ANNALES
UNIVERSITATIS SCIENTIARUM BUDAPESTINENSIS DE ROLANDO EÖTVÖS NOMINATAE

SECTIO GEOLOGICA

TOMUS XI.
1967

REDIGUNT
B. GÉCZY
J. KISS
L. STEGENA

BUDAPEST
1968

ANNALES
UNIVERSITATIS SCIENTIARUM BUDAPESTINENSIS DE ROLANDO EÖTVÖS NOMINATAE

SECTIO BIOLOGICA
incepit anno MCMLVII
SECTIO CHIMICA
incepit anno MCMLIX
SECTIO GEOLOGICA
incepit anno MCMLVII
SECTIO GEOGRAPHICA
incepit anno MCMLXV
SECTIO HISTORICA
incepit anno MCMLVII
SECTIO IURIDICA
incepit anno MCMLIX
SECTIO MATHEMATICA
incepit anno MCMLVIII
SECTIO PHILOLOGICA
incepit anno MCMLVII
SECTIO PHILOSOPHICA ET SOCIOLOGICA
incepit anno MCMLXII

МЕТЕОРОЛОГИЧЕСКИЕ ИССЛЕДОВАНИЯ НА ПИЛОТИРУЕМЫХ КОСМИЧЕСКИХ КОРАБЛЯХ

К. Я. КОНДРАТЬЕВ
(Ленинград)
(Поступила: 1. 10. 1966)

SUMMARY

The paper is a review of meteorological research carried out by analysing the observations, films and photos of the Earth, made by astronauts (using published data).

The following two groups of problems are discussed in particular:

1. Interpretation of cloud-photos (nephanalysis).
2. Investigation of the optical inhomogenities of the trophosphere and stratosphere (shining layer).

Удивительные успехи космонавтики, достигнутые за последние годы, открывают широкие перспективы научных исследований, осуществляемых человеком в космосе. Уже имеющийся опыт показывает, что полеты в космос важны не только с точки зрения изучения космоса, но очень ценны также для познания нашей планеты. Более того, основные научные результаты всех выполненных до сих пор околоземных космических полетов относятся преимущественно к области геофизики и, более всего, метеорологии и физики атмосферы. Цель настоящей статьи состоит в том, чтобы обсудить первые результаты метеорологических наблюдений и исследований по физике атмосферы из космоса, проведенных с участием космонавтов, и высказать некоторые соображения о перспективах дальнейших исследований в этом направлении. Прежде всего мы рассмотрим проблемы, относящиеся к метеорологическим исследованиям в интересах прогнозов погоды и климата.

Несомненно, что в настоящее время метеорология и физика атмосферы вступают в период революционных преобразований и это связано в значительной степени с появлением новых методов исследований. С одной стороны, в ближайшие годы впервые будут реализованы возможности осуществления системы сбора метеорологической информации в планетарных масштабах и в синоптические сроки; с другой, — огромные успехи вычислительной техники, приведшие к созданию электронных вычислительных машин

большого быстродействия и объема памяти, позволят осуществлять эффективную обработку и интерпретацию данных с целью прогноза погоды и климата. Хотя многие стороны процессов, определяющих изменения погоды и климата (в особенности разнообразные количественные характеристики), остаются неясными или недостаточно изученными, тем не менее бесспорно, что сочетание качественно нового объема метеорологической информации с эффективными методами ее обработки и анализа должно привести к существенному усовершенствованию прогнозов. В статье автора [Кондратьев, 1966] обсуждены основные черты возможной системы метеорологических наблюдений в планетарных масштабах. В качестве основных компонентов такой системы названы следующие:

1. Совокупность обычных методов наблюдений (наземные метеорологические, аэрологические, радиометеорологические, корабельные, самолетные и др.).

2. Метеорологические спутники.

3. Система метеорологических шаров-зондов, морских буев и наземных автоматических метеостанций в сочетании со спутниками, осуществляющими сбор и передачу получаемой информации.

4. Пилотируемые орбитальные космические лаборатории.

5. Лунная метеорологическая обсерватория для наблюдений Земли.

Нет необходимости высказывать здесь комментарии по поводу роли обычных методов наблюдений. Следует лишь подчеркнуть, что, несмотря на создание любых других систем получения метеорологической информации, значение обычных методов всегда останется существенным (это, в частности, отчетливо демонстрирует опыт использования спутниковых метеорологических данных). Разумеется, обычные методы будут в дальнейшем совершенствоваться и, прежде всего, по линии автоматизации процесса измерений, обработки и передачи информации.

Хотя еще не в деталях, но в принципе определилась и роль спутниковых метеорологических данных (эта проблема обсуждена в монографии автора [Кондратьев, 1963]). Подобные данные следует рассматривать как очень важное дополнение к обычной метеорологической информации. В случаях отсутствия такой информации (акватории океанов, труднодоступные области земного шара) спутниковые данные приобретают особую роль, становятся уникальными. Важной их особенностью является специфичность спутниковой метеорологической информации. Это либо изображения облачного покрова (телевизионные или инфракрасные), количественные методы интерпретации которых (в особенности в рамках численных методов прогноза) пока еще почти не разработаны, либо сведения об уходящем излучении, качество которых пока-что невысоко, и пути практического использования (снова следует упомянуть о численных методах) не найдены. Намечаются довольно ясные перспективы получения при помощи метеорологических спутников данных о вертикальном профиле температуры. Однако относительно возможностей располагать сведениями о полях атмосферного давления и ветра (с необходимой степенью точности) до сих пор трудно сказать что-либо достаточно определенное даже в принципиальном смысле.

Отмеченная специфичность спутниковой метеорологической информации побудила предложить для получения сведений о давлении, температуре, скорости и направлении ветра в труднодоступных районах сочетание обычных методов автоматических измерений на шарах-зондах и морских буях со сбором и передачей этих данных через спутники в наземные центры обработки и анализа информации. Со спутников должно осуществляться в данном случае также прослеживание перемещений шаров-зондов и буев с целью определения скорости и направления ветра, а также морских течений. В этой связи и возникает третий из упомянутых выше компонентов планетарной системы метеорологических наблюдений. Назовем этот компонент планетарными автоматическими метеорологическими станциями — ПАМС (в число ПАМС могут входить, в частности, арктические и антрактические наземные автоматические метеостанции).

В настоящее время разработано несколько проектов ПАМС [Lajenesse et al., 1965, Stanford, 1964, National Academy Washington, 1965], основные особенности которых рассмотрены в обзоре [Кондратьев, 1966].

Бесспорно, что из пяти перечисленных в начале настоящей статьи компонент системы метеорологических наблюдений в планетарных масштабах наиболее важное значение имеют первые три. Роль пилотируемых орбитальных космических лабораторий и лунной метеорологической обсерватории может быть лишь вспомогательной, хотя и весьма существенной.

Остановимся в этой связи сначала на краткой характеристике принципиальных возможностей использования пилотируемых орбитальных космических лабораторий. Заметим прежде всего, что участие человека в осуществлении научных программ на борту спутника имеет в частности, следующие преимущества: 1. возможность сознательного выбора объектов исследования, 2. контроль за функционированием сложной аппаратуры, 3. испытания новых приборов (в том числе контроль за калибровками, который трудно осуществить автоматически), 4. визуальные наблюдения.

Последнее преимущество с точки зрения метеорологии является особенно привлекательным. Очевидно, что присутствие на борту космического корабля квалифицированного синоптика-наблюдателя позволит реализовать возможность „наглядного" синоптического анализа и прогноза по данным наблюдений особенностей структуры облачного покрова. Своевременные штормовые предупреждения являются одним из примеров возникающих в связи с этим возможностей. Передача телевизионных изображений облачного покрова, получаемых с помощью метеорологических спутников, позволила существенно улучшить прогнозы погоды, особенно в тех районах, где сеть обычных метеорологических наблюдений отсутствует (океаны) или очень редка (труднодоступные районы суши). Однако метеорологические спутники выводились и будут в дальнейшем запускаться только на орбиты, расположенные над земной поверхностью довольно высоко (порядка 1000 км). Для исследовательских и практических целей важное значение имеет получение фотографий значительно большего пространственного разрешения с гораздо меньших высот, при осуществлении возможности сознательного выбора объектов фотографирования. Очень существенно последовательное (через короткие промежутки времени) фотографирование быстро изменяющихся облачных систем. Все эти специфические условия могут

быть лучше и надежнее всего реализованы с помощью наблюдателей-космонавтов.

Опыт анализа данных измерений уходящего излучения, полученных при помощи метеорологических спутников серии „Тайрос", убедительно свидетельствует о важности других, названных выше преимуществ наблюдений из космоса с участием человека. Напомним, например, что качество всех данных измерений уходящего излучения оказалось либо неудовлетворительным, либо не вполне удовлетворительным из-за неконтролировавшегося изменения чувствительности радиометров со временем (причины этого явления до сих пор не ясны). Разумеется, в дальнейшем можно ввести автоматический контроль чувствительности, что существенно повысит надежность данных. Однако лишь присутствие наблюдателя внесет решающий вклад в выяснение причин рассматриваемого явления.

В еще большей степени это относится к возможности сознательного анализа метеорологической ситуации и выбора объектов исследования. По тем-же данным результатов „Тайрос" обнаружено, что в верхней части тропосферы существуют аэрозольные слои (повидимому, перистые облака), которые оптически неактивны в видимой области спектра (незаметны на телевизионных изображениях облачного покрова), но являются интенсивными источниками инфракрасного теплового излучения. Естественно, что выбор и исследование подобных спорадически появляющихся объектов надежнее всего осуществить с участием наблюдателя. Несомненно, что в будущем космические инженеры и механики смогут обеспечивать также профилактический осмотр и ремонт аппаратуры.

К настоящему времени накоплен значительный опыт фотографирования космонавтами облачного покрова и последующего анализа полученных материалов. На первой стадии этих исследований были изучены оптимальные условия фотографирования облачности из космоса с точки зрения выбора спектрального диапазона чувствительности фотопленки. Интересный опыт в этом направлении был получен в результате полета В. М. Ширра на космическом корабле МА—8 3 октября 1962 г. С. Д. Соулс [Soules, 1963] описал научные результаты этого полета.

С помощью камеры Хассельблад, модел 500—С В. М. Ширра получил тринадцать черно-белых фотографий облачного покрова и земной поверхности. При этом каждый кадр был разделен на части шестью желатиновыми светофильтрами (с добавлением нейтральных фильтров для выравнивания яркостей), выделявшими различные участки спектра в пределах диапазона длин волн 380—720 мкм. Для съемок применялась сенсиблизированная панхроматическая пленка Кодак с чувствительностью ASA—64. Астронавту была рекомендована экспозиция 1/125 сек при диафрагме 5,6. Фактическая использованная экспозиция равнялась 1/250 сек (астронавт располагал портативным экспонометром). Обработка пленки произведена 6 октября 1962 г. Перед этим осуществлялась засветка пленки от стандартного источника света через оптический клин.

Фотографии, полученные В. М. Ширрой, относятся к южной части Атлантического океана и Бразилии. На рис. 1 приведены две фотографии для Атлантического океана, заснятые на 5-м витке при высоте солнца около 15° вблизи горизонта и примерно 7° — на переднем плане изображения.

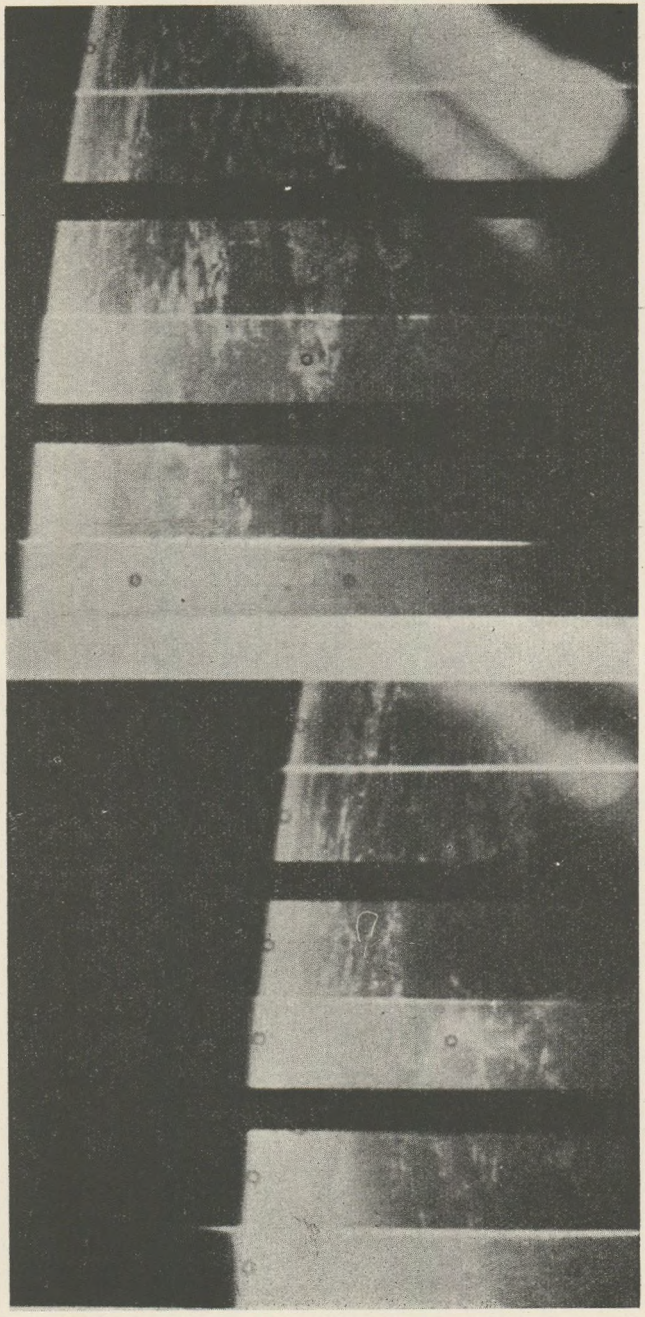

Рис. 1. Фотографии облачности в южной части Атлантического океана

Расположение полос изображения соответствует следующей последовательности светофильтров (слева направо): голубой, зеленый, нейтральный, желтый, красный, темно-красный. Отчетливо видно, как с увеличением длины волны уменьшается яркость атмосферной дымки и изображение становится все более контрастным. Более резко очерчена в области длинных волн и линия горизонта. Наблюдаемые на рис. 1 цепи кучевых облаков вытянуты по направлению ветра.

На некоторых фотографиях над линией горизонта заметен слой яркости, местоположение которого примерно совпадает с уровнем тропопаузы (16 км). Повидимому, это хорошо известный по данным наземных наблюдений аэрозольный слой под тропопаузой. С. Л. Соулс отмечает, что была предпринята попытка фотометрической обработки фотографий, оказавшаяся, однако, не вполне удачной, т.к. прозрачность иллюминатора космического корабля изменялась со временем, ввиду его загрязнения в период запуска. Можно было получить лишь относительные сенситограммы. На рис. 1 отмечены кружками точки, для которых определялось отношение плотностей почернения. Хотя выбранные пары точек не были идентичными, известное сопоставление контрастов все-же возможно. Для рис. 1 б отношения яркостей вершины слоистокучевого облака и безоблачного участка составляют следующие значения для различных светофильтров: нейтральный – 1,46; зеленый – 1,37; желтый – 1,28; красный – 1,18.

В альбоме фотографий [Кондратьев и др., 1964] прокомментированы двадцать цветных фотографий, заснятых советскими космонавтами. Рассмотрим некоторые из приведенных в работе [Кондратьев и др., 1964] примеров, иллюстрируя их черно-белыми изображениями. Фотографии, полученные космонавтами, выявляют весьма детальную картину так называемых внутримассовых облаков, развивающихся в однородной по своим свойствам воздушной массе. Эти облака возникают под влиянием конвективных движений в атмосфере, развивающихся главным образом благодаря сильному прогреву земной поверхности. К ним относятся кучевые облака хорошей

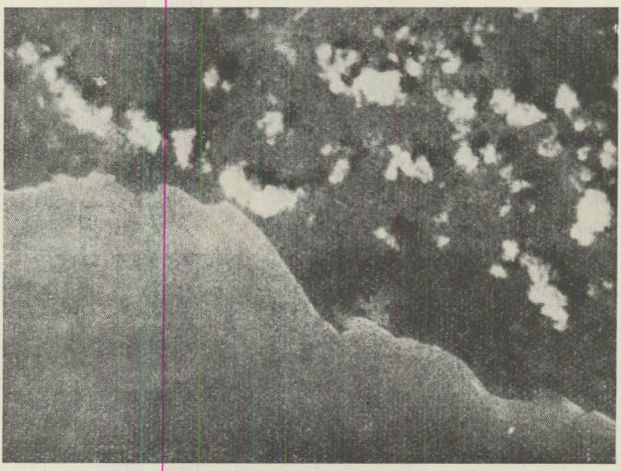

Рис. 2. Кучевые облака хорошей погоды над сушей

погоды и мощные кучевые облака. Очень сильное влияние на облака этого типа оказывают тепловые свойства земной поверхности и ее рельеф.

На рис. 2 представлен типичный случай образования кучевых облаков хорошей погоды в утренние часы над сушей, более прогретой, чем поверхность моря. Обращает на себя внимание полное отсутствие облаков над морем (в этом случае восходящие потоки слабы из-за малой разности температуры водной поверхности и воздуха). Фотографии на рис. 3 отчетливо иллюстрируют влияние орографии на конвективную облачность. Здесь изображен случай кучевых и мощных кучевых облаков, развивающихся над склонами гор.

Рис. 3. Кучевые и мощные кучевые облака, развивающиеся над склонами гор

Обширная группа облаков, представленных на фотографиях Земли из космоса, связана с существованием в тех или иных районах циклонов. Различие термодинамических свойств воздушных масс вблизи фронтов, входящих в системы циклонов, приводит к образованию огромных облачных массивов, многоярусных систем облаков, простирающихся на сотни и тысячи километров. Фотографии, заснятые со сравнительно небольших высот, позволяют изучать „тонкую" структуру подобных облачных систем.

Рис. 4 иллюстрирует случай обширных массивов перистых, перисто-слоистых и слоистых облаков на территории циклона, связанных с теплым фронтом.

Во многих случаях характер расположения облаков позволяет судить о направлении ветра. Относящийся к подобной ситуации пример изображен на рис. 5, где ряды кучевых облаков вытянуты по направлению ветра.

Американские астронавты Д. А. Макдивитт и Э. Х. Уайт („Джемини 4") осуществили фотографирование облачных систем на черно-белую (с применением различных светофильтров) и цветную пленку (высота космического корабля над земной поверхностью изменялась в пределах от 160 до 290 км).

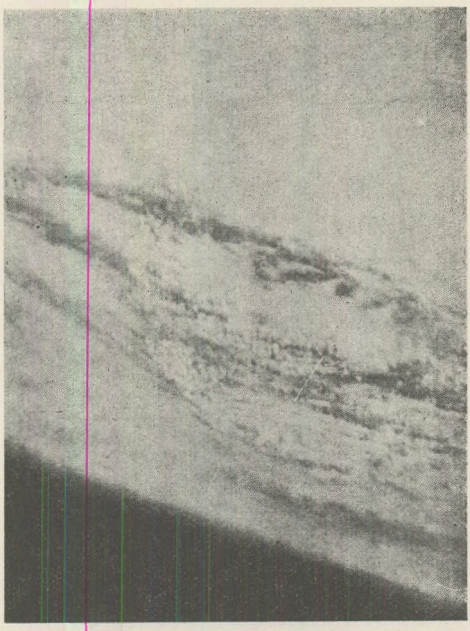

Рис. 4. Слоистообразные и перистые облака среднего и верхнего ярусов, входящие в облачную систему теплого фронта. В нижней части снимка — высококучевые облака

Полученные фотографии, проанализированные К. М. Наглером и С. Д. Соулсом [Nagler–Soules, 1965], особенно отчетливо демонстрируют возможности детального анализа систем конвективной (ячеистой) облачности с размерами ячеек, колеблющихся в пределах от 40 до 80 км. Достигаемая при этом высокая разрешающая способность, получение цветных изображений, возможность фотографировать одну и ту же облачную систему через короткие промежутки времени составляют отчетливые преимущества использования фотографий, полученных космонавтами, по сравнению с телевизионными снимками облачных систем с метеорологических спутников.

Данные фотографирования облачности с пилотируемых космических кораблей, которое было осуществлено американскими космонавтами ранее, подтвердили, в частности, что оптимальный диапазон спектральной чувствительности телевизионных трубок должен быть ограничен длинами волн 5000–7200 Å (см. рис. 1).

Рис. 5. Ряды кучевых облаков, вытянутые по направлению ветра над океаном

Для фотографирования с космического корабля „Джемини 4" использовалась модифицированная камера Хассельбад, Модель *С* с углом зрения 35°, снабженная пятью кассетами с 70 мм пленкой по 55 кадров размером 60 мм² (только одна кассета предназначалась для фотографирования облачности). Применялась фотопленка Кодак эктахром MS с чувствительностью ASA 64.

В качестве объектов фотографирования были избраны около двенадцати типов облачности (вихри, ячеистые облака, грозовые облака, тени перистых облаков, тропические штормы и др.). Во время и до полета космонавты получали инструкции по выбору объектов, основанные на анализе синоптической ситуации по данным обычных и спутниковых метеорологических наблюдений. Всего Д. А. Макдивиттом и Э. Х. Уайтом было отснято около 200 кадров, из которых примерно 100 представляют интерес с точки зрения метеорологии (снимки относятся к южной части США, Африке, южной Азии и океанам в зоне широт 32,5° ю.ш. – 32° 5 с.ш.). На фотографиях хорошо различимы объекты с размерами 18–24 м (дороги, аэродромы, следы кораблей и др.). В ряде случаев из-за сравнительно малой высоты космического корабля космонавты не смогли наблюдать и идентифицировать характерные спиралеобразные системы облачности штормов. В работе [Nagler–Soules, 1965] приведены и прокомментированы семь фотографий.

Как и на рассмотренных выше фотографиях советских космонавтов, отмечается, в частности, отсутствие кучевых облаков над большей частью океанических областей (см. также [Bulban, 1965]). Случай кучевых облаков хорошей погоды изображен на рис. 6, относящемся к району Багамских

островов. Эта фотография иллюстрирует также некоторые возможности определения глубины моря в зонах мелководья, поскольку в таких условиях в большей или меньшей степени проявляется отражение солнечной радиации от дна моря.

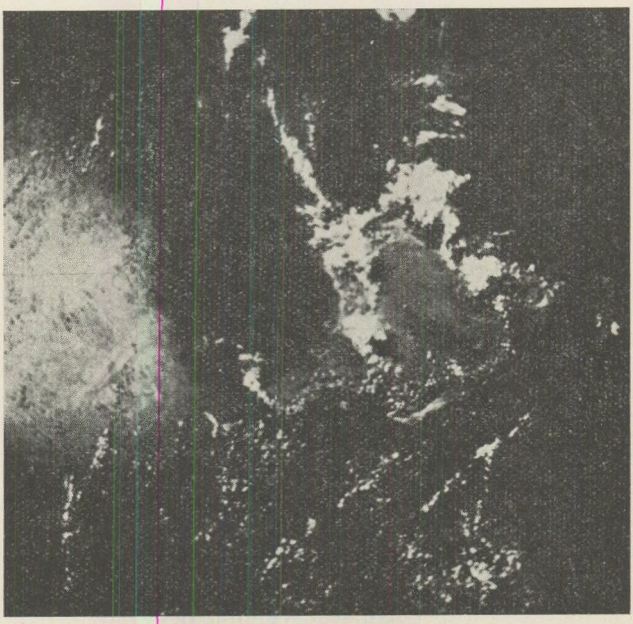

Рис. 6. Кучевые облака хорошей погоды в районе Багамских островов

В левой части фотографии зафиксирован солнечный блик с маленькими черными пятнами, представляющими собой тени, отбрасываемые облаками (сами облака незаметны из-за большой яркости морской поверхности в области блика). Как показали Г. В. Розенберг и Ю. А. Мулламаа [1965], наблюдения особенностей такого рода солнечных бликов (солнечной дорожки) позволяют получить известное представление о направлении и скорости ветра вблизи водной поверхности. Принципиальная возможность решения этой задачи определяется зависимостью от поля ветра высокочастотной компоненты временного и пространственного спектров водной поверхности, а также функцию распределения наклонов водной поверхности в области больших углов наклона. Авторы показали, что с точки зрения определения скорости ветра наиболее удобно использование таких параметров солнечной дорожки как положение максимума яркости отраженного света и поперечного (по отношению к направлению дорожки) градиента яркости. При доступной точности наблюдений ошибка определения скорости ветра не должна превосходить ± 2 м/сек. Однако направление ветра может быть найдено лишь очень приближенно. Интересно упомянуть в связи с этим, что заманчивы возможности судить о параметрах волнения заключены также в использовании корреляционных характеристик рассеянных морской поверхностью радиоволн в диапазоне 8 мм – 4 м [Калмыков и др., 1965].

Фотография, изображенная на рис. 7, демонстрирует интересное явление образования вихрей в подветренной стороне гористых островов, аналогичное (по внешним проявлениям) классическому случаю возникновения вихрей за препятствием, известному из гидродинамики. Этот случай подробно обсуждался при анализе телевизионных изображений, полученных при помощи метеорологических спутников [Conover, 1964, Chopra, 1965, Бугаев, 1965]. Рассматриваемая фотография, относящаяся к району Канарских островов, позволяет, однако, располагать гораздо более детальной

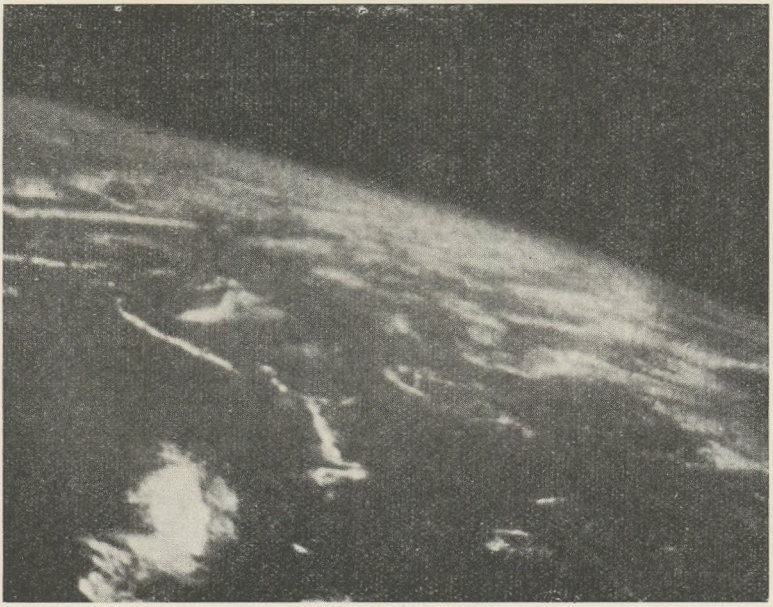

Рис. 7. Цепи кучевых облаков в районе Канарских островов, обусловленные влиянием орографии

картиной. Отметим, например, что хорошо заметные на рис. 7 тонкие линии (цепи) кучевых облаков не могли быть зафиксированы на фотографиях со спутников „Тайрос".

Рис. 8, на котором представлена фотография безоблачного участка подстилающей поверхности в районе штата Техас (США), любопытен в отношении возможности судить о горизонтальной неоднородности влажности почвы. Темные участки земной поверхности соответствуют здесь более влажным участкам с низкой отражательной способностью. Альтернативное предположение по поводу интерпретации темных зон состоит в том, что ливни, прошедшие на несколько дней до момента фотографирования, вызвали потемнение подстилающей поверхности либо в результате увлажнения, либо вследствие усиления роста зеленой растительности (возможно, что оба эти фактора существенны). В любом случае потемнение подстилающей поверхности в засушливой зоне является, однако, показателем выпадения осадков.

Наряду с фотографированием, важное значение имеют визуальные наблюдения. Уже наблюдения, осуществленные первыми космонавтами, указали на широкие возможности в этом направлении (оценка синоптической ситуации на основе анализа характера облачных систем, обнаружение грозовых очагов и зон штормов, наблюдение областей океанических течений по цветовым контрастам воды и др.).

Рис. 8. Безоблачный участок подстилающей поверхности в центральной части Техаса с темными зонами, свидетельствующими о выпадении осадков

Обратимся теперь к обсуждению тех результатов исследований, которые принадлежат области атмосферной оптики. Сюда относятся прежде всего наблюдения так называемых слоев яркости над горизонтом. Такого рода наблюдения были осуществлены Д. Х. Гленном [1962], В. В. Николаевой-Терешковой [1965], К. П. Феоктистовым [1965] и др.

Д. Х. Гленн [1962] наблюдал на ночной стороне Земли слой яркости, имевшей угловую ширину около 1,5—2° на угловой высоте от 6 до 8° над линией горизонта. Этот слой мог быть отчетливо обнаружен по временному (на время порядка нескольких секунд) исчезновению звезд вблизи горизонта при заходе их за горизонт по мере движения космического корабля. Внимательное визуальное прослеживание позволяло наблюдать полосу, параллельную линии горизонта, которая была отлична по цвету от расположенных ниже облаков. Полоса наблюдалась на всех трех витках, когда корабль находился на ночной стороне Земли и была гораздо лучше заметна при лунном освещении (хотя и в этом случае не имела резко очерченных краев). Д. А. О'Киф высказал предположение, что наблюдав-

шаяся Д. Х. Гленном полоса яркости является кажущейся и обусловлена оптическими эффектами в стеклах иллюминатора (такая интерпретация вызывает, однако, сомнения).

В. В. Николаева-Терешкова [1965] и К. П. Феоктистов [1965] осуществили не только визуальные наблюдения, но и фотографирование полос яркости, которые могут быть интерпретированы вполне достоверно.

Г. В. Розенберг [1965] проанализировал принципиальные возможности наблюдений планетарных атмосфер с космических кораблей в условиях сумерек. В работе отмечены прежде всего два возможных и существенно различных случая подобных наблюдений. Одна из ситуаций такова (рис. 9), что линия визирования наблюдателем находящимся в некоторой точке на высоте h над земной поверхностью, в области тени проходит целиком в области тени и упирается в неосвещенную часть поверхности. Во втором случае линия визирования проходит на некоторой минимальной высоте y над поверхностью планеты и определенная ее часть находится в освещенной зоне атмосферы (рис. 9). Существенное различие рассматриваемых ситуаций состоит в том, что в первом случае наблюдателя достигает только многократно рассеянный свет, а во втором — набладается также и первично рассеянный свет, причем вклад много-кратного рассеяния может быть достаточно малым.

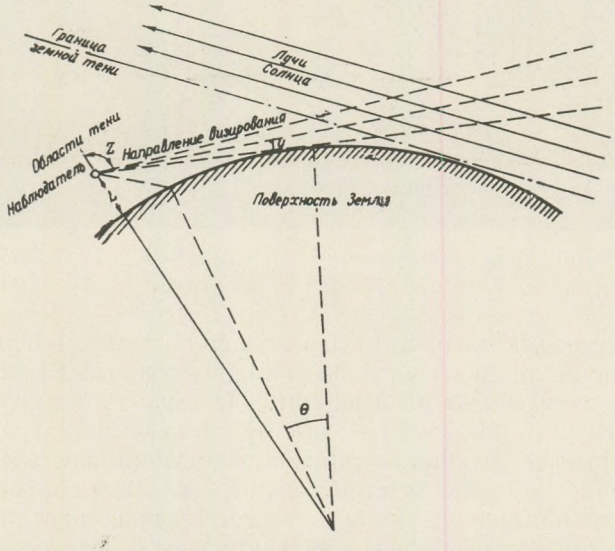

Рис. 9. Условия наблюдений сумеречной атмосферы с космического корабля

Второй случай значительно более интересен с точки зрения интерпретации данных наблюдений. Анализ данных измерений яркости атмосферы, осуществленных в таких условиях, позволяет изучать оптические свойства атмосферы на различных высотах. Более трудной является интерпретация данных, полученных при измерениях яркости только многократно рассеянного света.

Наблюдения светового ореола из точки, находящейся в зоне тени, позволяют по неоднородностям ореола судить о наличии облачности и аэрозольных слоев в атмосфере. Так, например, при наличии слоя повышенной мутности в направлении визирования свет окажется сильно ослабленным, что выразится в уменьшении яркости светового ореола. На рис. 10 приведена фотография ореола, заснятая В. В. Николаевой-Терешковой 17 июня 1963 г. с космического корабля „Восток 6" [Розенберг и др., 1965], иллюстрирующая подобный пример (рис. 9 характеризует схему эксперимента). Горизонтальная протяженность линии горизонта составляет около 500 км. Горизонтальная неоднородность яркости ореола обусловлена тем, что направление визирования не совпадало с направлением на Солнце. Отчетливая видимость края Земли позволила осуществить привязку по высоте с точностью порядка 1 км.

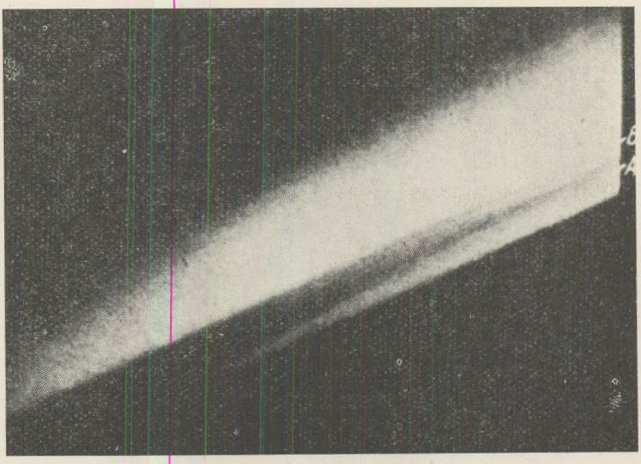

Рис. 10. Фотография сумеречного ореола. „Восток 6", 17 июня 1963 г.

Хорошо заметные на рис. 10 две полосы пониженной яркости А и Б отражают наличие здесь слоев повышенной мутности. Высотный фотометрический разрез, изображенный на рис. 11, характеризует спады яркости еще более четко (I — яркость, y — высота перигея направления визирования; Θ — угловые расстояния от горизонта до точки пересечения направления визирования с земной поверхностью, отнесенные к центру Земли, — см. рис. 9). Отрицательные значения Θ соответствуют визированию ниже линии горизонта. В этом случае яркость света обусловлена только многократным рассеянием (как видно, вклад многократного рассеяния в яркость сумеречного ореола весьма мал).

На рис. 12 изображена зарисовка сумеречного ореола по данным визуальных наблюдений на корабле „Меркурий 8" [NASA, 1965]. Последовательность окрасок ореола в направлении вверх от линии горизонта была следующей: от оранжевой к синей, голубой, снова синей, голубой и, наконец (в верхней части ореола), — белесоватой.

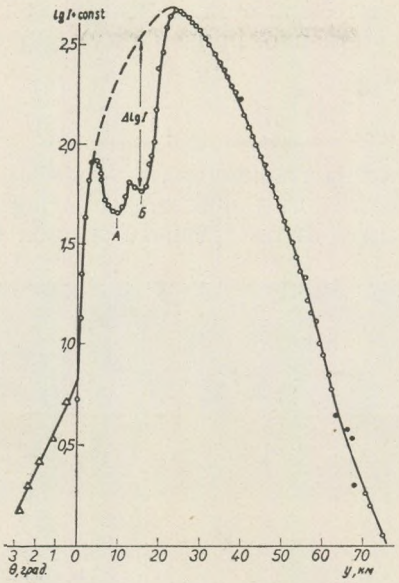

Рис. 11. Распределение яркости в сумеречном ореоле, изображенном на рис. 10

Приближенная теория, предложенная Г. В. Розенбергом [1965] показывает, что в рассматриваемом случае яркость ореола определяется следующим простым соотношением:

$$I(y) = I_0\omega_0 T(y) m\tau(H) \tag{1}$$

Здесь: $I_0 w_0$ — яркость и угловой размер диска Солнца; $T(y)$ — прозрачность атмосферы на всем протяжении направления визирования; m — атмосферная масса для направления визирования в точке пересечения им эффективной границы земной тени; $(\overline{H})$ — эффективная высота земной тени вдоль направления визирования; $\tau(\overline{H})$ — вертикальная оптическая толща рассеяния света атмосферой над уровнем $\overline{H}$. Прозрачность $T(y)$ увеличивается, а оптическая толща $m\tau(\overline{H})$ убывает с высотой. Это и определяет появление плавного максимума яркости на рис. 11. При отсутствии каких-либо аэрозольных неоднородностей в атмосфере зависимость $\ln I$ от y должна иметь плавный ход с одним максимумом.

Логарифмируя (1), получим

$$\ln I = \text{const} + \ln T(y) + \ln [m\bar{\tau}(H)]. \tag{2}$$

Если в рассматриваемой области отсутствует поглощение, то

$$-\ln T(y) = \tau_m(y) + \tau_a(y) \tag{3}$$

где τ_m, τ_a — оптические толщи, обусловленные молекулярным и аэрозольным рассеянием, соответственно, причем $\tau_m(y)$ определяется формулой

$$\tau_m(y) \approx 80 \frac{9 \cdot 10^{-3}}{\lambda^4} \frac{p(y)}{p(o)} \tag{4}$$

Здесь λ — длина волны в микронах, p — атмосферное давление.

Сильная зависимость τ_m от длины волны решающим образом влияет на спектральный состав света от сумеречного ореола. Быстрое убывание τ_m с

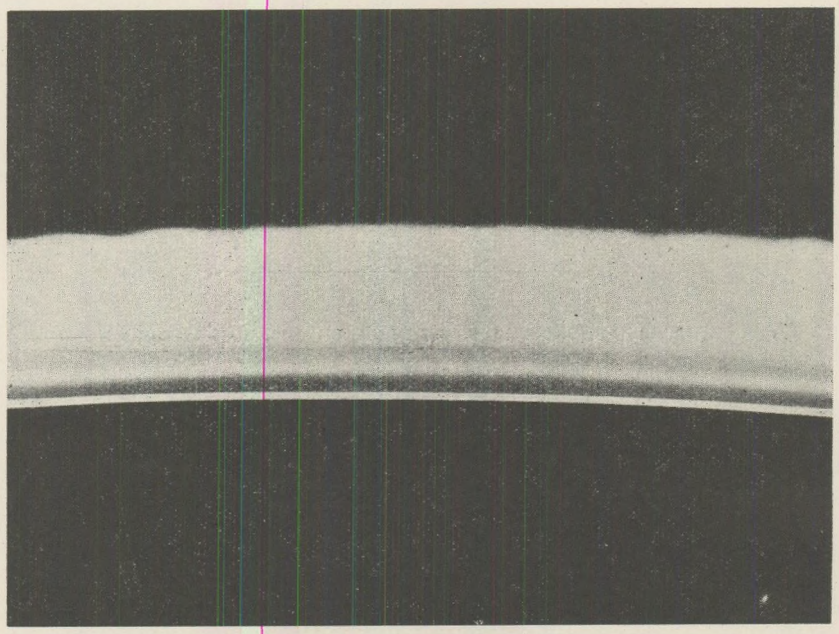

Рис. 12. Зарисовка полос яркости сумеречного ореола

высотой обусловливает появление главного максимума яркости сумеречного ореола (рис. 11). Нарушения плавного хода $\ln I$ в зависимости от y, как уже отмечалось, обусловлены неоднородностями вертикального распределения аэрозоля. Вертикальный профиль $\Delta \ln I$ (рис. 11) характеризует особенности вертикального распределения концентрации аэрозоля. В рассматриваемом случае (рис. 10, 11) Г. В. Розенберг и В. В. Николаева-Терешкова [1965] обнаружили аэрозольные слои на высотах $11{,}5 \pm 1$ км (тонкий, слабо выраженный слой) и $19{,}5 \pm 1$ км (значительно более мощный слой с довольно четкой верхней границей). Первый из этих слоев представляет собой хорошо известное явление скопления аэрозоля под тропопаузой. Существование второго — было ранее надежно установлено по данным прямых (аэростатные заборы проб) и косвенных (прожекторный метод, наземное сумеречное зондирование) исследований.

К. П. Феоктистов [1965] осуществил фотографирование сумеречного ореола на цветную пленку. На рис. 13 приведено черно-белое изображение полосы зари, а также схематическая зарисовка К. П. Феоктистова, характеризующая зависимость яркости B от высоты H с указанием

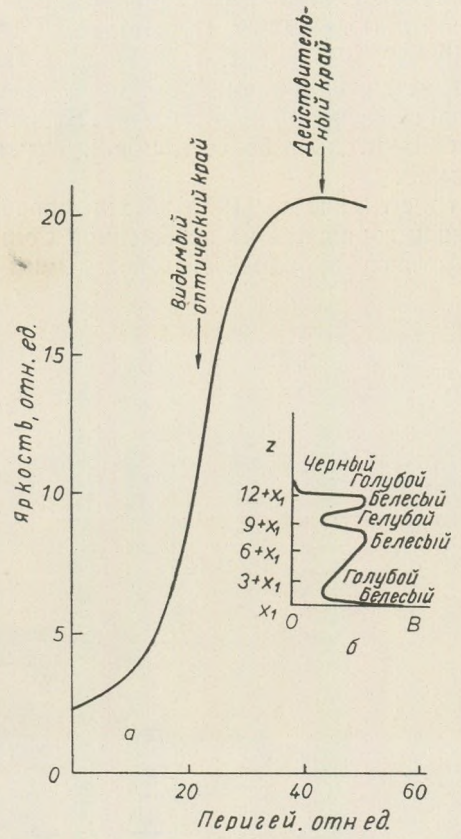

Рис. 13. Распределение яркости по высоте в зоне зари

наблюдавшейся последовательности цветов зари (цветные фотографии зари можно найти в альбоме [Кондратьев, 1964]). Как отмечено в работе Феоктистова [1965], смена окрасок зари от красно-оранжевой у каря Земли к голубой при переходе к космосу обусловлена селективным ослаблением света зари на пути через различные толщи атмосферы. Спады яркости на кривой рис. 13 отражают существование аэрозольных слоев, что находится в полном согласии с обсужденными выше результатами наблюдений В. В. Николаевой-Терешковой [1965]. Подобные слои наблюдались с корабля „Восход" как ночью, так и днем, а число их изменялось от одного до трех (иногда они вообще отсутствуют). Слабая светящаяся полоса наблю-

далась на высоте 2,5—3° над краем планеты на ночной стороне при лунном освещении.

Следует заметить, что на ночной стороне Земли вблизи линии горизонта всегда наблюдается „слой дымки", который в действительности представляет собой полосу свечения ночного неба [NASA, 1965]. Эта полоса неоднородна: имеет „облачную" структуру, причем линейные размеры неоднородностей изменяются от 30 до 300 км. По данным Д. А. Макдивитта и Э. Х. Уайта [NASA, 1965] при отсутствии Луны структура ночного горизонта характеризуется наличием трех полос: верхняя представляет собой упомянутую полосу свечения ночного неба. Вторая, ниже расположенная полоса, является значительно более тусклой, а третья — наиболее слабой и трудно различимой.

К. П. Феоктистовым [1965] были продолжены наблюдения светового ореола вблизи горизонта на освещенной Солнцем стороне Земли, а также выполнено фотографирование световой дымки над краем планеты.

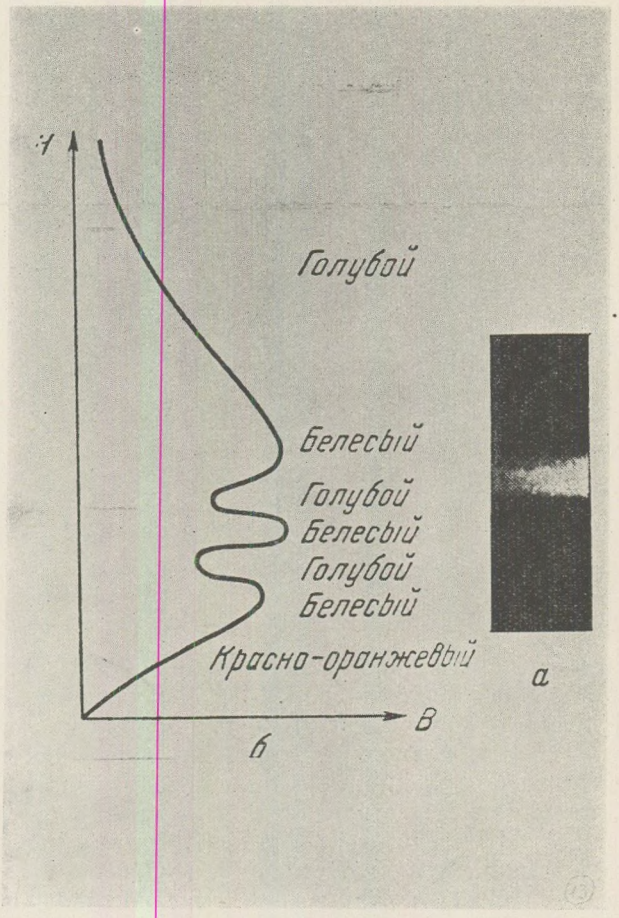

Рис. 14. Схематический фотометрический разрез светового ореола вблизи горизонта

Эти наблюдения показали, что дымка интенсивнее в синей части спектра, чем в красной, и практически полностью вуалирует не только рельеф земной поверхности у горизонта, но и тропосферную облачность. Оптический горизонт Земли может быть зафиксирован лишь как линия максимального вертикального градиента яркости (см. фотометрический разрез светового ореола вблизи горизонта на рис. 14а). На рис. 14б указана последовательность окрасок ореола (x, $\approx 7 \div 10$ км – высота оптически фиксируемого края планеты над земной поверхностью) по данным схематической зарисовки К. П. Феоктистова.

Интересные фотографии дневного ореола Земли получены с космического корабля „Джемини 4" [NASA, 1965]. Фотографирование велось с использованием панхроматической пленки и двух светофильтров: голубого (область пропускания 400–470 ммк с центром около 432 м ммк) и красного (диапазон пропускания 640–710 ммк с центром при 675 ммк). После полета снимки подвергались фотометрической обработке (пленка была заранее прокалибрована). Просмотр фотографий показал, что верхняя граница дымки проявляется более или менее одинаково как в красной так и в голубой области спектра, но „голубая" дымка значительно более „размыта" чем „красная". В таблице указаны полученные для различных фотографий величины превышения высоты дымки в голубой области спектра по сравнению с красным диапазоном (верхняя граница ореола фиксировалась по уровню, для которого значение яркости было равно одной трети максимального). Иногда наблюдался очень протяженный (до высоты 200 км) голубой ореол, но возможно, что он был кажущимся и обусловленным загрязненностью иллюминатора или другим рассеянным светом.

Для характеристики вертикального градиента яркости ореола определялась разность высот уровней, которым соответствуют плотности почернения, равные половине и четверти максимальной. В красной области эти величины варьируют от 4,0 до 6,0 км при среднем значении 4,8 км. Пределы изменения для голубой области составляют $5{,}2 \pm 8{,}6$ км, а среднее значение – 7,2 км. При этом существенно, что дневной ореол обладает значительной горизонтальной неоднородностью.

Г. В. Розенберг, А. Б. Сандомирский и Г. И. Трифонова [1965] предложили приближенную теорию яркостного профиля дневного горизонта Земли. Эти авторы показали, в частности, что оптический горизонт планеты должен располагаться в диапазоне высот 10–20 км, причем, положение его существенно зависит от длины волны.

Сделанные в работе расчеты позволили оценить влияние аэрозольных слоев на вертикальный профиль яркости светового ореола вблизи горизонта на дневной стороне Земли. На рис. 15 изображена зависимость $\lg(1-e^{-2\tau(y)})$ – величины, характеризующей относительное изменение яркости ореола с высотой, от высоты перигея y направления визирования. При построении внешней кривой учтено наличие двух аэрозольных слоев на высоте около 11 и 19 км по данным [Розенберг, 1965]. Как видно, в условиях дневного освещения наличие первого слоя почти незаметно. Влияние второго слоя проявляется гораздо более существенно как появление полосы повышенной яркости, расположенной вдоль дневного горизонта и являющейся довольно

Таблица

Превышение высот „голубой" дымки по сравнению с „красной"

Номер фотографии	Превышение высоты „голубой" дымки, км		Угол рассеяния, град
	единичные	средние	
7	4,35		
8	4,00	4,2	53
9	4,30		
10	7,2		
11	7,0	6,7	68
12	6,0		
13	7,3		
14	8,5	7,3	83
15	6,1		
16	4,5		
17	5,4	4,8	99
18	4,5		
19	5,2		
20	5,0	5,1	113
21	5,2		
22	5,5		
23	5,7	5,8	125
24	6,3		
25	5,7		
26	6,9	6,4	133
27	6,6		
28	7,8		
29	8,7	7,7	138
30	6,5		

размытой. Эти результаты отчетливо демонстрируют преимущество наблюдений сумеречного ореола с точки зрения исследований оптических неоднородностей атмосферы. Следует подчеркнуть, однако, что этот вывод справедлив лишь по отношению к оптическим неоднородностям, рассмотренным выше. В случае-же, например, серебристых облаков, расположенных на высоте около 80 км, весьма благоприятны с точки зрения их обнаружения из космоса не только сумеречные, но и дневные наблюдения [Розенберг, 1966].

Программа экспериментов на пилотируемых космических кораблях предусматривает решение ряда задач, относящихся к числу так наз. обратных задач спутниковой метеорологии, имеющих целью определение структурных параметров и состава атмосферы по данным измерений различных характеристик уходящего излучения. К числу подобных задач относится определение высоты верхней границы облачного покрова по данным измерений поглощения солнечной радиации, обусловленного 0,76 мк полосой кислорода, в толще атмосферы выше облака. Теория этого метода, развитая М. С. Малкевичем [1964], Д. К. Уорком и Д. М. Мерсером [1965], подтверждает, что измерения уходящей радиации в полосе и вне полосы поглощения кислорода позволяют определить поглощенную толщей

атмосферы солнечную радиацию, а затем рассчитать атмосферное давление на уровне верхней границы облака (поскольку кислород можно считать равномерно перемешанным в атмосфере газом, то его содержание в толще атмосферы выше фиксированного уровня определяется величиной давления на этом уровне и некоторыми известными параметрами).

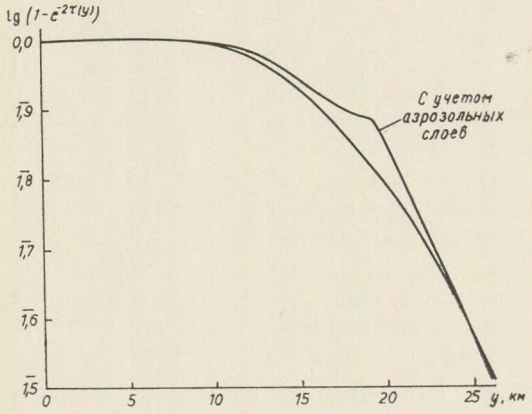

Рис. 15. Относительное изменение яркости светового ореола вблизи горизонта с высотой на дневной стороне Земли

Ф. Саиди и др. [1965] описали прибор, предназначенный для определения высоты верхней границы облачного покрова со спутников по поглощению солнечной радиации кислородом в толще атмосферы выше облака. Прибор представляет собой комбинацию фотоаппарата и спектрографа. Диспергирующим элементом спектрографа, который служит для получения данных о спектральном составе отраженной облаком солнечной радиации в области 0,76 мк полосы поглощения кислорода, является реплика размером 3,0×3,2 см с 1200 штрих/мм и с блеском при 0,76 мк в первом порядке. Спектральная разрешающая способность составляет ~5 Å.

Методика обработки результатов измерений состоит в сравнении измеренных величин пропускания солнечной радиации толщей атмосферы выше облака (отношения интенсивностей радиации в полосе поглощения при длине волны 7630 Å и вне полосы) и соответствующих расчетных величин, вычисленных для различных значений атмосферного давления на уровне верхней границы облака. По совпадению измеренных и вычисленных величин определяется атмосферное давление, а затем высота верхней границы облака.

Испытания прибора, осуществленные при полете самолета над однородным слоем высоко-кучевых облаков (самолет пролетал на высоте 30 м над облаком, а прибор был направлен в надир), обнаружили систематическую завышенность определенного предложенным методом атмосферного давле-

ния (следовательно, заниженность высоты облаков) по сравнению с действительным значением на 137 мб. Расчет показывает, что ошибка измерений пропускания радиации не превосходит $\pm 0{,}01$, что соответствует ошибке определения давления ± 30 мб. Упомянутое систематическое расхождение можно объяснить влиянием поглощения солнечной радиации в отражающей радиацию толще облаков, что в конечном счете сводится к необходимости учитывать различие альбедо облака в полосе и вне полосы поглощения кислорода. Приближенный теоретический расчет подтверждает подобное предположение. В связи с этим предложена методика введения поправки, учитывающей различие альбедо в полосе и вне полосы поглощения в зависимости от толщины облачного покрова. Без введения такой поправки ошибка опеределения высоты облаков может колебаться в пределах от 300 до 2200 м.

В своей работе Ф. Саиди, А. В. Морган и Д. К. Уорк [1965] описали предварительные результаты испытания описанного выше прибора на космическом корабле „Джемини – 5". Это испытание оказалось очень удачным. Обработка трех спектров с целью определить уровень верхней границы облаков дала следующие результаты в сопоставлении с данными расчетов по аэрологическим зондированиям:

Измеренная высота (мб)	Рассчитанная высота (мб)	Характер облачности
980	960	слоистые облака
440	–	внутритропическая зона конвергенции
320	350 – 220	тропический шторм „Дорин"

Интересные доклады космонавтов о программах исследований на космических кораблях, выполненных в 1965 г., были сделаны на XVI конгрессе по астронавтике в Афинах (сентябрь 1965 г.).

В сообщениях П. И. Беляева и А. А. Леонова сделан краткий обзор исследований на космическом корабле „Восход 2", результаты которых уже освещались в советской печати.

Американские космонавты Г. Купер и Ч. Конрад сообщили о 16 из 17 экспериментов (один опыт был секретным), осуществленных на „Джемини – 5". Были, в частности, произведены визуальные наблюдения метеоритов, следов самолетов в стратосфере, особенностей геологической и иной структуры земной поверхности, изучена возможность визуальной оценки глубины водных бассейнов в прибрежной полосе. Сделаны наблюдения зодикального света и получены фотографии млечного пути. Изучался электрический заряд космического корабля. С помощью спектрометра измерялось излучение космического пространства в области длин волн от 0,2 до 12 мк. Другой спектрометр использован для измерений отраженной солнечной радиации в полосе поглощения кислорода (0,76 мк) с целью определения высоты верхней границы облаков (результаты этих измерений были рассмотрены выше). Произведены фотографирование Земли из космоса, а

также инструментальные и визуальные наблюдения за запуском ракеты с земной поверхности.

Перспективы метеорологических исследований на орбитальных космических кораблях очень широки и разнообразны. В особенности это касается решения многочисленных обратных задач спутниковой метеорологии.

В настоящее время начинают обсуждаться также и возможности метеорологических наблюдений Земли человеком с других небесных тел, например, Луны.

Лунная метеорологическая обсерватория для наблюдений Земли (ЛМО), проект которой предложен в работе [NASA, 1965], может сыграть важную роль с точки зрения возможности визуального или инструментального прослеживания наиболее крупномасштабных метеорологических процессов в атмосфере.

Отсутствие на Луне атмосферы позволяет осуществлять с поверхности Луны измерения солнечной постоянной, данные которых имеют фундаментальное значение для решения проблемы „Солнце-погода". Значительный интерес представляют измерения потоков уходящего излучения Земли как планеты с помощью аппаратуры, установленной на поверхности Луны. Таже аппаратура может быть использована и для измерений составляющих радиационного баланса лунной поверхности и ее радиационной температуры.

Поскольку Луна обращена к Земле все время одной стороной, достаточно располагать на поверхности Луны всего лишь одной обсерваторией для наблюдений всей земной поверхности и атмосфер по мере вращения Земли вокруг своей оси. В этой связи для метеорологии особый интерес представляет получение инфракрасных изображений Земли, которые позволят в любой момент времени располагать данными о распределении облачного покрова, температуре и высоте верхней границы облаков, а также температуре подстилающей поверхности (в районах отсутствия облачности) для целого полушария.

Несомненно, что потребуется продолжительное время, прежде чем широкие возможности метеорологических наблюдений из космоса будут реализованы. Важно, однако, что уже имеющиеся результаты являются весьма обнадеживающими.

ЛИТЕРАТУРА

Бугаев, В. А., Минина Л. С. (1965): О грядовой структуре облачности. Метеор. и гидрол., № 5.

Калмыков, А. И., Островский, И. Е., Розенверг, А. Д., Фукс, И. М. (1965): О влиянии структуры морской поверхности на пространственные характеристики рассеянного ею радиоизлучения. Известия ВУЗ, Радиофизика, т. VIII., № 6.

Кондратьев, К. Я. (1963): Метеорологические спутники. Гидрометеоиздат.

Кондратьев, К. Я., Крошкин, М. Г., Морачевский, В. Г. (1964): Наша планета из космоса. Гидрометеоиздат.

Кондратьев, К. Я. (1966): О планетарной системе метеорологических наблюдений. Метеорология и гидрология, № 8.

Кондратьев, К. Я., Гаевский, В. Л., Конашенок, В. Н., Решетников, А. И. (1966): Лунная метеорологическая обсерватория для наблюдений Земли. Космич. исслед., т. IV, вып. 2.

Малкевич, М. С. (1964): Некоторые вопросы интерпретации поля уходящей радиации Земли. I. Определение температуры подстилающей поверхности и высоты верхней границы облаков. Труды ГГО, вып. 166.

Розенберг, Г. В., Мулламаа, Ю. А. Р. (1965): О некоторых возможностях определения скорости ветра над океанической поверхностью по наблюдениям с искусственных спутников Земли. Изв. АН СССР, сер. физ. атм. и океана, № 3.

Розенберг, Г. В., Николаева-Терешкова, В. В. (1965): Стратосферный аэрозоль по измерениям с космического корабля. Изв. АН СССР, сер. физики атмосферы и океана, т. 1, № 4.

Розенберг, Г. В. (1965): О сумеречных исследованиях планетных атмосфер с космических кораблей. Изв. АН СССР, сер. физ. атм. и океана, т. 1. № 4.

Розенберг, Г. В., Сандомирский, А. Б., Трифонова, Г. И. (1965): Яркостный профиль дневного горизонта планеты Земля. Изв. АН СССР, сер. физ. атм. и океана, т. 1, № 12.

Розенберг, Г. В. (1966): О наблюдаемости серебристых облаков с космических кораблей. Известия АН СССР, сер. физики атм. и океана, т. 2, № 1.

Феоктистов, К. П., Розенберг, Г. В., Сандомирский, А. Б., Сергеевич, В. Н., Сонечкин, Д. М. (1965): Некоторые результаты оптических наблюдений с космического корабля „Восход". Исслед. космич. пространства, „Наука", Москва.

Bulban, E. J. (1965): Crew of Gemini 5 vehicle provided detailed storm data. Aviation Week and Space technology, v. 83, N 12.

Chopra, K. P., Hubert, L. F. (1965): Karman vortex streets in wakes of islands. AJ. AA Journ, v. 3, N 10.

Conover, J. H. (1964): The identification and significance of orographically induced clouds observed by Tiros satellites. Journ. of Appl. Meteor., v. 3, N 3.

Glenn, J. H., O'Keefe, J. A. (1962): The Mercury – Atlas – 6 space flight. Science, v.136, N 3522.

Lajenesse, P., Millerdet, C., Turriere, J. (1965): Global meteorological system using satellites. Lab. Central de Telecommunications, Paris Pl. 601, 185A, Issue 1 – april 5 th.

Nagler, K. M., Soules, S. D. (1965): Cloud photography from the Gemini 4 Spaceflight. Bull. Am. Meteor. Soc., v. 46, N 9.

NASA, Washington (1965 : Manned Space Flight Experiments Symposium. Gemini Missions III and IV, Oct. 18 – 19, 1965.

National Academy of Siences, Washington (1965): The feasibility of a global observation and analysis experiment.

Saiedy, F., Hilleary, D. T., Morgan, W. A. (1965): Cloud-top altitude measurments from satellites. Appl. Optics, v. 4, N 4.

Saidy, F., Morgan, A. W., Wark, D. Q. (1965): Determination of cloud altitudes from Gemini-Titan – 5. Nature, v. 208, N 5012.

Soules, S. D. (1963): Spectral reflectance photography of the Earth from Mercury Spacecraft MA – 8. Meteor. Sat. Lab. Rep. N 22, Nov.

Stanford University (1964): Stanford worldwide acquisition of meteorological information. Dept. of Aeronautics and Astronautics, Ed. by L. R. Talbert.

Wark, D. Q., Mercer D. M. (1965): Absorption in the atmosphere by the oxygen "A" band. Appl. Optics, v. 4, N 7.

THE PROBLEM OF MAGNETIC STABILITY IN THE LIGHT OF THERMOMAGNETIC RESEARCH

by

P. MÁRTON

(Geophysical Institute of Loránd Eötvös University)

(Received: 17 September 1967.)

SUMMARY

One of the fundamental assumptions of the palaeomagnetic method is that the natural remanent magnetization (NRM) of rocks dates from the time of their origin and undergoes no substantial change during their later life. Only rocks about which this assumption has been proved by reliability studies are suitable for palaeomagnetic investigations. Thermomagnetic work done by the author raises some doubts as to the invariability of the ferromagnetic constituents of rocks hitherto considered as relatively stable. These ferromagnetic constituents may in certain cases hemselves be products of alteration.

Introduction

The reliability of palaeomagnetic measurements is checked by field methods on the one hand and laboratory methods on the other. Field methods are of a fundamentally geometric nature, whereas laboratory methods are based on measurements of rock magnetism, involving the reproduction in the laboratory of all the conceivable influences that might during its life have affected the magnetism of a rock and inferences concerning its magnetic stability from its behaviour under such simulated influences. However, laboratory influences are incomparably shorter in duration than natural influences whose duration can be measured in terms of million years. This is why laboratory experiments are designed so as to affect the rock samples much more "rudely" than the influences actually observed in nature, and the criteria of stability are very rigorous indeed.

The most widely used stability checks are a. c. demagnetization (one type of which is so-called magnetic washing) and d. c. demagnetization (i. e. the measurement of the remanent coercive force H_c'). Further procedures falling under the head of reliability checking include X-ray diffraction and microscopic procedures aimed at identifying mineralogically and chemically the mineral or minerals carrying the magnetism of the rock, chemical analysis and X-ray

microanalysis. Another widely used set of techniques is of the thermal type, e.g. the Thellier-method of repeated heating, or a variant of it, the method of thermal demagnetization. Thermal methods further include the measurement of Curie temperatures and the determination of the temperature dependence of saturation magnetization. A substantial drawback of thermal methods at large is that their application more often than not destroys the original mineralogical constitution of the rock.

The destructivity of thermal methods, the way they affect the original minerals, becomes apparent particularly when they are applied to rocks bearing titanomagnetite of low Curie temperature. Titanomagnetites whose Curie point is close to that of magnetite, and magnetite proper, exhibit a much greater thermal stability and resistance to changes in chemical composition when exposed to rapid heating than low Curie-point titanomagnetites. This is why it is commonly considered that for the purposes of palaeomagnetic measurements only rocks containing titanomagnetite of high Curie point (close to Fe_3O_4 in composition) are suitable. It is, however, questionable whether thermostable magnetites and titanomagnetites carry a magnetism developed at the time of origin of the rock.

When investigating this point the fact that thermal energy is capable of effecting changes of state in titanomagnetites turns out a blessing in disguise, because the changes due to thermal causes provide an insight into the possible processes of alteration of titanomagnetites as carriers of rock magnetism.

Experimental part

It is these processes of alteration that the author has studied by recording and comparing the susceptibility-vs-temperature, $\varkappa(T)$ and thermal demagnetization graphs of volcanic rock samples from Hungary. The temperature dependence of susceptibility has been recorded by means of an automatic magnetic torsion balance whose principle is the same as that of the device constructed by Larochelle [1961]. The heating rate has been set so as to cover the interval from 20 to 600 degrees centigrade in 20 min. Measurements were performed on natural samples wrapped in aluminium foil. Thermal demagnetization was performed as usual by heating the samples to increasing temperatures and cooling them to room temperature in a zero field.

The experiments performed so far gave results that can be classed into four types, to be presented below.

Type 1. (Fig. 1.) Sample No. 651, Miocene andesite, Nyesettvár Peak, Mátra Mountains.

At low temperatures (about 80 to 350° C), $\varkappa$ increases directly as temperature, then decreases first gradually from 450 to about 520° C and quite rapidly at higher temperatures. The paramagnetic value is attained at $T_C = 555°$ C. (Curie points were estimated by finding the intersection of the steepest section of the $\varkappa(T)$ graph with the temperature axis [Like, 1966].) The cooling curve indicates a strong increase of susceptibility after the first heating (1a).

The graphs of repeated heating and cooling (1b and 1c) essentially reproduce the circumstances brought about by the first heating.

According to the thermal demagnetization graph (1d), the sample gained 90% of its NRM below 360° C.

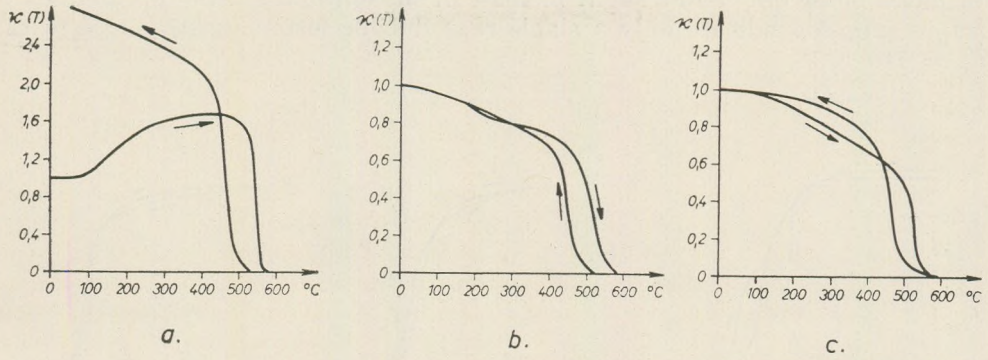

Graph 1a
First heating and cooling

Graph 1b
Second heating and cooling

Graph 1c
Third heating and cooling

Temperature dependence of initial susceptibility, $\varkappa = \varkappa(T)$, referred to the value at room temperature. The paramagnetic value corresponds to $\varkappa = 0$

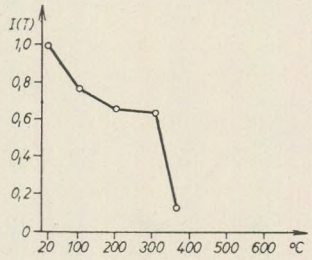

Graph 1d
Thermal demagnetization graph of NRM, $I = I(T)$, referred to the value at room temperature

Fig. 1. Sample No. 651, Miocene andesite, Nyesettvár Peak, Mátra Mountains

A confrontation of the two types of graph shows that on graph 1a the original phases carrying the NRM of the rock are not represented even by vague traces. Their presence is indicated in the first $\varkappa(T)$ graph only indirectly by an increase up to about 400° C, which suggests changes of phase: heating to 400° C resulted in changes of state in all the original ferromagnetic constituents. The product of change is a ferromagnetic phase of $T_C = 555°$ C whose susceptibility at room temperature is much stronger than that of the original constituent (see the first cooling graph, 1a) and another phase whose Curie point continuously changes from about 400° C to room temperature (1a, b, c).

Type 2. (Fig. 2.) Sample No. 846, Cretaceous trachydolerite, Jánosi-Nagyvölgy Valley, Mecsek Mountains.

The first $\varkappa(T)$ graph (Fig. 2a) indicates a first Curie point at about 420° C and another one at 530° C. The cooling graph indicates essentially one ferro-

magnetic phase only and a slight increase of susceptibility. The repeated $\varkappa(T)$ graphs (2b, 2c) indicate only a single reproducible ferromagnetic phase with $T_C = 540°$ C.

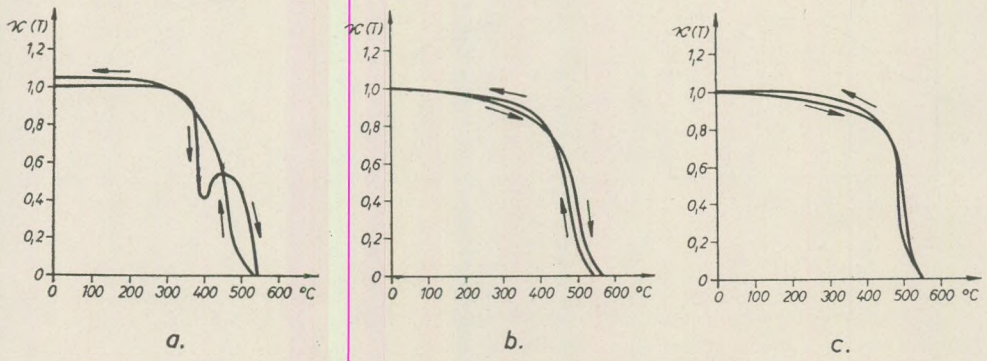

Graph 2a
First heating and cooling

Graph 2b
Second heating and cooling

Graph 2c
Thid heating and cooling

Temperature dependence of initial susceptibility $\varkappa = \varkappa(T)$, referred to the value at room temperature. The paramagnetic value corresponds to $\varkappa = 0$.

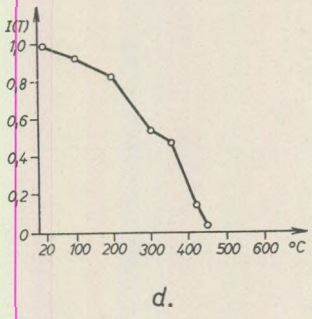

Graph 2d
Thermal demagnetization graph of NRM, $I = I(T)$, referred to the value at room temperature

Fig. 2. Sample No. 846, Cretaceous trachydolerite, Jánosi-Nagyvölgy Valley, Mecsek Mountains

According to the thermal demagnetization graph (2d), the full original remanent magnetization of the sample came to exist at a temperature below 450° C.

Confrontation of the results of the two methods reveals that the remanent magnetization of the original sample is due to a single ferromagnetic phase of $T_C = 420°$ C, whereas the appearance of the other phase of higher Curie temperature is due to changes brought about by heating. According to the repeated $\varkappa(T)$ graphs, the original phase of $T_C = 420°$ C is completely altered into the phase of $T_C = 540°$ C.

Type 3. (Fig. 3.) Sample No. 239, Pliocene basalt, Pécskő Peak near Salgótarján.

The first $\varkappa(T)$ heating graph essentially indicates a single ferromagnetic phase of $T_C = 290°$ C. On the corresponding cooling graph, this phase already exhibits a Curie temperature of 335° C (graph 3a). The repeated $\varkappa(T)$ graphs also reveal a single ferromagnetic phase whose Curie point is displaced towards higher temperatures by repeated heating. On the second $\varkappa(T)$ graph, $T_C = 360°$ C (3b); on the third, $T_C = 490°$ C. (3c)

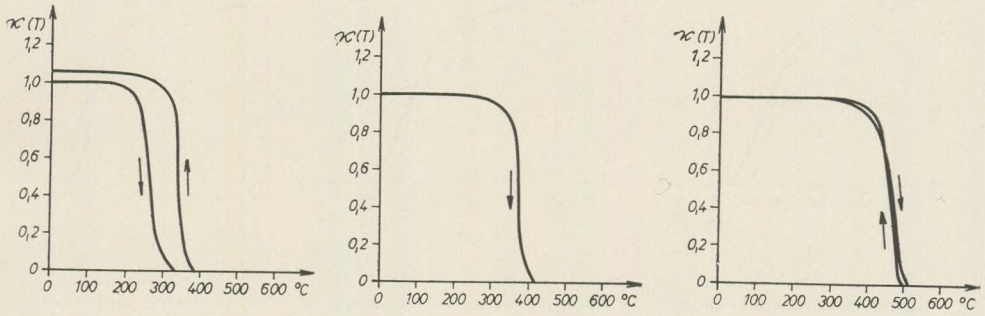

Graph 3a
First heating and cooling

Graph 3b
Second heating and cooling

Graph 3c
Third heating and cooling

Temperature dependence of initial susceptibility $\varkappa = \varkappa(T)$, referred to the value at room temperature. The paramagnetic value corresponds to $\varkappa = 0$.

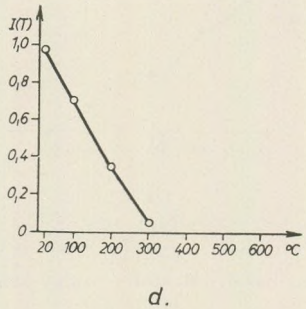

Graph 3d
Thermal demagnetization graph of NRM, $I = I(T)$, referred to the value at room temperature

Fig. 3. Sample No. 239, Pliocene Basalt, Pécskő Peak near Salgótarján

According to the thermal demagnetization graph (3d), the full original remanent magnetization of the sample came to exist at a temperature below 300° C.

Unlike the first two types, the first $\varkappa(T)$ graph and the thermal demagnetization graph are not in contradiction: on the contrary, both show that the NRM of the sample is due to the ferromagnetic phase whose T_C is at 290° C. This phase, too, passes gradually into one of higher Curie temperature, although considerably slower than those of the first two types.

Type 4. (Fig. 4.) Sample No. 715, Pleistocene basalt [Márton – Szalay, 1968], Kovácsi Hills, near Vindornyaszőllős (in a group of extinct basalt volcanoes north of the west end of Lake Balaton).

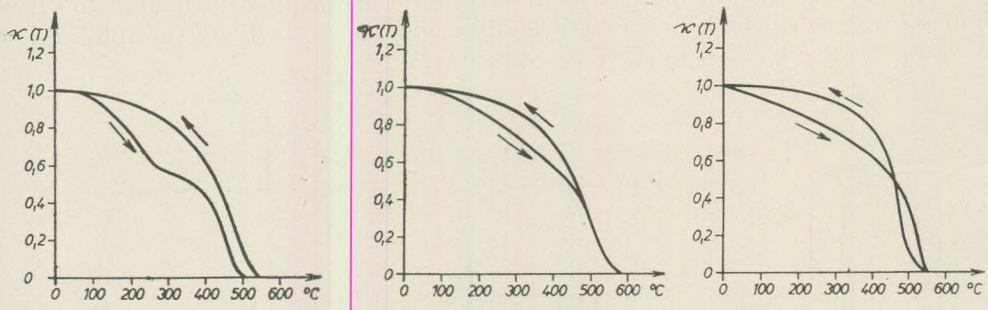

a. Graph 4a — First heating and cooling

b. Graph 4b — Second heating and cooling

c. Graph 4c — Third heating and cooling

Temperature dependence of initial susceptibility $\varkappa = \varkappa(T)$, referred to the value at room temperature. The paramagnetic value corresponds to $\varkappa = 0$

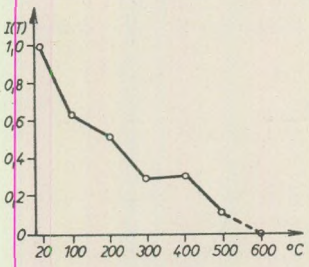

d. Graph 4d

Thermal demagnetization graph of NRM, $I = I(T)$, referred to the value at room temperature

Fig. 4. Sample No. 715, Pleistocene basalt [Márton – Szalay 1968], Kovácsi Hills near Vindornyaszőllős

The first $\varkappa(T)$ heating graph indicates a vague lower-temperature Curie point at about 250° C and a well-defined higher-temperature one at 460° C. The corresponding cooling graph shows, however, already a phase of $T_C =$ = 530° C and one of lower and gradually changing Curie temperature (3a). On the repeated $\varkappa(T)$ graphs, the latter phase appears with Curie points in the 400 to 450° C range whereas the Curie temperature of the higher-temperature phase shifts to $T_C = 550°$ C (4b and 4c).

According to the thermal demagnetization graph (4d), remanent magnetization is impressed upon the rock between 400 and 500° C on the one hand and below 300° C on the other.

The $\varkappa(T)$ and thermal demagnetization graphs are in agreement also in the case of this type. It is, however, remarkable that the $\varkappa(T)$ heating graphs are almost fully reproducible in the temperature interval from room temperature to about 400 or 500° C, over the temperature range of the phase of continuous Curie temperature. This indicates the relative stability of the phase in question.

Conclusions

In all the rock samples investigated, alterations due to heating resulted in ferromagnetic products whose Curie temperatures were higher than those of the original ferromagnetic phases. Changes of this sort can be interpreted by assuming the original phases to have been more or less oxidized [Ade-Hall et al. 1965, Verhoogen 1962].

In all four rock types investigated, heating brings about a more or less intense secondary alteration. Experiments carried out under identical external circumstances suggest that the nature and intensity of these secondary magnetic changes are controlled by the physical parameters (temperature) and chemical composition (redox potential) of the nonmagnetic constituents of the rock. Hence, the alterations affecting the ferromagnetic phases are independent of the Curie temperatures of these latter. Indeed, in Type 1 (No. 651), alteration began at about 100° C, at a temperature lower than the Curie point. In Type 2 (No. 846) alteration set in at the Curie point of about 420° C; in Type 3 (No. 239) above 300° C, i. e. above the Curie point, whereas in Type 4 (No. 715) the phase of lower Curie temperature altered very little if at all between 20 and 400° C.

The measurements discussed above reveal that although the rapid processes of alteration are independent of Curie temperature, they are temperature-dependent in the sense that at a given rate of heating the transition is not initiated below a given threshold temperature. Considering the accelerating effect of temperature rise on chemical processes [Lengyel et al. 1960], it seems likely that ferromagnetic phases in a given environment may become unstable not only as a result of a heat treatment of short duration relatively high above room temperature, but also at ambient temperature if there is enough time in geohistorical terms.

Whereas the first alterations, contemporaneous with the initial cooling of the lava and due to magmatic vapours and gases, do not, of course, invariably affect the NRM (Ade-Hall et al. 1965), the above-outlined processes, going on for long spans of time at ambient temperature, invariably result in a more or less profound change of remanent magnetization.

Returning now to the question originally raised, as to whether the magnetization of rocks containing ferromagnetic constituents of high Curie temperatures that give rise to reproducible $\varkappa(T)$ graphs can be regarded as primary, the measurements discussed above and their interpretation do not give an unequivocally positive answer, as only the phases produced by heating were found to give reproducible $\varkappa(T)$ graphs. Hence, rocks of high Curie temperatures with $\varkappa(T)$ graphs stable under repeated rapid heating may indicate one of three things: either their ferromagnetic phases are stable to begin with against

the chemical influence of the embedding minerals, or their ferromagnetic phases had undergone alteration at the time of the first cooling of the lava, or they came to exist as the result of gradual alteration during the life of the rock. For palaeomagnetic purposes, it is only the first group with the ferromagnetic constituents stable to begin with that will yield high-degree reliability. All other cases are to be treated with a great deal of caution.

REFERENCES

Ade-Hall, J. M., Wilson, R. L., Smith, P. J. (1965): The petrology, Curie points and natural magnetizations of basic lavas. Geophys. Journ. Roy. Astr. Soc. 9, No. 4. pp. 323–336.

Carmichael, C. M. (1965): The present state of rock magnetism with particular reference to the magnetic ulvospinel system. Journ. of Geomagn. and Geoelectricity, 17. No. 3–4. pp. 311–314.

Irving, E. (1964): Palaeomagnetism. John Wiley, New York.

Khramov, A. N. et al. (1961): Metodika paleomagnitnich issledovanij. Gostoptechizdat, Moscow.

Larochelle, A. (1961): Design of a Curie point meter. Geol. Surv. of Canada Bull. 69.

Lengyel, B., Proszt, J., Szarvas, F. (1960): Általános és szervetlen kémia (General and inorganic chemistry). Tankönyvkiadó, Budapest.

Like, C. B. (1966): An examination of the magnetic properties of basalts. Pure and Applied Geophysics, 65, pp. 132–146.

Márton, P., Szalay, E. (1968): Paläomagnetische Untersuchungen der Basaltlaven in Ungarn. Acta Geol. Hung. (in press).

Nagata, T. (1961): Rock Magnetism. Maruzen, Tokyo.

Petrova, G. N. (1961): Razlichnie laboratornie metodi opredeleniya geomagnitnoy stabilnosti gornich porod. Izv. AN. SSSR. 11, pp. 1585–1588.

Verhoogen, J. (1962): Oxidation of iron-titanium oxides in igneous rocks. J. Geol. 70, p. 168.

GRAVITY INTERPRETATION AND INFORMATION THEORY III. THE METHOD OF SECOND DERIVATIVES

by

A. MESKÓ

(Geophysical Institute of Loránd Eötvös University)

(Received: 28 September 1967.)

SUMMARY

The behaviour of the second-derivative method and its formulas of approximation is studied by applying the filter theory. It is shown that the second vertical derivative is the limit of various procedures of residual computation. An essential deficiency of the transfer function of the second derivative method, the overemphasizing of the high-frequency range, is pointed out. A comparison of the transfer functions of the variously proposed formulas of approximation with that of the fundamental procedure permits to define a measure of the approximation furnished by the formulas. Attention is called to the direction-dependent properties of approximate formulas, which may give rise to substantial errors in interpretation. A sequence of coefficients accurately approximating the second vertical derivative is given.

Introduction

In previous papers, the author has undertaken a systematic investigation of linear transformations of gravity maps, using the concepts and mathematical tools of information theory (Meskó 1965, 1966a). He discussed basic concepts and formulas as well as the ways of simply representing two-dimensional transfer functions by various graphs. Averaging over circles, formulas of smoothing and computation of regionals were investigated as applications of the theory.

The present paper is concerned with the second-derivative method, perhaps the most common device to transform original gravity survey maps into more informative ones. The aim of this method is to emphasize features presumably due to geological structures of practical importance and to clear away the regional component of the field. Hence, the second-derivative method is a special sort of residual method, an instance of high-pass filtering.

The connection between second derivatives and residuals, the filtering properties of formulas of approximation proposed by various authors and their relative merits are discussed in the paragraphs below.

Connexion between the second-derivative method and other methods of computing residuals

Residuals are obtained by subtracting the regional component from a measured gravity field. Hence, to any procedure of establishing the regional component there may be assigned a procedure of computing regionals. In the space domain the relation

$$g_{res}(x, y) = g_{0r}(x, y) - g_{reg}(x, y) \tag{1}$$

holds; in the frequency domain, we have the relationship

$$G_{res}(\omega, \psi) = G_{0r}(\omega, \psi) - G_{reg}(\omega, \psi). \tag{2}$$

If the transfer function of computing the regional component is $S_{reg}(\omega, \psi)$, then the right side of (2) may be given the form

$$G_{or}(\omega, \psi) - G_{reg}(\omega, \psi) = G_{or}(\omega, \psi) - G_{or}(\omega, \psi) \cdot S_{reg}(\omega, \psi) =$$
$$= G_{0r}(\omega, \psi)[1 - S_{reg}(\omega, \psi)],$$

whence the transfer function of computing the residual is, clearly,

$$S_{res}(\omega, \psi) = 1 - S_{reg}(\omega, \psi). \tag{3}$$

Let us now define the regional component of the field as the mean of the gravity measurement results at the four survey points adjacent to the point of reference.*

$$g_{reg}(x_0, y_0) = \frac{1}{4}\{g(x_0 + s, y_0) + g(x_0 - s, y_0) + g(x_0, y_0 + s) + g(x_0, y_0 - s)\}. \tag{4}$$

By (1), the appropriate residual is

$$g_{res}(x_0, y_0) = g(x_0, y_0) - \frac{1}{4}\{g(x_0 + s, y_0) + g(x_0 - s, y_0) + g(x_0, y_0 + s) + g(x_0, y_0 - s)\}.$$

Multiplication of both sides by $-4/s^2$ and some simple transformations yield

$$-\frac{4}{s^2} g_{res}(x_0, y_0) = \frac{1}{s}\left\{\frac{g(x_0 + s, y_0) - g(x_0, y_0)}{s} - \frac{g(x_0, y_0) - g(x_0 - s, y_0)}{s}\right\} +$$
$$+ \frac{1}{s}\left\{\frac{g(x_0, y_0 + s) - g(x_0, y_0)}{s} - \frac{g(x_0, y_0) - g(x_0, y_0 - s)}{s}\right\};$$

hence, the residual is seen to be related to the second difference quotient. To express this fact in a more striking form, let us write

$$-\frac{4}{s^2} g_{res}(x_0, y_0) \approx \frac{\partial^2 g(x_0, y_0)}{\partial x^2} + \frac{\partial^2 g(x_0, y_0)}{\partial y^2}. \tag{5}$$

* Here and in the following we shall invariably consider a regular square grid of survey points.

However, by the Laplace equation,

$$\frac{\partial^2 g}{\partial x^2} + \frac{\partial^2 g}{\partial y^2} = -\frac{\partial^2 g}{\partial z^2}, \tag{6}$$

so that, in the final reckoning, we obtain the following approximate equation:

$$\frac{4}{s^2} g_{res} \approx \frac{\partial^2 g}{\partial z^2}.$$

This approximation improves as s tends to zero:

$$\lim_{s \to 0} \frac{4}{s^2} g_{res} = \frac{\partial^2 g}{\partial z^2}. \tag{7}$$

The connexion between the limit formed using the residual on the one hand and the second vertical derivative on the other can further be illuminated by investigating the transfer properties of the two operations. Let us first of all establish the transfer function of the second derivative. For the purpose we shall write up the Fourier transform of a function transformed by that procedure. Next, we decompose the result into a product of two factors, one of which is the Fourier transform of the original function. The second factor is none other than the desired transfer function. Accordingly,

$$F[g_{out}(x, y)] = F\left[\frac{\partial^2}{\partial z^2} g_{in}(x, y)\right] = F\left[-\left(\frac{\partial^2}{\partial x^2} + \frac{\partial^2}{\partial y^2}\right) g_{in}(x, y)\right] =$$

$$= \int_{-\infty}^{+\infty} \int_{-\infty}^{+\infty} \left[-\left(\frac{\partial^2}{\partial z^2} + \frac{\partial^2}{\partial y^2}\right) g_{in}(x, y)\right] e^{-j(\omega x + \psi y)}\, dx\, dy.$$

Integrating by parts twice, with respect to the variables x and y, and making use of the fact that both the function $g_{in}(x, y)$ and its partial derivatives with respect to x and y become zero at infinity, we obtain

$$F[g_{out}(x, y)] = \int_{-\infty}^{+\infty} \int_{-\infty}^{+\infty} (\omega^2 + \psi^2) g_{in}(x, y) e^{-j(\omega x + \psi y)}\, dx\, dy = (\omega^2 + \psi^2) F[g_{in}(x, y)].$$

This is, in fact, the desired decomposition into products. Accordingly, the transfer function of computing the second derivative is

$$S(\omega, \psi) = \omega^2 + \psi^2. \tag{8}$$

Let us note that an entirely similar procedure consisting essentially of successive integrations by parts will yield the transfer function also of the operation

$$g_{out}(x, y) = \sum_j \sum_k c_{jk} \frac{\partial^{j+k}}{\partial x^j \partial x^k} g_{in}(x, y). \tag{9}$$

The transfer function in question is

$$S(\omega, \psi) = \sum_j \sum_k c_{jk} (i\omega)^j (i\psi)^k. \tag{10}$$

The case of the second vertical derivative is that particular case of (9) when $c_{02} = c_{20} = -1$ and $c_{jk} = 0$ for any other j, k.

The transfer function of the operation represented by Eq. (4) is

$$S_{reg}(\omega, \psi) = \frac{e^{j\omega s} + e^{-j\omega s} + e^{j\psi s} + e^{-j\psi s}}{4} = \frac{\cos \omega s + \cos \psi s}{2}.$$

The transfer function of $4/s^2$ times the corresponding residual is

$$\frac{4}{s^2} S_{res}(\omega, \psi) = 2 \cdot \frac{2 - (\cos \omega s + \cos \psi s)}{s^2} =$$

$$= \frac{1 - \cos \omega s}{2\left(\frac{s}{2}\right)^2} + \frac{1 - \cos \psi s}{2\left(\frac{s}{2}\right)^2} = \left(\frac{\sin \frac{\omega s}{2}}{\frac{s}{2}} \right)^2 + \left(\frac{\sin \frac{\psi s}{2}}{\frac{s}{2}} \right)^2.$$

Now if $s \to 0$, then, using the limit $\lim_{x \to 0} \frac{\sin x}{x} = 1$, we may write

$$\lim_{s \to 0} \frac{4}{s^2} S_{res}(\omega, \psi) = \omega^2 + \psi^2.$$

In the above simple deduction the reader might take exception to the seemingly arbitrary procedure of selecting from the survey grid the four points adjacent to the point of reference. It can be shown, however, that the final result is not affected by the nature of the procedure used for computing the regional effect. After multiplication with a suitable constant the difference between gravity at a given point and some mean of gravity in its environment approaches the second derivative under an appropriate limit formula.

If e.g. we consider as the regional effect the mean of values measured at points lying on the circumference of a circle, we find that the transfer function of the operation is

$$S_{reg}(\omega, \psi) = J_0(\sqrt{\omega^2 + \psi^2} \cdot r) = J_0(\varrho r).$$

$4/r^2$ times the corresponding residual is

$$\frac{4}{r^2} S_{res}(\varrho) = \frac{4[1 - J_0(\varrho r)]}{r^2}. \tag{11}$$

Let us look into the behaviour of the transfer function as r tends to zero. To find the limit of the right side of (11) we may use L'Hospital's rule and apply several relationships between Bessel functions of various kinds:

$$\frac{dJ_0(z)}{dz} = -J_1(z);$$

$$\frac{dJ_1(z)}{dz} = \frac{1}{2}[J_0(z) - J_2(z)];$$

$$J_0(0) = 1;\ J_1(0) = J_2(0) = 0.$$

These relationships turn the right side of (11) into

$$\lim_{r\to 0} 4 \cdot \frac{1 - J_0(\varrho r)}{r^2} = \lim_{r\to 0} \frac{2\varrho J_1(\varrho r)}{r} = \lim_{r\to 0} \varrho^2[J_0(\varrho r) - J_2(\varrho r)] = \varrho^2.$$

It holds indeed also in this case that

$$\lim_{r\to 0} \frac{4}{r^2} g_{res} = \frac{\partial^2 g}{\partial z^2}.$$

The graph of the transfer function (11) is shown as Fig. 1. for the cases $r = 2s$, $r = \sqrt{2}s$, $r = 1$ and $r \to 0$ The independent variable of the graphs is relative frequency, $\varrho' = \varrho s$. It is clear that, as r decreases, the transfer functions of the residuals tend towards the transfer function of the second derivative. Let us further note that the discrepancies between transfer functions are slight in the low-frequency range but become significant at higher frequencies.

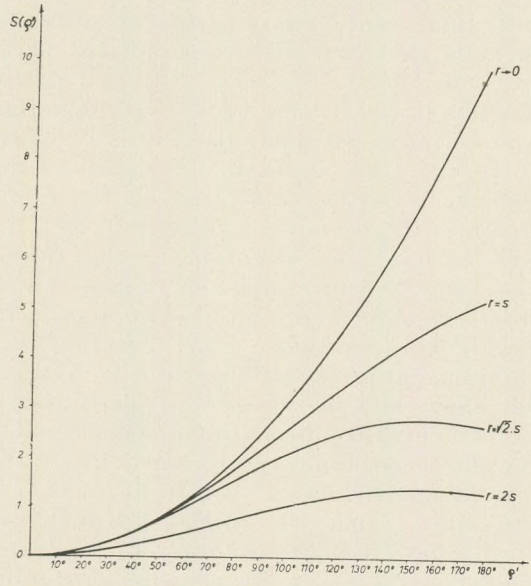

Fig. 1. Transfer functions showing the effect of decreasing the radius used in computation of residuals

The fact that the procedures for computing residuals all tend to a limit represented by the second vertical derivative has severally been resorted to justify the latter procedure. It has been the aim of several authors to set up formulas that approximate the second vertical derivative as closely as possible. The necessity of such approximations is due to the fact that, the gravity field being given by a set of values measured at distinct points rather than by an analytical formula, the second derivative cannot be obtained analytically, but only as a function of values measured at a number of survey grid points.

In the present paper, we shall investigate approximate formulas of the forms

$$g_{out}(x, y) = \frac{1}{s^2} \sum_{k=1}^{n} c_k \overline{g_{in}(r_k)} \tag{12}$$

and

$$g_{out}(x, y) = \frac{1}{s^2} \sum_{k=1}^{n} c_k g_{in}(x + x_k, y + y_k), \tag{13}$$

where $\overline{g_{in}(r_k)}$ means the average of values measured at points of a circumference of radius r, whereas x_k and y_k are multiples of the grid interval s, i.e. (13) refers to a square survey grid. The formulas proposed by the individual authors differ in the choice of the weights c_k as well as in the geometry of the circles and grid patterns . The general form of the transfer functions of the operations (12) and (13) has already been determined (e.g. Meskó 1965). The specific transfer functions of the individual approximations can be obtained by substituting into this general formula the particular values of the parameters c_k and r_k, or c_k, x_k and y_k.

The transfer function of the second derivative method has been established above (8). A comparison of transfer functions and the evaluation of the goodness of approximation offered by the individual formulas is fairly easy. Of two approximations, that one is better whose transfer function comes more close to the transfer function of the second derivative.

Before, however, turning our attention to the individual formulas of approximation, a few remarks concerning the transfer function of the second derivative are in order. (8) is the equation of a two-argument transfer function represented by a paraboloid of rotation. The operation is of the nature of a high-pass filtering and has no preferred direction. It does, as a matter of fact, remove the regional effect and in doing so it clarifies the gravity picture. The amplification of the high-frequency components is, however, excessive. This may give somewhat misleading results particularly if the data contain errors of measurement or reduction which appear as a high-frequency noise. The high-frequency range is further distorted by aliasing; moreover, the highest-frequency oscillations are due to near-surface bodies of little practical interest. For this reason, the principle proper of second-derivative reduction cannot be regarded as ideal. It would be useful to replace it by a procedure whose transfer function assigns maximum amplification to the

medium frequency range with a decrease in amplification at higher frequencies. Applying some formula approximating the second derivative *after* a smoothing of the original set of data gives a bandpass-type filtering of the desired properties. This procedure, found to be rather useful in practice, goes, however, beyond the concept of the second vertical derivative. Rather than approximating a pre-selected analytical procedure, it is aimed at getting, although in a somewhat intuitionistic way, a filtering best fitting some reasonable criterion of suitability, without regard to the degree of approximation between the working function and some pre-selected analytical procedure or other.

The most suitable filtering can, however, also be approximated by purposeful designing. As a first approximation, a bank of band-pass filters can be proposed, with not too steep cut-off and with both the lower and upper cutoff frequencies variable for the purpose of adaptation to the depth range to be prospected. The method of second derivatives admits of no such flexibility. The application of filtering theory has rendered the second-derivative method obsolete, having shown up that its transfer function is far from optimal.

Nor will the results of the author's investigations into the transfer properties of formulas approximating the second derivative be presented below with the purpose of estimating their relative merits. The viewpoint adopted below is that the re-interpretation of maps transformed earlier by one or another of these formulas will be facilitated by the knowledge of their transfer functions. E.g. the fictitious nature of "structural trends" surmised on a transformed map may be revealed by a check into the orientation-dependence of the formula used in transformation. If the transformed map exhibits a large number of small anomalies and the formula used tends to overemphasize high-frequency components, then one should suspect that a substantial portion of the anomalies is fictitious and quite independent from any cause essential to the geophysical investigation in hand.

Investigation of formulas approximating the second vertical derivatives

The transfer functions of Eqs. (12) and (13) are (M e s k ó 1965, 1966a)

$$S(\omega', \psi') = S(\varrho') = \frac{1}{s^2} \sum_{k=1}^{n} c_k J_0(\varrho' \mu_k) \tag{14}$$

and

$$S(\omega', \psi') = \frac{1}{s^2} \sum_{k=1}^{n} c_k e^{(\omega' \xi_k + \psi' \eta_k)}, \tag{15}$$

where the dimensionless parameters μ_k, ξ_k and η_k are defined by the equations

$$\mu_k s = r_k; \quad \xi_k s = x_k; \quad \eta_k s = y_k, \tag{16}$$

and the dimensionless frequencies ϱ', ω' and ψ' by the equations

$$\varrho' = \varrho s, \quad \omega' = \omega s, \quad \psi' = \psi s. \tag{17}$$

It is the transfer functions given by (14) and (15) that have to be confronted with the transfer function (8) of the second vertical derivative; this means testing the goodness of approximation furnished by the approximate equality

$$\varrho'^2 \equiv \omega'^2 + \psi'^2 \approx \frac{1}{s^2} \sum_k c_k J_0(\varrho' \mu_k). \tag{18}$$

Multiplying both sides of Eq. (18) by s^2 we transform (18) into

$$\varrho'^2 \approx \sum_k c_k J_0(\varrho' \mu_k). \tag{19}$$

It is now this approximation that is to be tested. It has the advantage of not containing explicitly the survey grid spacing. Using (15) we may obtain in a like manner the approximate equality

$$\varrho'^2 \approx \sum_k c_k e^{i(\omega' \xi_k + \psi' \eta_k)}. \tag{20}$$

Forming the weighted average over a circle realizes an orientation-independent transfer, provided averages are formed by integration. This is not, however, the case in practical work. Instead of integration, a summation is performed. The transfer function of the sum of values measured at a finite number of points has been investigated in a previous paper (M e s k ó, 1965), with the result that, in the case of low dimensionless frequencies the approximation is quite good even if the number of points is quite small, but that in the high-frequency range the fit between summation and integration is not by far so good.

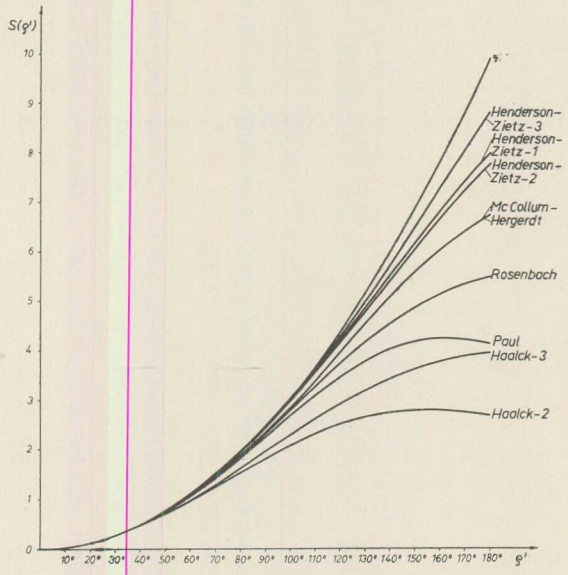

Fig. 2. Transfer functions of some second derivative formulas

Even if Eq. (19) introduces a further approximation, its use is justified for the purpose of a first orientation among the average transfer properties of the approximative formulas.

With the single exception of Paul's formula (P a u l, 1961) the formulas have been taken from the book written by K. J u n g (1961). The graphs of the transfer functions are shown as Figs. 2 and 3. The goodness of fit to the second vertical derivative deteriorates from top to bottom in the enumeration below:

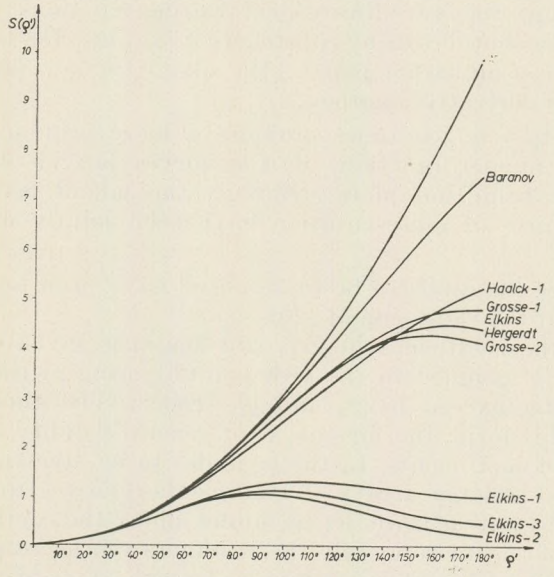

Fig. 3. Transfer functions of some second derivative formulas

Henderson-Zietz	No. 3.
Henderson-Zietz	No. 1.
Henderson-Zietz	No. 2.
Baranov	
McCollum-Hergerdt	
Rosenbach	
Haalck	No. 1.
Grosse	No. 1.
Elkins-Hergerdt	
Grosse	No. 2.
Paul	
Haalck	No. 3.
Haalck	No. 2.
Elkins	No. 1.
Elkins	No. 3.
Elkins	No. 2.

Let us emphasize once more that the transfer functions represented by the graphs in Figs. 2 and 3 refer to the hypothetical case that the average over the circle has been determined by integration. Let us now consider a regular square grid of survey points in which averages over circles are computed from a finite number of values (four in the case of circles of radii $r = s, \sqrt{2s}$ and $2s$, eight in the case of $r = \sqrt{5}$). These averages computed from actual survey grid patterns are orientation-dependent and so are their linear combinations (cf. in this respect Meskó 1965, Figs. 6 through 9). The two-argument transfer functions do not possess a symmetry of rotation any more: the surfaces representing the two-dimensional transfer functions can be illustrated either by drawing contours or by constructing profiles. The latter procedure has been resorted to in an earlier paper (Meskó, 1966b), likewise in connexion with the second-derivative method.

Representation by contours provides a more profound insight into the nature of the transfer function. Profile curves provide less comprehensive information but bring out more strikingly the salient features. This is why the two procedures of representation have been jointly used in the present paper.

The transfer functions to be represented have been found by means of a modified form of the right side of (20).

Thus far, the coefficient in Eq. (20) has been given one index only, to indicate its being assigned to the k-th point figuring in the computation (i.e. whose coordinates exceed by x_k and y_k, respectively, those of the point of reference). In this form, the formula is of general validity and can be applied to any system of coefficients. In the formulas to be investigated, however, we are faced with symmetric arrays of coefficients referring to a square grid pattern. To profit by this feature, let us double-index the coefficients: the indices will be chosen so as to represent the distances of the respective grid points from the point of reference, as measured along the axes of the grid. Grid spacing is taken here as unit distance. E.g. if c_{00} is the coefficient referring to the point of reference, then c_{01} is that of the two points lying on the y axis at unit distance from the point of reference. Using this notation, we may rewrite (20) to read

$$\omega'^2 + \psi'^2 \approx c_{00} + 2 \sum_{k=1}^{n} c_{k0} \cos k\omega' + 2 \sum_{l=1}^{n} c_{0l} \cos l\psi' + 4 \sum_{k=1}^{n} \sum_{l=1}^{n} c_{kl} \cos k\omega' \cos l\psi'. \tag{21}$$

The transfer function has no imaginary part and assumes identical values in the four quadrants of the frequency plane. Hence it is sufficient to represent its first quadrant. The relative frequency domain to be investigated is, consequently,

$$0 \leqq \omega' \leqq \pi,$$

$$0 \leqq \psi' \leqq \pi;$$

or, introducing the dimensionless frequencies

$$f_1' = \frac{\omega'}{2\pi}, \qquad f_2' = \frac{\psi'}{2\pi},$$

it is

$$0 \leqq f_1' \leqq 0{,}5; \quad 0 \leqq f_2' \leqq 0{,}5.$$

The transfer functions of a few widely used formulas are shown in Figs. 4 through 11.

The transfer functions behave fairly similarly near the origin ($\varrho' < 0{,}15$). The contours are almost regular, i.e. circles concentric about the origin. This means that the transfer of low-frequency (or, in other words, long-wave) components is fairly independent of orientation. Beyond $\varrho' = 0{,}15$, however, the differences between the transfer functions increase. Some of the formulas assign an amplification of more than ten to a part of the high-frequency range (Baranov, Henderson-Zietz), whereas the amplification of some nowhere exceeds 3.0 (Elkins, Peters). In the transfer functions of some of the formulas, amplification is a monotonically increasing function

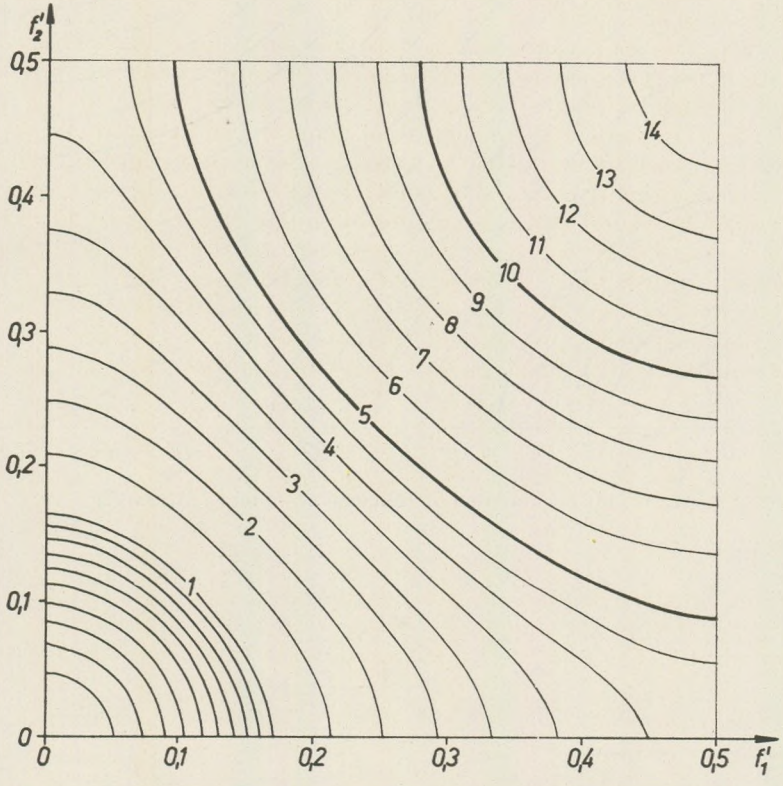

Fig. 4. Transfer function of Baranov's formula

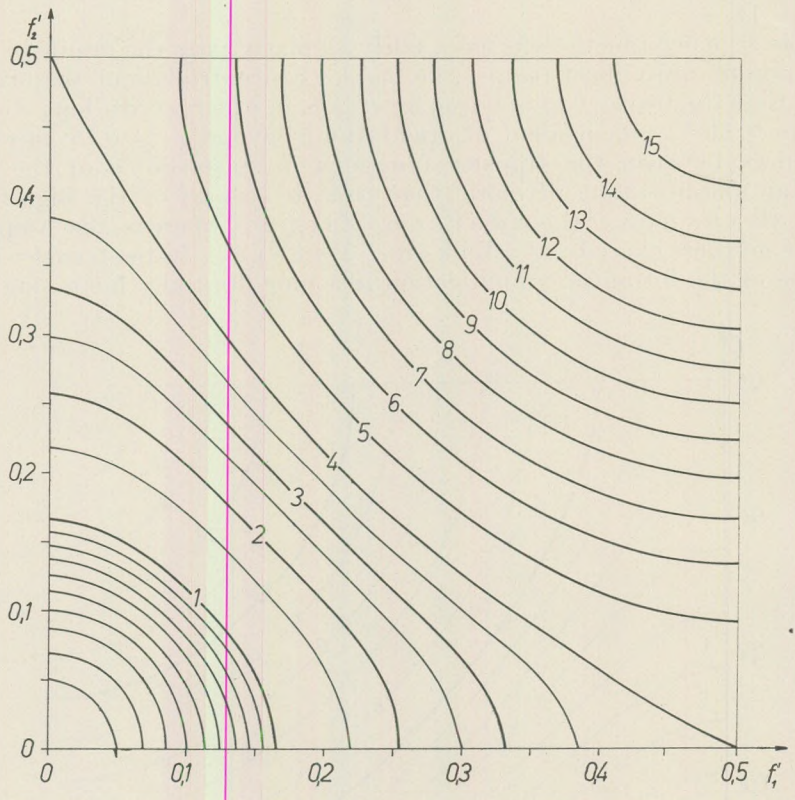

Fig. 5. Transfer function of Henderson – Zietz's formula 2

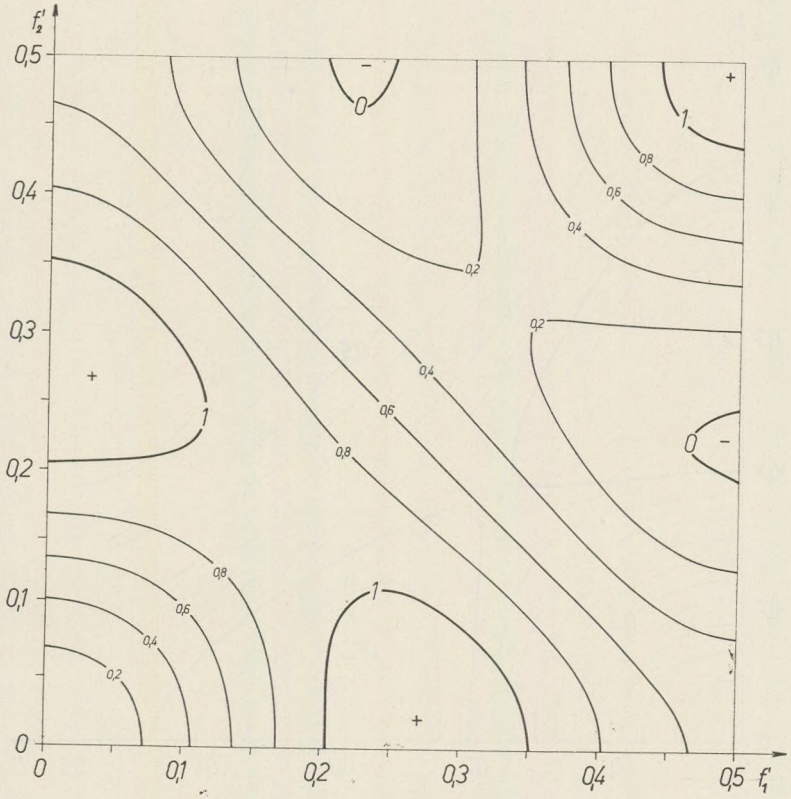

Fig. 6. Transfer function of Elkins' formula 2

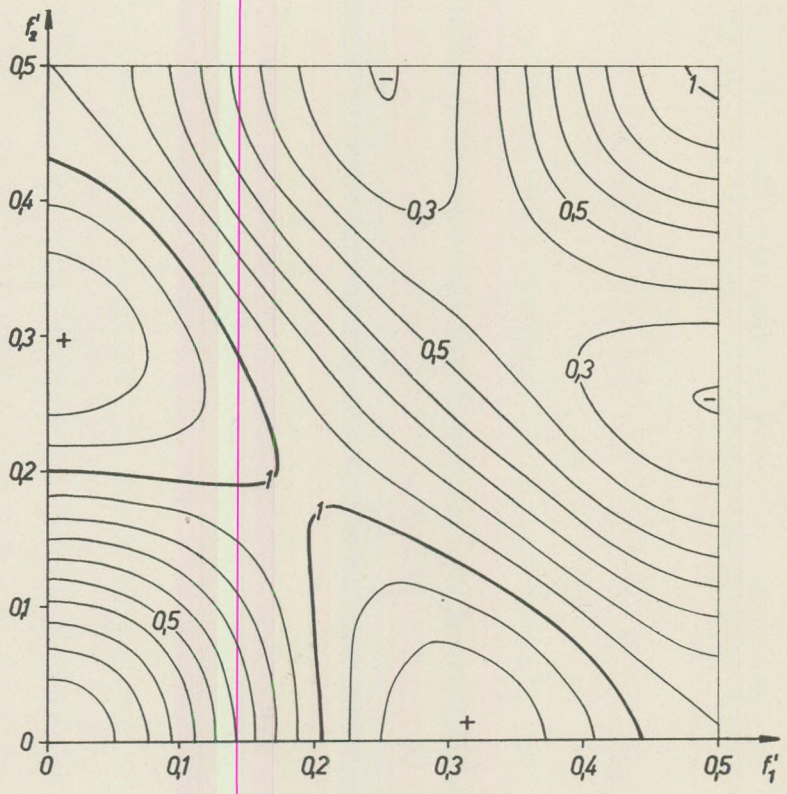

Fig. 7. Transfer function of Elkins' formula 3

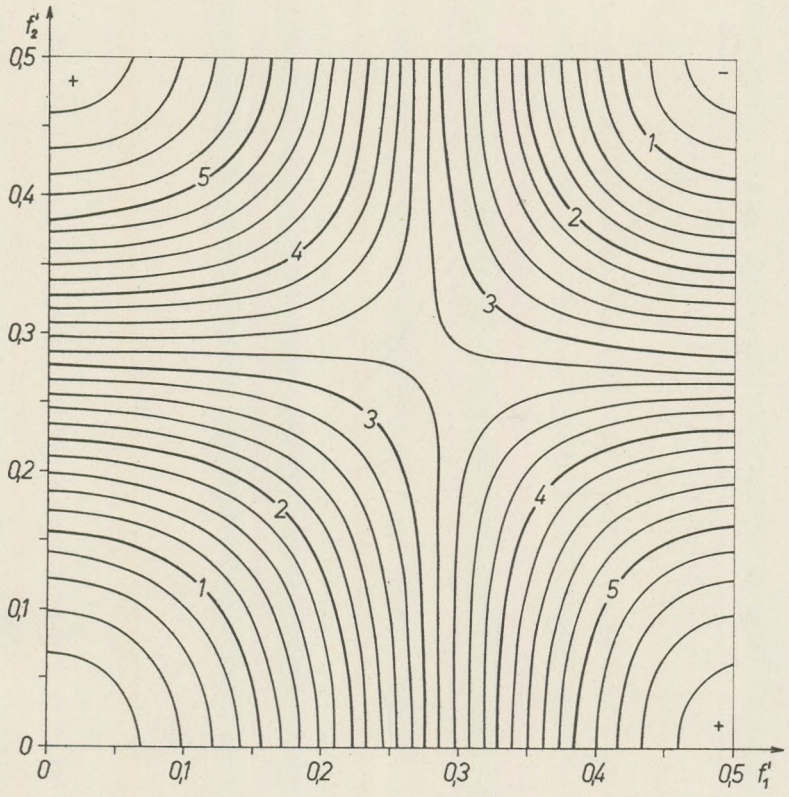

Fig. 8. Transfer function of Elkins – Hergerdt's formula

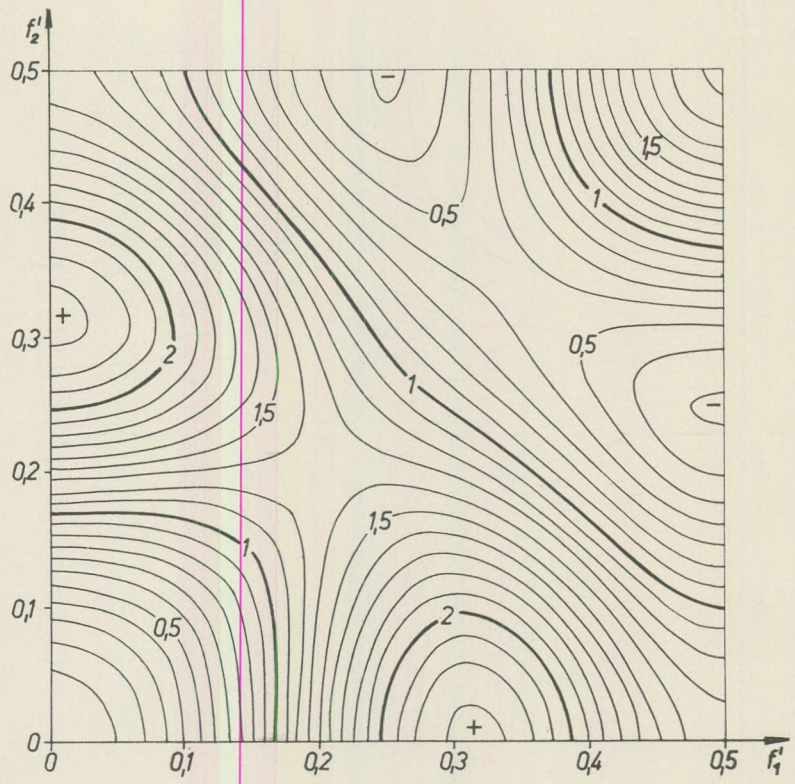

Fig. 9. Transfer function of Peters' formula

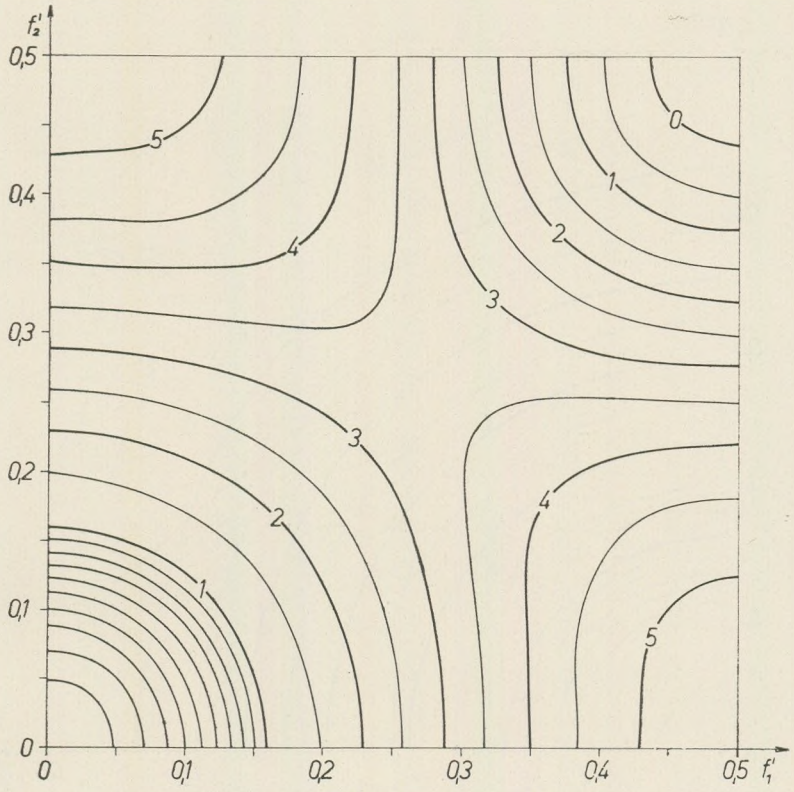

Fig. 10. Transfer functions of Paul's formula

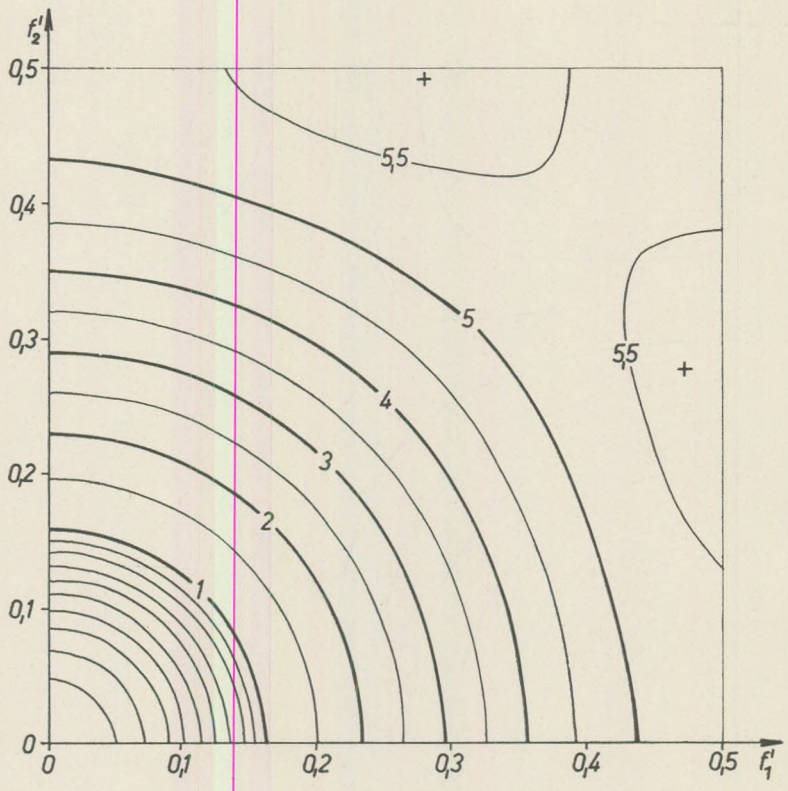

Fig. 11. Transfer function of Rosenbach's formula

of ϱ'. In others, an initial increase represented by a line including angles of 45° with the frequency axes is followed by a substantial drop (P a u l, E l k i n s - H e r g e r d t). Most transfer functions are orientation-dependent to a high degree. On the other hand, the dependence on orientation of the Rosenbach formula is negligible even in the high-frequency raneg.

More strikingly than by the contours, dependence on oirientation is revealed by the curves of intersection of the transfer surfaces with concentric cylinders. In order to represent these curves of intersection, we have plotted the ordinates of the transfer surface at the intersection vs. the polar angle, with the radius of the cylinder as parameter. (See M e s k ó 1965, Fig. 7.) Computations have been performed for the parameters $\varrho' = k \cdot 30°$ ($k = 1, 2, \ldots, 6$).

If transfer were independent of orientation, the curves would in fact be lines parallel to the coordinate axis. The deviation of the actual curve from

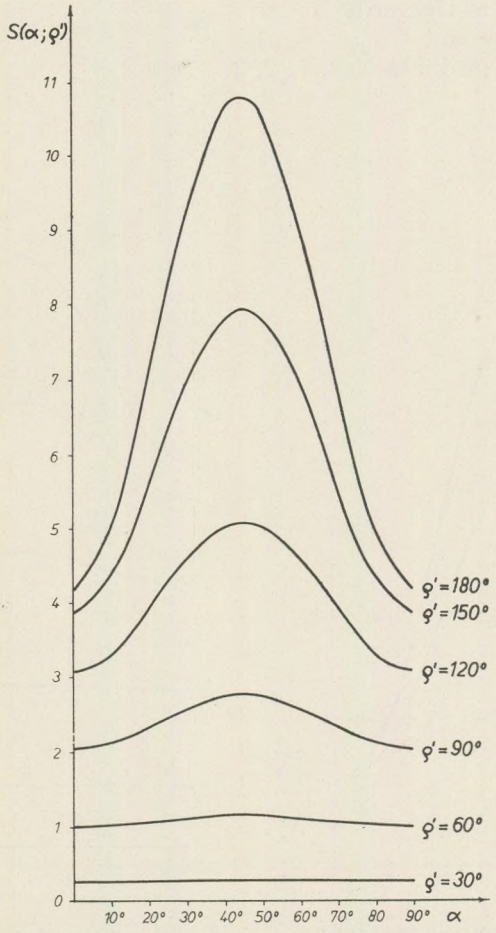

Fig. 12. Curves representing the transfer function of Baranov's formula

this hypothetical case is a measure of orientation dependence. In an earlier paper (M e s k ó 1966b) sets of curves for the transfer functions of the Elkins – 2, Henderson-Zietz – 2, Rosenbach and Haalck – 1 formulas have already been published. In the present paper we give, to further illustrate the point, the orientation-dependence of the following formulas: Baranov (Fig. 12), Henderson-Zietz 3 (Figs. 13), McCollum-Hergerdt (Fig. 14), Grosse 1 and 2 (Figs. 15 and 16), Elkins-Hergerdt (Fig. 17).

The orientation-dependence of transfer is

weak for Rosenbach and Haalck No. 3,
middling for Elkins Nos. 1, 2, 3, Grosse Nos. 1, 2, Haalck Nos. 1, 2, Elkins-Hergerdt McCollum-Hergerdt
strong for Baranow and Henderson-Zietz Nos. 1, 2, 3.

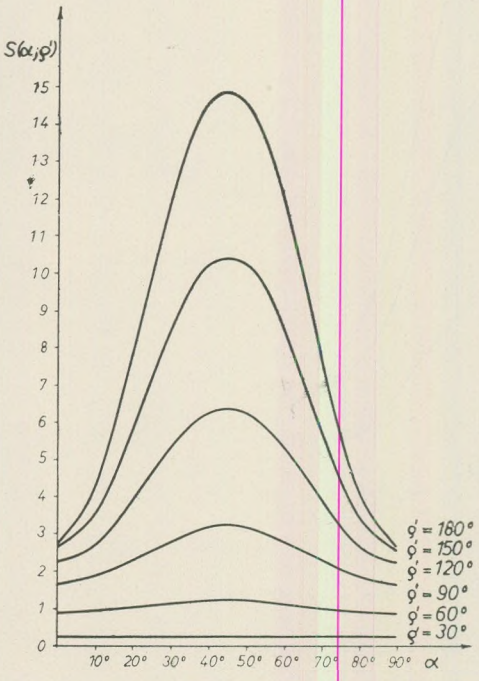

Fig. 13. Curves representing the transfer function of Henderson – Zietz's formula 3

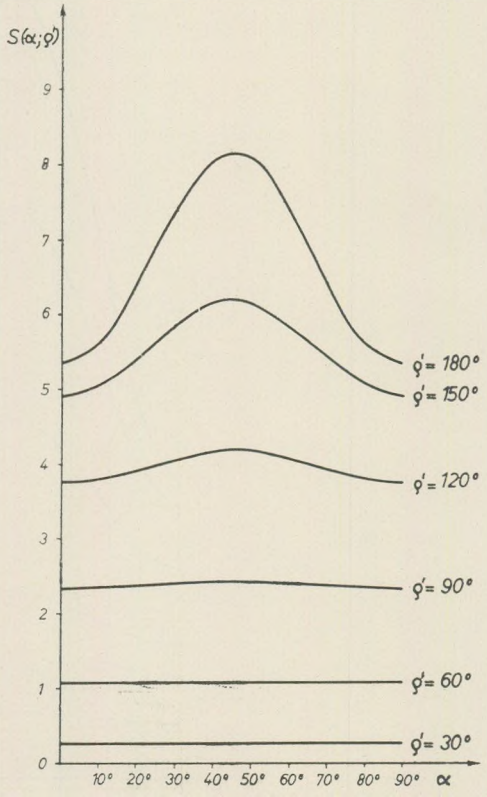

Fig. 14. Curves representing the transfer function of McCollum – Hergerdt's formula

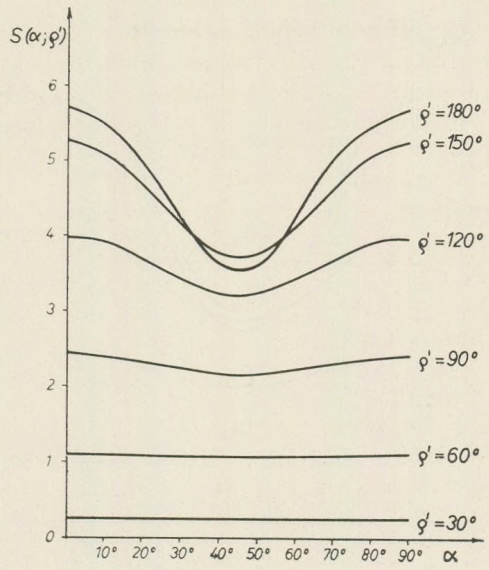

Fig. 15. Curves representing the transfer function of Grosse's formula 1

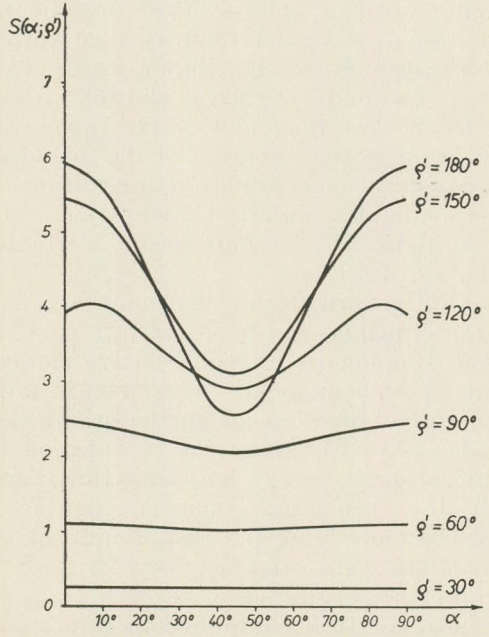

Fig. 16. Curves representing the transfer function of Grosse's formula 2

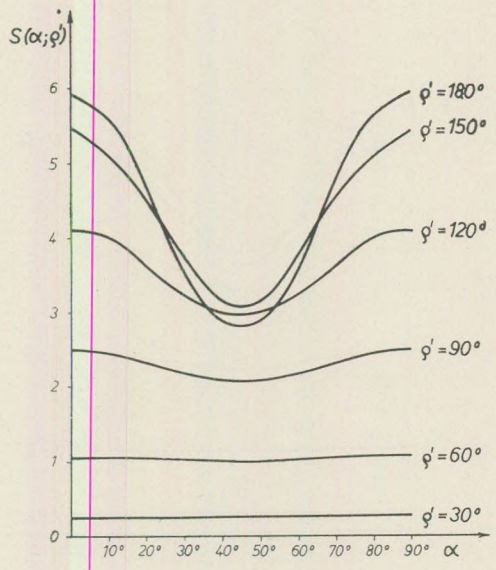

Fig. 17. Curves representing the transfer function of Elkins – Hergerdt's formula

The formulas may be roughly divided in two classes by the fact that those in Figs. 12 to 14 assign a stronger than average amplification to the 45° direction, whereas the rest assign a weaker than average amplification to it. It is apparent that if amplification is stronger than average in the 45° direction, the isoanomals on the map of second derivatives will tend to exhibit two preferred orientations parallel to the two diagonals of the square survey grid. A lower than average amplification in the direction of the diagonals will make the directions of the grid lines show up as preferred orientations. In both cases, there are two mutually perpendicular preferred orientations: cf. the series of maps resulting from transformation by various second derivative formulas e.g. in Grosse, 1957 or Jung, 1961.

For small values of φ', orientation-dependence is low for all formulas. Hence, the preferred orientations of isoanomals are particularly striking when the map exhibits also components of high relative frequency. The preferred orientations apparent on such maps are, of course, in no way related to any geological reality. The directions depend on the orientation of the coordinate system defined on the map. Changing the orientation of the grid pattern (without changing the original survey map and the transformation formula) will affect the result, too. The orientation-dependence of the transfer functions elucidates the cause underlying the grid orientation error first mentioned by Rosenbach (1954). The simplest way for avoiding this error is selecting a formula whose transfer function is orientation-independent. This at once eliminates the need for trial computations and complicated corrections proposed by some authors (Grosse, 1957).

Let us add that, whereas the above considerations have revealed the second-derivative method to be unsuitable in principle and have proposed the use of appropriate band-pass filters in its stead, it is nevertheless of a theoretical interest to construct a series of coefficients approximating it. The inverse Fourier transform yields that in the interval

$$-\pi \leqq \omega' \leqq \pi; \qquad -\pi \leqq \psi' \leqq \pi$$

the transfer function of the second derivative can be approximated by the transfer function of the formula

$$g_{ont}(x, y) = \frac{1}{s^2}\left\{\frac{2\pi^2}{3} + \sum_{k=1}^{\infty} \frac{2}{k}(-1)^k [g_{in}(x \pm ks, y) + g_{in}(x, y \pm ks)]\right. \tag{22}$$

The fransfer function is shown as Fig. 18. for the case $k_{\max} = 7$. It is seen to provide a better approximation of the second derivative than any one of the preceding formulas. Moreover, it is orientation-independent to a fairly high degree.

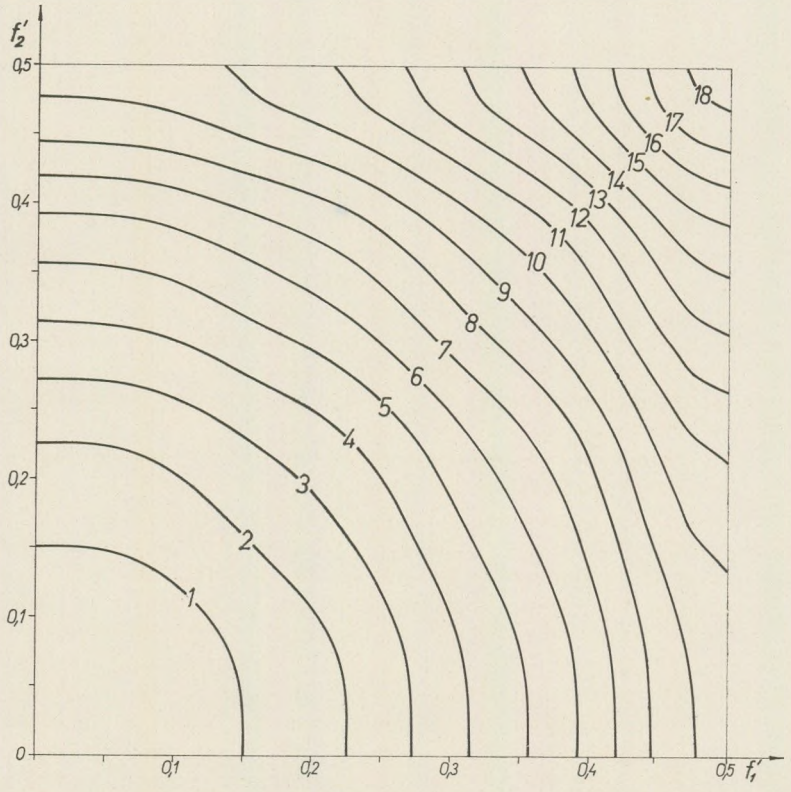

Fig. 18. Transfer function of the "exact" formula

REFERENCES

Grosse, S. (1957): Gravimetrische Auswerteverfahren für höhere Potentialentwicklungen. Freiberger Forsch. C 40, Berlin.

Jung, K. (1961): Schwerkraftfverfahren in der angewandten Geophysik. Akademische Verlagsgesellschaft, Leipzig.

Meskó, A. (1965): Gravity interpretation and information theory. Annales Univ. Sci. Budapestinensis IX. 15–29.

Meskó, A. (1966/a): Gravity interpretation and information theory II. Smoothing and computation of residuals. Annales Univ. Sci. Budapestinensis, X. 15–27.

Meskó, A. (1966/b): Two-dimensional filtering and the second derivative method. Geophysics, XXXI. 606–617.

Paul, M. K. (1961): On computation of second derivatives from gravity data. Pure and applied geophys. 48.

ПРЯМОЙ МЕТОД ИНТЕРПРЕТАЦИИ МНОГОСЛОЙНЫХ ГРАФИКОВ КАЖУЩЕГОСЯ СОПРОТИВЛЕНИЯ $\varrho_k(r)$, ПОЛУЧЕННЫХ НАД ГОРИЗОНТАЛЬНО-СЛОИСТОЙ СТРУКТУРОЙ С ВЭЗ

П. С. ШАЛАТ

(Геофизический Институт Университета имени Роланда Этвеша)

(Поступила: 18. 12. 1967)

SUMMARY

The paper deals with theoretical aspects of direct geoelectrical interpretation. A quick computing process and an outline program are given for the interpretation of vertical geoelectrical-sounding curves recorded above horizontal structures.

Теоретические основы

Доклад ставит себе целью разработать прямой метод интерпретации при помощи вычислительных машин данных ВЭЗ-графиков.

Во-первых рассмотрим случай горизонтальнослоистой структуры (рис. 1.).

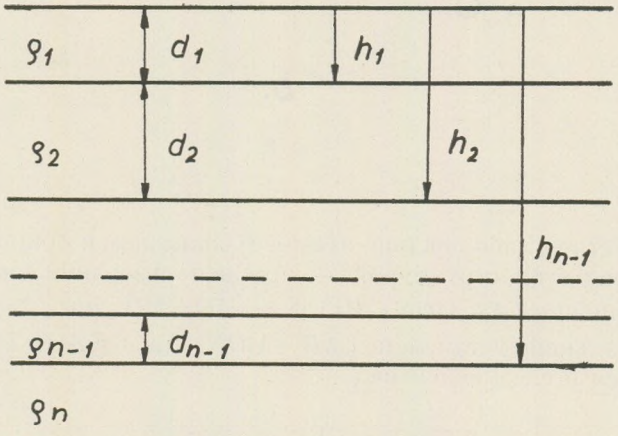

Рис. 1.

Обозначения:

$d_1, d_2, \ldots d_j, \ldots d_{n-1}$ — толщины слоев.

$h_1, h_2, \ldots h_j, \ldots h_{n-1}$ — глубины контактов.

$\varrho_1, \varrho_2, \ldots \varrho_j, \ldots \varrho_{n-1}, \varrho_n$ — сопротивления слоев.

$k_1, k_2, \ldots k_j, \ldots k_{n-1}$ — коэффициенты отражения:

$$k_j = \frac{\varrho_{j+1} - \varrho_j}{\varrho_{j+1} + \varrho_j}. \tag{1}$$

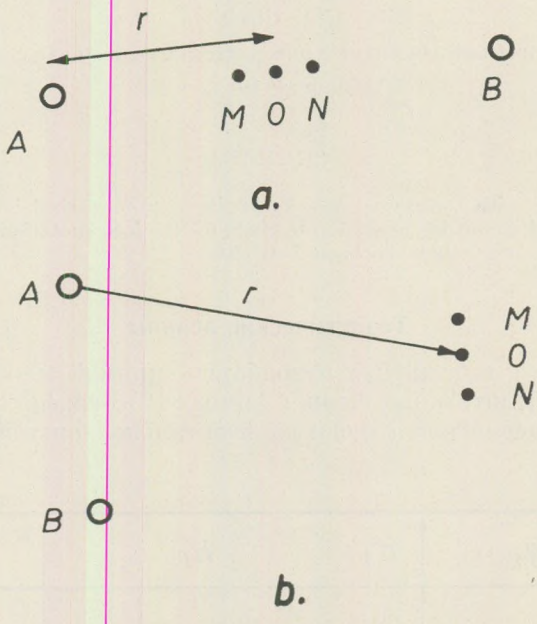

Рис. 2.

Как известно (Заборовский, Koefoed) кажущееся сопротивление $\varrho_k(r)$, полученное над этой структурой — при использовании симметрично-градиентной установки ($A-MON-B$, где $r=\overline{AO}=\overline{BO}$, рис. 2a), или дипольной-экваториальной установки ($AB-MON$, где $r=\overline{AO}=\overline{BO}$, рис. 2b) — представляется в следующем виде:

$$\varrho_K(r) = \varrho_1\left\{1 + 2r^2\int_0^\infty K_i(m)\cdot J_1(mr)\cdot m\cdot dm\right\}. \tag{2}$$

Здесь $K_i(m)$ так называемая керн-функция зависит только от структуры. Например, над двухслойной средой:

$$K_2(m) = \frac{1}{1 - k_1 e^{-2mh_1}}, \tag{3}$$

над трехслойной средой:

$$K_3(m) = \frac{k_1 e^{-2mh_1} + k_2 e^{-2mh_2}}{1 + k_1 k_2 e^{-2m(h_2 - h_1)} - (k_1 e^{-2mh_1} + k_2 e^{-2mh_2})}. \tag{4}$$

Над многослойной средой керн-функцию можно получить из формул Flathe:

$$u = e^{-2m}, \tag{5}$$

$$K_i(m) = K_i(u), \tag{6}$$

$$K_{i+1}(u) = \frac{P_{i+1}(u)}{H_{i+1}(u) - P_{i+1}(u)}. \tag{7}$$

Здесь $P_{i+1}(u)$ и $H_{i+1}(u)$ являются полиномами, получающимися из следующих рекурсивных формул:

$$P_{i+1}(u) = P_i(u) + H_i(u^{-1}) \cdot k_i u^{h_i}, \tag{8}$$

$$H_{i+1}(u) = H_i(u) + P_i(u^{-1}) \cdot k_i u^{h_i}. \tag{9}$$

Первые члены:

$$P_2(u) = k_1 u^{h_1}. \tag{10}$$

$$H_2(u) = 1. \tag{11}$$

Возвращаемся к формуле 2, где $J_1(mr)$ функция Бесселя первого порядка первого рода.

Как показали Schlichter, Weber, Koefoed зная $\varrho_K(r)$ из формулы 2 – по трансформации Hankel – Fourier – можно вычислить керн-функцию $K_i(m)$ в следующем виде:

$$K_i(m) = \int_0^\infty \frac{\varrho_K(r) - \varrho_1}{2\varrho_1 r} \cdot J_1(mr) \cdot dr. \tag{12}$$

Отношение между керн-функцией и кажущимся сопротивлением выражается в формуле 2 и в формуле 12. Эти формулы – равнозначные.

Из керн-функции $K_i(m)$ – как показали Pekeris и Koefoed – можно получить толщины и сопротивления слоев.

Koefoed внедрил выражение $G_i(m)$ так что

$$G_i(m) = \frac{K_i(m)}{1 + K_i(m)} = \frac{P_i(u)}{H_i(u)}. \tag{13}$$

Функция $G_i(m)$ при $m \to \infty$, асимптотически стремится к функции

$$Y_i(m) = k_1 e^{-2md_1}. \tag{14}$$

Иначе говоря из графика $\ln G_i(m)$

$$\ln G_i(m) \to \ln k_1 - 2md_1 \qquad (\text{при } m \to \infty), \tag{15}$$

при больших значениях m точки будут ложиться на прямую линию с наклоном $-2d_1$. Отрезок, отсекаемый этой прямой на оси ординат, будет равен $\ln k_1$. Если все точки лягут на одну прямую, то $d_2 = \infty$ (двухслойная среда). В противном случае определив таким образом d_1 и k_1 мы вычисляем другую почти такую же функцию $G_{i-1}(m)$, следующим образом (P e k e r i s, K o e f o e d):

$$G_{i-1}(m) = -k_1 \frac{1 - G_i(m)/Y_i(m)}{1 - k_1^2 G_i(m)/Y_i(m)}. \tag{16}$$

Это такая же функция, как $G_i(m)$, но относительно $(i-1)$-слойной среды. Можно посмотреть график ее — в логарифмическом масштабе — и по нему определить поочереди d_2 и k_2. Асимптота у функции $G_{i-1}(m)$, при больших значениях m:

$$Y_{i-1}(m) = k_2 e^{-2md_2}. \tag{17}$$

Дальше вычисляется третья функция $G_{i-2}(m)$, если все точки не ложатся на одну прямую, (т.е. если $d_3 \neq \infty$) и т.д. пока получается

$$G_2(m) = k_{i-1} e^{-2md_{i-1}}. \tag{18}$$

Очерк расчета

Мы хотели бы составить быструю программу, с которой можно вычислить параметры слоев из графика $\varrho_K(r)$.

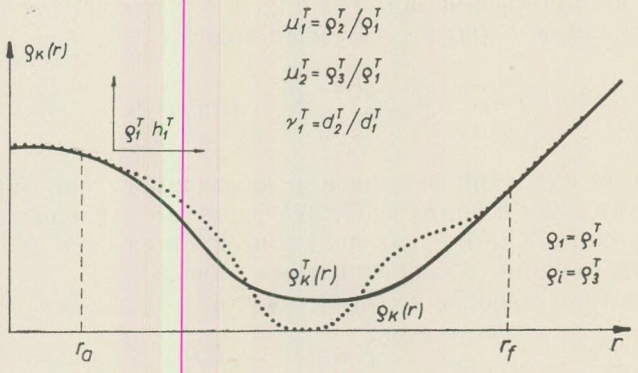

Рис. 3.

Рассмотрим данный полевой, измеренный над слоистой средой график ВЭЗ. Это $-\varrho_K(r)$, обозначенный точками на рис. 3. Легко можно найти такой график из трехслойных теоретических палеток, который в начале и в конце совпадает с $\varrho_K(r)$. Это $\varrho_K^T(r)$, беспрерывная линия на рис. 3.

Параметры теоретического трехслойного графика $\varrho_K^T(r)$:

$$h_1^T,\ h_2^T,\ \varrho_1^T,\ \varrho_2^T,\ \varrho_3^T,$$

или

$$h_1^T,\ \varrho_1^T,\ \mu_1^T = \varrho_2^T/\varrho_1^T, \qquad \mu_2^T = \varrho_3^T/\varrho_1^T, \qquad \nu_1^T = d_2^T/d_1^T,$$

$$k_1^T = \frac{\varrho_2^T - \varrho_1^T}{\varrho_2^T + \varrho_1^T}, \qquad k_2^T = \frac{\varrho_3^T - \varrho_2^T}{\varrho_3^T + \varrho_2^T}.$$

Переделаем формулу 12 следующим образом:

Прибавим $[\varrho_K^T(r) - \varrho_K^T(r)] \equiv 0$ к числителю функции под знаком интеграла:

$$K_i(m) = \int_0^\infty \frac{\varrho_K(r) - \varrho_1 + \varrho_K^T(r) - \varrho_K^T(r)}{2\varrho_1 r} \cdot J_1(mr) \cdot dr, \tag{19}$$

или

$$K_i(m) = \int_0^\infty \frac{\varrho_K(r) - \varrho_K^T(r)}{2\varrho_1 r} \cdot J_1(mr)\, dr + \int_0^\infty \frac{\varrho_K^T(r) - \varrho_1}{2\varrho_1 r} \cdot J_1(mr)\, dr. \tag{20}$$

Здесь второй интеграл — по формуле 12 — равняется с трехслойной керн-функцией, т.е. с формулой 4, при значениях

$$h_1 = h_1^T = d_1^T,\ h_2 = h_2^T = d_2^T + d_1^T,\ k_1 = k_1^T\ \ k_2 = k_2^T.$$

Итак

$$\int_0^\infty \frac{\varrho_K^T(r) - \varrho_1}{2\varrho_1 r} \cdot J_1(mr) \cdot dr = K_3^T(m) =$$

$$= \frac{k_1^T e^{-2md_1^T} + k_2^T e^{-2m(d_1^T + d_2^T)}}{1 + k_1^T \cdot k_2^T e^{-2md_2^T} - (k_1^T e^{-2md_1^T} + k_2^T e^{-2m(d_1^T + d_2^T)})}. \tag{21}$$

Первый интеграл в формуле 20

$$\int_0^\infty \frac{\varrho_K(r) - \varrho_K^T(r)}{2\varrho_1 r} \cdot J_1(mr) \cdot dr = K_i^0(m). \tag{22}$$

Иначе говоря

$$K_i(m) = K_i^0(m) + K_3^T(m). \tag{23}$$

Если мы знаем параметры теоретического трехслойного графика $\varrho_K^T(r)$, тогда легко можно вычислить керн-функцию $K_3^T(m)$ по формуле 21.

В дальнейшем исследуем расчет функции $K_i^0(m)$ по формуле 22. Если $\varrho_K(r)$ и $\varrho_K^T(r)$ в начале и в конце совпадают, тогда их разница будет

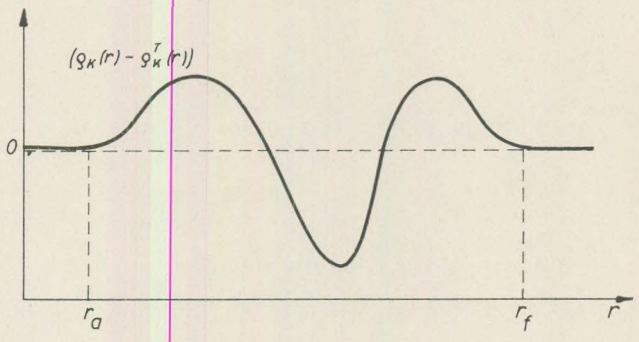

Рис. 4.

$$\varrho_K(r)-\varrho_K^T(r)=0 \quad \text{при} \quad \begin{cases} r<r_a \\ r>r_f \end{cases},$$

(см. на рис. 4), т.е.

$$K_i^0(m)=\int_{r_a}^{f}\frac{\varrho_K(r)-\varrho_K^T(r)}{2\varrho_1 r}\cdot J_1(mr)\cdot dr. \tag{25}$$

Это — интеграл с конечными пределами.

Для вычисления интеграла 25, промежуток от r_a до r_f разбивается на n частей, $r_a=r_0$, $r_f=r_n$.

$$K_i^0(m)=\sum_{j=1}^{n}\int_{r_{j-1}}^{r_j}\frac{\varrho_K(r)-\varrho_K^T(r)}{2\varrho_1 r}\cdot J_1(mr)\cdot dr. \tag{26}$$

В каждой части вычислим аппроксимирующую функцию выражения $\dfrac{\varrho_K(r)-\varrho_K^T(r)}{2\varrho_1}$ так, что

$$f(r)=\frac{\varrho_K(r)-\varrho_K^T(r)}{2\varrho_1}\approx a_j r+b_j \quad \text{при} \quad r_{j-1}<r<r_j. \tag{27}$$

Иначе говоря в каждой части промежутка функция $a_j r+b_j$ стремится к функции $f(r)$.

С этим приближением из формулы 26 получается, что

$$K_i^0(m) \approx \sum_{j=1}^{n} \int_{r_{j-1}}^{r_j} (a_j r + b_j) \cdot \frac{J_1(mr)}{r} \cdot dr = \sum_{j=1}^{n} a_j \cdot \int_{r_{j-1}}^{r_j} J_1(mr) \cdot dr +$$

$$+ \sum_{j=1}^{n} b_j \cdot \int_{r_{j-1}}^{r_j} \frac{J_1(mr)}{r}\, dr. \tag{28}$$

Возникает проблема: при каких значениях m надо вычислить функцию $G_i(m)$, чтобы получить $Y_i(m)$.

Посмотрим первые функции $G_i(m)$

По формулам 13, 8, 9, 10, 11:

$$G_{i+1}(m) = \frac{P_{i+1}(u)}{H_{i+1}(u)} = \frac{P_i(u) + H_i(u^{-1}) \cdot k_i u^{h_i}}{H_i(u) + P_i(u^{-1}) \cdot k_i u^{h_i}}, \tag{29}$$

или

$$G_{i+1}(m) = \frac{P_i(u) + H_i(u^{-1}) \cdot k_i u^{d_1+d_2+\ldots+d_i}}{H_i(u) + P_i(u^{-1}) \cdot k_i u^{d_1+d_2+\ldots+d_i}}. \tag{30}$$

С этой рекурсивной формулой из функции

$$G_2(m) = \frac{k_1 u^{d_1}}{1} \tag{31}$$

получаются следующие члены:

$$G_3(m) = \frac{k_1 u^{d_1} + k_2 u^{d_1+d_2}}{1 + k_1 k_2 u^{d_2}} \tag{32}$$

$$G_4 = \frac{k_1 u^{d_1} + k_2 u^{d_1+d_2} + k_3 u^{d_1+d_2+d_3} + k_1 k_2 k_3 u^{d_1+d_3}}{1 + k_1 k_2 u^{d_2} + k_1 k_3 u^{d_2+d_3} + k_2 k_3 u^{d3}} \tag{33}$$

$$G_5(m) = \frac{\begin{array}{c} k_1 u^{d_1} + k_2 u^{d_1+d_2} + k_3 u^{d_1+d_2+d_3} + k_1 k_2 k_3 u^{d_1+d_3} + k_4 u^{d_1+d_2+d_3+d_4} + \\ + k_1 k_2 k_4 u^{d_1+d_3+d_4} + k_1 k_3 k_4 u^{d_1+d_4} + k_2 k_3 k_4 u^{d_1+d_2+d_4} \end{array}}{\begin{array}{c} 1 + k_1 k_2 u^{d_2} + k_1 k_3 u^{+d_2+d_3} + k_2 k_3 u^{d_3} + k_1 k_4 u^{d_2+d_3+d_4} + \\ + k_2 k_4 u^{d_3+d_4} + k_3 k_4 u^{d_4} + k_1 k_2 k_3 k_4 u^{d_2+d_4} \end{array}}. \tag{34}$$

и т.д.

По правилу полной индукции можно доказать, что самый низкий показатель числителя d_1, и то знаменателя — 0 ($e^\circ = 1$). Дальше можно показать, что из числителя можно вынимать u^{d_1}, потому что каждый член содержит u^{d_1}. Например:

$$G_5(m) = u^{d_1} \cdot \frac{\begin{array}{c} k_1 + k_2 u^{d_2} + k_3 u^{d_2+d_3} + k_1 k_2 k_3 u^{d_3} + k_4 u^{d_2+d_3+d_4} + k_1 k_2 k_4 u^{d_3+d_4} + \\ + k_1 k_3 k_4 u^{d_4} + k_2 k_3 k_4 u^{d_2+d_4} \end{array}}{\begin{array}{c} 1 + k_1 k_2 u^{d_2} + k_1 k_3 u^{d_2+d_3} + k_2 k_3 u^{d_3} + k_1 k_4 u^{d_2+d_3+d_4} + \\ + k_2 k_4 u^{d_3+d_4} + k_3 k_4 u^{d_4} + k_1 k_2 k_3 k_4 u^{d_2+d_4} \end{array}}. \quad (35)$$

Когда будут члены, содержащие u, меньше чем 10^{-4}. Если $e^{-2md_j} < 10^{-4}$ (36)

где тольщина d_j самая маленькая из значений $d_1, d_2, \ldots d_i$.
Т.е.

$$md_j > 4{,}6. \quad (37)$$

При больших значениях m можно писать

$$G_i(m) = k_1 e^{-2md_1} \cdot \frac{1 + \sum\limits_l c_l}{1 + \sum\limits_l d_l}, \quad (38)$$

где величины c_l и d_l приблизительно $10^{-3} - 10^{-4}$. (Предполагая, что $|k_1| > 0{,}1$).

Иначе говоря, пусть мощность самого тонкого слоя d_j равна единице, если

$$m > 4{,}6. \quad (39)$$

тогда

$$G_i(m) \approx Y_i(m) \quad (40)$$

На основании этих предварительных счетов вычислим функцию $G_i(m)$ при значениях

$$m_l = \left(\sqrt[4]{2}\right)^l \quad \text{при} \quad -16 \leq l \leq 16 \quad (41)$$

т. е. при

$$m\colon\ 1/16,\ 2^{-\frac{15}{4}},\ 2^{-\frac{14}{4}},\ \ldots\ 2^{-\frac{1}{4}},\ 1,\ 2^{\frac{1}{4}},\ \ldots\ 2^{\frac{15}{4}},\ 16.$$

В дальнейшем посмотрим, как разбивать целеобразно промежуток $[r_a, r_f]$.

Перепишем интеграл 28, при $m = m_l$

$$K_i^0(m_l) = \sum_{j=1}^{n} a_j \int_{r_{j-1}}^{r_j} J_1(m_l r) \cdot dr + \sum_{j=1}^{n} b_j \int_{r_{j-1}}^{r_j} \frac{J_1(m_l r)}{r}\, dr \quad (42)$$

Пусть

$$m_l r = R; \quad r = \frac{R}{m_l}; \quad dr = \frac{dR}{m_l}. \quad (43)$$

Блок-схема программы

I. Вычисление нескольких теоретических кривых

$$\varrho_K^T(r)$$

Форм. 2, 4

II. Вычисление интегралов

$$V_k = \int_{(\sqrt{2})^{k-1}}^{(\sqrt{2})^{k}} J_1(R)dR$$

$$Z_k = \int_{(\sqrt{2})^{k-1}}^{(\sqrt{2})^{k}} J_1(R)\cdot\frac{1}{R}\,dR$$

Несколько $\varrho_K^T(r)$ на магнитной ленте, в медленной памяти.
Это МП.

Интегралы V_k и Z_k в быстрой памяти.
Это БП.

III. Данный полевой график $\varrho_K(r)$ на перфокарте

$$n, \varrho_K(r_1), \varrho_K(r_2), \ldots \varrho_K(r_n).$$

IV. Параметры совпадающего графика $\varrho_K^T(r)$; h_1^T, ϱ_1^T, μ_1^T, μ_2^T, ν_2^T на перфокарте.

V. III. и IV. ВХОД.

VI. Быстрая память машины.

МП: $\varrho_K^T(r)$.

VII Из МП $\varrho_K^T(r_1), \varrho_K^T(r_2), \ldots \varrho_K^T(r_n)$

VIII. Вычисление

$$f(r) = \frac{\varrho_K(r) - \varrho_K^T(r)}{2\varrho_2}$$

IX. Приближение $f(r)$ в частях $r_{j-1} < r < r_j$

$$f(r) = a_j r + b_j$$

X. $K_3^T(m_l)$ из VI.
из формулы 21.

XI.

$$K_i^0(m_l) = \sum_{j=m}^{n} a_j \cdot \frac{1}{m_l} V_{10l+j} + \sum_{j=m}^{n} b_j Z_{10l+j}$$

БП: V_k Z_k

XII. $K_i(m_l) = K_0^i(m_l) + K_3^T(m_l)$.

XIII. $G_i(m_l) = \dfrac{K_i(m_l)}{1 + K_i(m_l)}$.

XIV. Асимптотические приближения, если $m \to \infty$

$$G_i(m) \to Y_i(m) = k_1\ e^{-2md_1}$$

XVII.

$$G_{i-1}(m_l) = -k_1 \frac{1 - G_i(m_l)/Y_i(m_l)}{1 - k_1^2 \cdot G_i(m_l)/Y_i(m_l)}.$$

XVIII. $G_{i-1} \to G_i$

XVI. ВЫХОД k_1 d_1.

XV. k_1, d_1 из $Y_i(m_l)$.

Из формулы 42 вытекает, что

$$K_i^0(m_l) = \sum_{j=1}^{n} a_j \cdot \frac{1}{m_l} \int_{m_l r_{j-1}}^{m_l r_j} J_1(R)\, dR + \sum_{j=1}^{n} b_j \int_{m_l r_{j-1}}^{m_l r_j} J_1(R) \cdot \frac{1}{R} \cdot dR. \tag{44}$$

Разбиваем промежуток r на n частей с следующими точками

$$r_j = \left(\sqrt[40]{2}\right)^j \quad \text{при} \quad -160 \leq j \leq 520, \tag{45}$$

т.е. при

$$r\colon\ 1/16,\ 2^{-\frac{159}{40}},\ 2^{-\frac{158}{40}},\ \ldots\ 2^{-\frac{1}{40}},\ 1,\ 2^{\frac{1}{40}},\ \ldots\ 1024\ \ldots\ 16\,384.$$

На основе вышеупомянутых нужно вычислить интегралы

$$V_k = \int_{(\sqrt[40]{2})^{k-1}}^{(\sqrt[40]{2})^{k}} J_1(R)\, dR \tag{46}$$

$$Z = \int_{(\sqrt[40]{2})^{k-1}}^{(\sqrt[40]{2})^{k}} J(R) \cdot \frac{1}{R} \cdot dR \tag{47}$$

$$\begin{gathered} k = 10\,l + j, \\ -160 \leq 10l \leq 160, \\ -160 \leq j \leq 520, \\ \hline -320 \leq k \leq 680. \end{gathered}$$

Это значит 2×1000 интегралов. Но если мы уже вычислили один раз эти интегралы, тогда больше не надо интегрировать. Зная значения V_k и Z_k при $-320 \leq k \leq 680$ и предполагая, что $f(r) \neq 0$ при $(\sqrt[40]{2})^m < r < (\sqrt[40]{2})^n$ тогда $K_i^0(m_l)$ получается из следующей формулы:

$$K_i^0(m_l) = \sum_{j=m+1}^{n} a_j \frac{1}{m_l} \cdot V_{10l+j} + \sum_{j=m+1}^{n} b_j Z_{10l+j} \tag{48}$$

Это значит только некоторые умножения и сложения, которые машина быстро вычислит. (Блок-схема программа).

ЛИТЕРАТУРА

Заборовский, А. И. (1963): Электроразведка.

Flathe, H. (1955): A practical method of calculating geo-electrical model graphs for horizontally stratified media. Geophys. Prosp. III. pp. 268 – 294.

Koefoed, O. (1966): A semi-direct method of interpreting resistivity observations. Geophys. Prosp. XIII. pp. 259 – 282.

Koefoed, O. (1966): Direct method of interpreting resistivity observations. Geophys. Prosp. XIII. pp. 568 – 591.
Mooney, H. M. et al: (1966). Resistivity computation method for layered earth models. Geophysics, XXXI. pp. 192 – 203.
Pekeris, C. L. (1940): Direct method of interpretation in the resistivity prospecting. Geophysics, V. pp. 31 – 42.
Schlichter, L. B. (1933): The interpretation of the resistivity prospecting method for horizontal structures. Physics, IV. pp. 307 – 322.
Weber, M. (1964): Ein direktes Verfahren zur Interpretation von geoelektrischen Messungen nach Schlumberger. Pure and Applied Geophys. LIX. pp. 123 – 127.

ROLE OF THE INHOMOGENEOUS MAGNETISATION OF ROCK SAMPLES IN ROCK-GENERATOR MEASUREMENT

by

P. SZEMERÉDY

(Geophysical Institute of Loránd Eötvös University)

(Received: 25 September 1967)

ZUSAMMENFASSUNG

Infolge der inhomogenen Magnetisation der Gesteinsprobe können die gemessene und die wahre magnetische Momentkomponente bei Rockgenerator-Messungen verschieden sein. Die zur Drehachse gehörige Asymmetrie der Verteilung der Magnetisation modifiziert das Frequenzspektrum der in der Indikatorspule auftretenden Wechselspannung. Als Wirkung der Asymmetrien verändert sich die Amplitude und das Phasenverhältnis der Grundfrequenz, und treten harmonische Oberwellen auf. Durch die Messung der Grösse und des Phasenverhältnisses der zweiten Oberwelle wird die Korrektion der Messergebnisse, und das Studium der Asymmetrienverhältnisse möglich sein.

In palaeomagnetic measurements on rocks the inhomogeneous magnetization of the rock sample introduces an error into the determination of the magnetization vector. The aim of the present paper is to show that for a rock generator it is possible to make the necessary corrections provided supplementary measurements are carried out and that there may be a way for measurement on samples of irregular shape.

In earlier rock-generator measurements, only the basic harmonic equalling the frequency of rotation of the generator was taken into consideration. Thus the information of the higher harmonics has been neglected. Of course, for extremely small magnetizations, as was the case with the samples for which the rock generator was designed in the first place, this was fully justified. It would be namely very difficult to analyze harmonics not rising above the thermal noise level. However, if the second harmonic is well above this level, it is logical to make use also of this one.

The inhomogeneity of the magnetization of the rock can approximately be resolved in two kinds of asymmetry of a magnetic rod of finite dimensions with respect to the axis of rotation of the rock generator. These are the following:

a) a magnetized rod rotating around the axis in the xy-plane is asymmetrical by having its magnetic centre displaced by a distance Δ against the axis of rotation.

b) The rod is off-center by a distance ε.

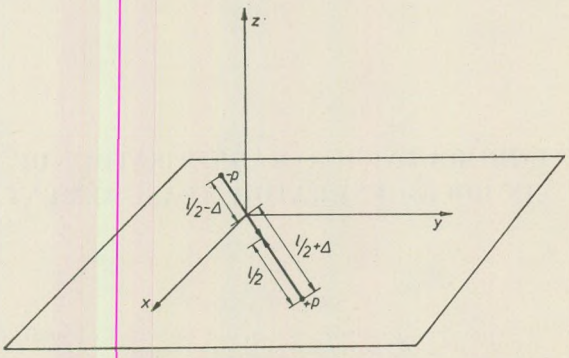

Fig. 1. Asymmetry (*a*): The magnetic centre of the rod displaced by a distance Δ against the axis of rotation

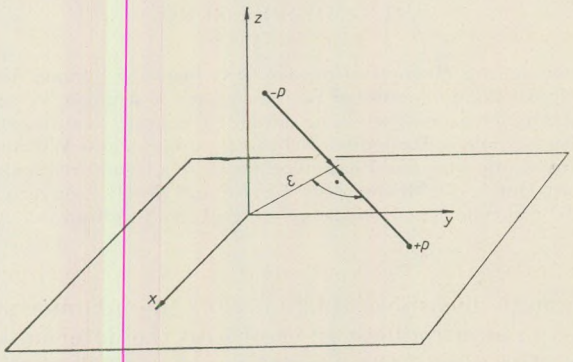

Fig. 2. Asymmetry (b): The rod is off-center by a distance ε

In order to avoid disturbing influences let us assume that in the space containing the rock sample there is no external magnetic field, that is, the geomagnetic field is eliminated or reduced to a negligible value by appropriate screening.

Let us find the value of the magnetic potential for an arbitrary point P of a surface bounded by a circular loop of radius R. It is apparent from the figure that it may be described by a function of the form

$$V = V(p, \Delta, \varepsilon, \varrho, \vartheta, L, l, t). \tag{1}$$

The electromotive force U generated in the circular loop of radius R is given by

$$U = -\frac{\partial}{\partial t} \int_0^R \int_0^{2\pi} -\mathrm{grad}_L V \, d\vartheta \, d\varrho. \tag{2}$$

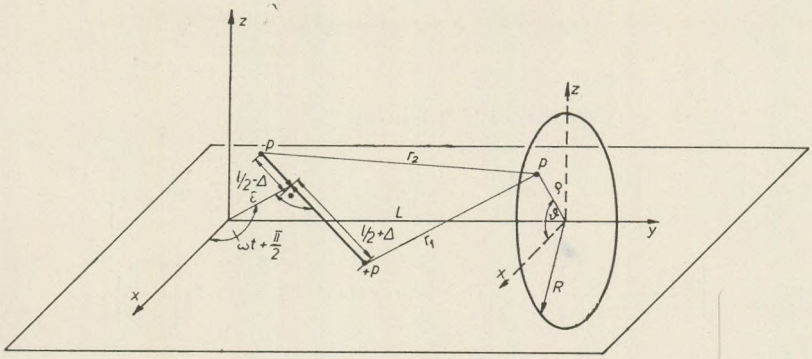

Fig. 3. Calculation of electromotive force in a circular loop

However, in the present case it is impossible to bring the expression of U into an analytical form, and even its series expansion is exceedingly complicated. That is why I shall in the following attempt only to estimate the influence of the asymmetries on the frequency spectrum of the electromotive force U.

Introducing the asymmetry parameters $\eta = \frac{\varepsilon}{l}$ and $\xi = \frac{\Delta}{l}$, the potential function assumes the form

$$V(p, \eta, \xi, \varrho, \vartheta, L, l, t) = p\left(\frac{1}{r_1} - \frac{1}{r_2}\right) = \frac{p}{l}\left[(\eta^2 + \xi^2 + a_1\eta + b_1\xi + c_1)^{-1/2} - \right.$$

$$\left. - (\eta^2 + \xi^2 + a_2\eta + b_2\xi + c_2)^{-1/2}\right]. \tag{3}$$

Let us note, however, that the symbols a, b, c themselves represent functions, which were, however, not written out in detail to avoid confusion.

Since η and ξ are less than unity and the functions a, b, c are bounded, the $V(\eta, \xi)$ function can be expanded in a fairly convergent Taylor series. Thus

$$V(\eta, \xi) = V(0, 0) +$$

$$+ \left(\frac{\partial V}{\partial \eta}\right)_{\eta=0} \eta + \left(\frac{\partial V}{\partial \xi}\right)_{\xi=0} \xi + \left(\frac{\partial^2 V}{\partial \eta^2}\right)_{\eta=0} \eta^2 + \left(\frac{\partial^2 V}{\partial \eta \partial \xi}\right)_{\eta=\xi=0} \eta\xi + \left(\frac{\partial^2 V}{\partial^2 \xi}\right)_{\xi=0} \xi^2 + \ldots \tag{4}$$

The function $V(0, 0) = V_0(\varrho, L, \vartheta, l, t)$ describes the magnetic potential of the symmetrically rotated magnetic rod at the point P, whereas the further terms of the expansion represent the accessory potentials due to the respective asymmetries.

Since the coefficients of the series are functions of time, they involve the frequency components. If the asymmetries are sufficiently small, it is enough to consider the second-order terms.

The method of estimating the frequency components shall be presented for the term $V(0, 0)$. The analysis of the rest of the coefficients is performed similarly.

$$V(0,\,0) = \frac{p}{l}\,(c_1^{-1/2} - c_2^{-1/2}). \tag{5}$$

Substituting c_1 and c_2, respectively, we have

$$V(0,0) = \frac{p}{l}\left\{\left[\frac{\varrho^2}{l^2} + \frac{L^2}{l^2} + \frac{1}{4} - \frac{1}{l}\,(\varrho\cos\vartheta\cos\omega t + L\sin\omega t)\right]^{-1/2} - \right.$$

$$\left. - \left[\frac{\varrho^2}{l^2} + \frac{L^2}{l^2} + \frac{1}{4} + \frac{1}{l}\,(\varrho\cos\vartheta\cos\omega t + L\sin\omega t)\right]^{-1/2}\right\}. \tag{6}$$

Let us denote the terms $\frac{\varrho^2}{l^2} + \frac{L^2}{l^2} + \frac{1}{4}$ by g and carry it before the braces. Then

$$V(0,0) = g^{-1/2}\,\frac{p}{l}\left\{\left[1 - \frac{1}{lg}\,(\varrho\cos\vartheta\cos\omega t + L\sin\omega t)\right]^{-1/2} - \right.$$

$$\left. - \left[1 + \frac{1}{lg}\,(\varrho\cos\vartheta\cos\omega t + L\sin\omega t)\right]^{-1/2}\right\}. \tag{7}$$

It can be shown that, introducing the notation

$$\frac{1}{lg}\,(\varrho\cos\vartheta\cos\omega t + L\sin\omega t) = \psi,$$

the condition $|\psi| < 1$ holds for any value of t.

In the following the function $V(0, 0)$ can be written as

$$V(0,0) = D\{(1-\psi)^{-1/2} - (1+\psi)^{-1/2}\}. \tag{8}$$

Expanding into a binomial series by ψ and rearranging we obtain the following expression:

$$V(0,0) = D\sum_{\mu=0}^{\infty}\frac{(4\mu+1)!!}{(4\mu+2)!!}\,\psi^{2\mu+1}. \tag{9}$$

Introducing the former expression of ψ, this becomes

$$V(0,0) = D\sum_{\mu=0}^{\infty}\frac{(4\mu+1)!!}{(4\mu+2)!!}\left(\frac{1}{lg}\right)^{2\mu+1}(\varrho\cos\vartheta\cos\omega t + L\sin\omega t)^{2\mu+1}. \tag{10}$$

Applying the binomial theorem, we have

$$V(0,0) =$$

$$= D\sum_{\mu=0}^{\infty}\frac{(4\mu+1)!!}{(4\mu+2)!!}\left(\frac{1}{lg}\right)^{2\mu+1}\sum_{k=0}^{2+1}\binom{2\mu+1}{k}\varrho^k\cos^k\vartheta\cos^k\omega t\,L^{2\mu+1-k}\sin^{2\mu+1-k}\omega t. \tag{11}$$

The component of the electromotive force induced in the loop by the potential $V(0, 0)$ is given by

$$-\frac{\partial}{\partial t}\int_0^R\int_0^{2\pi} -\mathrm{grad}_L\, V(0,0)\, d\vartheta\, d\varrho.$$

If the prescribed operations are performed avoiding derivation with respect to time, the following expression results:

$$D\sum_{\mu=0}^{\infty} S_\mu(L, l, R)\sum_{k=0}^{\mu} r_{2k}(L, R)\cos^{2k}\omega t \sin^{2\mu+1-2k}\omega t,$$

where the terms corresponding to odd values of k have fallen out owing to the cyclic integration of $\cos^k\vartheta$ from 0 to 2π.

Expanding this function in a Fourier series, and carrying out the prescribed summations, we get a series of the form

$$A_1 \sin\omega t + A_3 \sin 3\omega t + A_5 \sin\ \omega t + \ldots$$

The negative of the derivative according to time of this series has the form

$$B_1 \cos\omega t + B_3 \cos 3\omega t + B_1 \cos 5\ t + \ldots$$

This is a pure cosine series containing odd harmonics only. Extending the procedure to the terms of the potential series quadratic in η and ξ, we obtain the following Fourier series:

$$\sum_{\alpha=0}^{\infty}[({}^0B_{2\alpha+1} + {}^2_\eta B_{2\alpha+1}\eta^2 + {}^2_\xi B_{2\alpha+1}\xi^2)\cos(2\alpha+1)\omega t +$$

$$+ {}_{\eta\xi}A_{2\alpha+1}\eta\xi \sin(2\alpha+1)\omega t] + \ldots +$$

$$+\sum_{\alpha=1}^{\infty}[({}^1_\eta A_{2\alpha}\eta + {}^1_\xi A_{2\alpha}\xi)\sin 2\alpha\omega t + {}^1_\eta B_{2\alpha}\eta\cos 2\alpha\omega t] + \ldots$$

Hence, the electromotive force generated in the indicator coil by the basic harmonic, that is, by the frequency of rotation of the rock sample, is

$$({}^0B_1 + {}^2_\eta B_1\eta^2 + {}^2_\xi B_1\xi^2)\cos\omega t + {}_{\eta\xi}A_1\eta\xi\sin\omega t = U_1 \qquad (12)$$

It is usual to consider these simply as the components of the magnetic moment vector. As a result, two types of error may occur if the magnetization is inhomogeneous. The first is an obvious phase error due to the arising sine term. The other is due to further terms added to the correct ${}^0B_1$ value obtained for the symmetrical case. It is apparent that in the knowledge of η and ξ it would be possible to carry out appropriate corrections of U_1. The study of the Fourier series reveals that the even harmonics are exclusively due to the asymmetries. Now this offers a possibility of determining the η and ξ values in question. Let us write up the second harmonic:

$$({}^1_\eta A\eta_2 + {}^1_\xi A_2\xi)\sin 2\omega t + {}^1_\eta B_2\eta\cos 2\omega t = U_2. \qquad (13)$$

Transformed, this becomes

$$U_2 = \sqrt{({}^1_\eta A_2\eta + {}^1_\xi A_2\xi)^2 + {}^1_\eta B_2^2\eta^2}\,\sin(2\omega t + \varphi), \tag{13}$$

where

$$\operatorname{tg}\varphi = \frac{{}^1_\eta B_2\eta}{{}^1_\eta A\eta + {}^1_\xi A_2\xi}.$$

In the knowledge of φ this system of equations can be solved for η and ξ. The phase angle φ is to be determined by measurement, which can be performed e.g. as follows. Let us change the sign of ω in the expression of U_2; this corresponds to a reversal of the rotation direction of the rock generator.

$$\operatorname{tg}\varphi' = -\frac{{}^1_\eta B_2\eta}{{}^1_\eta A_2\eta + {}^1_\xi A_2\xi}. \tag{15}$$

Since $\varphi = -\varphi'$, the angle φ can be determined from the observed phase difference.

Now the only problem left over is that of determining the Fourier coefficients A and B, assumed to be known above. These involve the instrumental constants, the length of the "magnetic rod" subjected to the measurements, and the magnetic pole strength. Since their computation is exceedingly cumbersome, it is best to determine them empirically, for instance by carrying out measurements on magnetic rods of known asymmetry.

The stated results can obviously be applied without further complications to the study of samples having a symmetry of rotation with respect to the axis of rotation. In rock-magnetic studies, cube-shaped samples are frequently employed. In this case the second harmonic is no more due to the asymmetries alone. A correction may be applied, however. One of the difficulties of rock magnetism measurements is that the cutting of the sample to the required shape takes a considerable amount of work. In routine measurements, it would be of considerable advantage if this could be somehow circumvented. The studies described above promise a solution also of this problem. If a sample of irregular shape is utilized, the asymmetry parameters and the approximate geometrical data of the sample permit the determination of magnetization to the required degree of accuracy. The necessary computations might be simplified by the aid of a computer programmed for this purpose.

REFERENCE

T. Nagata: Rock Magnetism, Maruzen, Tokyo 1953.

SOME GEOPHYSICAL AND GEOLOGICAL ASPECTS OF CRUSTAL STRUCTURE EVOLUTION IN THE HUNGARIAN BASIN

by

B. BALKAY* and L. STEGENA**

(* ALUTERV, Budapest,** Geophysical Institute of Loránd Eötvös University)

(Received: 20 December 1967.)

SUMMARY

As a result of research into the fundamental changes undergone by the Hungarian Basin region during the Alpine cycle of mountain building, the authors have reached the conclusion that a substantial portion of the events that had taken place since the Cretaceous (the Austrian phase of orogeny) can be ascribed to a thinning by some 8 to 10 kilometres of the crust beneath the basin. This thinning, spread out over the interval from the Cretaceous to the Pleistocene, was the prime mover of subsidence in the basin. Subsidence was further intensified by the load of sediments deposited on the basin bottom.

Structural evolution in the Hungarian Basin* region during the Alpine cycle of mountain building can be roughly subdivided as follows (Fig. 1.) (Balkay 1959, 1960, 1961).

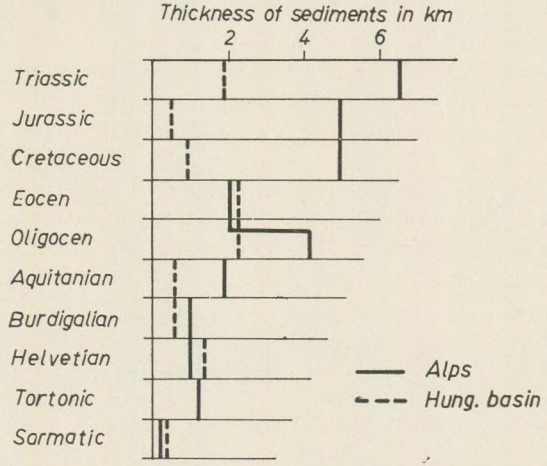

Fig. 1. The greatest thickness of sediments, in the Alps and in the Hungarian Basin (after Balkay, 1960)

* The term Hungarian Basin as used here means the Hungarian portion of the Carpathian Basin.

1. Relative quiet and slow epicontinental-type sedimentation up to the Lower Cretaceous.

2. The subsidence of a so-called flysch trough of north-south trend across the middle of the basin; volcanism, largely diabase eruptions, closely associated with the trough (Dank 1963); slight block-faulting in the Barremian.

3. In spite of strong block-faulting, thrust-faulting and mountain building of German style in the Austrian phase of orogeny, the Hungarian Basin behaved in an infinitely more passive way than the geosynclinal zones all around it, where large-scale folding and napping took place.

4. In the Eocene and Lower Oligocene, the Hungarian basin shows for the first time rates of deposition equalling those in the Alps. Sporadic volcanism in the Eocene is followed by a quite large-scale activity in the Oligocene. Volcanism is accompanied by tensile stresses and is plugged in as the compressive stresses of the Savian phase of orogeny build up in the uppermost Oligocene (Balkay 1961).

5. Volcanism returns with a vengeance at the time of the intensely tensile Styrian phase of orogeny: in various regions it continues throughout the Helvetian, Sarmatian and Tortonian, and even into the Pannonian, producing an estimated maximum thickness of 2000 metres of volcanics and followed by intense hydrothermal activity (Fig. 2). In these stages of the Miocene, rates of subsidence in the basin exceed those in the Alps.

6. The most rapid subsidence in the entire Alpine history of the basin sets in with the Pannonian: with a maximum thickness of 3500 metres or more, and a mean thickness of the order of 1500 metres (Kertai 1957) for an estimated 11 million years, it represents a pronouncedly geosynclinal rate of subsidence.

7. In the Pleistocene, subsidence is still fairly rapid in some isolated places, but on the whole it is slowing down. At present, precision levelling still proves the slow elevation of the mountains rising above the basin and the slow subsidence of the basin proper.

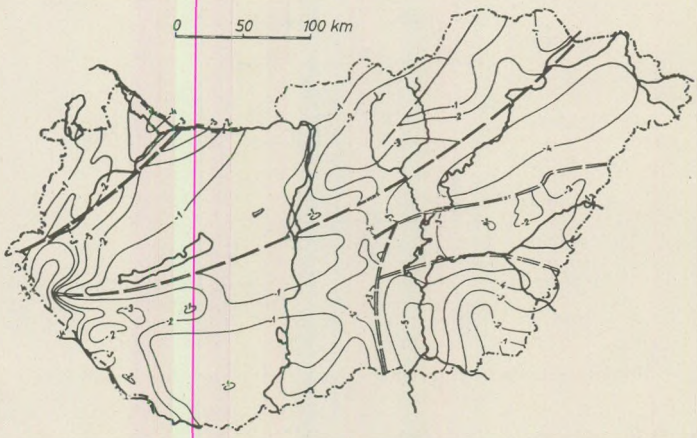

Fig. 3. The isobaths of the crystalline basement in Hungary in kilometers (after Körössy, 1964)

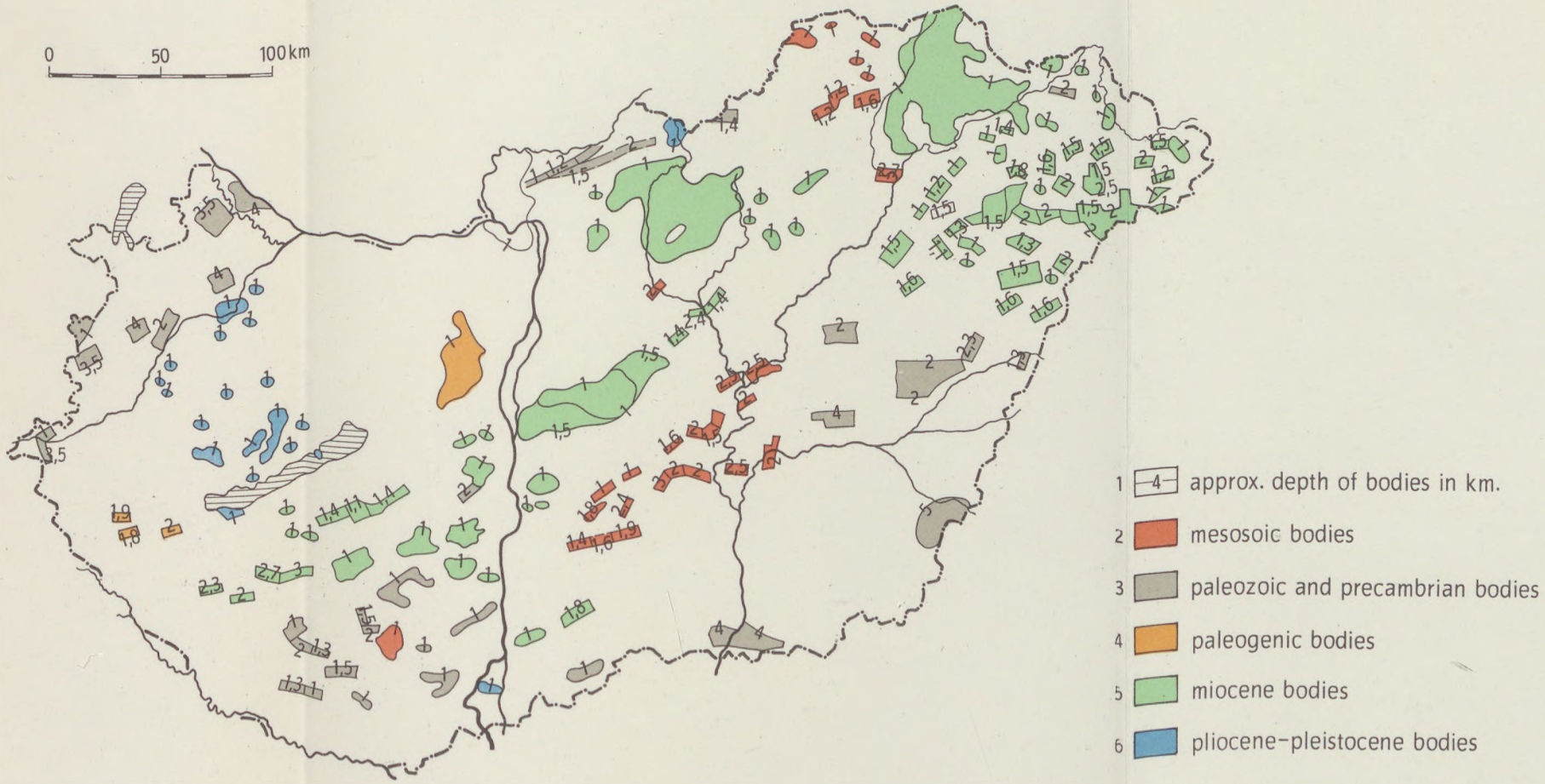

MÁFI. Eng. sz: 28/1968. 600 pld.

Fig. 2. The age and depth of the magnetic bodies in Hungary (after Posgay, 1967)

All in all, the main trend of evolution that emerges from the above facts is that, starting from a rather stable and decidedly un-volcanic state, the basin acquired in the course of these events a substantial mobility going hand in hand with an intense volcanism. Volcanism had reached its paroxysm in the Miocene; subsidence, in the Pannonian. The mean thickness of sediments deposited from the end of the Lower Cretaceous to the present day is about 2.5 km; their maximum thickness is of the order of 6000 metres (Sághy–Vándor – Varga 1967) (Fig. 3).

The common cause of these events was, in the opinion of the authors, a crustal revolution that took place since the Lower Cretaceous; by a mechanism that is open to discussion (see the last paragraphs of the present paper), this resulted in a thinning of the crust by some 8 to 10 kilometres. By isostasy, such a thinning is obviously accompanied by a subsidence that attracts a great deal of waste from the rising mountains all around: the deposited waste represents a load that entails further subsidence and so on. Subsidence was not uniform all over the basin: the differences resulted in the formation of sub-basins, profound faults and the concentration of volcanism along these faults.

Geophysical measurements and their evaluation (Gálfi – Stegena 1957, Balkay 1959, Stegena 1964, Mituch – Posgay 1965, Mituch 1966, 1967) have proved the Moho interface to be at a depth of 23 to 27 km below the surface (Fig. 4). On the other hand, a "standard continental" crust is 33 km thick (Press 1961); the "standard crust" of the Russian Platform is 35 km thick (Subbotin et al. 1965).

A thin crust would not in itself warrant any inferences as to the process of thinning, or as to the connexion between thinning and subsidence. However, seismic work all over the world has brought evidence that young subsidences are everywhere underlain by thin crust. Let us look into this point in some detail.

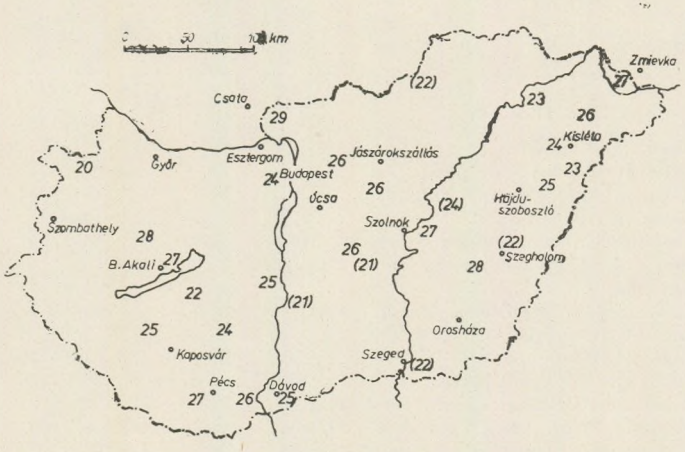

Fig. 4. The depth of the Moho-discontinuity in kilometers in Hungary, based on measurements by Gálfi, Mituch, Posgay and Stegena

In the Eastern United States, the Great Valley basin, of about the same area and age as the Hungarian Basin, has a crust 20 km thick (Eaton, 1963) (Fig. 5). Crustal thickness below the surrounding mountains is 30 to 50 km (Pakiser – Steinhart 1964).

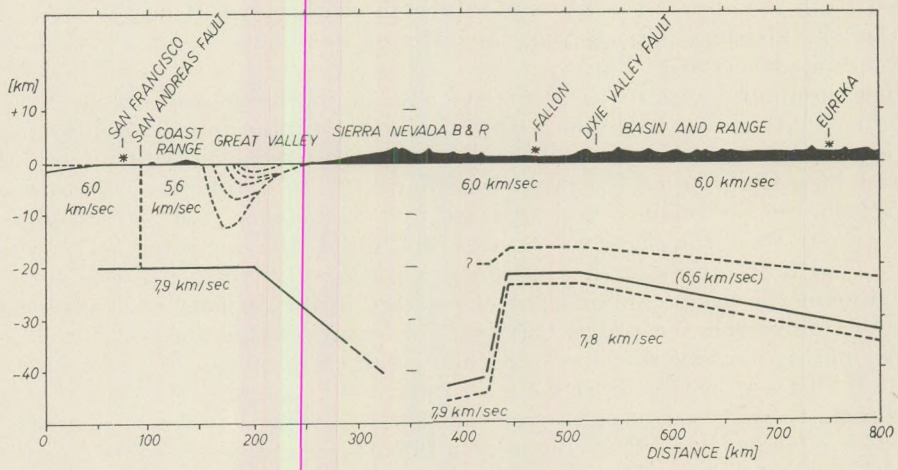

Fig. 5. Crustal structure beneath the Great Valley depression (after Eaton, 1963)

Table

The thickness (H), the vertical mean velocity (V) of the Earth's crust and the boundary-velocity of the M layer (P), in various Earth areas

(After Stegena 1966)

	H (km)	*V* (km/s)	*P* (km/s)
I. PLATFORMS AND SHIELDS			
a) Ancient platforms and shields			
– Baltic shield (Litvinenko et al. 1962)	36 – 40	6,6	8,0
– Russian platform (Godin et al. 1959)	36 – 40	6,4 – 6,8	8,2
– Finland (Vesanen, 1965)	35	6,4	8,4
– Arkansas (Woolland, 1965; Pakiser, Steinhart, 1964)	43	6,4 – 6,5	8,1 – 8,2
– Interior Plains, USA (Stuart et al., 1964; Pakiser, Steinhart, 1964)	40 – 50	6,1 – 6,8	8,0 – 8,5
– Keweenaw, Wisconsin (Steinhart, Meyer, 1961)	36 – 42	6,3 – 6,4	8,1
– Alberta, Canada (Richards, Walker, 1959)	43	6,6	8,2
– Yilgarn, Australia (Bullen, 1965)	32 – 39	6,0(?)	8,2
b) Younger, tectonically activised platforms			
– Coastal Plains, USA (Stuart et al., 1964; Pakiser, Steinhart, 1964; Cram, 1961, Tatel et al., 1954)	30 – 40	5,8 – 6,5	8,1 – 8,2
– German Herzinium (German Research Group, 1964; Closs, 1965)	30	6,1 – 6,3	8,2
– Turkmenian platform (Kosminskaya, Risnitsenko, 1964)	30 – 35	6,5	8,2

II. MOUNTAINS

a) Paleozoic mountains			
– Appalachian Highlands (Stuart et al., 1964; Pakiser, Steinhart, 1964)	33 – 39	6,0 – 6,7	8,1 – 8,2
– Rheinisches Schiefergebirge (German Research Group, 1964; Closs, 1965)	~30	6,1	8,2
– Schwarzwald (German Research Group, 1964; Closs, 1965)	~28	6,4(?)	8,2
– Nura Tau, Bukhara (Kosminskaya, Risnitsenko, 1964)	~40	6,2 – 6,3	8,2
b) Alpine mountains			
– Alps (Closs, 1965; Peterschmidt et al., 1964; Fuchs et al., 1963)	~55	6,2 – 6,4	8,1 – 8,2
– Carpathians (Sollogub, 1966)	~55	(7,1 Ivrea?)	–
– Dinaric mountains (Prosen, 1966)	~55	–	–
– Rocky Mountains (Stuart et al., 1964; Pakiser, Steinhart, 1964; Pakiser, 1965)	~50	6,5	7,9 – 8,2
– Sierra Nevada (Eaton, 1963)	~50	6,2 – 6,4	7,9 – 8,0
– Tien-Shan, Pamiro-Alai (Kosminskaya, Risnitsenko, 1964; Kosminskaya, 1958)	50 – 70	6,0 – 6,1	8,1
– Kopet-Dag (Godin et al., 1962)	~55	–	–

III. BASINS AND PLATFORM SUBSIDENCES

a) With crustal thinning			
– Great Valley, USA (Stuart et al., 1964; Pakiser, Steinhart, 1964; Eaton, 1963)	~20	6,0 – 6,1	7,9
– Hungarian basin (Stegena, 1964)	20 – 27	6,0 – 6,1	8,1
– Poplain (Di Filippo, Peronaci, 1961)	~35	5,7	8,2
– Black Sea (Kosminskaya, Risnitsenko, 1964)	23 – 26	5,6 – 6,1	8,2 – 8,4
– Dnepr graben (Sollogub et al., 1966)	38	6,4(?)	8,2
b) With crustal thickening			
– Ferghana depression (Kosminskaya, Risnitsenko, 1964)	53	6,2	8,3

In the Basin and Range province (in the US, between the Sierra Nevada and the Rocky Mountains), the basins are underlain by thin, the ranges by thick crust (Thompson – Talwani 1964).

The Po Basin depression in Italy has a thinner crust than its surroundings (Carrozzo–Morelli 1965, Di Filippo – Peronaci 1961). The crust of the Black Sea is also very thin (Fig. 6) (Subbotin et al. 1965, Kosminskaya – Risnitsenko 1964).

A crustal-research profile across the Ukrainian Platform has shown up three subsidences with thin crust and three shields with thick crust (Sollogub et al., 1966), (Fig. 7).

In the Tien-Shan and Pamir regions it has likewise been established that mountain ranges are underlain by a thick crust, basins by a thinner one (Krestnikov – Nersesov 1962, Khain 1964).

There is a great deal of further evidence to support the hypothesis just proposed. Only one region of young subsidence with a thick crust has so far been discovered. It is the Ferghana Basin (Kosminskaya and Risnitsenko 1964) with a crustal thickness of about 50 km. Its very special

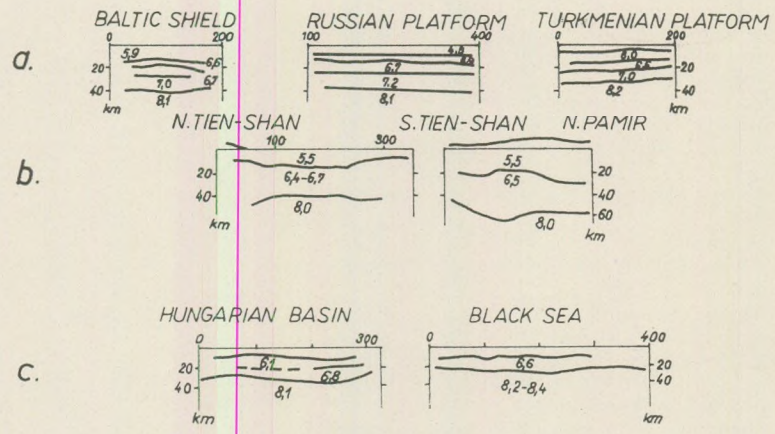

Fig. 6. Crustal structure of platforms and shields (*a*), alpine mountains (*b*), and subsidences. (*c*) (*a* and *b* after Kosminskaya – Risnitsenko, 1964, *c* after Stegena, 1967)

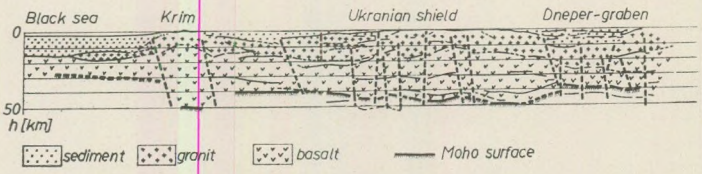

Fig. 7. Crustal structure from the Black Sea to the Voronesh Massiv (After Sollogub et al. 1966)

position, however, among the tall mountains of the Alai Pamir, and its intensely folded, relatively young structure make it an exception that does not detract from the general validity of the theorem that

subsidences all over the world possess a thin or very thin crust

and its corollary that

subsidence and crustal thinning are causally correlated, syngenetic.

There is further considerable support to the statement that

the prime mover of subsidence very probably is crustal thinning.

If we accept the hypothesis that subsidence owing to crustal thinning was brought about by an isostatic mechanism, then a thinning by 8 to 10 km of the crust corresponds to a subsidence of about one kilometre.

The "standard" (mean) upper mantle is denser by 0.4 to 0.5 gcm^{-3} than the crust (Press 1961, Subbotin et al. 1965). This is a sufficiently confirmed figure which can be derived among others also from the mean elevation of continental regions, as follows (Fig. 8.). Let us imagine that we have removed sea water, bottom sediment and basaltic crust from the oceans and replaced it by mantle matter of equal weight. Then the mean continental surface overtops the mean oceanic surface resulting from the above operation

by 5 km in a fairly good approximation. By the condition of buoyant equilibrium,

$$\delta_2 h_2 = \delta_1 (h_1 + h_2);$$

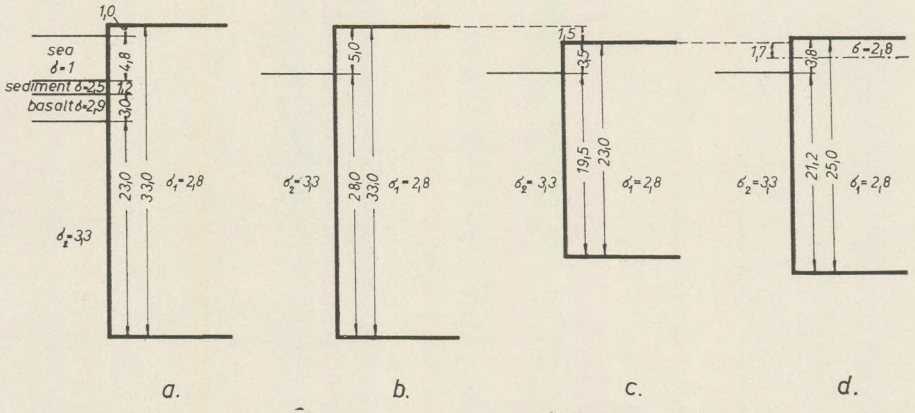

Fig. 8. Crustal structures in isostatic equilibrium. *a)* means "normal" crust, *b)* the same, with marine structure computed for crustal material, *c)* crust thinned by 10 kilometers; the surface subsides 1,5 kilometers; *d)* at the top of a thinned crust 2 kilometers of sediment, the old surface subsided by 1,7 kilometers more

whence, substituting for $h_1 + h_2$ the mean crustal thickness of 33 km of the continents, for δ_1 the density of the continental crust, 2.8 gcm^{-3}, and for h_1, the above value of 5 km, we obtain

$$\Delta\delta = \delta_2 - \delta_1 = 0.5 \text{ gcm}^{-3}.$$

Now let us remove in thought one kilometre of crustal matter from the bottom of the crust. Using the same formula for buoyant equilibrium, and substituting $\delta_2 = 3.3$, $\delta_1 = 2.8$ gcm^{-3} and $h_1 + h_2 = 32$ km, we obtain $h_1 \sim 4.85$. That is, a thinning of the crust by one kilometre entails a subsidence by about 0.15 kilometre. Hence, 10 km of thinning results in a subsidence of 1.5 km. Since the upper mantle below the Carpathian Basin is supposed to be less dense (Renner – Stegena 1965, Stegena 1967), a subsidence of one kilometre is the most probable value.

It is further easy to show that 2.5 km of sediment, gradually deposited into the depression brought about by the above mechanism, accounts for further 1.5 km of subsidence. If in the above fictive experiment we add one kilometre of crustal matter to the top of the crust, rather than removing one kilometre from its bottom, we obtain with the new equilibrium condition the value of 5.15 km for h_1; that is, the former surface will lie at an altitude of 4.15 km, which corresponds to a sinking of 0.85 km against the original situation. 2.5 km of unconsolidated sediment exert the same pressure as about 1.8 km of crustal matter. Hence, the restoration of isostasy requires a subsidence of $1.8 \cdot 0.85 \sim$ $\sim$ 1.5 km purely on account of the sedimentary load.

Thus our fundamental assertion is proved.

There remains to be discussed the mechanism by which the supposed crustal thinning and subsidence could have taken place. Evidence is insufficient to solve this problem in a satisfactory manner: still, we feel that the following considerations are sufficiently justified.

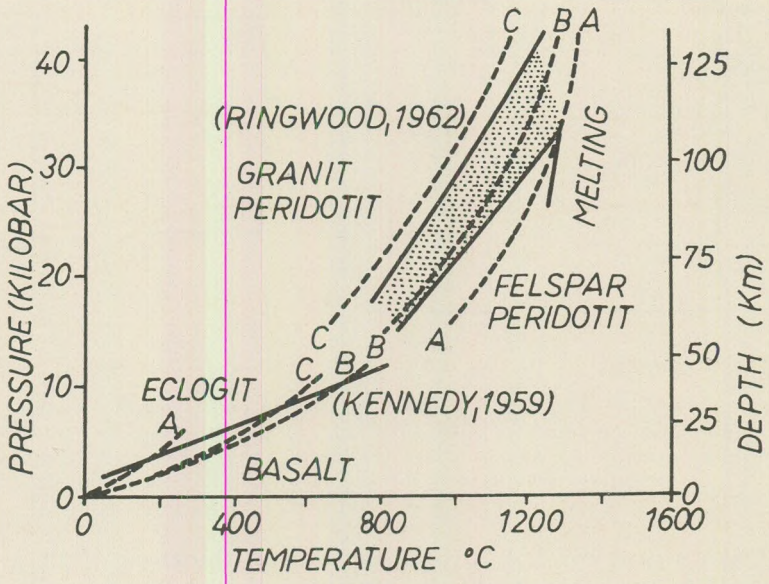

Fig. 9. The basalt-eclogite transition curve (after Wyllie, 1963)

1. Supposing the Moho interface to be due to a basalt-eclogite phase change occurring at about 10^3 bars and a temperature of about 500° C (Fig. 9), it is an obvious conclusion that changes in temperature will shift this phase interface up or down, as the case may be (Fermor 1914, Wyllie 1963, Yoder – Tilley 1961).

2. Supposing the Moho interface to represent a change in the chemical composition of rocks, with basalt above it and an ultrabasic rock (peridotite) beneath it, displacements of the Moho interface necessarily entail the displacement of matter (e.g. by a magmatic-current mechanism).

If one of the above two hypotheses is true (which is not necessarily the case: both have been criticized, see e.g. Stegena 1966b), then decision is easy. The basalt-eclogite phase interface is shifted downwards by temperature rises. The density of basalt being less than that of eclogite, the formation of basalt at the expense of eclogite should entail an elevation of the region in question. If, as many authors suppose, heat flow in the Hungarian basin is higher than average (to prove this conclusively will require some further research), then the basalt-eclogite phase transition hypothesis may be summarily rejected (Fig. 10). (The present heat flow through rocks represents the heat balance of about 10 million years ago: this is the time required for the heat to surge from the depth of the Moho interface.)

The hypothesis of magmatic currents can be raised in the form of assuming, with E. Szádeczky-Kardoss (1968) that, previous to the Pannonian, the rising branch of a fairly small convection cell was situated beneath the Carpathian Basin: turning into the horizontal, this current eroded away, partly by selective migration presumably, some of the crust in the basin, and deposited it where the descending branch of the cell dipped under, that is, beneath the Carpathian ranges.

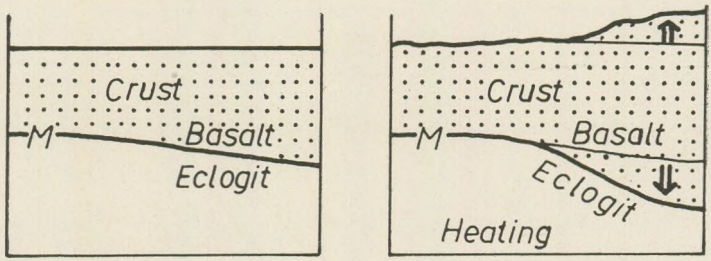

Fig. 10. Heating causes submergence, after the basalt-eclogite transition theory

REFERENCES

Balkay, B. (1959): Crustal structure below Hungary. Annales Univ. Sci. Bp, Sectio Geol. *2.*

Balkay, B. (1960): Probleme der tektonischen Spannungsverteilung im Karpatenraum. Geologische Rundschau *50.*

Balkay, B. (1961): On the Neozoic magma tectonics of Hungary. Acta Geol. Acad. Sci. Hung. *7.*

Bullen, K. E. (1965): Crustal thickness in Australia. Annals of the IGY, XXX.

Carrozzo, M. T. – Morelli, C. (1965): Model Earth calculations and correlations with Moho depths. Boll. di Geofisica, *28.*

Closs, H. (1965): Results of explosion seismic studies in the Alps and in the German Federal Republic. The Upper Mantle Symposium, New Delhi.

Cram, I. H. (1961): Crustal structure refraction survey in South Texas. Geophysics.

Dank, V. (1963): A délalföldi neogén medencék. (The Neogene basins of the southern part of the Great Plains). Földtani Közlöny *93.*

Di Filippo – Peronaci (1961): Struttura della crosta terrestre nelle Pre-Alpi Lombardo-Venete quale risulta dello studio del terremoto del Garda del 19. 2. 1960. Ann. Geofisica, *4.*

Eaton, Y. P. (1963 : Crustal structure from San Francisco, California to Eureka, Nevada from seismic-refraction measurements. Jour. of Geophys. Res. *20.*

Fermor, L. L. (1914): The relationship of isostasy, earthquakes and volcanicity to the Earth's infraplutonic shell. Geol. Magazin *51.*

Fuchs, K. et al. (1963): Krustenstruktur der Westalpen. Gerlands Beitr. *3.*

German research group for explosion seismology (1964): Crustal structure in Western Germany. Zeitschr. f. Geophys. *5.*

Gálfi, J. – Stegena, L. (1957): Tiefenreflexionsversuche in Ungarn zum Studium der kontinentalen Aufbauung. Geol. Rundschau.

Godin, Y. N. et al. (1959): Progress in geophysical methods for prospecting for oil and gas in the USSR. World Petrol Congress 5, New York.

Godin, Y. N. et al. (1962): Osobennosti strojenija zemnoi kori zapada Srednej Azii. Dokladi AN USSR *4.*

Khain, V. Y. (1964): Evolucia zemnoj kori i vozhmosnie formi yeye swjazi s processami w verchney mantii. Sovietskaya Geologia *6.*

Kertai, Gy. (1957): A magyarországi medencék és kőolajtelepek szerkezete. (Structure of Hungarian basins and oilfields). Földtani Közlöny *87*, 383–394.

Krestnikov, V. N. – Nersesov, I. L. (1962): Tektonicheskoe stroienie Pamira i Tien Shana. Sovietskaya Geologia *11.*

Kosminskaya, I. P. – Risnitsenko, Y. V. (1964): Seismic studies of the Earth's crust in Eurasia. in Research in Geophysics, *2.*

Kosminskaya, I. P. (1958): Stroienie zemnoi kori po seismicheskim dannim. Bull. M. O-Va Isp. Prirodi, Otd. Geol. *4.*

Kőrössy, L. (1964): Tectonics of the Basin Areas of Hungary. Acta Geol. VIII. Budapest.

Litvinenko, I. V. – Nekrasova, K. A. (1962): Osobennosti glubinnogo seismicheskogo zhondirovaniya na Baltiiskom stite. GSZ Zemnoi Kori v SSSR, Moscow.

Mituch, E. (1966): A magyarországi kéregkutatás folytonos harántszelvényezéssel kapott eredményei. (Results of seismic crustal research with continuous profiling in Hungary). Geofizikai Közlemények, XV. 1–4.

Mituch, E. (1967): A földkéregkutatás legújabb eredményei Magyarországon. (Newest results of seismic scrustal research in Hungary). Geofizikai Közlemények, XVI. 1–2.

Mituch, E. – Posgay, K. (1965): A hazai szeizmikus kéregkutatás fejlődése és eddigi eredménye. (Evolution and results of seismic crustal research in Hungary). Földtani Kutatás, *2.*

Pakiser, L. C. – Steinhart, J. S. (1964): Explosion seismology in the Western Hemisphere. in Research in Geophysics, *2.*

Posgay, K. (1967): A magyarországi földmágneses hatók áttekintő vizsgálata. (A comprehensive survey of geomagnetic masses in Hungary). Geofizikai Közlemények XVI. 4.

Press, F. (1961): The Earth's crust and upper mantle. Science, 133. 3463.

Renner, J. – Stegena, L. (1966): Magyarország mélyszerkezetének gravitációs vizsgálata. (Gravity research of deep structure of Hungary). Geofizikai Közlemények, XIV. 1–4.

Sághy, Gy. – Vándor, B. – Varga, I. (1967): A kisalföldi refrakciós mérések földtani eredményei. (Geological results of seismic refraction measurements in Little Hungarian Plains). Földtani Közlöny *97*, 160–166.

Sollogub, V. B. – Pavlenkova, N. I. – Tsekunov, A. V. – Hilinskij, L. A. (1966): Glubinnoe stro'enie zemnoi kori vdoly meridionalnogo peresetsenia Chernoje More Voronezhski Massiv. Geofizichesky Sbornik AN USSR, 15.

Stegena, L. (1966a): Il principio dell'attualismo e la superficie Moho. Boll. di Geofisica VIII 31.

Stegena, L. (1966b): On the possibility of diffusion at the M discontinuity. Boll. di Geofisica VIII. 32. 309–317.

Stegena, L. (1967): A Magyar Medence kialakulása. (Evolution of the Hungarian Basin). Földtani Közlöny.

Stegena, L. (1964): The structure of the Earth's crust in Hungary. Acta Geologica 1–4.

Subbotin, S. I. – Naumchik, G. L. – Rakhimova, I. Sh. (1965): Influences of upper mantle processes on the structure of the Earth's crust. Tectonophysics, 2. 2/3.

Szádeczky-Kardoss, E. (1968): A Föld szerkezete és fejlődése. (The Earth's structure and evolution). Akadémiai Kiadó, Budapest, in press.

Szénás, Gy. (1965): A geofizikai térképezés földtani alapjai Magyarországon. (The geological principles of geophysical mapping in Hungary). ELGI Évkönyv II.

Thompson, G. A. – Talwani, M. (1964): Geology of the crust and mantle. Science, 3651.

Wyllie, P. J. (1963): The nature of the Mohorovicic discontinuity, a compromise. Journ. of Geophys. Res. 15.

Yoder, H. S. – Tilley, C. E. (1961): Origin of basalt magma: an experimental study of natural and synthetic rock systems. Journ. of Petr. 3.

CORRELATION OF QUANTITATIVE PETROGRAPHIC CHARACTERISTICS OF PYROXENE ANDESITES IN THE VOLCANIC COMPLEX OF THE SOUTHWESTERN CSERHÁT HILLS

by

P. ÁRKAI

(Geochemical Research Laboratory of the Hungarian Academy of Sciences)

(Received: 30th August 1967)

SUMMARY

The paper deals with quantitative microscopic characteristics of pyroxene andesite lava rocks, relationships between the individual characteristics and their possible use as volcanologic and petrographic facies indices. The characteristics in question include:

1. mineral composition and its changes,
2. textural features of the rock (grain size and seed number distributions of the constituent minerals),
3. the chemical composition of rock-forming minerals, as function of grain size.

Analysis of the above characteristics yields several parameters indicative of rate of cooling, and permits to separate volcanic from subvolcanic rocks, to recognize hypomagmatic-, endo- and exometamagmatic processes, and to reconstruct the process of crystallization.

Outline of the geology and volcanology of the Southwestern Cserhát Hills

The subsurface geology of this region is little known. According to T. Szalay (1956), the basin basement consists of Upper Triassic Dachstein limestone at a depth of about 1200 to 1400 m. It is overlain by Upper Eocene limestone, Lower Oligocene clay marl, and Middle Oligocene clay.

The oldest outcropping sediment is Upper Oligocene (sandy clay, sandstone, marl).

The Burdigalian stage of the Lower Miocene is represented by rags of Anomya sandstone, and by terrestrial gravel and conglomerate. Part of the latter is of uncertain age, though.

The deposits of the Helvetian stage of the Middle Miocene are fairly extensive. The Helvetian includes three horizons: the lower consists of terrestrial deposis, the middle of marine sandstone and schlier, the upper of a calcareous byrozoan and brachiopod sandstone.

Lower Tortonian volcanics

According to J. Noszky (1940), the andesites of the Cserhát Hills are uniform products of a volcanic activity of short duration. F. Schafarzik (1880, 1892) distinguished three types of andesite (augite andesite with augite microlites, augite-hypersthene andesite and hypersthene andesite). A. Vendl stated (1932) the three groups to be linked by all sorts of transitional types. Among the andesite dykes of the Middle Cserhát, Gy. Buda (1965) has found evidence of three phases of eruption, which successively had furnished (1) hypersthenic augite andesite (dyke), (2) augite andesite (dyke) and (3) intensely vitreous augite andesite (sheets). The work of I. Kubovics (1963a, 1966) in the NW and NE Mátra Mountains has laid down the foundations of a parallelization of the volcanics of the Cserhát and Mátra. In the following we shall use terms defined in Kubovics (1966), based in their turn on the terminology proposed by Szádeczky-Kardoss – Pantó – Széky-Fux (1960). The parallelization of the volcanics of the Southwest Cserhát and the Western Mátra is given in Table I. Of the andesite types enumerated therein, bronzitic augite andesite, "amafic andesite" and microandesite are characterized as to chemical composition in Table II.

Table I. Parallelisation of volcanics in the Southwest Cserhát and Western Mátra

Southwest Cserhát		Western Mátra		
Western part	Eastern part (Ecskend Plateau)			
		andesitogenic potash trachyte	middle andesite group	middle complex of volcanics
	microandesite	microandesite		
vacuolar andesite	vacuolar andesite	vacuolar andesite		
amafic andesite	amafic andesite	amafic andesite		
		augite-based andesite		
	andesite tuff, agglomerate	fine-grained andesite tuff		
bronzitic augite andesite	bronzitic augite andesite	bronzitic pyroxene andesite		
	andesite tuff?	andesite tuff with lapilli and pumice		
		hypersthene andesite		
		andesite-dacite tuff		
		middle plagioclase-rhyolite tuff		
		hypoandesite	lower andesite group	lower complex of volcanics
		andesite tuff		

There is no obstacle to extending this parallelization to the entire Cserhát region. The term "amafic andesite" covers those andesites that contain very rare phenocrysts of pyroxene or none at all (the augite andesites of earlier authors).

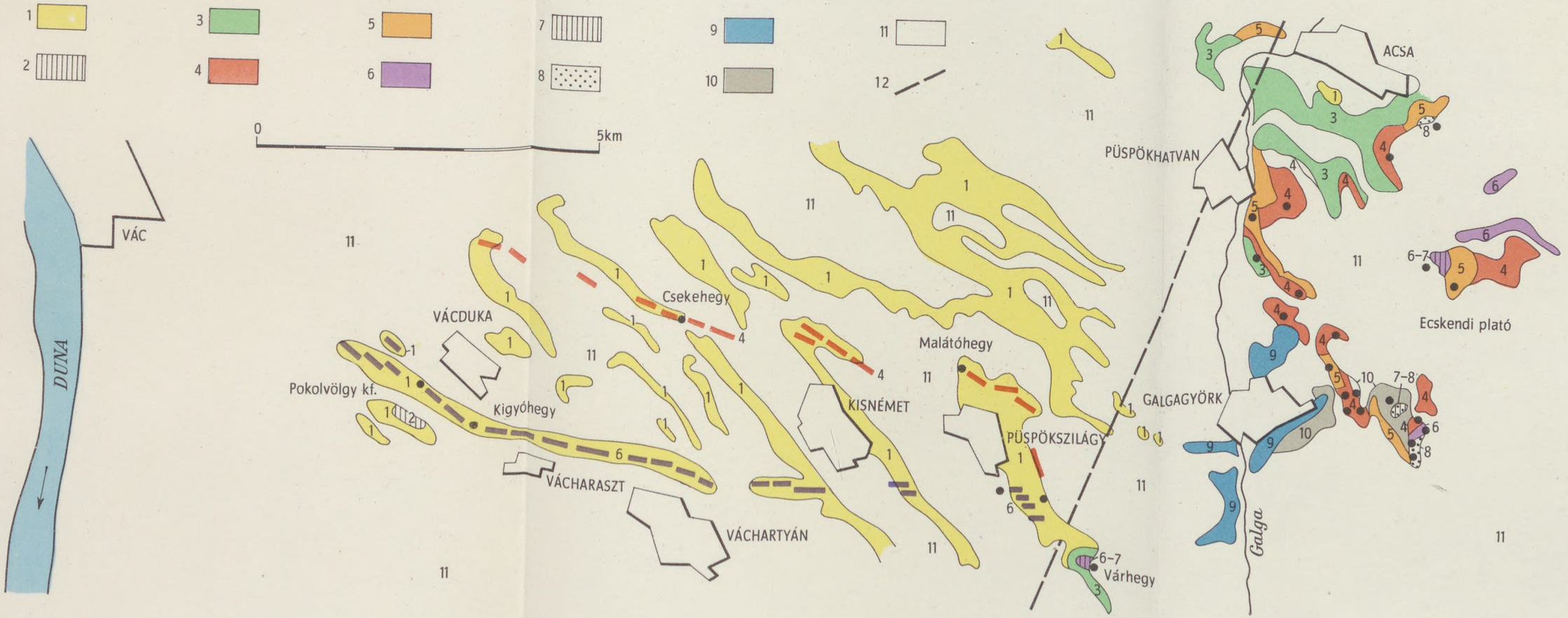

Fig. 1. Geological map sketch of the Southwest Cserhát area. Legend:

1. Upper Oligocene sandy clay; 2. Burdigalian gravel: 3. Helvetian Schlier and sandy limestone; 4. to 8. Lower Tortonian Volcanics; 4. Bronzitic augite andesite. 5. Andesite tuff and agglomerate, 6. Amafic andesite, 7. Vacuolar andesite, 8. Microandesite, 9. Sarmatian limestone, 10. Pannonian sands, clays, 11. Pleistocence loess, Recent floodplain deposits, 12. Tectonic line, ● Sampling localities.

MÁFI. Eng. sz. 28/1968. 600 pld.

Table II. Chemical composition of andesites

	Bronzitic augite andesite, North Dyke, Cseke Hill	Amafic andesite, South Dyke, Pokol Valley	Microandesite Ecskend Plateau, Acsa
Analyst	G. Csajághy	G. Csajághy	K. Emszt
SiO_2	55.51	56.42	56.02
TiO_2	0.92	1.24	1.05
Al_2O_3	15.14	15.44	16.23
Fe_2O_3	1.97	2.66	2.49
FeO	5.00	6.90	7.51
MnO	0.12	0.13	0.09
MgO	4.96	2.52	2.91
CaO	8.30	6.20	7.07
Na_2O	2.50	2.88	4.09
K_2O	2.03	2.77	1.50
H_2O-	0.84	0.85	0.13
H_2O+	2.90	2.05	0.59
P_2O_5	0.17	0.21	0.33
CO_2	0.06	0.00	0.00
	100.42	100.27	100.01

The volcanism of the Cserhát region arose along a fault pattern engendered by tensile stresses of the Styrian phase of orogeny at the Helvetian-Tortonian boundary. Differentiation resulted in a gradual acidifying of the lava within one and the same cycle of eruption. The southward increase of the SiO_2 content suggests an oblique structural feature not unlike a Benioff line. The close volcanologic connection between the Mátra and Cserhát is proved by more and more abundant evidence as work proceeds: (1) the volcanics of the Southwest Cserhát correspond to the middle andesite group of the Mátra and constitute a marginal facies of the latter, (2) andesite dykes and sheets are contemporaneous, easily parallelized, (3) close connection with the Mátra is due to the simultaneous eruption of magmas formed under identical geological conditions, although there are differences in intensity and volume of products.

The upper part of the Tortonian was a period of erosion.

In the lower part of the Sarmatian stage of the Upper Miocene, sediments are predominantly calcareous (brackish Potamides limestone and sandy limestone with miliolinids). Erosion in the Upper Sarmatian is indicated according to F. Szentes (1943) and I. Sándor (1937) by a terrestrial gravel complex.

The Pannonian stage includes lacustrine detritic sediments (sands, sandstones, clays).

Mineralogical and petrographical work

In the course of his work on the Southwest Cserhát, the author wished to trace the variation in space of the following parameters:

1. the mineralogical composition of rocks and the changes in volume percentages of the mineral constituents,

2. the textural parameters of rocks (seed number graphs, grain size distribution graphs of the mineral constituents),

3. the chemical composition of principal minerals and its changes vs. grain size,

4. the chemical composition of rocks and their changes.

For this purpose, a total of 50 samples from one subvolcanic profile and three volcanic ones were examined. Desisting from a detailed quantitative description of the individual types of pyroxene andesite, the author shall concentrate below upon the interpretation of the parameters enumerated above, as well as on their suitability as indices of facies and their correlation.

I. Variation of mineralogical composition

The mineral constitution of a rock depends partly on the chemical composition of the magma, and partly on the geological, physical and chemical features of the locus of solidification. The former is largely reflected by the phenocrysts, the latter by the minerals of the matrix.

Table III shows the mean volume percentages of mineral constituents in pyroxene andesite lava rocks of the Southwest Cserhát.

Table III. Mineral constituents in pyroxene andesite lava rocks of the SW Cserhát. Based on 50 measurements

	1	2	3	4	5	6
	volume percent					
Tabular, lathy plagioclase (phenocrysts + matrix)	41	37	30	45	39	41
Xenomorphic plagioclase (matrix)	12	5	28	4	4	12
Augite	15	19	10	12	10	9
Bronzite	7	9	—		—	—
Opaques	4	1	7	2	2	6
Clay minerals	7	7	19	1	14	8
Carbonate minerals	—	2	3	4	—	—
Glass	14	20	3	22	31	24
Total	100	100	100	100	100	100

1: bronzitic augite andesite dyke, 2: bronzitic augite andesite sheet, 3: amafic andesite dyke, 4: amafic andesite sheet, 5: vacuolar andesite, 6: microandesite.

1. The cooling rate of the magmatic melt emplaced at the locus of solidification is indicated first and foremost by the products of late crystallization in the matrix, such as xenomorphic plagioclase, opaque constituents and glass. Hypidiomorphic laths of plagioclase and xenomorphic grains have already been distinguished by Schafarzik (1880, 1892). Although there are transitions between the two groups, they are usually easy enough to distinguish. Plagioclase laths usually consist of 2 or 3 twin elements and possess

well-defined grain boundaries. Xenomorphic plagioclases are more acid, and more often exhibit undulatory extinction. They are among the last products of crystallization of the matrix. Their outlines are vague; their borders contain opaque inclusions whose abundance increases from the centre outwards. The percentages of the minerals mentioned are closely correlated (Figs. 2 and

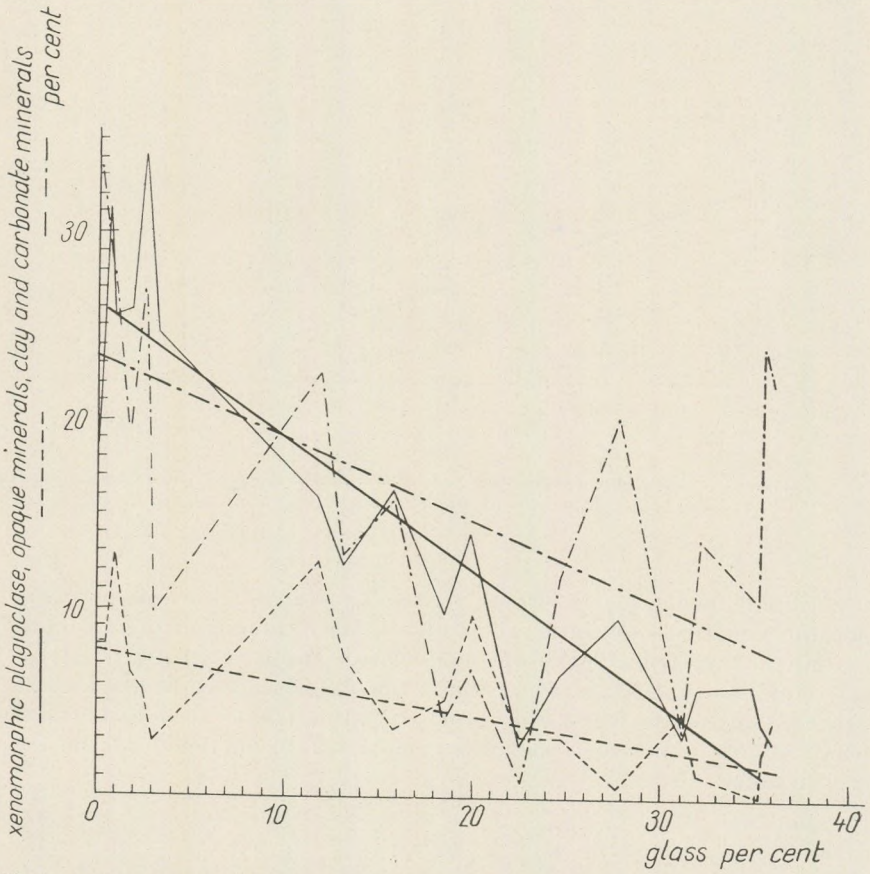

Fig. 2. Content of xenomorphic plagioclases, opaque constitutents, clay minerals and carbonate minerals vs. glass content in the amafic andesite group

3). An increase in the percentage of glass entails decreases in the percentages of automorphic opaque constituents, xenomorphic plagioclase, clay minerals and carbonates. The coefficients of these correlations are as follows:

$$r_{glass-opaque} = -0.5$$
$$r_{glass-xen.\ plag.} = -0.7$$
$$r_{glass-clay+carb.} = -0.5$$
$$r_{xen.\ plag.-opaque} = 0.6$$
$$r_{xen.\ plag.+opaque-glass} = -0.4$$

The last one is a partial correlation coefficient. The correlation as shown above is somewhat understated as actual correlation is impaired by differences in the percentages of phenocrysts between the rock samples, in the intensity of

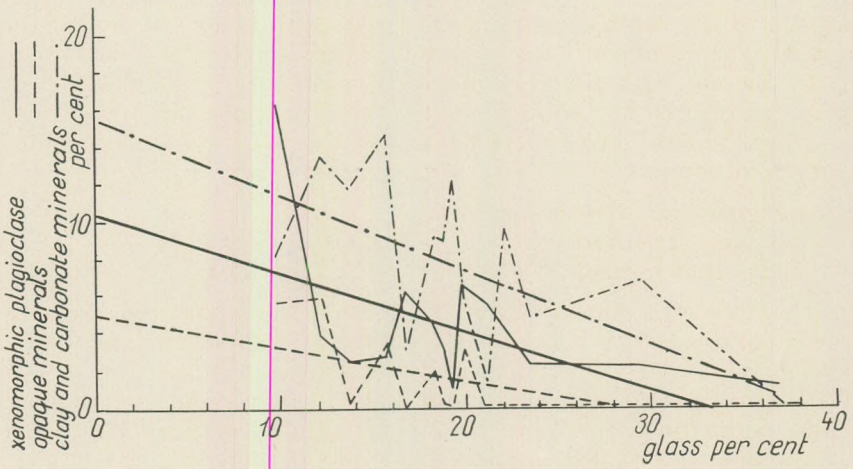

Fig. 3. Content of xenomorphic plagioclases, opaque constituents, clay minerals and carbonate minerals vs. glass content in bronzitic augite andesites

the hypo-and metamagmatic effects that have affected the opaques and volatile-bearing constituents above all, and by measurement errors. Xenomorphic grains and automorphic laths of plagioclase exhibit a strong positive correlation ($\sim 0{,}8$), so that confronting the entire plagioclase content of a rock with the other constituents will yield about the same coefficients of correlation as above. Correlations between the constituents can be modeled by the following linear functions:

amafic andesite	$y_1 = 8-0.2x,\ y_2 = 26-0.7x,\ y_3 = 24-0.4x$
bronzitic augite andesite	$y_1 = 5-0.2x,\ y_2 = 10-0.3x,\ y_3 = 15-0.4x$

where x is glass, and $y_{1,\,2,\,3}$ denote opaque constituents, xenomorphic plagioclases, and volatile-bearing minerals, in that order.

The expression

$$\frac{\text{xenomorphic plagioclases} + \text{opaques}}{\text{glass}}$$

is termed the cooling quotient. It varies inversely as the rate of cooling. E.g. in exposure IA/1−4, a vertical profile of a bronzitic augite andesite sheet 25 metres thick gave the following cooling quotients, upward from the contact with the underlying rock:

distance from contact, metres	2	5	17	22
cooling quotient	1.18	1.51	0.266	0.032.

The transverse profile in the Pokol Valley Quarry of the southern amafic andesite dyke gave, for a total width of 10 m:

distance from contact, metres	0.25	1	5
cooling quotient	16.71	27.20	99.00.

Comparison of the cooling quotients of rocks containing widely different percentages of porphyric constituents is liable to be misleading, so that it is preferable to operate with the percentages of xenomorphic plagioclase, opaques and glass referred to the total amount of matrix taken as 100 percent. The various volcanological facies of the Southwest Cserhát gave the following ranges of cooling quotients:

plugged subvolcanic horizon	100 to 10
volcanic pipe horizon	10 to 0.4
lava sheet horizon	3 to 0.05.

2. The following considerations shall be based upon the transvaporisation theory of Szádeczky-Kardoss (1958, 1959a, 1959b) which can be regarded as sufficiently proved by laboratory and field evidence.

The distinction of the products, often highly convergent, of hypomagmatic, endo- and exometamagmatic processes is often fairly difficult, and more often than not requires a detailed comparative study of the geological surroundings. The variance graphs shown as Figs. 2 and 3 permit to determine the origin of the volatile-bearing minerals provided the volume percentual mineral constitution of a sufficient number of rock samples is known. In these graphs, the percentage of glass is a rough indicator of the rate of cooling of the magmatic melt emplaced at the locus of solidification. In amafic andesites, the volatile-bearing minerals exhibit a minimum about the middle of the graph. The decreasing flank of the minimum indicates that rocks of lower rates of crystallization do more readily absorb transvaporizing volatiles. On the other hand, higher percentages of volatiles occurring together with high percentages of glass are due to the higher hypomagmatic volatile content of rapidly solidifying marginal facies such as contacts, degassing scoriaceous lava surfaces etc. Hence, high percentages of glass and volatiles, found in the same rock, indicate an intense hypomagmatic influence. Metamagmatic effects are revealed by a combination of low percentages of glass and high percentages of volatile-bearing minerals, as it is the unstable glass that is decomposed first. In such cases xenomorphic plagioclase tends to be less abundant than would be expected on the basis of the glass percentage. An exometamagmatic influence (oxidation) results in a decreased abundance of the opaque constituents.

The depth of volatile absorption by the magma can also be determined. If it took place at great depth, no sample of the rock will be without volatile-bearing minerals. Now since in the Southwest Cserhát both groups of andesites include low-volatile (ortho) rocks, it is justified to assume that absorption took place at a level not far below the level of solidification. A further argument in favour of this hypothesis is that the volatile-bearing minerals include calcite, hematite, limonite in some instances, and pyrite, montmorillonite in others, but no epidote; furthermore, vacuolar, scoriaceous "maizestones" are fairly frequent, indicating volatile intake at low pressure and temperature.

The application of the above findings to the various rock types of the Southwest Cserhát leads to the following conclusions. (1) Hypomagmatic influences resulted in the absorption of volatiles at a level not far below the level of solidification. Its products include montmorillonite, calcite, limonite and pyrite largely in the form of spherulites and cavity fillings. The central portions of the magmatic rock bodies are orthomagmatic, their marginal portions hypomagmatic in character. (2) Endometamagmatic processes are largely connected with the group of amafic andesites; even there, they are mostly embryonal. In the south dyke (Pokol Valley) one encounters fissure fillings of pyrite, calcite, montmorillonite, veins and nodes of opal and cristobalite, montmorillonite, and pyrite in the vacoular andesite and microandesite of the Ecskend plateau, fissure fillings of calcite in the bronzitic augite andesite. According to I. Csalagovits (1958), in the region of Bercel and the Szanda Hill, the products of hydrothermal migration of solutions are, in the order of time and decreasing temperature: (*a*) siderite, limonite, (*b*) montmorillonite, (*c*) calcite, (*d*) opal. The hydrothermal traces encountered in the Southwest Cserhát represent the last, decaying, epithermal phase of thermal activity. (3) Exometamagmatic alteration has resulted in the formation of clay minerals and limonite; its typical structural forms are spheroidal exfoliation and pseudoagglomerates, most abundant in the top zones of lava sheets. The order of alteration of the mineral constituents of orthomagmatic rocks is the same under hypomagmatic, endo- and exometamagmatic influences: glass and the pyroxenes of the matrix are decomposed first, the plagioclases of the matrix only later on.

II. Interpretation of texture

The quantitative method of the degree of crystallinity, first proposed by E. Szádeczky-Kardoss, represents an important advance as compared to the qualitative assessments exclusively used before.

Intra-Carpathian ore formations are connected with rocks whose degree of crystallinity is 4 to 6. The mean degree of crystallinity of the entire Cserhát is about 3.1 or 3.2. In the Soutwest Cserhát, the following local values have been established:

bronzitic augite andesite:	
Northern dyke	4.7 to 3.9
Plateau of Ecskend	4.4 to 3.5
amafic andesite:	
Southern dyke	4.9 to 4.1
Plateau of Ecskend	3.9 to 3.8
vacuolar andesite, ditto	3.4
microandesite, ditto	4.6 to 3.2.

The results of the author's texture examinations are presented in the form of cumulative distribution graphs; the grain size distributions of the individual constituents are illustrated by simple distribution graphs.

According to Szádeczky-Kardoss (1967), transvaporization affects grain size along the contact between magma and host rock in one of

two possible ways: (1) rapid cooling and the removal of heat by the volatiles results in a decrease of grain size; (2) at greater depth, the penetrating hot volatiles decrease viscosity and thus increase grain size. In the Southwest Cserhát, the first of the two effects is predominant. The usual notion about this point is that mean grain size is decreased by accelerated cooling, both in the porphyric grain size group and in the matrix. This is not, however, invariably reflected by our graphs: curves crossing each other are fairly frequent. (Fig. 4).

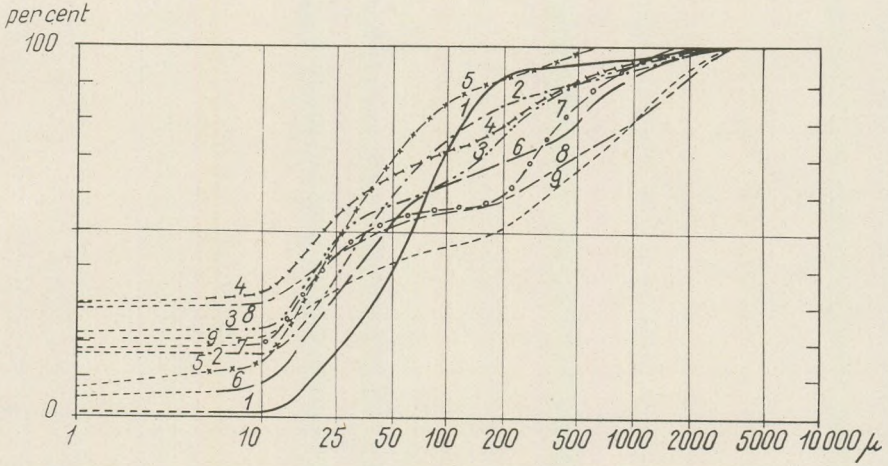

Fig. 4. Cumulative grain size distribution curves of Southwest Cserhát pyroxene andesiste

1. Amafic andesite, South Dyke, Pokol Valley; 2. Ditto, Kígyó Hill; 3. Amafic andesite, Ecskend Plateau, Sample No. III/1;4. Vacuolar andesite, Ecskend Plateau, Sample No. III/3; 5. Microandesite, Ecskend Plateau, Sample No. III/4; 6. Bronzitic augite andesite, North Dyke, Malátó Hill; 7 Ditto, Cseke Hill; 8. Bronzitic augite andesite, Ecskend Plateau, Sample No. IA/4; 9. Ditto, Sample No. IA/2

Grain size distribution and cooling rates are closely related (Szádeczky-Kardoss, 1967). Flat cooling graphs entail grain size distribution curves with sharp peaks. The main difficulty of establishing a mathematical relationship between cooling graph and grain size distribution is that it is only the last section of the cooling graph that can be computed from the size and temperature at the time of emplacement of the volcanic and subvolcanic magma bodies. The hypothesis that most phenocrysts had formed earlier than that is, however, sufficiently confirmed. A preliminary calculation has shown the correlation between the mean cooling rate after emplacement and the mean grain size in the matrix to have a coefficient of -0.7 to -0.9. The coefficient for the phenocrysts is practically zero.

A comparison of fifty cumulative curves from the Southwest Cserhát, eleven from the Middle Cserhát and numerous ones from the Mátra (the latter from Kubovics 1966) suggests the following:

(1) the curves of subvolcanic rocks are steeper and of the one-peak type;

(2) the curves of volcanic rocks are flatter and have two peaks.

(3) As to the evolution of volcanism, unidirectional changes in the features of the volcanic rocks can be demonstrated also for the Southwest Cserhát, particularly as regards the quality and abundance of phenocrysts. The abundance of plagioclase phenocrysts exhibits a gradual decrease. Bronzite does

not occur except in the lava rock of first eruption; it is accompanied by lots of porphyric augite. In amafic andesite, augite phenocrysts are rather scarce, and in the rocks of later formation, augite is restricted to the matrix. Mineral constitution is in the first place a function of cooling rate (S z á d e c z k y -

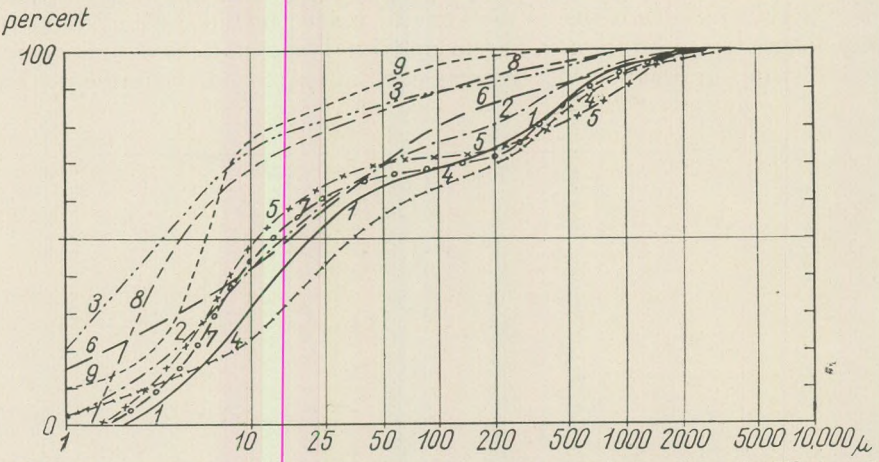

Fig. 5. Cumulative grain size distribution curves of pyroxene andesites from the Western Mátra (after I. Kubovics)

1. Bronzitic pyroxene andesite, lower horizon; 2. Ditto, middle horizon; 3. Ditto, upper horizon; 4. Bronzitic pyroxene andesite dyke ; 5. Amafic andesite sheet; 6. Amafic andesite dyke; 7 Vacuolar andesite, lower horizon; 8. Vacuolar andesite, upper horizon; 9. Microandesite

K a r d o s s 1967): slow cooling about 1000° C gives rise in an andesitic magma to pyroxenes in dependence on vapor pressure; slow cooling about 900° C to amphiboles; slow cooling about 800° C to phenocrysts of biotite. Rapid cooling between 1000 and 800° C gives rise to amafic andesites, microandesites. It is the first eruption, penetrating a cold environment, that begins to crystallize at a relatively great depth; this early crystallization can be identified with the medium-overcooled phase of the cooling graphs; its long duration is proved by the presence of ortho- and clinopyroxenes and the abundance of phenocrysts. At the time of the later eruptions, the host rock is already warmed up, the isotherms have risen, so that the formation of phenocrysts sets in later and later, at higher levels, nearer and nearer to the point of effusion. The phase of medium overcooling is shortened, the rate of cooling accelerates, entailing a scarcity of phenocrysts and resulting in an amafic andesite. Microandesite, the final product of the cycle is formed out of a lava that contained no phenocrysts at all when it poured out over the surface.

The way the grain size distributions of the mineral ingredients reflect the geological environment and the rate of cooling can be shown on lathy plagioclase: the difference between volcanic rocks (considered as such up to a maximum thickness of 30 m) and subvolcanic ones (minimum thickness, 5 m) is as follows.

facies	big phenocrysts	medium grains	matrix
volcanic	maximum at 1000 to 5000 microns	intermediate maximum	maximum at 10 to 25 microns
subvolcanic	ditto	minimum	maximum at 50 to 100 microns

III. Seed number graphs and their applications

Seed number is the number of individual crystals per a given volume of rock. It is a parameter connected with the cooling history of magmatic rocks and permits a refinement of volcanologic facies in their physical and chemical aspects. There are several ways of working with seed numbers. In earlier work (Árkai 1967) relative seed numbers were largely used. Relative seed number is the volume percentage of a mineral in a given grain size class, divided by the measured mean grain size within the grain size class in question, and multiplied with a constant known from the theory of grain size distributions: $R = k\frac{V\%}{d}$. By means of the integrating stage, seed numbers per unit length can also be determined. Relative seed number and seed number per unit length are related by the approximate formula $100\,R \approx 1$ seed number per cm. Seed numbers are usually plotted vs. grain size on bilogarithmic paper. (Figs. 6 and 7.)

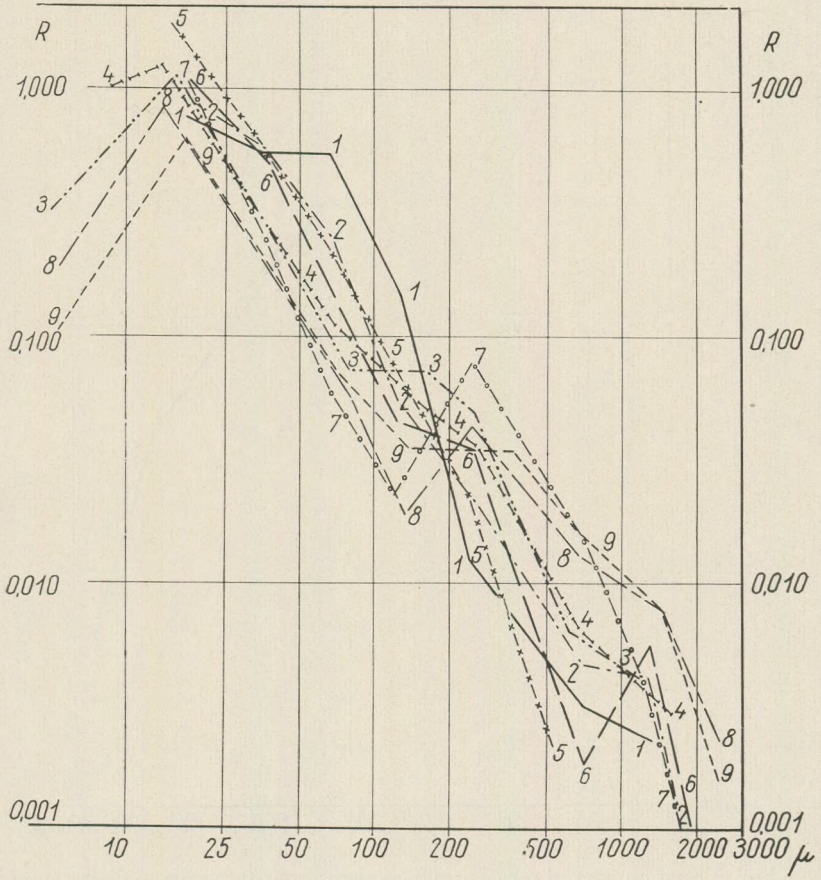

Fig. 6. Relative seed number graphs of Southwest Cserhát pyroxene andesites (for legend see Fig. 4.)

Seed number graphs and cumulative grain size distribution curves are closely related. Both are suitable for comparative studies. Of the manifold uses of seed number graphs, only their use as facies indicators will be dealt with here. Resolution is sharpest in the middle portion of the seed number graph, between 100 and 500 microns. In rocks rich in glass, there is a sharp break with a minimum at 100 to 200 microns and a maximum at 200 to 500 microns. The graphs of subvolcanic rocks are almost straight in the middle section. The amplitude of the minimum is proportional to the rate of cooling of

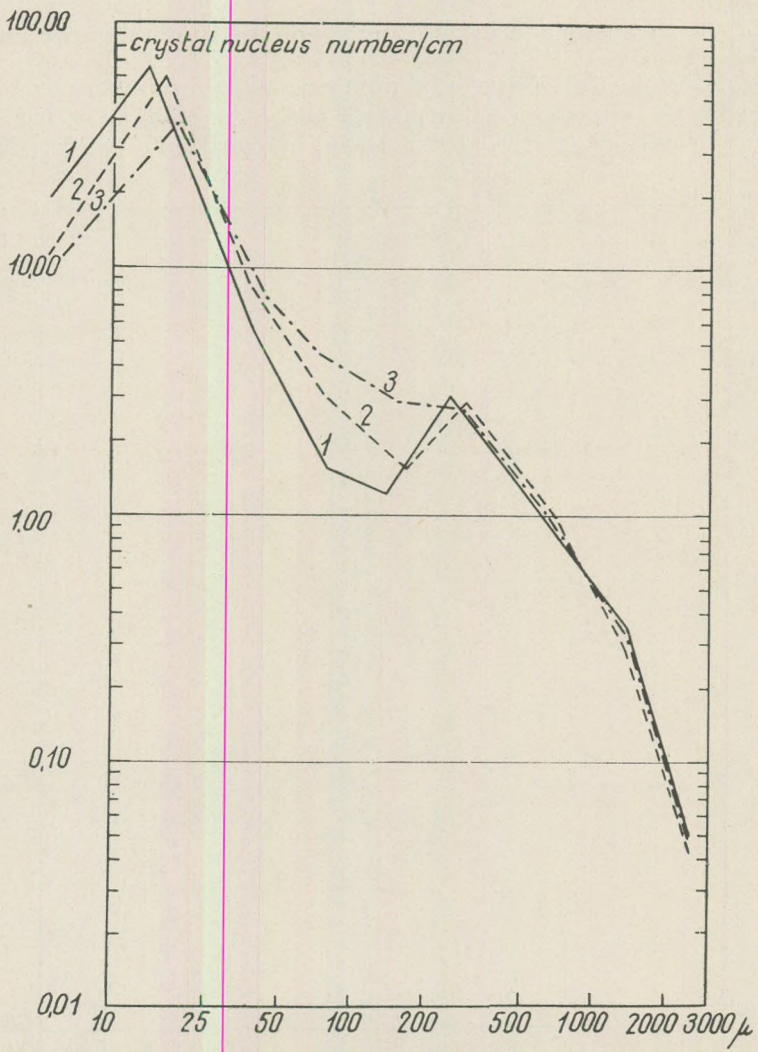

Fig. 7. Seed number graphs of plagioclase in bronzitic augite andesite sheet
1. 0.1 m from contact, 2. 0.2 m from contact, 3. 1.0 m from contact

the emplaced magma. (Fig. 7.) The decrease of seed number in the grain size range below the peak of the matrix indicates the decreasing probability of seed formation, the formation of glass.

Seed number graphs of the Middle Cserhát dykes, computed from data published by Gy. Buda (1965), indicate that both in the north and south dyke, there are alternating sections representing the pipes of subvolcanic bodies on the one hand and of volcanoes on the other. As regards the relative abundances of these sections, the north dyke appears as the root region of a number of volcanoes, whereas the south dyke seems to have communicated more with subvolcanic bodies. Also in the Southwest Cserhát, the difference between the Pokol Hill and Kígyó Hill exposures of the south dyke reflects differences in origin. Although the andesite dykes came to exist as a result of post-tectonic intrusion, the Upper Oligocene sandy clay was hampering the unobstructed flow of the magma towards the surface. This is why both endings of the south dyke are of a plugged, subvolcanic type, whereas a less profound transvaporization in the middle portion suggests an open communication with a number of volcanoes on the surface. A similar phenomenon has been described from the Mátra by Kubovics (1963a, 1963b).

IV. Relationship of quality to abundance in the principal rock-forming minerals

Confrontation of the chemical composition of mineral ingredients with grain size distribution and grain shapes is primarily informative as to the course of the crystallization process. The author has, on his specimens from the Southwest Cserhát, determined by universal-stage methods the chemical composition of 300 grains of plagioclase and 60 grains of pyroxenes.

The plagioclase phenocrysts of bronzitic augite andesite are bytownitic to labradoric in composition; the class of 200 to 500 microns is largely labradoric, the matrix, acid labradoric. On the basis of composition, several groups could be distinguished within the large and medium grain size classes.

Large grain class		Class of 200 to 500 microns		Matrix	
An per c.	Vol. per c.	An per c.	Vol. per c.	An per c.	Vol. per c.
North dyke (Cseke Hill)					
76	8				
67	56	63	50		
56	36	55	50	55	100
Ecskend Plateau (Püspökhatvan)					
76	19	76	23		
66	62	65	46	64	40
57	19	54	31	53	60

Here, An per c. means the percentage of An in the grains, Vol per c. the volume percentage of grains containing that much An within the entire population of plagioclase grains. Between the individual grain size classes, considerable over-

laps are observed. The mean compositions in per cent An of the individual grain size classes are as follows.

North dyke (Cseke Hill)		
63.7	59.0	55.0
Ecskend Plateau (Püspökhatvan)		
66.2	64.2	57.0

Presented in this form, the above data do not unequivocally represent the differences in chemical composition between the two varieties of rock. To improve this situation, abundances have also to be taken into consideration. Multiplication of the An percentages obtained with the respective volume percentages yields parameters expressive of the chemical composition of the entire population of plagioclases:

	Large grain size class	Class of 200 to 500 microns	Matrix	Total
North dyke (Cseke Hill)	525	1130	860	2515
Ecskend Plateau	1320	520	1050	2890

Hence, the plagioclases of andesite sheets are more basic also in the absolute sense. The formation of the most basic plagioclases had begun even before the crystallization of pyroxenes; plagioclase inclusions with 76 percent An have been observed in bronzite, with 68 percent An in augite. According to Gy. Buda (1965), the order of formation of the minerals is a function of magma composition, plagioclases tending to crystallize earlier in a magma high in Ca. This phenomenon is apparent in the bronzitic augite andesites of the Southwest Cserhát, too. In the more basic andesite sheets, the relative abundance of crystals with 76 percent An is 19 percent; in dyke andesite, it is only 8 percent. The more acid plagioclases with 65 to 55 percent An crystallized simultaneously with the pyroxenes.

As regards zoning and inclusions, there are substantial differences between the volcanic and subvolcanic facies of bronzitic augite andesite. The plagioclases of the dyke rock are without inclusions (1, Plate 1), with reverse zoning at the deeper levels and elongate unzoned grains higher up. Plagioclases in the volcanic lava sheets form three groups: one with a border without inclusions about a resorbed core (2, Plate 1), one with a wreath of inclusions indicative of rapid continuation of growth (3, Plate 1), and one of grains without inclusions. The crystals of the medium grain size class are usually without inclusions. The chemical composition of the individual plagioclase groups is as follows:

An per cent

type with inclusionless border		type with wreath of inclusions	inclusionless grain type
core	border		
76	68	67	76
75	57	66 – 57	65
		57	56

The plagioclases of first formation, those with 76 percent An, became resorbed in the convection currents: their growth continued when they came once more into suitably cool surroundings. At that stage, plagioclase with 68 to 66 percent An was formed. The wreath of inclusions is a sign of continued growth, not necessarily preceded by resorption. Not all phenocrysts carry features of all the phases of crystallization: this is a result of the inhomogeneous temperature and composition of the magma.

In determining the composition of pyroxenes in bronzitic augite andesite, the author has adopted the procedures proposed by Hess (1949) and Ruegg (1964) and measured the parameters γ/c, $2V$ and occasionally a/c. In orthorhombic pyroxenes, chemical composition has been inferred from $2V$.

North dyke	77 percent En
Ecskend plateau (Püspökhatvan)	
middle horizon	73 percent En
upper horizon	78 percent En

The composition of the monoclinic pyroxenes is as follows.

Locality	2V	γ/c	Chemical composition
North dyke			
Cseke Hill	55°	41.5°	$Mg_{43}Fe_{11}Ca_{46}$
Malátó Hill	52°	42°	$Mg_{43}Fe_{15}Ca_{42}$
Ecskend Plateau			
Middle horizon	52°	42°	$Mg_{43}Fe_{15}Ca_{42}$
Upper horizon	56°	43°	$Mg_{40}Fe_{15}Ca_{45}$

The monoclinic pyroxenes are augitic in composition, frequently twin-lamellar. Bronzite crystals with augite borders are encountered in both the dyke and lava sheet rocks. According to Poldervaart and Hess (1951), in basaltic magmas the crystallization of pyroxenes proceeds along two entirely different paths. In the augite sequence, iron content gradually increases in the course of crystallization. This explains the changes of composition in our pyroxenes. Some of the plagioclases in the Ecskend Plateau region had formed earlier than the pyroxenes: according to the Poldervaart-Hess augite sequence, monoclinic pyroxenes are indeed later formations. This is confirmed in the case of the orthorhombic pyroxenes by the decrease of the En percentage. The monoclinic pyroxenes of amafitic andesite are formed in the matrix in the late phases of crystallization ($Mg_{35}Fe_{25}Ca_{40}$). (In the other branch of pyroxene crystallization we find the sequence orthorhombic pyroxene – pigeonite – augite.)

Crystallization of plagioclases in amafic andesite begins in a more basic environment, at 85 to 80 percent An and ends usually at 55 percent and in more crystalline rocks at 50 to 48 percent An. Strong reverse zoning prohibits a quantitative evaluation of the chemical composition of the entire plagioclase population. It is very important that even under highly different grain size distributions the mean An contents of the individual grain size classes are about the same.

In the south dyke, inclusions indicating rapid continuation of growth, arranged parallel to the crystallographic axes, are most frequent (4, Plate I).

Reverse and oscillatory zoning with subsequent resorption is the rule (1, 2, Plate 2). The plagioclases of volcanic amafic andesite exhibit an irregular type of wreath of inclusions, a result of resorption. (3, 4, Plate 2). The inner inclusion-bearing portion is invariably more basic (80 per cent An) than the inclusionless border (65 per cent An).

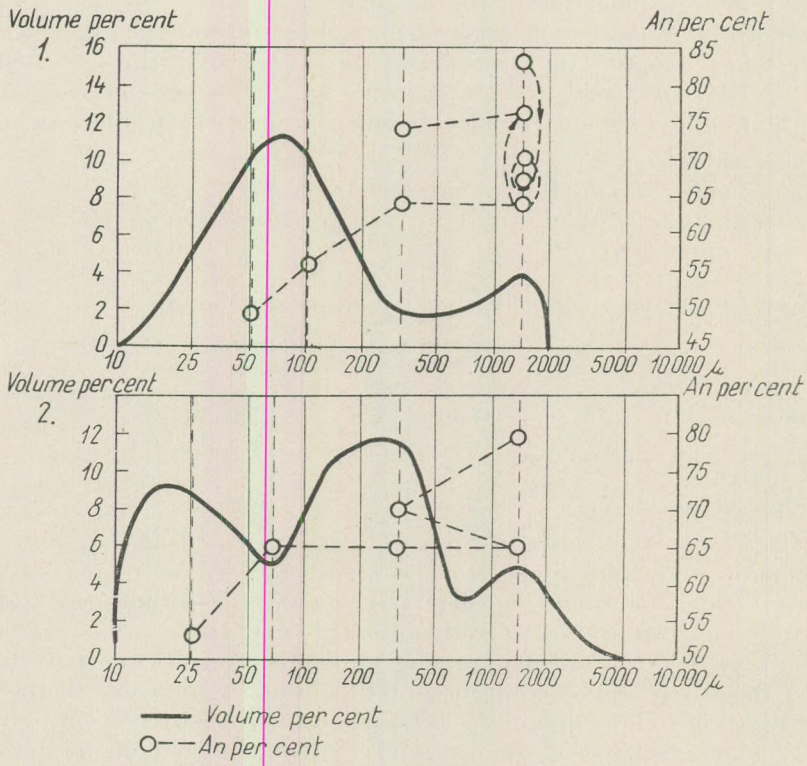

Fig. 8. 1. subvolcanic (South Dyke, Pokol Valley) and 2. volcanic (Ecskend Plateau) facies of amafic andesite: grain size distribution of plagioclases and An percentages. The dashed line indicates the advance of crystallization

Crystallization of plagioclase begins also in microandesites at 80 per cent An, just as in amafic andesites. One or two percent of the grains larger than 500 microns are of such composition. It is remarkable that the scoriaceous marginal facies with a lower content of grains from 200 to 500 microns is more basic (76 to 70 percent An) than the main mass of rock (65 to 55 per cent). The crystallization of plagioclase in the matrix ends at about 55 to 50 per cent An.

The plagioclases of microandesite are inclusionless: the basic interior is surrounded by a narrow, more acid border.

The evidence outlined above justifies the following general conclusions.

(1) During crystallization, the An content of plagioclases gradually varies over the 80 to 50 percent range. In the individual grain size classes, certain An percentages are more frequent than others (Fig. 8).

(2) The chemical compositions of the plagioclases of the individual grain size classes exhibit some overlap. The progress of crystallization is indicated in the figure by dashed lines joining the most frequent compositions.

(3) Differences in grain size are indicative of succession of formation (i.e. bigger crystals are earlier formations) only if the chemical composition of the grains is nearly identical.

(4) The chemical composition of the total plagioclase population cannot be determined except on the basis of a very large number of measurements and then only by tedious computation taking into consideration also relationships of abundances of grain size vs. abundances of composition.

The crystallization of pyroxene andesites is an involved process. In an attempt at interpreting it, let us first characterize the crystallization of plagioclases. The first step is seed formation whose probability (i.e. the number of seeds) increases with overcooling up to a certain limit: beyond that, the tendency to crystallize slackens and glass is formed. Crystallization is initially controlled by temperature (overcooling), later on by diffusion. In keeping with the phase diagram, the first plagioclase seeds are basic (85 to 80 percent An), but the rate of growth of crystals of this composition soon decereases and the formation of plagioclase with 75 to 70 percent An becomes more probable: this means that either the growth of the basic crystals of early formation is arrested or the basic crystals acquire acid borders. The relative frequencies of the two occurrences depend partly on viscosity but largely on the rate of orvercooling. The abundant formation of new seeds tends to indicate rapid overcooling. The inverse relationship between the frequency of occurrence of zoning and the abundance of 200 to 500 micron size grains of plagioclases is remarkable. In that portion of the south dyke where zoning is most intense there is no 200 to 500 micron class to speak, of; in the Cseke Hill portion of the north dyke, where this class is most abundant, there are no zoned crystals at all. Now it is just this grain size class that consists of the early basic crystals that had failed to grow bigger, on the one hand, and of the late seeding of acid crystals, on the other. Hence, the portions with 80 to 60 percent An of the large and medium grain size classes are more or less simultaneous formations. Their grain size distribution is informative of the rate of cooling before emplacement or outflow. As soon as the lava pours out, acid crystals with 60 to 55 per cent An begin to form, but rate of growth is still fairly rapid owing to high temperature, low viscosity and rapid de-gassing, so that the acid crystals forming at this juncture may attain the size of the large-grain class. This phenomenon is, of course, absent in sub-volcanic and dyke rocks. In volcanic rocks, the probability of seed formation increases for a short while after outflow, but rapid cooling prevents the growth of the crystals thus formed into the medium-size class (this is why there is a minimum on the seed number graphs). The process outlined above is, of course, much more complicated in reality. Resorption indicates convection currents; the numerous variants of zoning and of the distribution of inclusions imply the inhomogeneity of

the magma: so that, in the final reckoning, we have to consider crystallization as a stochastic process.

Let us finally collate the volcanological and petrographical evidence obtained by a variety of methods. Fig. 9. shows for the last phase of crystallization the volume percentages of xenomorphic plagioclase, opaque constituents, and glass, all functions of the rate of cooling, vs. the slope of the central section, itself a function of cooling, of the relative seed number graph. Fig. 9.

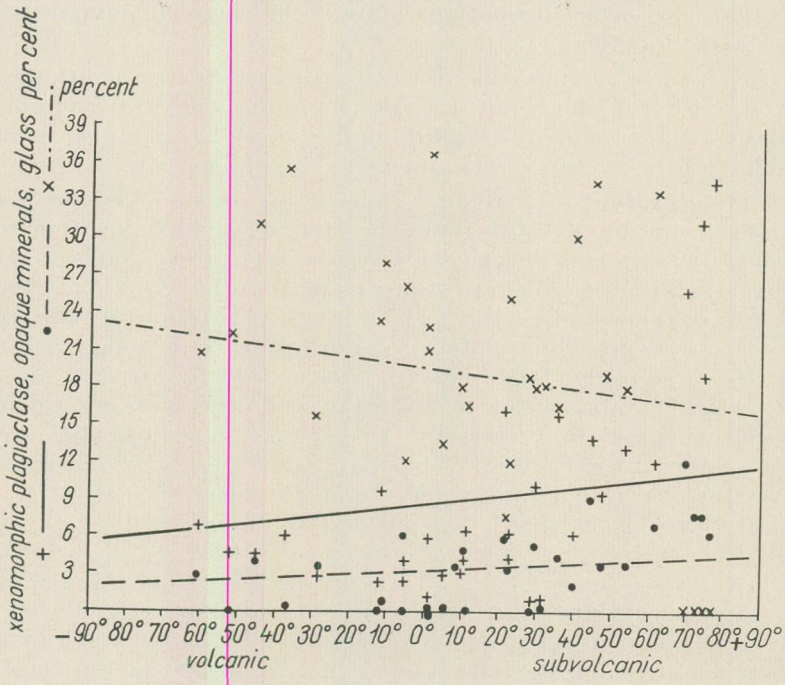

Fig. 9. Slope of middle section of relative seed number graph vs. volume percentages of the minerals figuring in the cooling-quotient formula

The subvolcanic rocks are seen to cluster on the right-hand side, the volcanic rocks of rapid cooling on the left-hand side of the diagram, with the following coefficients of correlation:

$$r_{slope-opaques} = 0.6$$

$$r_{slope-xen.\ plag} = 0.45$$

$$r_{slope-glass} = -0{,}5$$

The relationships involved can be approximated with linear functions as follows:

$$y_1 = 3 + 0.05\,x; \qquad y_2 = 8.6 + 0.13\,x;$$

$$y_3 = 19.5 - 0.13\,x;$$

where x is slope in degrees, $y_{1,2,3}$ are the volume percentages of opaque constituents, xenomorphic plagioclases, and glass, in that order. Correlation is weakened, besides the factors enumerated on p. 92. also by the uncertainties affecting relative seed numbers.

Correlation between cooling coefficient, mean size of plagioclase laths in the matrix and seed numbers of these latter is shown in Fig. 10.

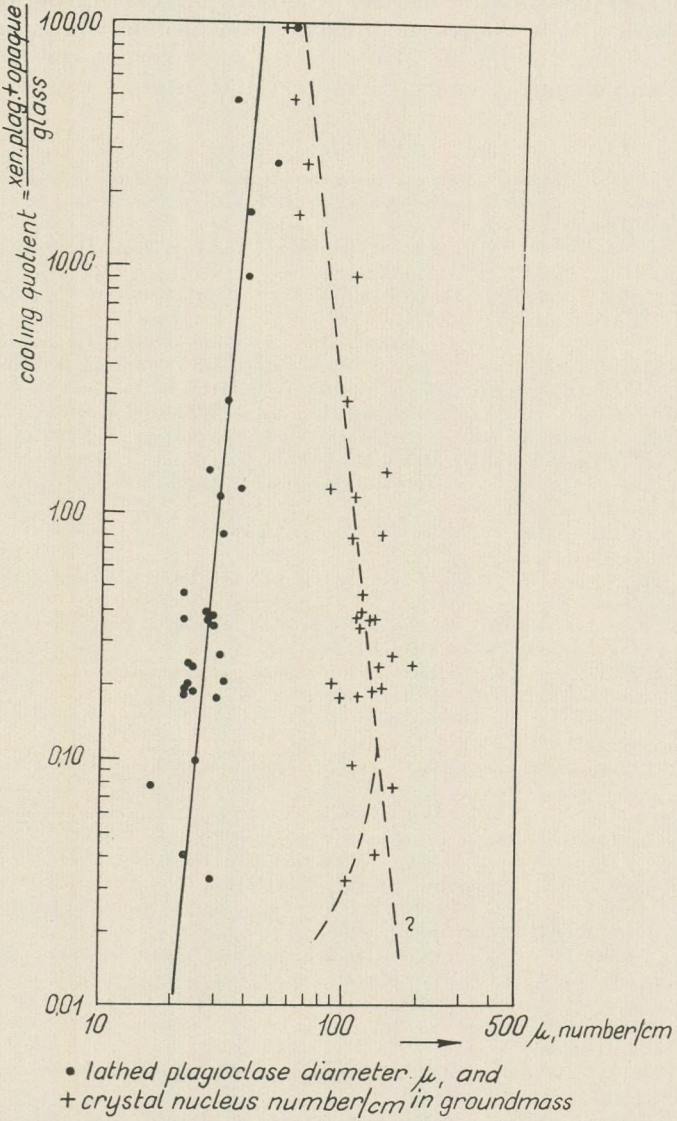

Fig. 10. Mean size of lathy plagioclases in matrix and seed number vs. cooling quotient

The correlation coefficients are

$$r_{\text{cooling coef.}-\text{mean size}} = 0.55$$

$$r_{cooling\ coef.-seed\ number} = -0.8$$
$$r_{mean\ size-seed\ number} = -0.8$$

The equations of these relationships are

$$y_1 = 30x^{0,07}; \qquad y_2 = 106x^{-0,12};$$

where x is the cooling coefficient and $y_{1,2}$ are mean grain size in microns and seed number per centimetre, in that order. An increase in the rate of cooling of the last phase entails a decrease of mean grain size; maximum seed number is related to a cooling coefficient of 0.1. These data permit the computation of the physical and chemical parameters of crystallization.

REFERENCES

Buda, Gy. (1965): Középső-cserháti piroxénandezittelérek földtani vizsgálata (Geological investigation of pyroxene andesite dykes of the Middle Cserhát Hills). B. Sc. Thesis, Eötvös University, Budapest.

Csalagovits, I. (1958): A Bercel–Szandahegy földtani viszonyai (Geology of the Szanda and Bercel Hill). B. Sc. Thesis, Budapest.

Hess, H. H. (1949): Chemical composition and optical properties of common clinopyroxenes. American Mineralogist, *34*.

Kubovics, I. (1963a): Az ÉNy-i Mátra földtani és vulkanológiai vizsgálata (Geological and volcanological investigation of the SW Mátra Mountains), Földtani Közlöny *93*.

Kubovics, I. (1963b): Az ÉK-i Mátra földtani és kőzettani vizsgálata (Geological and petrographical investigation of the NE Mátra Mountains), Földtani Közlöny *93*.

Kubovics, I. (1966): Az ÉK- és Ny-Mátra ásvány-kőzettani vizsgálata (Mineralogy and petrography of the NE and W Mátra Mountains). Candidate's Thesis.

Noszky, J., sen. (1940): A Cserháthegység földtani viszonyai (Geology of the Cserhát Hills), Budapest.

Poldervaart, A. – Hess, H. (1951): Pyroxenes in the crystallization of basaltic magmas. Journal Geol. *59*.

Ruegg, N. R. (1964): Use of the angle A_1/c in optical determination of the composition of augite. American Mineralogist *49*.

Sándor, I. (1937): A Cserhát származiai és pontusi-pannóniai koru üledékei (Sarmatian and Pontian-Pannonian deposits of the Cserhát). D. Sc. Thesis, Budapest.

Schafarzik, F. (1880): A Cserhát DNy-i végének eruptiv kőzetei (Eruptive rocks of the SW end of the Cserhát Hills), Földtani Közlöny *10*.

Schafarzik, F. (1892): A Cserhát priroxén andezitjei (Pyroxene andesites of the Cserhát). Földt. Int. Évk. *9*.

Szalay, T. (1956): A Dunakönyök és a Naszály vidékének tektonikai vázlata (Structural sketch of the Danube bend and of the Naszály Mountain area), Geofizikai Közlemények *5*.

Szádeczky-Kardoss, E. (1958): A vulkáni hegységek kutatásának néhány alapkérdéséről (On some fundamental problems of the study of volcanic regions), Földtani Közlöny *88*.

Szádeczky-Kardoss, E. (1959a): A magmás kőzetek új rendszerének elvi alapjai (Principles of a new system of magmatic rocks). MTA Műsz. Tud. Oszt. Közl. *22*.

Szádeczky-Kardoss E. (1959b): A földkéreg, a magma és a könnyenillók (Crust, magma and volatiles). MTA Geokém. Konf. 1959.

Szádeczky-Kardoss, E. (1967): On igneous rock textures, mineralogical composition and cooling curves. Acta Geol. Ac. Sci. Hung. *11*.

Szádeczky-Kardoss, E. – G. Pantó – V. Széky-Fux (1960): A preliminary proposition for developing a uniform nomenclature of igneous rocks. Int. Geol. Cong. Rep., 21. Ses., Copenhagen.

Szentes, F. (1943): Aszód távolabbi környékének földtani viszonyai (Geology of the brodaer environment of Aszód), Budapest.

Vendl, A. (1932): A Cserhát piroxénandezitjairól (On the pyroxene andesites of the Cserhát Hills), Mat. és Term. Tud. Ért.

Árkai, P. (1967): A Délnyugat-Cserhát magmás kőzetfáciesei (Magmatic rock facies of the Southwest Cserhát), ELTE Természettud. Kara, Tanulmányok a természettudományok köréből.

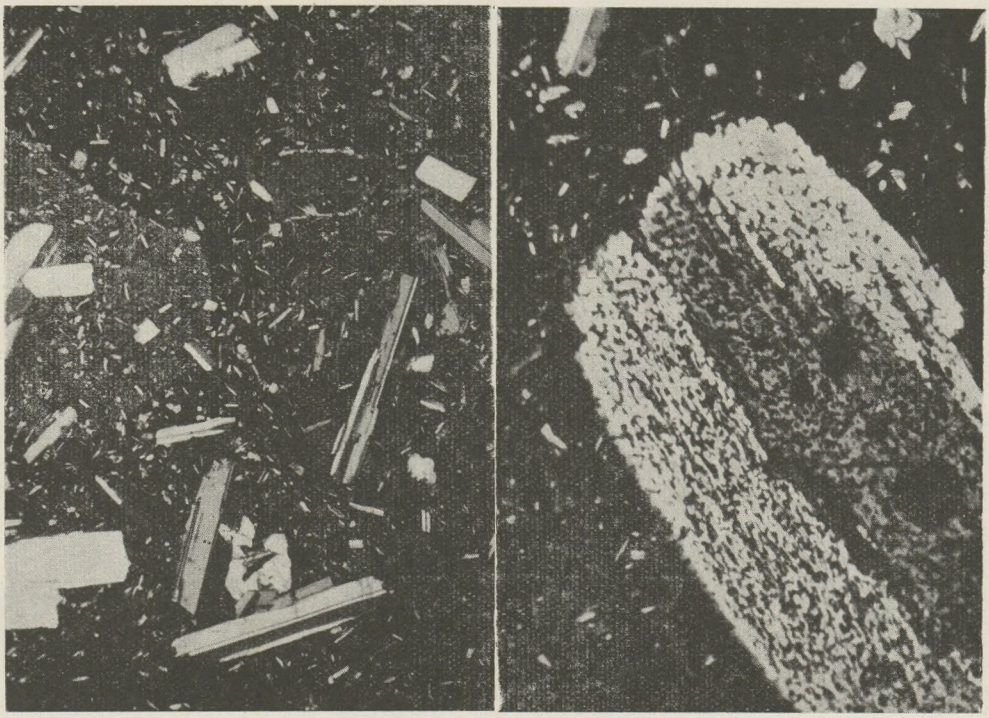

Plate 1.

1. Bronzitic augite andesite, North Dyke, Cseke Hill. Porphyric plagioclases with no inclusion and bronzite with augite wreath. × N, 40x.
2. Bronzitic augite andesite, Ecskend Plateau. Plagioclase with inclusions at the middle. × N, 40x

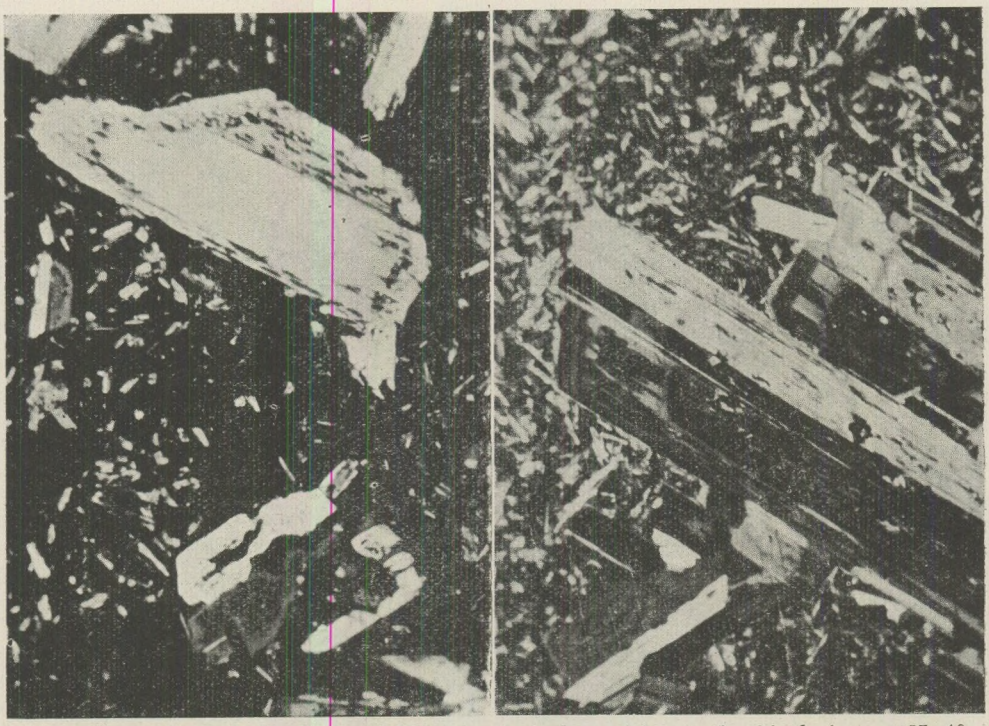

3. Bronzitic augite andesite, Ecskend Plateau, plagioclase with wreath of inclusions, ×N, 40x.
4. Amafic andesite, South Dyke, Pokol Valley. Zoned plagioclase with inclusions, ×N, 40x.

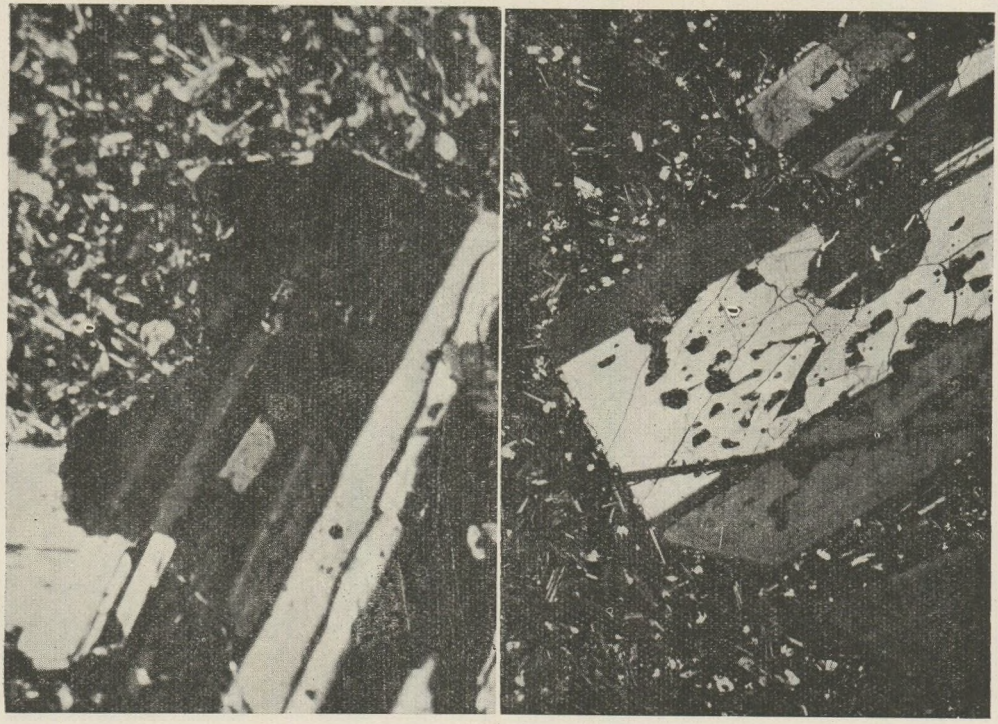

Plate 2.

1. Amafic andesite, South Dyke, Kígyó Hill. Zoned, resorbed plagioclase with inclusions. × N, 40x.
2. Amafic andesite, South Dyke, Kígyó Hill. Resorbed plagioclase with inclusions. × N, 40x.

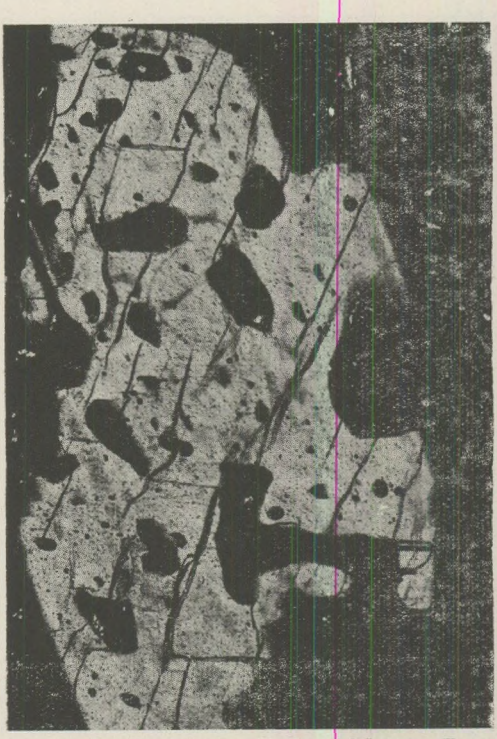

3. Amafic andesite, Ecskend Plateau. Resorbed plagioclase with inclusions. ×N, 100x.
4. Amafic andesite, Ecskend Plateau. Resorbed plagioclase with inclusions. //N, 40x.

NOTICE HISTORIQUE SUR LES VESTIGES VÉGÉTAUX DES TUFS BASALTIQUES DES ALENTOURS DE GLEICHENBERG

Dr. h. c. E. VADÁSZ
(Institut de Géologie, Université, Eötvös Budapest)
(Reçu: le 1. IX. 1967)

Les produits variés, andésitiques et basaltiques de volcanisme miocène dans la partie orientale de la Styrie, dans les collines précurseurs des Alpes et sur le marge du bassin, furent décrits dans un traité fondamental par Stur (1871) qui fit mention aussi des vestiges végétaux rencontrés dans le tuf basaltique. Un an après la parution de son ouvrage, les roches volcaniques des alentours de Gleichenberg furent étudiées par J. Szabó, Professeur de minéralogie et géologie à l'Université de Budapest, au cours d'une excursion de plusieurs jours à l'occasion de laquelle il a fait collection de plusieurs troncs d'arbre fossiles dans la carrière la plus vaste ouverte dans le tuf basaltique, celle près de Feldbach. Szabó a donné la description de l'examen de ces vestiges dans une communication en hongrois (Szabó 1873). Depuis, le volcanisme basaltique de cette région a fait le sujet d'études modernes qui en ont fort bien éclairci et les lignes générales et les détails (Winkler 1913, Heritsch 1922). La flore du tuf a été décrite de façon exemplaire, très illustrative par B. Kubart (1924) et E. Hofmann (1933). Ces ouvrages n'ont cependant pas fait mention de la communication de Szabó*. Kubart explique qu'à cause de la cessation des travaux dans la carrière de Feldbach il lui était impossible de faire un levé de la succession des couches ou des observations précises quant à la position et les conditions de gite des vestiges végétaux. «Dies ist umsomehr zu bedauern, als das Material ganz hervorragend gut erhalten ist, und so schon mit Rücksicht auf das im allgemeinen nicht so gut erhaltene Gleichenberger Material eine ausserordentlich wertvolle und erwünschte Bereicherung unserer Kenntnisse über die Tertiärflora der Oststeiermark

* Ces descriptions phytopaléontologiques parurent toutes après la mort de Szabó en 1894: mais leurs auteurs ont certainement connu la littérature phytopaléontologique hongroise, et ont même étudié des phytofossiles d'origine hongroise; ils ont même eu des contacts personnels avec des géologues et paléontologues hongrois; l'auteur de ces lignes a rencontré dans la correspondence de L. Lóczy sen. une lettre écrite par B. Kubart au temps quand ce dernier fut adjoint à l' Université de Graz (1890), dans laquelle Kubart s'enquiert des galets de «dolomie de tourbe» carbonifères de Secul, Transylvanie.

geboten hätte. Die Hölzer sind *nicht* lignitisiert, sondern bloss gebräunt, zeigen also den gleichen Erhaltungszustand wie das kürzlich behandelte Spondylostrobusholz, das auch von Basaltmassen überdeckt worden war, und lassen sich so auch ohneweiters mit dem Rasiermesser schneiden.» (K u b a r t 1924, p. 6.)

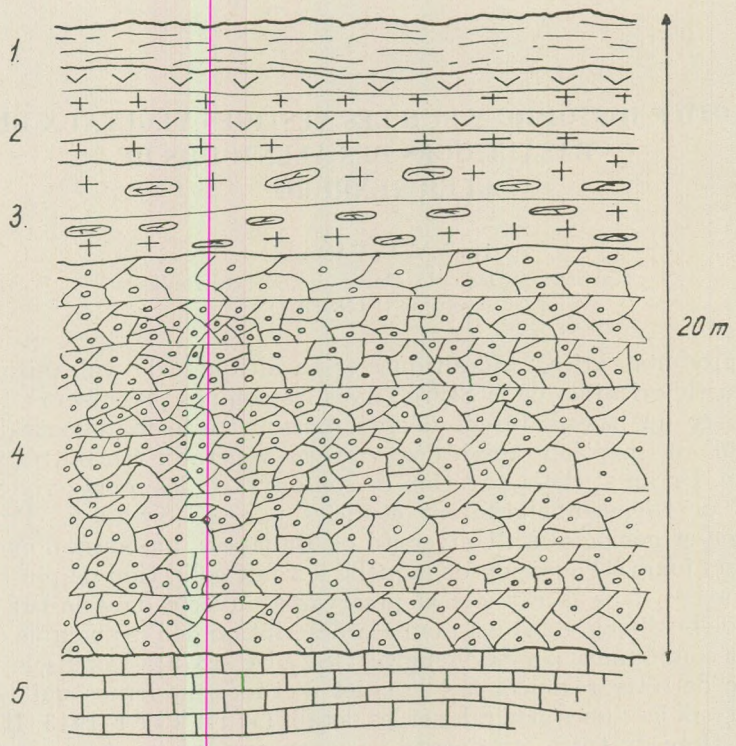

Fig. 1. La succession des couches à Gleichenberg, selon les notes de J. S z a b ó
1. Sol à produits d'altération de basaltes, 2. tuf basaltique peu compacte, 3. tuf basaltique plus dur, à débris végétal, 4. tuf stratifié à galets de quartz et débris de calcaire sarmatien, 5. calcaire sarmatien

L'auteur de ces lignes n'a trouvé non plus aucune trace de données afférant à ces points dans la littérature géologique concernant la Styrie. Il ne sera donc peut-être pas sans intérêt de citer la description qu'en a fait J. S z a b ó (elle se trouve dans le tome XVIII de ses notes d'observation manuscrites, datant des années 1872—74), ainsi qu'une esquisse de la succession stratigraphique, fondée sur cette description, et les notes de A. K o c h (ancien adjoint de S z a b ó qui fut à l'époque de ces évènements professeur de minéralogie et pétrographie à l'Université de Kolozsvár et devint par la suite Professeur de géologie et paléontologie à l'Université de Budapest) concernant l'étude microscopique de ces vestiges de bois par L. J u r á n y i, Professeur de botanique (nos Figs. 2. et 3. reproduisent le manuscrit, inédit jusqu'ici, de K o c h).

La description du gîte par J. S z a b ó suit.

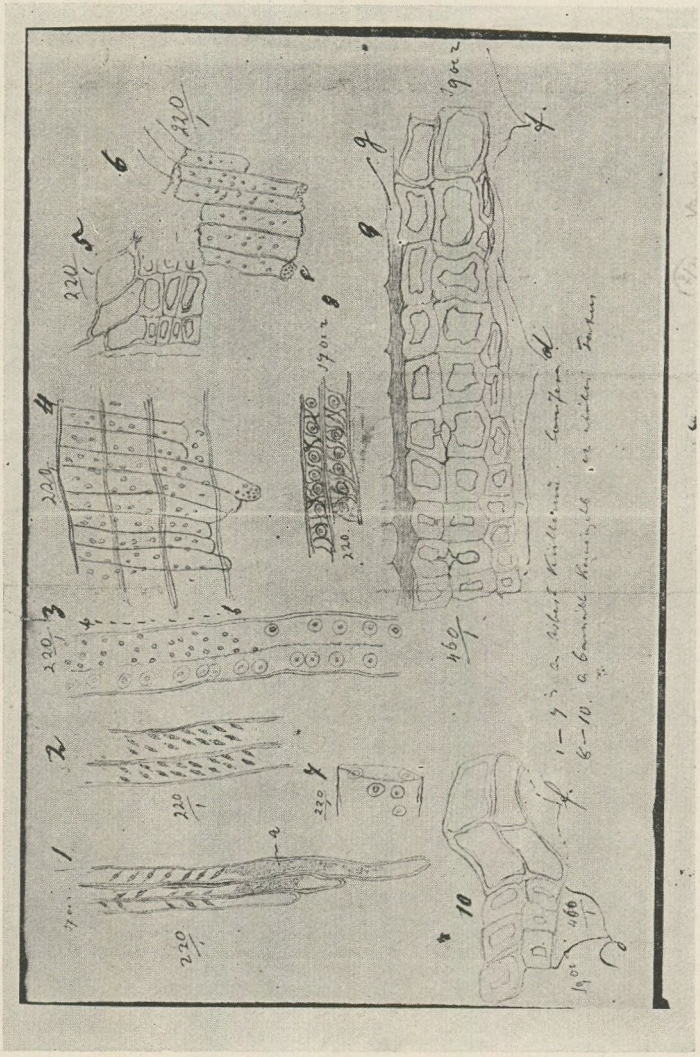

Fig. 2. Dessin microscopique et détermination par le Prof. Jurányi des bois fossiles récoltés par J. Szabó à l'occasion de son excursion à Gleichenberg, le 5. 9. 1873

«Au SW de Feldbach, près du village de Leitersdorf, c'est la carrière du propriétaire Kaintz la plus vaste de toutes les carrières de la région et qui donne la roche la plus dure. Celle-ci est un tuf de basalte, gisant en couches. L'épaisseur visible de la roche est en somme toute de 20 mètres environ. La couche supérieure est une argile basaltique, espèce de limon rouge; au-dessous de celui-ci il y a 2 à 3 m de tuf basaltique altéré, tuf qui n'est pas exploité à cause de son altération profonde. En-dessous il y a deux couches d'épaisseur semblable, en pierre de meilleure qualité celles-ci; c'est elles qui contiennent les arbres sous forme d'inclusions.

«En ce qui concerne la position des inclusions il est remarquable que toutes sont parallèles aux couches, ayant pour la plupart la forme de planches plates: puisque ces morceaux sont souvent longs d'un pied ou d'un demi-pied, cette position est fort bien visible. Leur état de conservation est fort variée. Quant à leur couleur, ils sont d'un brun rougeâtre, ressemblant à un bois torréfié ou à quelques lignites. Ils ne sont guère pétrifiés, puisqu'allumés, ils brûlent assez bien. Quelques-uns sont cependant tellement pourris sur place qu'ils tombent en poussière à la touche, tandis que d'autres sont plus frais et il y en a même de si bien conservés qu'ils se coupent au couteau et qu'on pourrait peut-être même polir. Hormis ces troncs il y a dans le matériel expédié à Budapest un bout de branche, long de 26 cm, ayant un diamètre de 5 cm, dont l'écorce même est conservée. D'après la détermination par Monsieur Jurányi, il s'agit d'un Taxus (cf). Une inclusion fort remarquable et dont on a beaucoup discuté sur les lieux est un vestige végétal sous forme d'une boule, constituée par une matière ressemblant à de l'amiante. Une fois libérée de la roche, la boule s'est révélée d'être composée de fibres de quelques 33 cm de longueur qui, allumées, brûlaient presque comme des fibres de chauvre. Monsieur Jurányi les a reconnu, ceux-ci aussi, comme vestiges de conifères (espèces de pins). Quelques-unes de ces fibres sont fortement attachées d'un de leurs bouts à la roche même. — C'est la pierre au-dessous de ces couches à vestiges végétaux qui est la plus dure et la plus recherchée pour le bâtiment.»

«Parmi les enclaves de ce tuf se rencontrent les morceaux des formations géologiques des alentours: des blocs de taille variée de calcaire grossier à Cérithes, à mollusques bien conservés, des blocs de trachyte et des cailloux de quartz provenant du gravier supérieur à Congéries: ces enclaves se manifestent partout dans cette carrière, du mur jusqu'au toit.»

Szabó mentionne encore que le médecin des bains de Gleichenberg possède un poisson fossile provenant de ces mêmes couches et dont le corps, conservé à deux tiers, porte une tête de 5 cm de diamètre. (Selon Heckel, il s'agissait d'un brochet.) Il considère les couches de tuf basaltique à pendage léger comme un produit de déposition aquatique («d'origine neptunique»).

Cette description du gîte complète la description des bois fossiles par Kubart; les observations de Szabó s'accordent bien avec ce que dit Kubart sur la conservation non-ligniteuse, non pétrifiée des bois qui brûlent et se coupent au couteau. On n'a pas réussi à retrouver les échantillons originaux de Szabó à Budapest: il ne nous était donc pas possible de vérifier les déterminations. Les

Fig. 3. Explication de la Fig. 2. écrite par A. Koch, Le texte en est le suivant:
Explication des dessins

1—7 Cellules du bois d'un Conifère fossile, d'une gerbe à aspect amianteux

1 et 2. Cellules de bois d'automne. Le 1er dessin montre les bouts allongés des cellules; dans quelques-unes il y a un contenu décomposé desséché.

a) et *b)* les ouvertures rondes des perforations en forme de fuseaux. Le 2ème dessin montre des morceaux de ce bois, en contact avec des raies; ici les perforations sont plus nombreuses du même côte de la paroi cellulaire.

3 et 7 Cellules de bois de printemps ou d'été à perforations de forme lenticulaire. La partie b—b de la cellule du 3ème dessin était en contact avec une raie.

4. Cellules de raie couchées sur cellules de bois.

6. Cellules de raie libérées: leurs bouts sont perforés en façon de tamis *c)*.

9 et 10. Coupe transversale d'un Taxus fossile *d)* cellules de bois d'automne à parois épaisses *f)* cellules de bois d'été à parois plus minces. *g)* sur le 9ème dessin est une raie.

8ème dessin coupe longitudinale du même Taxus, avec des perforations lenticulaires (à double cercle) avec des bandes spirales entre eux.

A rajzok magyarázata

1–7. fossil conifera fasejtjei.
Azbest küllemű kőlegekből.

1 és 2. őszi fasejtek. Az 1ső ábrán e sejtek nyilt végei egyesekben a szétszedt zsugorodott tartalom a). ugyanezekben b. nél az orsó alakú vermek kerek nyilásaival. – A 2ik ábra ugyan e fasejtek azon darabjait mutatja, hol ezek bél sugarakkal érintkeznek, itt a vermek nagyobb számmal lépnek fel a sejtfal ugyanazon oldalain.

3. és 7. tavaszi s nyári fasejtek lencse alakú vermekkel. A 3ik ábrában vaskos sejt b–b darabja bélsugárnak érintkezett.
4. fasejteken fekvő bélsugár sejtek.
6. Kiszabadított bélsugár sejtek. egymással érintkező vezlapjaik rosta nemüleg átlikgatva c.,

9 és 10 harántmetszet fossil Taxusból
d vastagfalú őszi fasejtek f vékonyabb falú nyári fasejtek. A 9ik ábrán g bélsugár.
8ik ábra hosszmetszet ugyanazon Taxusból rajta a lencse alakú (kettős körű) vermek s ezek közt lefutó spiral szalagok.

esquisses au crayon des images microscopiques de la texture, dont les photocopies sont joints au présent article, ne contredisent pas à Pseudotsuga, indiquée par Kubart. Cependant, Kubart n'a pas mentionné de vestige fibreux «ressemblant à de l'amiante» comme celui décrit par Szabó. Aussi, E. Hofmann mentionne un cône silicifié de Conifère (Picea sp.). De tels cônes blancs silicifiés, bien conservés, étiquetés «Gleichenberg» se trouvent aussi dans la collection botanique du Musée National Hongrois: l'un d'eux porte un morceau d'un grès brun grisâtre à ciment argileux, se composant de graines de quartz à peine émoussées. La fibrosité ressemblant à de l'amiante et les cônes silicifiés rappellent nettement l'état de conservation, due à des agents post-volcaniques, des vestiges silicifiés de la localité classique du Pannonien inférieur à Megyaszó dans la Montagne de Tokaj (Horváth 1954). L'examen phytopaléontologique comparatif en révélera peut-être l'identité taxonomique (Kubart, 1924). Tout cela indique que les couches de tuf de la grande carrière abandonnée de Feldbach ont livré deux sortes de vestiges végétaux à l'état de conservation nettement différent. L'un de ces types provient de l'ancienne flore vivante des alentours: il est légèrement pourri, non pétrifié. Il s'agit ici de débris flottants de bois. L'autre type est silicifié, et provient des torrents (barranco) dévalant des flancs du volcan, torrents qui ont transporté de plus des galets, des débris de grès et de calcaire sarmatien. Ce fait est prouvé par la stratification aquatique des couches décrites par J. Szabó, ainsi que par la dureté changeante de la roche. Ce processus composé d'éléments de destruction (érosion) et construction (déposition) fixe dans le temps et dans le cadre local l'âge du volcanisme basaltique. Heritsch (1922, p. 59), citant les études détaillées de Winkler, dit: «Ihre Entstehung fällt in die Zeit nach der Ablagerung der Hauptmasse der pontischen Bildungen, beziehungsweise der Belvedereschotter.» Dans l'état présent de nos connaissances nous sommes d'avis que le volcanisme basaltique de la Styrie orientale est contemporain du volcanisme du même type au N du Lac Balaton, sur la marge de la Petite Plaine Hongroise: c'est dire qu'il a duré jusqu'à la limite Pannonien supérieur – Pléistocène, et que ses manifestations post-volcaniques (geyserites, sources thermales) se sont peut-être poursuivies même dans le Pléistocène. Compte tenu de l'analogie de Megyaszó, les vestiges végétaux silicifiés sont les éléments remaniés provenant de dépôts plus anciens (Pannonien inférieur).

LITTÉRATURE

Stur, D. (1871): Geologie der Steiermark, Graz.

Szabó, J. (1873): Bazalt és trachyt Gleichenberg vidékén (Basalte et Trachyte dans les environs de Gleichenberg). Földtani Közlöny *3*, 163–168.

Winkler, A. (1913): Jahrbuch der Geol. Reichsanst.

Winkler, A.: Zeitschrift f. Vulkanologie, I.

Heritsch, F. (1922): Geologie der Steiermark, Graz.

Kubart, B. (1924): Beiträge zur Tertiärflora der Steiermark, Graz.

Hofmann, E. (1933): Pflanzenreste aus dem Gebiete v. Gleichenberg in Oststeiermark (Verh. d. Geol. Bundesanst. Wien.)

Horváth, E. (1954): A megyaszói Csordáskút kovásodott fatörzseinek vizsgálata (Étude des troncs d'arbre silicifiés de la localité dit de Csordáskút près de Megyaszó). Botanikai Közl. *44*.

DEFORMED JURASSIC AMMONOIDS FROM ÚRKÚT (BAKONY MOUNTAINS, TRANSDANUBIA)

by

B. GÉCZY

(Institute of Palaeontology, Eötvös University, Budapest)

(Received: 30th Sep. 1967)

SUMMARY

On the basis of 36 species of ammonites, the ammonitico rosso marl of Csárda Hill near Úrkút belongs to the Levesquei (-Meneghinii) Zone of the uppermost Toarcian. In lithology and fauna, the Úrkút beds closely agree with the deposits of identical age exposed at Csernye: previous lithological and faunistical differences between the two regions gradually disappear during the Toarcian. At the Liassic-Dogger boundary the ammonitico rosso marl passed into a silex at Úrkút: the subsidence of the sea bottom had begun earlier here than at Csernye. Presumably in the Cretaceous, the strata of Csárda Hill underwent a structural deformation amounting to a 15 percent average compression. The major axis of the ellipse of deformation is oriented NNW-SSE, parallel to the structural trend of the Urkut area.

It was Chief Geologist Dr. J. Cseh Németh who in 1960 called my attention to the Jurassic ammonites of Csárda Hill at Úrkút in the Bakony Mountains. With the kind assistance of Dr. Cseh Németh and Dr. J. Noszky I collected a faunule from the waste tip of the open-cast manganese ore pit, which has been closed down since. Examining the fossils I was struck by the strong deformation of most specimens. In order to establish the orientation of the deformation I collected in 1967 a larger fauna from undisturbed strata. I am indebted to Dr. J. Fülöp and Dr. J. Konda of the Hungarian Geological Institute for the sponsoring of this collecting campaign and to Geologist Z. Szabó of the Úrkút Manganese Mine for kindly given assistance. I have myself performed at the Palaeontological Institute of Eötvös University the treatment of the fauna and the measurement of its distortion. In my computations I was assisted by E. Koblinger. The photos reflect the excellent workmanship of Á. Szabó.

An up-to-date review of the geology of the Úrkút region in the southwestern Bakony Mountains is due to Cseh Németh (1967). Csárda Hill proper is situated NW of the village of Úrkút. On the southern flank of the hill, on the southeastern rim of the opencast pit, there is a small exposure of

Jurassic rocks, accessible and easy to investigate. Collecting locality I is situated on the western rim of the pit face, locality II some 15 metres farther east. At both localities, ammonites occur in a well-stratified pink knotty marl

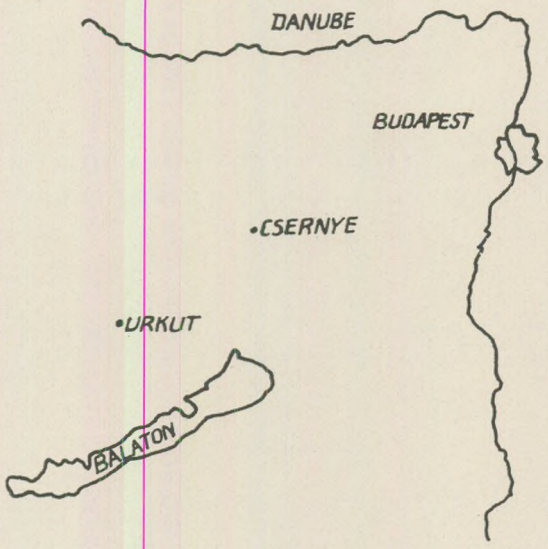

Fig. 1. Map sketch of the Úrkút area

that, according to the classification of Aubouin (1965), corresponds to the "ammonitico rosso marl" facies. At locality I, the strata dip 22° towards 255° at locality II they dip 15° towards 120°. Collection of centimetre accuracy was possible only at Locality II. The ammonitebearing layers are underlain by the manganese carbonate deposit and overlain by cherty radiolarian limestone and silex. Whereas finding out the exact nature of contact with the underlying deposit will require further exposure, contact with the overlying strata is easily observed. The two localities have yielded the following species of ammonites.

Phylloceras? baconicum Hantken in Prinz, 1904
Calliphylloceras beatricis (Bonarelli, 1897)
Calliphylloceras altisulcatum (Prinz, 1904)
Calliphylloceras altisulcatum magnum Géczy, 1967
Calliphylloceras altisulcatum quadratum Géczy, 1967
Calliphylloceras spadae (Meneghini, 1867–1881)
Calliphylloceras cf. *supraliasicum* (Pompeckj, 1893)
Calliphylloceras supraliasicum planulatum Géczy, 1967
Calliphylloceras connectens frechi (Prinz, 1904)
Holcophylloceras ultramontanum (Zittel, 1869?)
Ptychophylloceras chonomphalum (Vacek, 1886)
Lytoceras sublineatum (Oppel, 1862)

Lytoceras subfrancisci Sturani, 1964
Lytoceras hoelderi Géczy, 1967
Lytoceras rasile Vacek, 1886
Lytoceras amplum kocsisi Géczy, 1967
Alocolytoceras ophioneum (Benecke, 1865)
Polyplectus pluricostatus (Haas, 1913)
Dumortieria dumortieri cf. *pannonica* Géczy, 1967
Dumortieria cf. *rhodanica* Haug, 1887
Dumortieria cf. *meneghinii* (Zittel M. S.) in Haug, 1887
Dumortieria meneghinii longilobata Géczy, 1967
Dumortieria sp.
Pleydellia cf. *aalensis* (Zieten, 1830?)
Pleydellia aalensis inaequicostata Géczy, 1967
Pleydellia cf. *burtonensis* (Buckman, 1902)
Pleydellia cf. *dudelangensis* (Maubeuge, 1950)
Pleydellia laevigata (Hantken in Prinz, 1904)
Pleydellia sp.
Hammatoceras sp. aff. *tenuinsigne* (Vacek, 1886)
Hammatoceras sp. aff. *planinsigne merlai* Géczy, 1967
Hammatoceras sp. aff. *brancoi* (Prinz, 1904)
Erycites fallifax (Arkell, 1957)
Erycites subquadratus Géczy, 1967
Erycites sp. aff. *telegdirothi* Prinz, 1904
Erycites elaphus Merla, 1934

On the basis of the *Dumortieria* and *Pleydellia* of stratigraphic relevance, the ammonite-bearing strata of Csárda Hill belong to the Levesquei Zone of the uppermost Toarcian, which in the subdivision of Donovan (1958) corresponds to the Meneghinii Zone of the Mediterranean region. Within this zone, the separation of the Northwest European subzones (Dispansum, Levesquei, Moorei, Aalensis) seems to be rather difficult. It was easy to divide the zone in two according to Donovan (subzones of *Dumortieria meneghinii* and *Pleydellia* sp.), because at Locality II the lowermost layer (No. 4) of 25 cm thickness contained two specimens of *Dumortieria* besides the predominant *Pleydellia* (10 specimens). Layer No. 3. of 20 cm thickness furnished 9 specimens of *Pleydellia* and one of *Dumortieria*. On the other hand, layer No. 2 of 24 cm thickness yielded *Pleydellia* only (11 specimens). The upper fossil-rich subdivision of Locality II corresponds to the subzone "*Pleydellia*" sp. = *aalensis*. At Locality I, this upper subdivision is partly eroded away: the *Pleydellia* (37) are accompanied by some *Dumortieria* (8).

The Csárda Hill fauna, placed into the uppermost Toarcian, is slightly younger than the ammonite-bearing complex of Shaft III of Úrkút (Géczy 1965, 1966, 1967). The fauna of Shaft III represents the Toarcian without its lowermost and uppermost zones (Tenuicostatum and Levesquei). The fauna of Csárda Hill completes the Toarcian succession overlying the manganese deposit.

Noszky (1961) suggested the Úrkút area to possess a complete Jurassic from the Lower Liassic to the Upper Oxfordian, carrying – among others – the index fossils of the Lower Toarcian (Bifrons Zone) and the Lower Aalenian

(Opalinum Zone). In his subdivision, the Csárda Hill fauna corresponds to the upper part of the Jurense Zone. The presence of the Opalinum Zone can be proved also at Locality II on Csárda Hill. Layer No. 1. is overlain by thick beds of silex. 5 cm below the lowermost bed of silex a softer marl has yielded a single specimen of *Leioceras* cf. *opaliniforme*, indicative of the Opalinum Zone. The first traces of silex formation are observed even below the Opalinum Zone, as low as Layer No. 4. The lithostratigraphic separation of the Liassic from the Dogger on the basis of the apparance of the silex is correct in the broad outline; the biochronological border is, however, between the first layers with chert nodes and the first silex beds.

Despite a distance of 40 kilometres, the uppermost Toarcian of Csárda Hill can be readily parallelized with the Csernye deposits described in earlier papers of the author (G é c z y 1966, 1967). In both regions, the uppermost Toarcian consists of ammonitico rosso marl. In both regions, ammonites are predominant; the accessory fauna, exclusively of cephalopods, includes a few belemnites and nautiloids. As far as lithology is concerned, the sole difference is in the level where the silex crops up; its first traces appear in Layer No. 4 on Csárda Hill but only in the Bajocian at Csernye. The uppermost Toarcian of Csernye abounds in Cancellophycus, no trace of which has so far been encountered at Úrkút.

As regards the species making up the faunas, Úrkút and Csernye are alike: all 36 species found in the Csárda Hill layers have already been recognized at Csernye. Nine of the 36 species are exclusive to Csernye and Úrkút *(C. altisulcatum quadratum, C. supraliasicum planulatum, C. connectens frechi, L. hoelderi, L. amplum kocsisi, D. dumortieria pannonica, D. meneghinii longilobata, P. aalensis inaequicostata, L. laevigata.)* Hence, 25 per cent of the Csárda Hill fauna is endemic in a broader sense of the term.

Fig. 2. Number of ammonites per cu. metre of rock at Úrkút (Localities I and II) and Csernye (Exposures *A* and *B*) in the Levesquei Zone

In regard of faunal density, there is a slight difference between the two faunas. In the Tűzköves ravine at Csernye, the thicker Exposure A gave on an average 204,68 specimens per cu. metre of marl; Exposure B, of lesser thickness, gave 126.6 ammonites per cu. metre. At Úrkút, densities similar to those of Exposure B have been established. On an average, one cu. metre of rock gave 124.7 specimens at Locality I, and 122.2 specimens at Locality II. This agreement may be taken to indicate either the uniformity over a large area of primary faunal density, or the uniformity of the conditions of fossilization, or both.

The Mediterranean forms regarded as indicators of great depth (the species of the superfamilies *Phylloceratacеae* and *Lytoceratacеae)* are dominant in both areas. At exposure A of Csernye, 78,9 percent of a total of 673 ammonites belonged to these two superfamilies. The corresponding figures for Exposure B are 82.3 percent of 152 specimens, for Locality I. of Úrkút, 63.5 percent of 156 specimens, for Locality II, 72 percent of 154 specimens. The lower percentage of Locality I is presumably due to the fact that it represents a slightly deeper portion of the Levesquei Zone. At Locality II, it is the rate of change that is remarkable: *Phylloceratacеae* and *Lytoceratacеae* make up 70.2 percent of 47 specimens in lowermost Layer No. 4., 66.6 percent of 39 specimens in Layer No. 3., 68.4 percent of 38 specimens in Layer No. 2, and finally 100 (!) percent of 13 specimens in Layer No. 1.

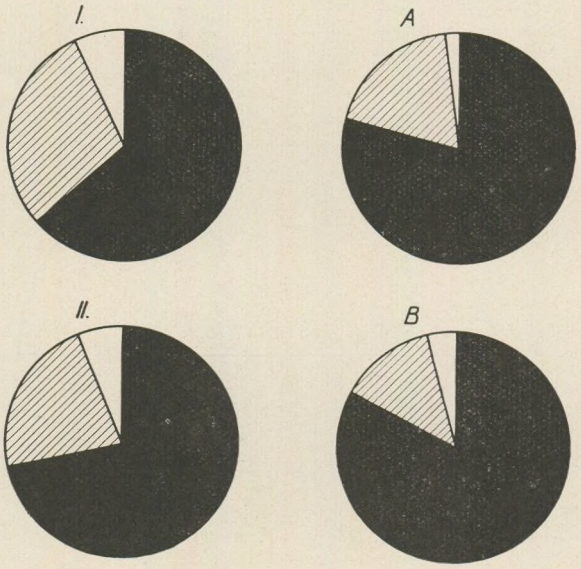

Fig. 3. Percentage distribution of ammonites at Úrkút (Localities I and II) and Csernye (Exposures *A* and *B*) in the Levesquei Zone. Black: *Phylloceratacеae* and *Lytoceratacеae*. Shaded: *Dumortieriinae*. White: *Hammatoceratinae*

The most frequent phylloceratid both at Úrkút and at Exposure B of Csernye is *Holcophylloceras ultramontanum*, making up 30.4 percent of all *Phylloceratacеae* at Úrkút and 27.3 percent at Csernye B. Figuring with 20.7 percent at Csernye, it is preceded there by *Phylloceras? baconicum* (26.1 percent).

The subfamily *Dumortieriinae* makes up 18.6 percent of the fauna at Csernye A. 13.1 percent at Csernye B, 28.9 percent at Úrkút I and 22.1 percent at Úrkút II.

The genera *Hammatoceras* and *Erycites* are most abundant at Úrkút I (7 percent).

At Úrkút, the presence of the manganese deposit in the lowermost Toarcian is a striking difference from Csernye where the lowermost Toarcian is taken up by a hiatus. The Toarcian fauna of Shaft III of Úrkút still differs in many respects from the fauna of the same age from Csernye. In the uppermost Toarcian, however, the previous differences are seen to disappear.

Both at Csernye and Úrkút, the ammonitico rosso marl lithofacies of the uppermost Toarcian and its pelagic macrofossils indicate an open sea deeper than neritic: this is borne out in particular by the substantial abundance of *Lytocerataceae* and *Phylloceratáceae*. At Úrkút, too, the ammonitico rosso marl passes into a deep-sea radiolarite. At Csernye, this change took place in the Bajocian: at Úrkút, the sudden subsidence of the sea bottom had set in by the beginning of the Dogger.

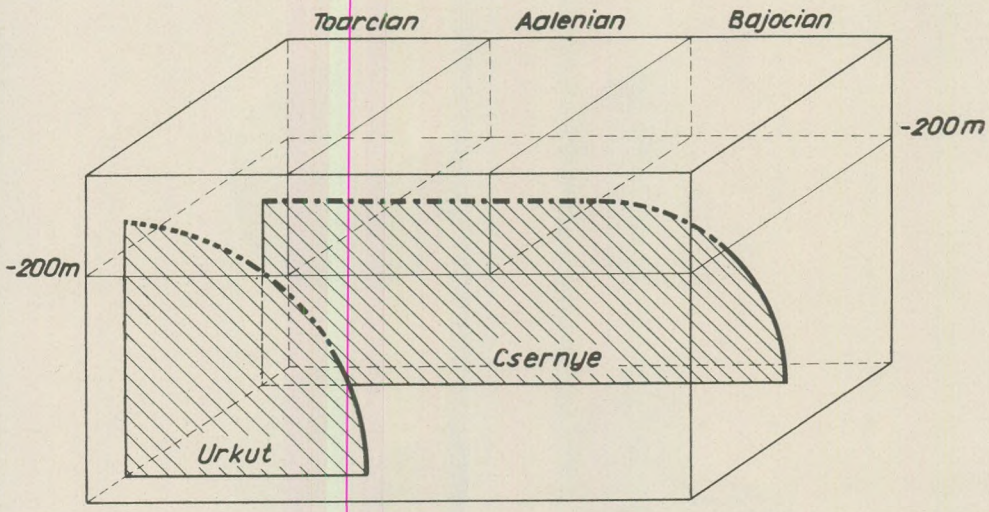

Fig. 4. Age difference of the ammonitico rosso — radiolarian silex contact at Úrkút and Csernye, with indication of bathymetric changes. Dashed: Ammonitico rosso. Continuous: radiolarite

Despite these analogies in lithology and composition, there is a substantial difference in the preservation of the two faunas. In both areas, the ammonites occur as casts whose upper sides are worse preserved than the lower. The Csernye casts, however, have preserved their original outlines, whereas those of Úrkút have undergone a deformation. Intensity of deformation is illustrated by Plates 7. and 8. for *Dumortieria* and by Plates 3. to 6. for *Erycites*. Since the growth of ammonites observes the rule of the logarithmic spiral, the original shape of the fossil and hence the intensity of deformation of the embedding rock can be reconstructed.

The measure of compression has been expressed by Langheinrich (1966) as follows:

$$\delta = \frac{\sqrt{r_1 \cdot r_3}}{r_2},$$

where δ is shortening, r_1 r_2 and r_3 are the radii of the elliptically deformed logarithmic spiral. Measurements on 20 specimens have given a range of 0.63 to 0.97 for δ, with a mean at 0.85. Hence ,the ammonites embedded in the layer have undergone a mean shortening of 15 percent. The questions that I feel

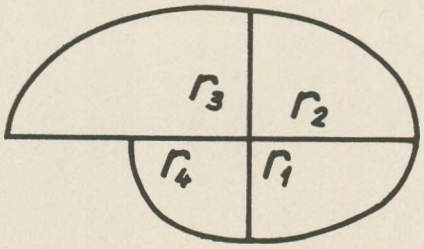

Fig. 5. Radii serving as measures of deformation of ammonites, after LANGHEINRICH (1966)

should be raised in this context are the following: what was the direction of the force that had brought about this deformation, what is the explanation of the fluctuation of deformation from one fossil to the next, and under what conditions and at what time did compression take place.

In order to determine the orientation of the ellipsoid of deformation, I measured by means of a miner's compass the orientation of the major axes of 62 elliptically deformed ammonites at Locality I and of 60 ammonites at Locality II. Besides the errors inherent in such a procedure, accuracy of measurement was impaired also by the density of joints that made it difficult to clear large surfaces of rock, as well as by the cohesion of the fossils with the underlying bed. Most measurements were performed on fossils first removed from the embedding rock and then replaced for the purpose of the measurement. These sources of error notwithstanding, the main direction of deformation could be established: it was found to be the same at both localities. On the basis of 120 measurements, the major axes of the elliptically deformed ammonites are directed NNW–SSE: more than 40 percent of the specimens lie in the angular interval between 165 and 175°. At locality I, the most abundant orientation was 170–350° (19'4%); at locality II it was 165–345° (16'6%). Part of this deviation might be due to a slight displacement of blocks loosened up by the working of the open pit.

This state of facts suggests a compressive force to have acted in a perpendicular direction (WSW–ENE).

The variations in intensity of deformation are presumably due to local factors. Specimens lying close to joints tend to be more deformed than those farther away; close to joints, shattered or sheared ammonites are none too rare. The compression indicated by the deformation of the fossils on the one hand and the stress that brought about the slickensides on the other are shown to be parallel in Fig. 2, Plate 5. Plastic deformation and fractures are due to the same compressive stress.

Deformation is beyond doubt subsequent to the embedding of the ammonites. Plastic deformation presupposes in itself the previous dissolution of the test. Early diagenetic atectonic deformation (consolidation, mudflows etc.)

may result in a plastic deformation of the ammonites, but in the case considered here the nature of the deformation and its correlation with structural features contradict such a hypothesis. At Úrkút the subsidence of the sea bottom in the

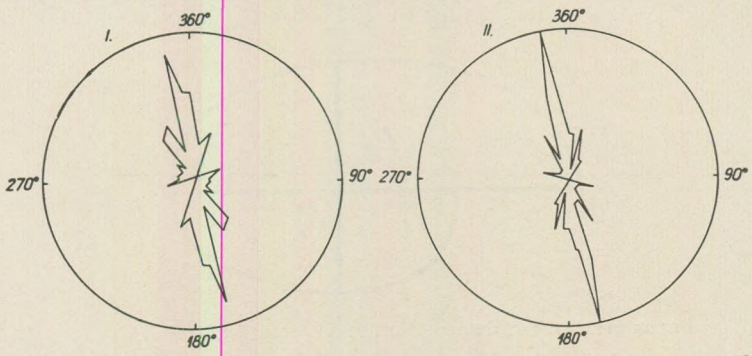

Fig. 6. Orientation of the deformation of ammonites at Localities I and II, Úrkút

Middle Jurassic would entail dilatation rather than compression: the deformation of the ammonites is, consequently, post-Jurassic in all probability. At the time of compression, the ammonite-bearing strata must have been covered with a thick succession of younger sediments: otherwise the unidirectional compression of the ammonites should have been accompanied by distension in the perpendicular direction. These sediments have been removed since. Compression is most probably due to the Cretaceous phases of mountain building that played an important role in molding the structure of the Bakony Mountains. This compression was then succeeded by fractures of the disjunctive type. According to Vigh and Noszky (1941), the Úrkút region is characterized by a "very strongly shattered block-faulted structure with the main faults tending NW–SE." That is, the fundamental structural trend did not change in subsequent times, either.

REFERENCES

Aubouin, J. (1965): Réflexions sur le faciès "ammonitico rosso". Bull. Soc. Géol. France. 7 ser. 6, Paris, 1964.

Cseh Németh, J. (1967): Úrkút és Eplény mangánterületeinek összehasonlítása. (Ein Vergleich der Manganerzlagerstätten von Úrkút und Eplény.) Földt. Közl. 97. Budapest.

Donovan, D. T. (1958): The Ammonite Zones of the Toarcian (Ammonitico Rosso Facies) of Southern Switzerland and Italy. Ecl. Geol. Helv. 51, Basel.

Géczy, B. (1966, 1967): Ammonoides Jurassiques de Csernye, Montagne Bakony. Geol. Hung. Ser. Pal. fasc. 34, 35. Budapest.

Géczy, B. (1967): Upper Liassic Ammonites from Úrkút, Bakony Mountains. Annal. Univ. Sci. R. Eötvös Sect. Geol. 10, Budapest.

Géczy, B. (1967): Csernyei jura biozónák és kronozónák (Biozones and Chronozones in the Jurassic of Csernye, Bakony Mts. Hungary.) Földt. Közl. 97, Budapest.

Langheinrich, G. (1966): Syndiagenetische Fossildeformation im untersten Lias (Hettangium) von Göttingen N. Jb. Geol. Paläont. Stuttgart.

Langheinrich, G. (1967): Bestimmung der tektonischen Gesteinsdeformation mit Hilfe deformierter Ammoniten. N. Jb. Geol. Paläont. Abh. 128, Stuttgart.

Noszky, J. (1961): Formations jurassiques de la Hongrie. Magy. Áll. Földt. Int. Évkönyve, 49, Budapest.

Vigh, Gy., Noszky, E. (1941): Vorläufiger Bericht über die geologischen Verhältnisse der Umgebung des Úrkúter Manganbergwerkers. Magy. Áll. Földt. Int. Évi Jel. 1936–1938-ról. Budapest.

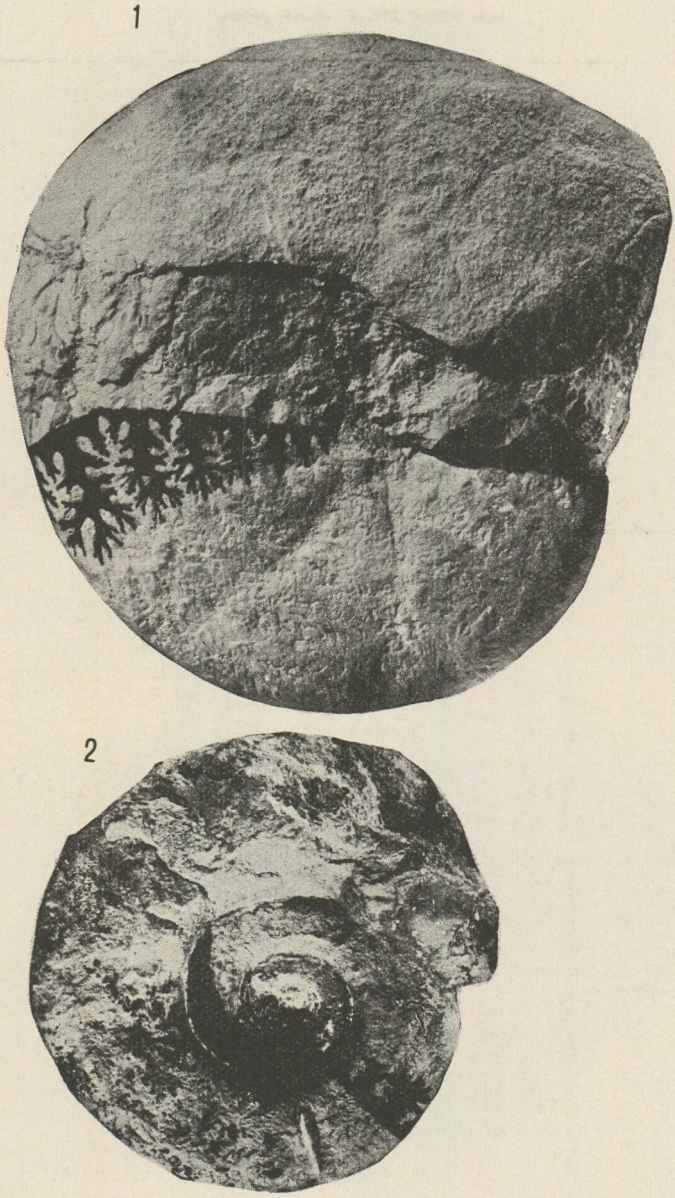

PLATE 1

1. *Calliphyloceras* sp.
2. *Alcolytoceras ophioneum* (Benecke, 1865)

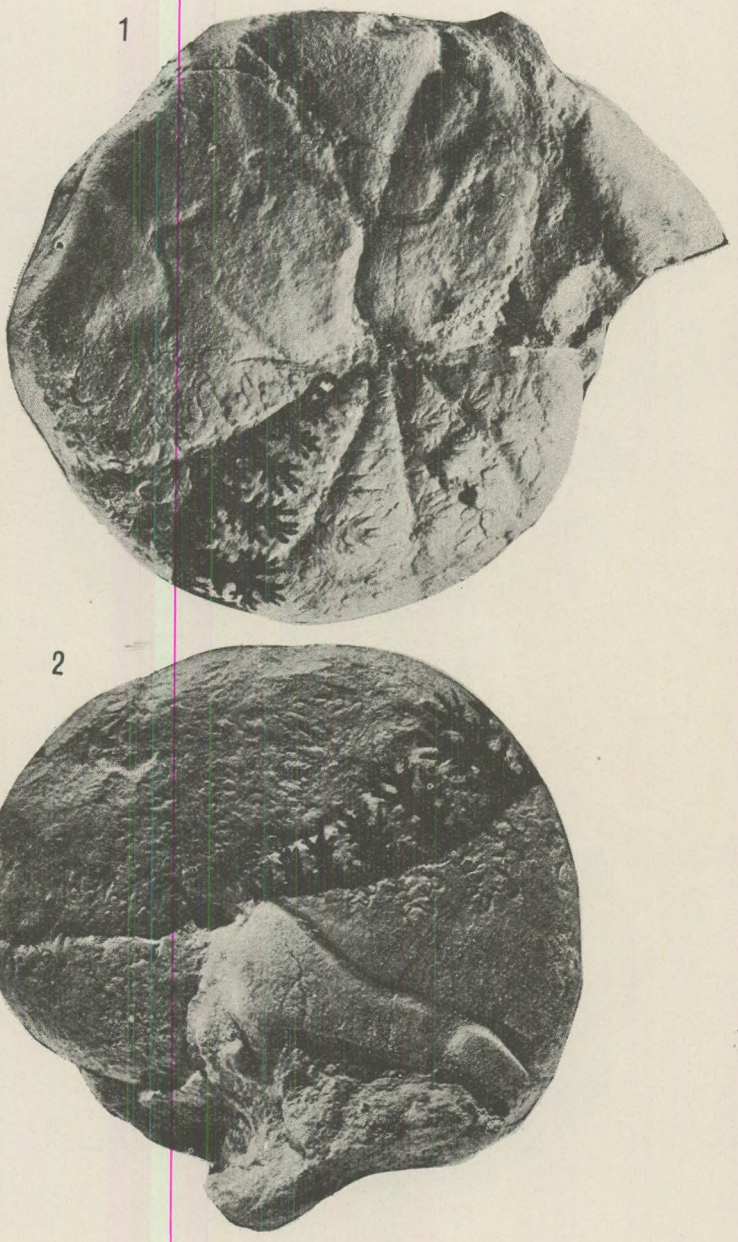

PLATE 2

1. *Calliphylloceras altisulcatum quadratum* Géczy, 1967
2. *Holcophylloceras ultramontanum* (Zittel, 1869) ?

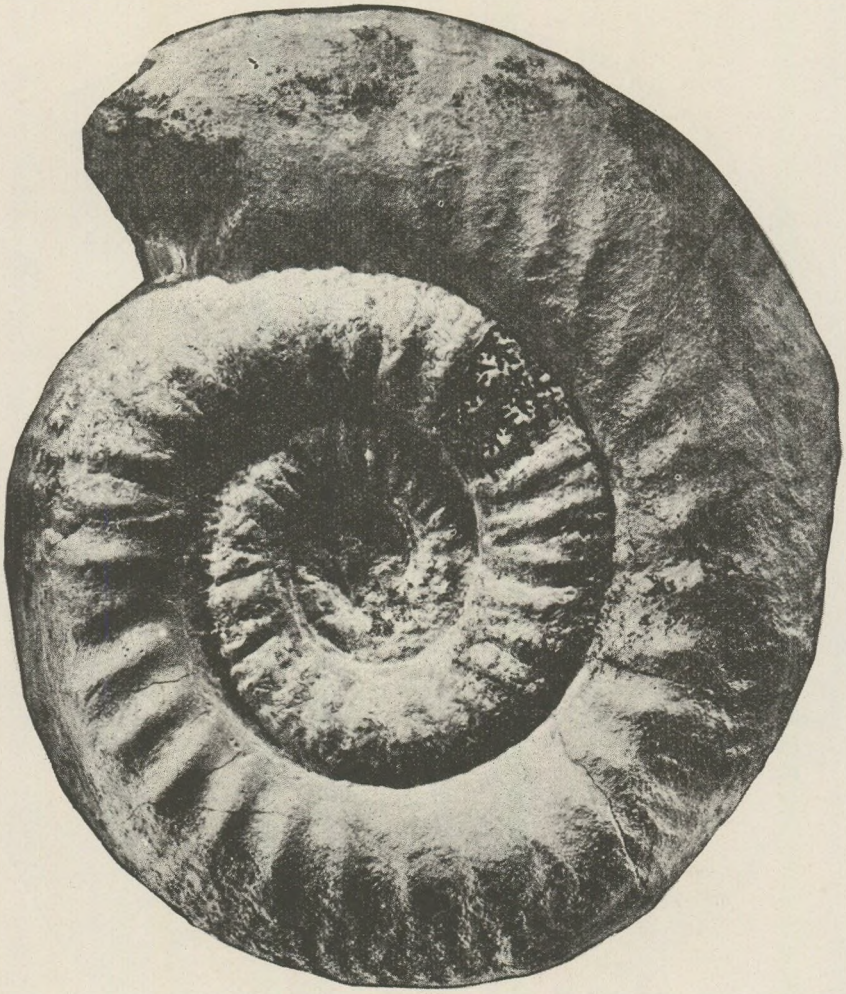

PLATE 3

Erycites subquadratus Géczy, 1967

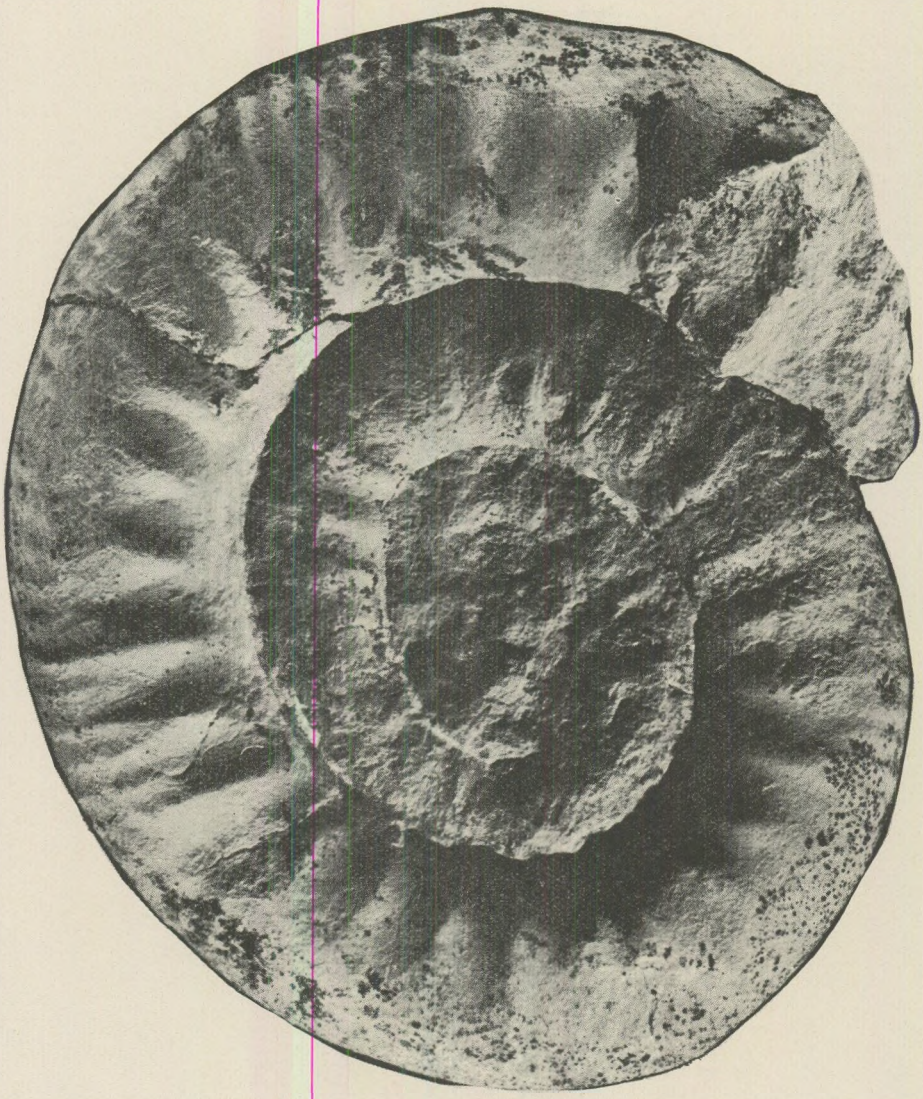

PLATE 4

Erycites elaphus Merla, 1934

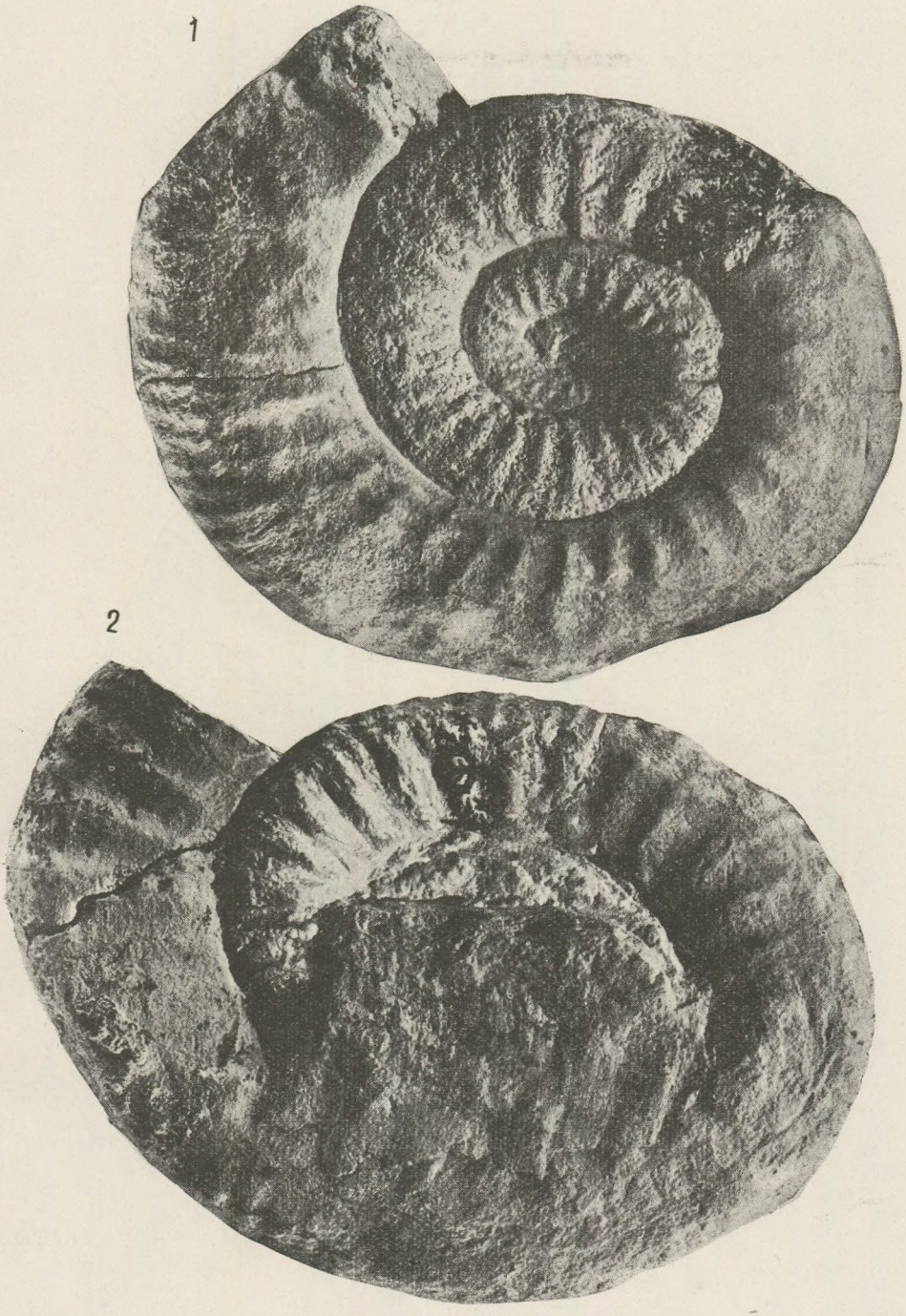

1. *Erycites elaphus* Merla, 1934
2. *Erycites sp.*

PLATE 5

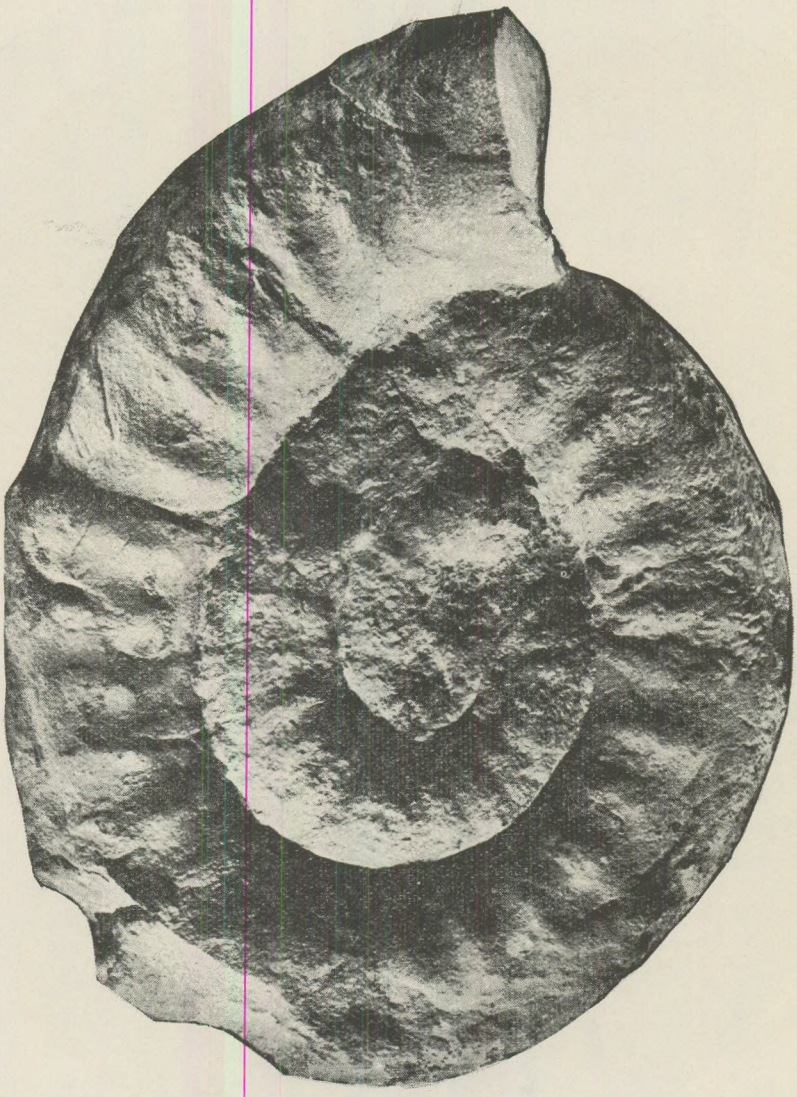

PLATE 6

Erycites elaphus Merla, 1934

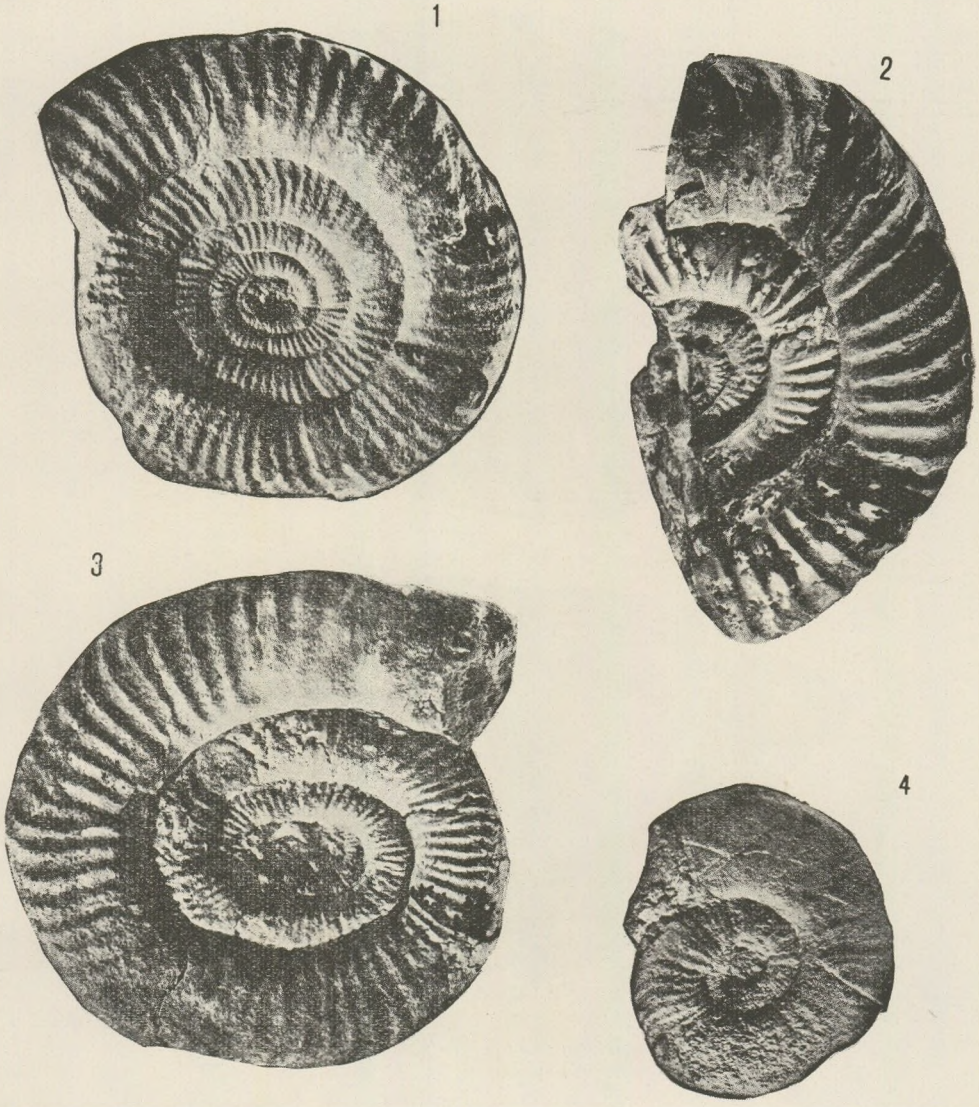

PLATE 7

1. *Dumortieria* sp.
2. *Dumortieria dumortieri* cf. *pannonica* Géczy, 1967
3. *Dumortieria* sp.
4. *Pleydellia* sp.

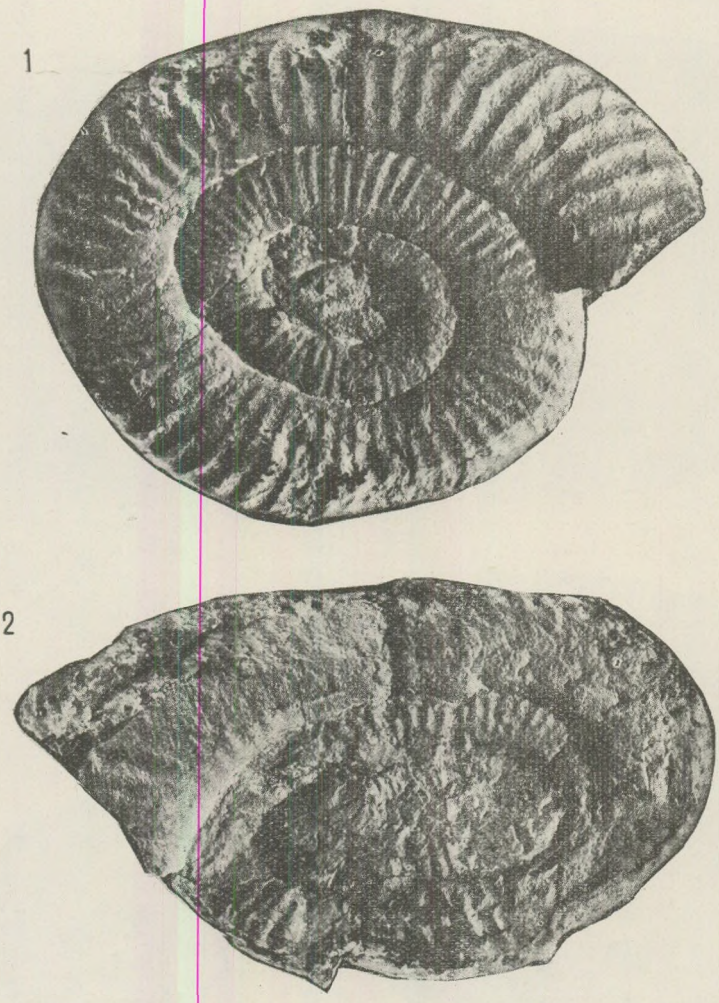

PLATE 8

1. *Dumortieria meneghinii* (Zittel M. S.) in Haug, 1887
2. *Dumortieria* sp.

PLANKTONIC FORAMINIFERA FROM THE OLIGOCENE AND LOWER MIOCENE OF HUNGARY

by

A. I. KENAWY

(Geology Department, Assiut University, Egypt, U.A.R.,
Institute of Paleontology, Loránd Eötvös University, Budapest)

(Received: 30 th. Sep. 1967)

SUMMARY

This paper lists and describes 49 species and subspecies of planktonic foraminifera from five Oligocene and Lower Miocene localities in Hungary. The analysis of a large number of samples makes possible the subdivision of this Oligocene and Lower Miocene into a number of zones, established for the first time in Hungary. This zonation correlates the Hungarian sections with each other and with other parts of the world. The Oligocene and Lower Miocene sections are divided into the following zones from bottom to top: *Globigerina ouachitaensis ouachitaensis*, *Globigerina ampliapertura*, *Globorotalia opima opima* and *Globigerina ciperoensis ciperoensis*. In spite of the fact that the age of these zones is still a matter of controversy, the author accepts the view expressed by Jenkins (1966) that the boundary between the Oligocene and Miocene should be placed between the *Globorotalia opima opima* Zone and *Globigerina ciperoensis ciperoensis* Zone. The ages of the studied sections are determined on the basis of these planktonic foraminiferal zones.

Introduction

This paper lists and describes planktonic foraminifera from the Oligocene and Lower Miocene rocks of 5 different localities in Hungary.

These are: Eger bore-hole (Wind Brickyard) Eger profile (Wind Brickyard), Novaj, Törökbálint and Ipolytarnóc (Text figure 1).

The ages of these localities are controversial. The present author will not discuss previous literature: the main purpose of the present work is to study the planktonic foraminifera of these localities and to define ages on the basis of these foraminifera.

About 134 samples from the Eger bore-hole, 23 samples from the Eger profile, 9 samples from Novaj, 20 samples from Törökbálint and 10 samples from Ipolytarnóc were investigated. The majority of the samples contain a large number of planktonic foraminifera excellently preserved, which facilitates the zonation and correlation of the profiles among each other, and with other parts of the world.

Planktonic foraminiferal zones: In the following paragraph a description of these foraminiferal zones in the different localities is presented *(Table I, 2.)*

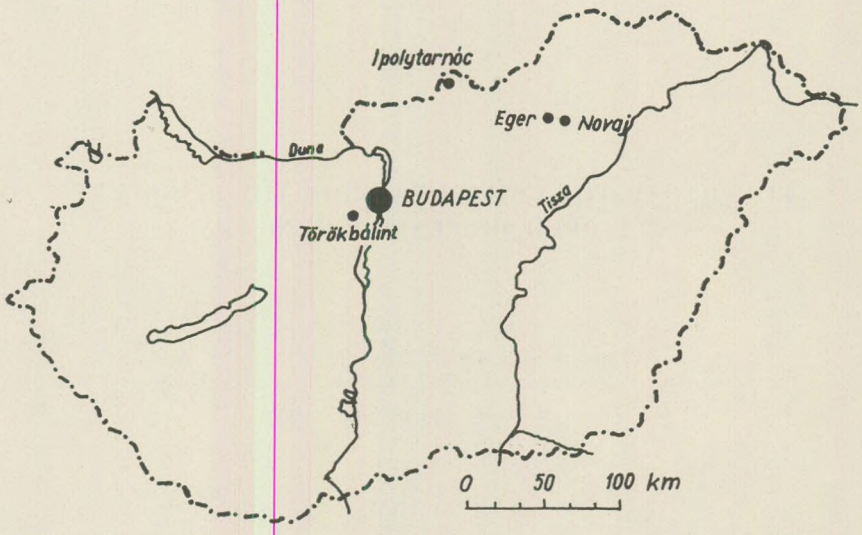

Fig. 1. Sketch map of Hungary showing the location of the studied localities (after R. M. Nyirő)

I. Globigerina ouachitaensis ouachitaensis Zone:

This zone is characterized by a large number of *G. ouachitaensis ouachitaensis* together with *G. linaperta, G. trilocularis* and *Globigerinita unicava unicava.* This zone contains a large number of benthonic foraminifera; among the most important index species is *Clavulinoides szabói.*

To this zone belong the lower marly layers of the Eger bore-hole from 80 to 40 m depth.

According to the presence of *Clavulinoides szabói,* the age of this zone is Rupelian.

II. Globigerina ampliapertura Zone:

This zone has a planktonic foraminiferal assemblage distinctly different from the previous one. This zone is characterized by the dominance of the well known *Globigerina ampliapertura* accompanied by. *G. ciperoensis angustiumbilicata, G. corpulenta, G. druryi, G. euapertura, G. linaperta, G. ouachitaensis gnaucki, G. parva, G. praebulloides praebulloides, G. praebulloides occlusa, G. rohri, G. senilis, G. yeguaensis, Globorotalia permicra, Globigerinita dissimilis, G. unicava primitiva, G. unicava unicava* and *Globoquadrina venezuelana.*

To this zone belong the sandy and glauconitic sandy and sandstone beds from 40 to 6 m depth in the Eger bore-hole.

This zone is also found in the Lepidocyclina limestone, in samples no. 308, 309 from Novaj.

Table 1.

Chart showing the occurrence of Planktonic Foraminifera at the localities studied in Hungary

a = abundant c = common f = frequent r = rare

	Rupelian	Upper Oligocene						Lower Miocene
	Globigerina ouachitaensis ouachitaensis Zone	Globigerina ampliapertura Zone		Globorotalia opima opima Zone				Globigerina ciperoensis ciperoensis Zone
	Eger bore-hole 80–40 m	Eger bore-hole 40–6 m	Novaj Sampl. Nos. 308–309	Eger bore-hole 6–0 m	Eger profile Samples Nos. 7–25	Novaj Samples Nos. 457–459	Török-bálint Samples Nos. 318–322 439	Ipolytarnóc
Globigerina ampliapertura Bolli	–	a	a	–	r	–	–	–
G. bollii Cita and Premoli	–	–	–	–	–	–	–	c
G. brazieri Jenkins	–	–	–	–	–	–	–	a
G. ciperoensis angulisuturalis Bolli	–	–	–	–	–	–	–	c
G. ciperoensis angustiumbilicata Bolli	–	f	r	–	–	–	–	–
G. ciperoensis ciperoensis Bolli	–	–	–	f	f	f	f	a
G. corpulenta Subbotina	–	–	–	–	–	–	–	–
G. druryi Akers	–	r	–	–	–	–	–	–
G. euapertura Jenkins	–	r	–	–	–	–	–	–
G. foliata Bolli	–	–	–	–	–	–	–	f
G. juvenilis Bolli	–	–	–	–	–	–	–	c
G. labiacrassata Jenkins	–	–	–	–	r	–	–	–
G. linaperta Finlay	f	f	r	–	–	–	–	–
G. nepenthes Todd	–	–	–	–	–	–	–	r
G. ouachitaensis gnaucki Blow and Banner	f	f	f	f	f	–	–	–
G. ouachitaensis ouachitaensis Howe and Wallace	a	f	f	–	–	–	–	–
G. parva Bolli	–	c	c	c	c	c	a	f
G. praebulloides leroyi Blow and Banner	–	–	–	f	c	f	c	a
G. praebulloides occlusa Blow and Banner	–	–	f	–	–	–	–	–
G. praebulloides praebulloides Blow	–	f	f	f	f	f	r	a
G. rohri Bolli	–	f	–	–	–	–	–	–
G. senilis Bandy	–	f	f	–	–	–	–	–
G. sp.	–	–	–	r	–	–	–	–
G. trilocularis d'Orbigny	f	r	r	–	–	–	–	–
G. turritilina praeturritilina Blow and Banner	–	f	f	–	–	–	–	–
G. turritilina turritilina Blow and Banner	–	f	–	–	–	–	–	–
G. woodi woodi Jenkins	–	–	–	–	–	–	–	a
G. woodi connecta Jenkins	–	–	–	–	–	–	–	a
G. yeguaensis Weinzierl and Applin	–	f	–	–	–	–	–	–
Globorotalia continuosa Blow	–	–	–	–	–	–	–	a
G. extens Jenkins	–	–	–	–	–	–	a	–
G. obesa Bolli	–	–	–	–	–	–	–	a
G. opima nana Bolli	–	–	–	a	a	a	a	r
G. opima opima Bolli	–	–	–	a	a	a	a	–
G. permicra Blow and Banner	–	–	c	–	–	–	–	–
G. postcretacea (Myatliuk)	–	–	–	–	–	–	f	–
G. saginata Jenkins	–	–	–	–	–	–	–	c
G. testarugosa Jenkins	–	–	–	–	–	–	–	c
Cassigerinella chipolensis (Cushman and Ponton)	–	–	–	–	–	–	–	f
Globigerinita dissimilis (Cushman and Bermudez)	–	r	–	–	–	–	–	–
G. martini martini Blow and Banner	–	f	–	–	–	–	f	–
G. unicava primitiva Blow and Banner	–	f	–	–	–	–	–	–
G. unicava unicava (Bolli, Loeblich and Tappan)	f	f	f	–	–	–	–	–
Globigerinoides primordius Blow and Banner	–	–	–	–	–	–	–	r
Globoquadrina dehiscens (Chapman, Parr and Collins)	–	–	–	–	–	–	–	f
G. larmeui Akers	–	–	–	–	–	–	–	f
G. venezuelana (Hedberg)	–	c	f	f	–	–	–	–
Globorotaloides suteri Bolli	–	–	–	f	–	–	–	–
G. variabilis Bolli	–	–	–	–	–	–	–	c

Table 2.
Distribution chart of Planktonic Foraminifera in the Oligocene and Lower Miocene at the localities studied in Hungary

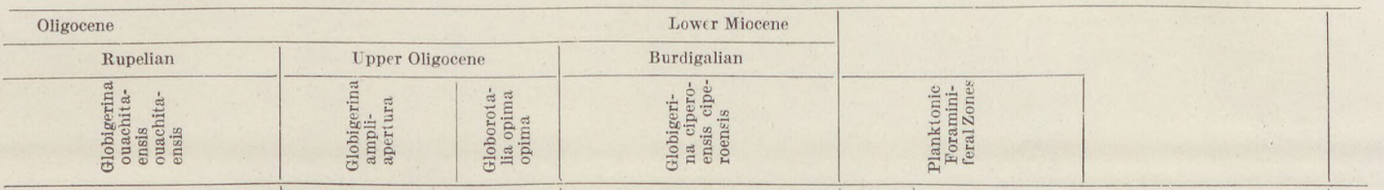

1	Globigerina ampliapertura Bolli	Globigerina
2	Globigerina bollii Cita and Premoli	
3	Globigerina brazieri Jenkins	
4	Globigerina ciperoensis angulisuturalis Bolli	
5	Globigerina ciperoensis angustiumbilicata Bolli	
6	G. ciperoensis ciperoensis Bolli	
7	G. corpulenta Subbotina	
8	G. druryi Akers	
9	G. euapertura Jenkins	
10	G. foliata Bolli	
11	G. juvenilis Bolli	
12	G. labiacrassata Jenkins	
13	G. linaperta Finlay	
14	G. nepenthes Todd	
15	G. ouachitaensis gnaucki Blow and Banner	
16	G. ouachitaensis ouachitaensis Howe and Wallace	
17	G. parva Bolli	
18	G. praebulloides leroyi Blow and Banner	
19	G. praebulloides occluosa Blow and Banner	
20	G. praebulloides praebulloides Blow	
21	G. robri Bolli	
22	G. senilis Bandy	
23	G. sp.	
24	G. trilocularis d'Orbigny	
25	G. turritilina praeturritilina Blow and Banner	
26	G. turritilina turritilina Blow and Banner	
27	G. woodi woodi Jenkins	
28	G. woodi connecta Jenkins	
29	G. yeguaensis Weinzierl and Applin	
30	Globorotalia continuosa Blow	Globorotalia
31	G. extens Jenkins	
32	G. obesa Bolli	
33	G. opima nana Bolli	
34	G. opima opima Bolli	
35	G. permicra Blow and Banner	
36	G. posteretacea (Myatliuk)	
37	G. saginata Jenkins	
38	G. testarugosa Jenkins	
39	Cassigerinella chipolensis (Cushman and Ponton)	Other genera
40	Globigerinita dissimilis (Cushman and Bermudez)	
41	G. martini martini Blow and Banner	
42	G. unicava primitiva Blow and Banner	
43	G. unicava unicava (Bolli, Loeblich and Tappan)	
44	Globigerinoides primordius Blow and Banner	
45	Globoquadrina dehiscens (Chapman, Parr and Colline)	
46	G. larmeui Akers	
47	G. venezuelana (Hedberg)	
48	Globorotaloides suteri Bolli	
49	G. variabilis Bolli	

This zone is Oligocene according to the findings of Bolli (1957) in Trinidad, Reiss and Gvirtzman (1964) in Israel and Mc Tavish (1966) in the British Solomon Islands.

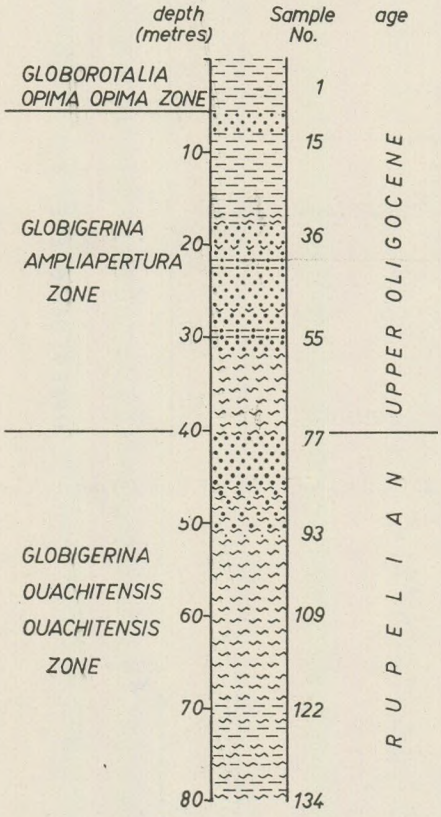

Fig. 2. Geological profile Eger bore-hole (Wind Brickyard)

III. Globorotalia opima opima Zone.

This zone includes a number of *Globorotalia* species that belong to the *opima opima* and *opima nana* forms, together with other planktonic foraminifera such as *Globigerina ciperoensis, G. labiacrassata, G. leroyi, G. praebulloides praebulloides, Globorotalia extens, G. postcretacea, Globoquadrina venezuelana* and *Globorotaloides suteri.*

The age of this zone is Oligocene according to Bolli (1957), Hofker (1963) and Reiss and Gvirtzman (1964).

To this zone belong the upper 6 m of the marly beds in the Eger bore-hole. This zone is found also in the Eger profile (Wind Brickyard) in samples 7 – 18 of the molluscan clay layers. To this zone belong also samples Nos. 457 – 459 of Novaj, samples Nos. 318 – 322 and sample 439 of Törökbálint.

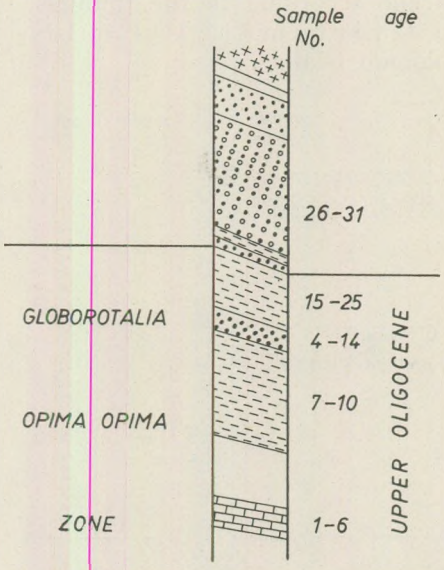

Fig. 3. Geological profile of Eger (Wind Brickyard)

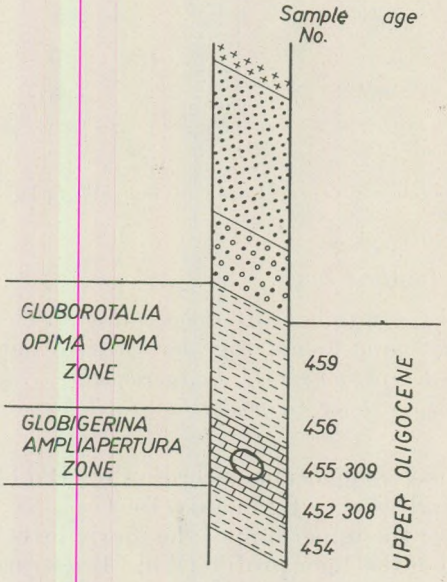

Fig. 4. Geological profile of Novaj

IV. Globigerina ciperoensis ciperoensis Zone:

This zone is characterized by the predominance of *Globigerina ciperoensis ciperoensis* together with other planktonic species that are restricted only to this zone such as: *Globigerina bolli, G. brazieri, G. ciperoensis angulisuturalis, G. foliata, G. juvenilis, G. nepenthes, G. woodi woodi, G. woodi connecta, Globorotalia continuosa, G. obesa, G. saginata, G. testarugosa, Cassigerinella chipolensis, Globigerinoides primordius, Globoquadrina dehiscens, G. larmeui* and *Globorotaloides variabilis.*

To this zone belong samples Nos. 1280 to 1289 of Ipolytarnóc.

The age of this zone is Burdigalian (Lower Miocene) according to Jenkins (1964, 1966).

Although this zonation is noted in many parts of the world and agrees in detail with that found by Bolli (1957), the age of these zones is a matter of interpretation.

From the above-mentioned four zones, we can conclude the following:

1. The Eger bore-hole belongs to 3 zones (Text fig. 2):

Globigerina ouachitaensis ouachitaensis Zone ..... Rupelian

Globigerina ampliapertura Zone .. .. Upper Oligocene

Globorotalia opima opima Zone ..... Upper Oligocene

2. The Eger profile belongs to one zone (Text fig. 3):

Globorotalia opima opima Zone ..... Upper Oligocene

3. Novaj belongs to two zones (Text fig. 4):

Globigerina ampliapertura Zone ..... Upper Oligocene

Globorotalia opima opima Zone ..... Upper Oligocene

4. Törökbálint belongs to one zone only:

Globorotalia opima opima Zone ..... Upper Oligocene

Owing to the presence of some Globorotalia species such as *G. subcretacea, G. extens,* and *G. permicra* especially in sample No. 439, the present author is inclined to consider Törökbálint younger than the Eger profile (Wind Brickyard).

5. Ipolytarnóc belongs to one zone:

Globigerina ciperoensis ciperoensis Zone ..... Lower Miocene

Intercontinental correlation

The zonation of the Oligocene and the Lower Miocene by means of planktonic foraminifera has been proved satisfactory by different authors in various parts of the world (Table 3.).

Drooger (1956) studied the planktonic foraminifera from the European type Oligocene-Miocene stages. He recorded the following species from the type rocks:

Aquitanian: *Globigerina bulloides, Globigerinoides trilobus.*
Chattian: *Globigerina globularis.*
Rupelian: *Globigerina* cf. *increbescens.*

Trinidad was one of the first areas where planktonic foraminifera were successfully used for the zonation of Cretaceous to Tertiary marls and calcareous clays. Most of the zones proposed in Trinidad are recognisable on a world-wide scale and can be used in intercontinental stratigraphic correlation. Using planktonic foraminifera, B o l l i (1957) has divided the Cipero formation of Trinidad into 13 zones. These zones begin with *Globigerina ampliapertura* and end with *Globorotalia menardii* in the Miocene. B o l l i (1957) considered the *Globigerina ampliapertura, Globorotalia opima opima, Globigerina ciperoensis ciperoensis* and *Globorotalia kugleri* zones to be of Oligocene age, the *Catapsydrax dissimilis* and *C. stainforthi* zones of Lower Miocene age.

B l o w and B a n n e r (in Eames et al. 1962) studied the Eocene-Oligocene and Lower Aquitanian Globigerinaceae, and recorded the following zones from base to top. *Globigerina oligocaenica* in the Rupelian, and *Globigerina ampliapertura, Globorotalia opima opima* and *Globigerina ouachitaensis ciperoensis* in the Aquitanian. They put the Oligocene-Miocene boundary at the base of the *G. ampliapertura* Zone while according to B o l l i (1957) the base of this zone coincides with the Eocene-Oligocene boundary.

B e r g g r e n (1963) in his review on the work of B l o w and B a n n e r (in E a m e s et al. 1962) placed the Oligocene-Miocene boundary within the *G. opima opima* zone.

H o f k e r (1963) recorded the following 6 species from the Oligocene rocks of northwestern Europe: *Globigerina opima opima, G. ouachitensis, G. ampliapertura, G. praebulloides, G. dissimilis* and *G. leroyi.*

H o f k e r concluded from this list that the *Globorotalia opima opima* zone of Trinidad is of Oligocene age.

R e i s s and G v i r t z m a n (1964), working on the Neogene stratigraphy of Israel, were able to correlate their zones with those established by Bolli in Trinidad, but they added the *Globigerina sellii* zone underneath the *Globigerina ampliapertura* zone.

J e n k i n s (1965) studied the planktonic foraminifera in the Lower Tertiary of New Zealand. Jenkins recorded 6 zones from the Oligocene and the Lower Miocene of New Zealand. These zones are from base to top: *Globigerina brevis, Globigerina angioporoides angioporoides, G. euapertura* in the Oligocene; and *Globoquadrina dehiscens, G. woodi woodi* and *Globigerina woodi connecta* in the Lower Miocene. Jenkins correlated his new zones with those of B o l l i (1957) in Trinidad.

M c T a v i s h (1966), working on the planktonic foraminifera of the British Solomon Islands, recorded 5 zones from the Oligocene and Lower Miocene. These zones are from base to top: *Globigerina (Globigerinita) martini, G. ampliapertura* and *Globorotalia kugleri* in the Oligocene; and *Globigerina (Globigerinita) dissimilis* and *Globigerinatella insueta* in the Lower Miocene. Mc Tavish did not record the *Globorotalia opima opima* and *Globigerina ciperoensis ciperoensis* zones.

Table 3.
Correlation table of the Hungarian Planktonic Foraminifera Zones with other studied localities

Age	Trinidad Bolli (1957, 1966)	Caribbean, Africa Blow and Banner (Eames et al., 1962)	Israel Reiss and Gvirtzman (1964)	Caribbean-Pacific Alpine-Mediterranean Banner and Blow (1965)	New Zealand Jenkins (1965, 1966)	British Solomon Islands McTavish (1966)	Hungary (1967)
Lower Miocene	↑	Globigerina ouachitaensis ciperoensis	↑	↑	↑	↑	
	Catapsydrax stainforthi	Globorotalia opima opima	Globigerinita stainforthi	N.6 Globigerinatella insueta Globigerinita dissimillis	Globigerinoides trilobus trilobus	Globigerinatella insueta	
	Catapsydrax dissimilis	Globigerina ampliapertura	Globigerinita dissimilis	N.5 Globoquadrina dehiscens praedehiscens G. dehiscens dehiscens		Globigerina (Globigerinita) dissimilis	Globigerina ciperoensis ciperoensis
Oligocene	Globorotalia kugleri	Not known	Globorotalia kugleri	N.4 Globorotalia (T.) kugleri	Globigerina woodi connecta	Globorotalia kugleri	Globorotalia opima opima
	Globigerina ciperoensis ciperoensis	Globigerina oligocaenica	Globigerina ouachitaensis ciperoensis	N.3 Globigerina angulisuturalis	Globigerina woodi woodi		Globigerina ampliapertura
	Globorotalia opima opima		Globorotalia opima opima	N.2 Globigerina angulisuturalis Globorotalia (T.) opima (s.s.)	Globoquadrina dehiscens		Globigerina ouachitaensis ouachitaensis
					Globigerina (G.) euapertura		
	Globigerina ampliapertura		Globigerina ampliapertura	N.1 Globigerina ampliapertura	Globigerina (S.) angiporoides angiporoides	Globigerina ampliapertura	
			unnamed			Globigerina (Globigerinita) martini	
			Globigerina sellii				

Jenkins (1966) studied the planktonic foraminifera from the type Aquitanian-Burdigalian rocks of France. He concluded that neither *G. ampliapertura* nor *Globorotalia opima opima* were found in the Lower Aquitanian, and that the absence of *G. opima opima* in the lower Aquitanian supports Hofker's opinion that the *Globorotalia opima opima* zone is of Oligocene age. Jenkins (1966) suggested that owing to the presence of *Globigerina ciperoensis ciperoensis* and *G. ciperoensis angulisuturalis*, the Lower Aquitanian samples of France are equivalent to the *G. ciperoensis ciperoensis* zone of Trinidad (Bolli 1957). He concluded that the Oligocene-Miocene boundary must be placed between the *Globorotalia opima opima* zone and the *G. ciperoensis ciperoensis* zone.

The present author agrees with the conclusion of Jenkins (1966) that the *Globigerina ampliapertura* zone and *Globorotalia opima opima* zone are Upper Oligocene, and the *G. ciperoensis ciperoensis* zone is Lower Miocene (Burdigalian). The boundary between the Oligocene and the Miocene should be placed between the *Globorotalia opima opima* zone and the *G. ciperoensis ciperoensis* zone.

SYSTEMATIC DESCRIPTIONS

Family CASSIDULINIDAE d'Orbigny. 1839

Sub-family CASSIDULININAE d'Orbigny. 1839

Genus Cassigerinella Pokorny. 1955

Cassigerinella chipolensis (Cushman and Ponton)

(Plate 1, Figures 1a – d)

1932 *Cassidulina chipolensis.* – Cushman and Ponton, p. 98, pl. 15, Fig. 2a – c.
1957 *Cassigerinella chipolensis* (Cushman and Ponton). – Bolli, p. 108, pl. 22, Fig. 3a – c.
1963 *Cassigerinella chipolensis* (Cushman and Ponton). – Hofker pp. 321 – 324, pl. 1, Fig. 1 – 2.
1964 *Cassigerinella chipolensis* (Cushman and Ponton). – Jenkins, p. 29, tab. 1.
1966 *Cassigerinella chipolensis* (Cushman and Ponton). – Jenkins, p. 1, pl. 1, Fig. 1a, 1b.

Description:

Test minute, consisting of subglobular chambers. The last whorl is composed of 4 pairs of inflated chambers alternating on each side of the axis of coiling. Periphery strongly lobulate. Wall calcareous, finely perforate. Sutures deeply depressed. Aperture elongate, loop-like in the apertural face.

Diameter: 0.15 mm

Occurrence: Rare in sample No. 1283, Ipolytarnóc.

Cushman and Ponton (1932) described this species from the Lower Miocene of Florida.

Family GLOBIGERINIDAE Carpenter, Parker and Jones, 1862

Sub-family GLOBIGERININAE Carpenter, Parker and Jones, 1862

Genus Globigerina d'Orbigny, 1826

Globigerina ampliapertura Bolli

(Plate 1, Fig. 3a – d, 4a – d, 5a, b)

1956 *Globigerina globularia Roemer.* – Drooger, p. 190, pl. 1, Fig. 1, 2.
1957 *Globigerina ampliapertura.* – Bolli, p. 108, pl. 22, Fig. 4 – 8.
1962 *Globigerina ampliapertura ampliapertura Bolli.* – Blow and Banner p. 83, pl. XI. A – D, Fig. 12b.
1965 *Globigerina ampliapertura Bolli.* – Jenkins, pl. 2, Fig. 11a – c.
1966 *Globigerina ampliapertura Bolli.* – McTavish, pl. 1, Fig. 27 – 28.

* The types and the figured specimens have heen deposited in the collections of the Natural History Museum at Budapest under Nos. M. 68. 283 & M. 68. 284.

** For the range and occurrence of the species see Table 3.

Table 4.

Cassigerinella chipolensis
Globigerina ampliapertura
bollii
brazieri
ciperoensis angulisuturalis
angustiumbilicata
ciperoensis
corpulenta
druryi
euapertura
foliata
juvenilis
labiacrassata
linaperta
nepenthes
ouachitaensis gnauki
ouachitaensis
parva
praebulloides leroyi
oculosa
praebulloides
rohri
senilis
trilocularis
turritilina praeturritilina
turritilina
woodi woodi
connecta
yeguaensis
Globigerinita dissimilis
martini martini
unicava primitiva
unicava
Globigerinoides primordius
Globoquadrina dehiscens
larmeui
venezuelana
Globorotalia continuosa
extens
obesa
opima nana
opima
permicra
postcretacea
saginata
testarugosa
Globorotaloides suteri
variabilis
Globigerinatella insueta
Catapsydrax stainforthi
Catapsydrax dissimilis
Globorotalia kugleri
Globigerina ciperoensis ciperoensis
Globorotalia opima opima
Globigerina ampliapertura
Miocene
Oligocene
Upper
Middle
Lower
Eocene
Palaeocene
Trinidad
Bolli 1957
and other authors
Lower & Middle Miocene
Piemont
Cita & Premoli 1967
Aquitanian
Sicily
Blow & Banner 1962
Globigerina woodi connecta
Globigerina woodi woodi
Globoquadrina dehiscens
Globigerina euapertura
Globigerina angiporoides angiporoides
Globigerina brevis
Lower Miocene
Oligocene
Eocene
New Zealand
Finlay 1939
Hornibrook 1958
Jenkins 1965
Globigerinoides triloba triloba
Globigerina woodi
Globoquadrina dehiscens dehiscens
Pre-Globoquadrina dehiscens dehiscens
Miocene
Australia
Jenkins 1960
Miocene
Ponce Limestone
Oligocene
Juana Diaz
Puerto Rico
Pessagno 1963
Gordon 1961
Globigerinatella insueta
Globigerina (G-ita) dissimilis
Globorotolia kugleri
Globigerina ampliapertura
Globigerina (G-ita) martini
Miocene
Oligocene
British
Solomon
Islands
McTavish 1966
Helvetian
Burdigalian
Aquitanian, upper
Aquitanian, lower
Stampian
Rupelian
E
M
B
C
G
EL
O
France, Germany
Jenkins 1966
Drooger 1956
Blow & Banner 1962
E = Escornebéou
B = Biarritz
C = Cambes
G = Gironde
EL = Elmsheim
O = Offenbach
M = Moulin de l'Eglise
Globigerina ouachitaensis ciperoensis
Globorotalia opima opima
Globigerina ampliapertura
Aquitanian
Oligocene
Rupelian (Globigerina oligocaenica)
Lattorfian
Upper
Middle
Lower
Eocene
Palaeocene
East Africa
Blow & Banner 1962
Miocene
Oligocene
North Sea Basin
Drooger & Batjes 1959
Oligocene, Boreal
NW Europe
Hofker 1963
Miocene
Venezuela
Blow 1959

Description:

Test medium, low trochospiral, consists of three whorls. The last whorl is composed of four chambers increasing in size as added; in the early whorls the chambers are spherical, in the later whorls they are compressed laterally. Periphery rounded, distinctly lobulate; wall calcareous, perforate, having a rough granular appearance, surface finelly pitted. Sutures distinct, slightly depressed, slightly oblique on the spiral side, radial on the umbilical side. Aperture high, in the form of an asymmetrical arch; umbilicus deep.

Diameter: 0.32 mm.

Occurrence: Abundant in the *Globigerina ampliapertura* zone in the Eger bore-hole and Novaj samples. Rare in the Eger profile samples.

Globigerina ampliapertura was described as *Globigerina globularis* by Drooger (1956) from the Oligocene of Biarritz, France.

Bolli (1957) described and illustrated this species from the *Globigerina ampliapertura* zone, Oligocene, Cipero formation, Trinidad.

GLOBIGERINA BOLLII CITA AND PREMOLI

(Plate 1, Fig. 2a–d)

1960 *Globigerina bollii.* – Cita and Premoli, p. 120, pl. 13, Fig. 12.
1966 *Globigerina bollii* Cita and Silva. – McTavish, p. 22, pl. 1, Fig. 25, 29–30.
1967 *Globigerina bollii.* – Cita and Premoli, pl. 1, Fig. 5a–c.

Description:

Test small, low trochospiral, composed of 3 whorls. The last whorl consists of 4 chambers. Chambers globular, last chamber smaller than the penultimate. Axial periphery rounded, equatorial periphery lobulate. Wall calcareous, finely perforate. Sutures distinctly depressed, radial on both the spiral and the umbilical surfaces. Umbilicus very narrow. Aperture a small arch at the base of the last-formed chamber, with a distinct lip.

Diameter: 0.23 mm.

Occurrence: Rare in sample No. 1288, Ipolytarnóc.

This species was originally described from the lower Miocene of northwestern Italy (1960).

GLOBIGERINA BRAZIERI JENKINS

(Plate 2, Fig. 1a–d)

1965 *Globigerina brazieri.* – Jenkins, p. 1098, text fig. 6. Fig. 43–51.

Description:

Test large, low trochospiral, composed of 3 whorls. The last whorl composed of 4 chambers, increasing very rapidly in size as added. Chambers inflated, slightly embracing. Equatorial periphery lobate, axial periphery rounded.

Wall calcareous, perforate, pitted. Sutures depressed, raidal on both spiral and umbilical sides. Umbilicus deep. Aperture umbilical, a high arch with a distinct lip.

Diameter: 0.55 mm.

Occurrence: Common in sample No. 1283, Ipolytarnóc.

Remarks: This species differs from *G. woodi woodi* Jenkins in possessing a high arched aperture, and in the rapid increase in the size of the chambers of the last whorl.

Jenkins (1965) described this species from the Lower Miocene of New Zealand.

GLOBIGERINA CIPEROENSIS ANGULISUTURALIS BOLLI

(Plate 3, Fig. 1a – d)

1957 *Globigerina ciperoensis angulisuturalis.* – Bolli, p. 109, pl. 22, Fig. 11a – c.
1960 *Globigerina ciperoensis angulisuturalis Bolli.* – Jenkins, p. 350, pl. 1, Fig. 4a – c.
1962 *Globigerina angulisuturalis Bolli.* – Blow and Banner (in Eames et al.) p. 84, pl. IX Aa – Cc.
1966 *Globigerina ciperoensis angulisuturalis Bolli.* – McTavish, p. 22, pl. 1, Fig. 19 – 20, 24.
1966 *Globigerina ciperoensis angulisuturalis Bolli.* – Jenkins, p. 4, pl. 1, Fig. 6a – c.

Description:

Test small, low trochospiral, composed of 2 1/2 whorls. The last whorl is composed of 5 chambers, increasing slowly in size as added; chambers spherical. Periphery rounded, lobate. Wall calcareous perforate, surface finely pitted. Sutures depressed, radial on both spiral and umbilical surfaces. The most characteristic feature is that this species possesses U-shaped, excavated intercameral sutures. Umbilicus small. Aperture arched, without a rim, interiomarginal.

Diameter: 0.28 mm.

Occurrence: Abundant in the *Globigerina ciperoensis ciperoensis* Zone of Ipolytarnóc.

GLOBIGERINA CIPEROENSIS ANGUSTIUMBILICATA BOLLI

(Plate 3, Fig. 4a – d)

1957 *Globigerina ciperoensis angustiumbilicata.* – Bolli, p. 109, pl. 22, Fig. 12a – 130.
1960 *Globigerina angustiumbilicata Bolli.* – Jenkins, p. 350, pl. 2, Fig. 2a – c.
1962 *Globigerina angustiumbilicata Bolli.* – Blow and Banner, p. 85, pl. IX Fig. X – Z.
1963 *Globigerina ciperoensis angustiumbilicata Bolli.* – Pessagno, p. 56, pl. 2. Fig. 8 – 9, 14.

1966 *Globigerina angustiumbilicata Bolli.* – McTavish, pl. 1. Fig. 33–34.
1966 *Globigerina angustiumbilicata Bolli.* – Jenkins, p. 4, pl. 1, Fig. 7a–c.

Description:

Test large, low trochospiral, composed of 2 1/2 whorls. The 4 chambers of the last whorl increase rapidly in size; chambers spherical. Periphery lobulate. Wall calcareous perforate, surface cancellate. Sutures radial, depressed on both the spiral and the umbilical sides. Umbilicus narrow and shallow. Aperture arched at the interior end, interiomarginal with a lip.

Diameter: 0.48 mm.

Occurrence: Frequent in the *G. ampliapertura* Zone, in the Eger bore-hole and at Novaj.

Globigerina angustiumbilicata was described by Bolli (1957) from the *Globigerina ciperoensis ciperoensis* Zone, Cipero formation, Trinidad.

GLOBIGERINA CIPEROENSIS CIPEROENSIS BOLLI

(Plate 2, Fig. 2a–d, 3a–d, 4a–d)

1954 *Globigerina ciperoensis.* – Bolli, p. 2, Text fig. 3, 3a; 4, 4a, 4b.
1956 *Globigerina ciperoensis Bolli.* – Drooger, pl. 1, Fig. 9a–c.
1957 *Globigerina ciperoensis ciperoensis.* – Bolli, p. 109, pl. 22, Fig. 10a–b.
1959 *Globigerina ciperoensis Bolli.* – Drooger and Batjes, p. 179, pl. 1.
1960 *Globigerina ciperoensis Bolli subsp, ciperoensis Bolli.* – Jenkins, p. 350, pl. 1. Fig. 5a–c.
1962 *Globigerina ouachitaensis ciperoensis Bolli.* – Blow and Banner, p. 90, pl. IX Fig. E–G.
1966 *Globigerina ciperoensis ciperoensis Bolli.* – McTavish pl. 1, Fig. 1–3, 6–7, 14–16.
1966 *Globigerina ciperoensis ciperoensis Bolli.* – Jenkins, p. 4, pl. 1, Fig. 9a–c.

Description:

Test medium, low to medium trochospiral, consists of four whorls of subglobular chambers, five chambers in each whorl, slightly increasing in size as added. Periphery strongly lobulate. Wall calcareous perforate, surface finely spinose, especially on the earlier chambers. Sutures distinctly depressed, radial both spirally and umbilically. Umbilicus large, deep, nearly quadrate in outline. Aperture arched interiomarginal.

Diameter: 0.55 mm.

Occurrence: Found in the *Globorotalia opima opima* Zone in the Eger bore-hole, Eger profile and at Novaj. Very rare at Törökbálint. Abundant in samples Nos. 1287, 1288 of Ipolytarnóc.

Bolli (1953) described and figured this species from the Globigerina ciperoensis zone, Lower Oligocene, Cipero formation, Trinidad.

GLOBIGERINA CORPULENTA SUBBOTINA

(Plate 3, Fig. 5a – d)

1953 *Globigerina corpulenta.* – Subbotina, p. 76, pl. X Fig. 1a – 4c.

Description:

Test medium, high trochospiral, consisting of about 3 whorls with 4 chambers in each whorl, increasing in size as added: chambers spherical. Periphery rounded, distinctly lobulate. Wall calcareous, perforate, surface pitted. Sutures distinctly depressed. Umbilicus broad, surrounded by the chambers of the last whorl. Aperture of each chamber opens into the umbilicus.

Diameter: 0.35 mm.

Occurrence: Rare in sample No. 29, *Globigerina ampliapertura* Zone, Eger bore-hole.

Subbotina (1953) described this species from the Upper Eocene of the Northern Caucasus, USSR.

Remarks: Our specimens from the Oligocene agree with those from the Upper Eocene. They are characterised by the turret-like spiral side and by the presence of a bladder-like "float" chamber, which is smaller than the chambers of the last whorl and located in our specimen between the first and the last chamber of the last whorl, giving it the shape of a bulla as in *Globigerinita.*

GLOBIGERINA DRURYI AKERS

(Plate 3, Fig. 3a – d)

1955 *Globigerina druryi.* – Akers, p. 654, pl. 65. Fig. 1a – 1c.

Description:

Test small, high trochospiral, consisting of two whorls, the last whorl consists of 3 subglobular chambers. Periphery rounded and distinctly lobulate. Wall coarsely perforate, hispid, umbilicus very narrow. Aperture arched, at the base of the last chamber, bordered by a narrow lip.

Diameter: 0.28 mm.

Occurrence: This species is rare in sample No. 29, Eger bore-hole.

G. druryi was described by Akers (1955) from the *Cibicides carstensis var. opimus* Zone, middle Miocene, Louisiana.

GLOBIGERINA EUAPERTURA JENKINS

(Plate 4, Fig. 1a – d)

1960 *Globigerina euapertura Jenkins,* p. 351, pl. 1, Fig. 8a – c.

Description:

Test medium, low trochospiral, composed of 5 whorls. The last whorl consists of 4 chambers, increasing in size as added. Chambers inflated, slightly embracing. Wall calcareous, perforate, surface hispid. Sutures slightly curved on the spiral side, radial, depressed on the umbilical side. Umbilicus deep, small. Aperture a low arch with a rim, interiomarginal.

Diameter: 0.32 mm.

Occurrence: Rare in sample No. 309, Novaj.

Jenkins (1960) recorded this species from the pre-*Globoquadrina dehiscens dehiscens* Zone to the middle of the *Globoquadrina dehiscens dehiscens* Zone in southeast Australia.

Remark: Jenkins (1960) considered this species to be intermediate in morphology between *Globoquadrina venezuelana* (Hedberg) and *Globigerina ampliapertura* Bolli.

GLOBIGERINA FOLIATA BOLLI

(Plate 3, Fig. 2a–d)

1957 *Globigerina foliata.* – Bolli, p. 111, pl. 24, Fig. 1a–c.
1959 *Globigerina foliata Bolli.* – Blow, pp. 177–178, pl. 10, Fig. 42a–c.
1960 *Globigerina foliata Bolli.* – Jenkins, p. 351, pl. 1, Fig. 9a–c.
1964 *Globigerina cf. G. foliata Bolli.* – Jenkins, p. 29. tabl. 1.
1966 *Globigerina foliata Bolli.* – Jenkins, p. 5. pl. 1, Fig. 11a–c.

Description:

Test small, low trochospiral, composed of 2 1/2 whorls. The last whorl is composed of 4 chambers increasing slowly in size; chambers spherical. Equatorial periphery lobate, axial periphery rounded. Wall calcareous, perforate, surface pitted. Sutures depressed, radial on both the spiral and umbilical sides. Umbilicus narrow. Aperture interiomarginal, umbilical with a thin lip.

Diameter: 0.25 mm.

Occurrence: A few specimens in sample No. 1287, Ipolytarnóc.

Bolli (1957) described this species from the *Catapsydrax dissimilis* Zone to the *Globorotalia menardii* Zone, Miocene, Trinidad.

GLOBIGERINA JUVENILIS BOLLI

(Plate 4, Fig. 2a–d)

1957 *Globigerina juvenilis.* – Bolli, p. 110, pl. 24. Fig. 5a–b.
1959 *Globigerina juvenilis Bolli.* – Blow, p. 178, pl. 10. Fig. 43a–b.
1960 *Globigerina juvenilis Bolli.* – Jenkins, pp. 351, 352, pl. 1, Fig. 10a–c, 11a–c.
1964 *Globigerina juvenilis Bolli.* – Jenkins, p. 29 tab. 1.
1966 *Globigerina juvenilis Bolli.* – McTavish p. 22, pl. 1, Fig. 17–18, 22.
1966 *Globigerina juvenilis Bolli.* – Jenkins, p. 5. pl. 1, Fig. 12a–c.

Description:

Test small, low trochospiral, composed of 3 whorls, the last whorl with 4 chambers, increasing rapidly in size. Chambers spherical. Equatorial periphery lobate, axial periphery rounded. Wall calcareous perforate, finely pitted. Sutures distinctly depressed, radial on both the spiral and the umbilical sides. Umbilicus very narrow. Aperture a low elongate slit with a lip.

Diameter: 0.25 mm.

Occurrence: Common in sample No. 1287, Ipolytarnóc.

GLOBIGERINA LABIACRASSATA JENKINS

(Plate 4, Fig. 3a – d)

1965 *Globigerina labiacrassata.* – Jenkins, p. 1102–1103, Fig. 64–71.

Description:

Test medium, low trochospiral, consisting of 2 1/2 whorls. The first whorl composed of 5 chambers, the later whorl composed of 4 embracing chambers. Periphery rounded, lobulate. Wall calcareous, fairly coarsely perforate. Sutures depressed, radial on both the spiral and umbilical surfaces. Umbilicus large, open. Apertura high arch with a distinct rim, interiomarginal.

Diameter: 0.4 mm.

Occurrence: Rare in sample No. 20, *Globorotalia opima opima* Zone, Eger profile.

Jenkins (1965) described this species from the *Globigerina angiporoides angiporoides* Zone to the lower part of the *Globoquadrina dehiscens* zone, Oligocene to Lower Miocene, New Zealand.

GLOBIGERINA LINAPERTA FINLAY

(Plate 4, Fig. 4a – d)

1939 *Globigerina linaperta.* – Finlay, p. 125, pl. 13, Fig. 54–57.
1957 *Globigerina linaperta Finlay.* – Bolli, p. 70, pl. 15, Fig. 15–17; p. 163 pl. 36. Fig. 5a–6.
1957 *Globigerina triloculinoides Plummer.* – Loeblich and Tappan, p. 183–184, pl. 62, Fig. 3a–c, 4a–c; pl. 56, Fig. 8a–c.
1958 *Globigerina linaperta Finlay.* – Hornibrook, p. 33, pl. 1, Fig. 19–21.
1962 *Globigerina linaperta linaperta Finlay.* – Blow and Banner p. 85. pl. XI. H.
1966 *Globigerina linaperta Finlay.* – McTavish, p. 24, pl. 2, Fig. 29, 31–33.

Description:

Test small, low trochospiral, consisting of about three whorls: the first whorl consists of about 4 embracing chambers, the later whorl of 3 chambers, rapidly enlarging in size. Periphery weakly lobulate. Wall calcareous, coarsely

perforate. Sutures radial, depressed. Umbilicus small. Aperture in the form of a large arch, bordered throughout its length by a distinct lip.

Diameter: 0.3 mm.

Occurrence: In the *G. ouachitaensis ouachitaensis* Zone, Eger bore-hole, and in the *G. ampliapertura* Zone, Novaj.

Finlay (1939) described this species from the middle Eocene of New Zealand.

Remarks: G. linaperta Finlay differs from *G. trilocularis* d'Orbigny in that its chambers are more compressed and by its wide low arched aperture which extends laterally to cover previous chambers, instead of centrally.

GLOBIGERINA NEPENTHES TODD

(Plate 4, Fig. 5a – d)

1957 *Globigerina nepenthes.* – Todd, p. 301, pl. 78, Fig. 7.
1957 *Globigerina nepenthes Todd.* – Bolli, p. 111. pl. 24. Fig. 3a – c.
1959 *Globigerina cf. nepenthes Todd.* – Drooger and Batjes, p. 179, pl. 1, Fig. 8.
1966 *Globigerina nepenthes Todd.* – McTavish, pl. 1, Fig. 12 – 13.
1967 *Globigerina nepenthes Todd.* – Cita and Premoli, pl. 1, Fig. 6a – c.

Description:

Test small, completely coiled, except the last-formed, protruding chamber. The last whorl is composed of 4 chambers. Chambers inflated. Periphery weakly lobulate. Wall calcareous, perforate, surface cancellate. Sutures depressed. Aperture large semicircular, arched, at the base of the last formed protruding chamber, bordered by a thick lip.

Diameter: 0.30 mm.

Occurrence: Only one specimen in sample No 1283, Ipolytarnóc.

Todd (1957) described this species from the Miocene of the Mariana Islands.

GLOBIGERINA OUACHITAENSIS GNAUKI BLOW AND BANNER

(Plate 5, Fig. 3a – d, 4a – d)

1962 *Globigerina ouachitaensis gnauki.* – Blow and Banner p. 91, pl. IX. Fig. L – N.

Description:

Test medium in size, high trochospiral, consists of 3 whorls. First whorl composed of 5 – 6 chambers; only the 4 chambers of the final whorl are visible on the umbilical side. Periphery rounded and distinctly lobulate. Wall calcareous, finely perforate, with cancellate and sightly hispid surface. Umbilicus deep. Aperture open, interomarginal, bordered by a rim.

Diameter: 0.48 mm.

Occurrence: Abundant in the *Globigerina ouachitaensis ouachitaensis* Zone, *G. ampliapertura* Zone and *Globorotalia opima opima* Zone, Eger bore-hole and *G. opima opima* Zone, Eger profile and Novaj.

This subspecies was described and illustrated by Blow and Banner (1962) from the *G. oligocaenica* Zone, Oligocene, Lindi area, East Africa.

GLOBIGERINA OUACHITAENSIS OUACHITAENSIS HOWE AND WALLACE

(Plate 5, Fig. 5a – d)

1932 *Globigerina ouachitaensis.* – Howe and Wallace, p. 74, pl. 10. Fig. 7a – b.
1959 *Globigerina bulloides d'Orbigny.* – Drooger and Batjes p. 175, pl. 1, Fig. 3.
1962 *Globigerina ouachitaensis ouachitaensis Howe and Wallace.* – Blow and Banner, p. 90. pl. IX. Fig. D, H – K.
1963 *Globigerina ouachitaensis Howe and Wallace.* – Hofker, p. 200, Textfig. 4, 5.

Description:

Test small, low trochospiral, consisting of about 3 whorls. The last whorl consists of about 4 subglobular chambers increasing in size as added. Periphery strongly lobulate. Wall calcareous perforate, surface strongly hispid. Sutures radial, depressed both on the spiral and umbilical sides. Umbilicus deep broad quadrate. Aperture of the last chamber distinct in the form of a low arch bordered by a rim-like thickening.

Diameter: 0.3 mm.

Occurrence: Abundant in the *Globigerina ouachitaensis ouachitaensis* Zone, Eger bore-hole; some specimens were found also in the *Globigerina ampliapertura* Zone.

GLOBIGERINA PARVA BOLLI

(Plate 5, Fig. 1a – d, 2a – d)

1956 *Globigerina cf. bulloides d'Orbigny.* – Drooger, pl. 1. Fig. 6.
1957 *Globigerina parva.* – Bolli, p. 108, pl. 22, Fig. 14.
1959 *Globigerina parva Bolli.* – Drooger and Batjes, p. 175, pl. 1, Fig. 4.
1962 *Globigerina officinalis Subbotina.* – Blow and Banner p. 88. pl. IXA – C, Fig. 16.
1963 *Globigerina parva Bolli.* – Pessagno, p. 56, pl. 2, Fig. 1 – 3.

Description:

Test small in size, low trochospiral, consists of three whorls. There are four chambers in the final whorl, increasing moderately in size as added. Chambers subglobular. Periphery distinctly lobulate. Wall calcareous, perforate, surface finely pitted. Sutures in both spiral and umbilical sides distinct, radial, depressed. Umbilicus small, closed. Aperture arched, interiomarginal.

Diameter: 0.25 mm.

Occurrence: Abundant in the *Globigerina ampliapertura* zone and *Globorotalia opima opima* zone in the Eger bore-hole, Eger profile, at Novaj and Törökbálint; frequent at Ipolytarnóc.

Globigerina parva was recorded by Bolli (1957) from the *Globigerina ampliapertura* zone, Oligocene, Cipero formation, Trinidad.

Remarks: This species differs from *G. officinalis* Subbotina in that the chamber of the last whorl increases moderatly in size as added; the most characteristic feature of *G. officinalis* is the shape and the diameter of the last semispherical chamber which is sometimes one-half the size of the entire test.

GLOBIGERINA PRAEBULLOIDES LEROYI BLOW AND BANNER

(Plate 6, Fig. 1a–d, 2a–d, 5a, b)

1953 *Globigerina globularis Roemer.* – Batjes, p. 161–162, pl. XI. Fig. 4a–c.

1962 *Globigerina praebulloides leroyi.* – Blow and Banner, p. 93, pl. IX. Fig. R–T.

1963 *Globigerina leroyi Banner and Blow.* – Hofker, p. 202, Text. Abb. 11.

1966 *Globigerina leroyi Blow and Banner.* – Jenkins, p. 5. pl. 1, Fig. 3a–c.

Description:

Test medium, low trochospiral, consisting of 3 whorls. Early chambers compressed, about 12 arranged in about 2 1/2 whorls; the last 3 1/2 chambers of the last whorl increase rapidly in size as added. Wall calcareous, finely perforate, hispid. Sutures distinctly depressed. Umbilicus deep and open. Aperture in the form of a symmetrical arch bordered by a thin rim.

Diameter: 0.27 mm.

Occurrence: In the *Globorotalia opima opima* zone, Eger profile and Törökbálint; abundant in the *Globigerina ciperoensis ciperoensis* Zone, Ipolytarnóc.

Batjes (1953) described this species as *Globigerina globularis* from the Oligocene of Belgium.

GLOBIGERINA PRAEBULLOIDES OCCLUSA BLOW AND BANNER

(Plate 7, Fig. 1a–d)

1957 *Globigerina cf. trilocularis d'Orbigny.* – Bolli, p. 110, 163, pl. 22, Fig. 9a–c, pl. 36, Fig. 3a–b.

1959 *Globigerina globularis Roemer.* – Drooger and Batjes, p. 174, pl. 1, Fig. 2.

1962 *Globigerina praebulloides occlusa.* – Blow and Banner, p. 93–94, pl. IX. u–w.

Description:

Test small, low trochospiral, consisting of three whorls. The first whorl consists of five inflated chambers, the last whorl of four subglobular to ovoid chambers. Periphery strongly lobulate. Wall calcareous, coarsely perforate, periphery hispid. Sutures depressed, slightly curved spirally, radial umbilically. Umbilicus very narrow, shallow. Aperture very low without a lip.

Diameter: 0.33 mm.

Occurrence: In sample No. 308, Novaj.

Bolli (1957) recorded this species as *Globigerina cf. trilocularis* from the *Globorotalia lehneri* Zone, middle Eocene, Navet formation to *Catapsydrax dissimilis* Zone, Miocene, Cipero formation, Trinidad.

Globigerina praebulloides occlusa was illustrated by Drooger and Batjes (1959) as *Globigerina globularis* from the Oligocene of the North Sea Basin.

GLOBIGERINA PRAEBULLOIDES PRAEBULLOIDES BLOW

(Plate 6, Fig. 3a–d, 4a–d)

1959 *Globigerina praebulloides.* – Blow, p. 180. pl. 8, Fig. 47a–c; pl. 9, Fig. 48.

1960 *Globigerina praebulloides Blow.* – Jenkins, p. 352, pl. 2, Fig. 1a–c.

1962 *Globigerina praebulloides praebulloides Blow.* – Blow and Banner p. 92. pl. IX. Fig. O–Q.

1966 *Globigerina praebulloides Blow.* – McTavish, pl. 1, Fig. 21, 23, 26.

1966 *Globigerina praebulloides Blow.* – Jenkins, p. 6. pl. 1, Fig. 15a–c.

Description:

Test small, low trochospiral, composed of about 3 whorls, the last whorl composed of 3 very rapidly increasing and globular chambers. Periphery rounded and distinctly lobulate. Wall calcareous perforate, surface strongly reticulate. Sutures distinctly depressed on the spiral and umbilical surfaces. Umbilicus broad, deep and open. Aperture a high arch, bordered by a thin rim-like lip.

Diameter: 0.52 mm.

Occurrence: In the *Globigerina ampliapertura* and *Globorotalia opima opima* Zone, Eger bore-hole and Novaj. Frequent also in the *G. ciperoensis ciperoensis* Zone, Ipolytarnóc.

Blow (1959) gave the range of *G. praebulloides* as *Catapsydrax stainforthi* Zone to *Globorotalia menardii menardii, Globigerina nepenthes* Zone in Venezuela.

Blow and Banner (in Eames et al., 1962) recorded it from the base of the *Globigerapsis semiinvoluta* Zone, upper Eocene, to the middle part of the *Globorotalia culturata (Globigerina nepenthes)* Zone, (Helvetian). They have split up *G. praebulloides* into a number of subspecies.

GLOBIGERINA ROHRI BOLLI

(Plate 8, Fig. 2a – d)

1953 *Globigerina venezuelana Hedberg.* – Beckmann, p. 392 pl. 10, Fig. 12 – 13.
1957 *Globigerina rohri.* – Bolli, p. 109, pl. 23. Fig. 1a – 4b.
1961 *Globigerina cf. rohri Bolli.* – Gordon, p. 452, pl. 1, Fig. 5a – c.
1963 *Globigerina rohri Bolli.* – Pessagno, pl. 56. pl. 3, Fig. 1 – 2.
1966 *Globigerina rohri Bolli.* – McTavish, pl. 1, Fig. 34, 38 – 39.

Description:

Test large, spherical, low trochospiral, consisting of about three whorls of rapidly enlarging, partially embracing chambers. The last whorl composed of about 3 globular chambers, laterally compressed. Periphery lobulate. Wall calcareous perforate, surface pitted. Sutures in the spiral surface slightly oblique, depressed: in the umbilical surface, radial, depressed. Umbilicus deep, open triangular in shape. Aperture arched, interiomarginal.

Diameter: 0.52 mm.

Occurrence: In the *G. ampliapertura* Zone, Eger bore-hole.

Globigerina rohri was first described by Bolli (1957). from the *Globigerina ampliapertura* zone (Oligocene) to the *Catapsydrax dissimilis* zone (Lower Miocene, Cipero formation, southern Trinidad).

GLOBIGERINA SENILIS BANDY

(Plate 7, Fig. 2a – d, 3a, b, 4a, b)

1949 *Globigerina ouachitaensis Howe and Wallace var. senilis.* – Bandy, p. 121. pl. 22. Fig. 5a – c.
1962 *Globigerina senilis Bandy.* – Blow and Banner (in Eames et al., 1962) p. 95, pl. XI R – U.

Description:

Test medium in size, subglobular, medium trochospiral, composed of three whorls, the last whorl composed of 4 inflated, laterally compressed chambers, the last chamber smaller than the penultimate. Periphery weakly lobulate. Wall calcareous perforate, surface reticulate, coarse granular. Sutures depressed in both spiral and umbilical sides. Umbilicus deep, nearly quadrangular. Aperture highly arched, bordered by a narrow rim.

Diameter: 0.38 mm.

Occurrence: In samples Nos. 126, 26, 21, Eger bore-hole, and in sample No. 309, Novaj.

Bandy (1949) described this species from the Upper Eocene, lower Oligocene and middle Oligocene of the Jackson formation, Alabama.

GLOBIGERINA TRILOCULARIS D'ORBIGNY

(Plate 9, Fig. 1a – d, 2a – d)

1944 *Globigerina trilocularis d'Orbigny.* – Bandy, p. 376, pl. 62, Fig. 7a – b.

1955 *Globigerina trilocularis d'Orbigny.* – Weiss, p. 308, pl. 1, Fig. 22–23.
1957 *Globigerina cf. trilocularis d'Orbigny.* – Bolli, p. 163, pl. 36, Fig. 3a–b.
1961 *Globigerina trilocularis d'Orbigny.* – Gordon, p. 452, pl. 1, Fig. 6a–c.

Description:

Test small, medium trochospiral, consisting of about 2 1/2 whorls; the last whorl is composed of 3 rapidly increasing globular chambers. Periphery rounded and distinctly lobulate. Wall calcareous, perforate, surface reticulate. Sutures depressed. Umbilicus small, depressed. Aperture arched, slit at the base of the last chamber and bordered by a rim.

Diameter: 0.32 mm.

Occurrence: In the *Globigerina ouachitaensis ouachitaensis* and *G. ampliapertura* zones, in Eger bore-hole, and in the *G. ampliapertura* Zone, at Novaj.

Weiss (1955) recorded *Globigerina trilocularis* from the Paleocene and Lower Eocene of Peru.

GLOBIGERINA TURRITILINA PRAETURRITILINA BLOW AND BANNER

(Plate 10, Fig. 2a–d)

1962 *Globigerina turritilina praeturritilina.* – Blow and Banner, p. 99. pl. XIII. A–C.

Description:

Test large, high trochospiral, consists of about three whorls, each whorl consists of about four chambers which increase gradually in size as added; they are slightly inflated; periphery rounded, lobulate. Wall calcareous, finely perforate, pitted. Sutures distinctly depressed in both spiral and umbilical surfaces. Umbilicus deep, broad. Aperture umbilical.

Diameter: 0.6 mm.

Occurrence: This species is rare in the *Globigerina ampliapertura* Zone of Eger bore-hole.

Blow and Banner (1962) described this subspecies from the Upper Eocene of East Africa.

GLOBIGERINA TURRITILINA TURRITILINA BLOW AND BANNER

(Plate 10, Fig. 3a–d)

1962 *Globigerina turritilina turritilina.* – Blow and Banner p. 98. pl. XIII. Fig. D–G.

Description:

Test large, high trochospiral, consisting of about 3 1/2 weakly embracing whorls, each whorl of about 4 chambers increasing in size as added: chambers

spherical. Periphery strongly lobulate. Wall coarsely perforate, finely cancellate. Sutures strongly depressed both in spiral and umbilical surface. Umbilicus deep, quadrate in outline between the last 4 chambers. Aperture arched, interiomarginal.

Diameter: 0.50 mm.

Occurrence: Aboundant in the *Globigerina ampliapertura* Zone, Eger borehole.

Blow and Banner (in Eames et al., 1962) recorded this species from the uppermost Bartonian and Lattorfian-Rupelian of East Africa.

Remarks: This species is like the holotype of Blow and Banner. It even shows the reduced-size final chamber in the last whorl.

GLOBIGERINA WOODI WOODI JENKINS

(Plate 9, Fig. 3a – d)

1960 *Globigerina woodi.* – Jenkins, p. 352, pl. 2. Fig. 2a – c.
1964 *Globigerina woodi.* – Jenkins, p. 29, pl. 1.
1966 *Globigerina woodi woodi.* – Jenkins, p. 6, pl. 1, Fig. 18a – c.

Description:

Test medium, low trochospiral, composed of 3 whorls: the last whorl composed of 3 spherical chambers; final whorl with 3 chambers increasing in size as added; last chamber larger than the penultimate. Periphery rounded, distinctly lobulate. Wall calcareous, perforate, coarsely pitted. Sutures distinctly depressed, radial on both spiral and umbilical sides. Umbilicus narrow, small. Aperture an extraumbilical, semicircular arch with a clear lip around its border.

Diameter: 0.42 mm.

Occurrence: Abundant in sample No. 1283, Ipolytarnóc.

Jenkins (1960) recorded this species from the base of the *G. woodi* Zone to the *Globorotalia menardii miotumida* Zone in a southeast Australian sequence.

GLOBIGERINA WOODI CONNECTA JENKINS

(Plate 10, Fig. 1a – d)

1964 *Globigerina woodi subsp. connecta.* – Jenkins, p. 72, Text fig. 1a – c.
1966 *Globigerina woodi cf. G. woodi connecta.* – Jenkins, p. 6, pl. 1, Fig. 17a – c.

Description:

Test small, low trochospiral, composed for the most part of the three last formed chambers, the last one comprising about half of the test. Chambers globular, increasing very rapidly in size as added. Periphery rounded, lobulate. Wall calcareous, perforate, finely cancellate. Sutures deeply depressed. Aperture a low arch, slightly rimmed.

Diameter: 0.35 mm.

Occurrence: Abundant in the samples of Ipolytarnóc.

Jenkins (1964) described and illustrated this species from the lower Miocene of Australia. In 1966, he recorded this species from the upper Aquitanian of France.

GLOBIGERINA YEGUAENSIS WEINZIERL AND APPLIN

(Plate 9, Fig. 4a–d)

1929 *Globigerina yeguaensis Weinzierl and Applin*, p. 408, pl. 43, Fig. 1a–b.
1957 *Globigerina yeguaensis Weinzierl and Applin.* – Bolli, p. 163, pl. 35, Fig. 15a–c.
1962 *Globigerina yeguaensis Weinzierl and Applin.* – Blow and Banner, p. 99. pl. XIII. Fig. H–M.

Description:

Test large, low trochospiral, consists of about 3 whorls, each whorl consists of 4 rapidly enlarging, inflated chambers. The chambers are subcircular. Periphery rounded, distinctly lobulate. Wall calcareous, coarsely perforate, hispid. Sutures distinctly depressed. Umbilicus broad, deep, open. Aperture in the form of an arch, bordered by a flap-like lip, interioumbilical.

Diameter: 0.50 mm.

Occurrence: This species occurs in the *G. ampliapertura* Zone, Eger bore-hole.

Remarks: Globigerina yeguaensis differs from *Globoquadrina venezuelana* in that it has a fairly open umbilicus and its aperture is protected by a lip. *Globigerina yeguaensis* has no rudimentary final chamber as has *Globoquadrina venezuelana.*

This species was originally described from the upper Claiborne (Middle Eocene) of Texas.

GLOBIGERINA SP.

(Plate 8, Fig. 1a–d)

Description:

Test large, compact; three whorls. The last whorl is composed of 4 inflated, sligthly compressed chambers, the rate of enlargement of the chambers increases during ontogeny. The equatorial periphery is strongly lobulate, the axial periphery is broadly rounded. Wall calcareous, coarsely perforate, surface cancellate and hispid. Sutures depressed, slightly curved on the spiral side, radial on the umbilical side. Umbilicus fairly broad, open and deep, square in outline. Aperture intraumbilical, a low arch without a distinct rim.

Diameter: 0.7 mm.

Occurrence: Rare in sample No. 13, Eger bore-hole.

Remarks: This species is characterized by a large compact test, inflated, compressed chambers, and a large broad, square umbilicus.

GENUS GLOBIGERINITA BRÖNNIMANN 1951
GLOBIGERINITA DISSIMILIS (CUSHMAN AND BERMUDEZ)

(Plate 11, Fig. 1a–d)

1937 *Globigerina dissimilis.* – Cushman and Bermudez, p. 25, pl. 3. Fig. 4–6.
1957 *Catapsydrax dissimilis (Cushman and Bermudez).* – Bolli, Loeblich and Tappan, pl. 7, Fig. 6a–c, 7a–b.
1957 *Catapsydrax cf. dissimilis (Cushman and Bermudez).* – Bolli, p. 166, pl. 37, Fig. 6a–b.
1962 *Globigerinita dissimilis dissimilis (Cushman and Bermudez).* – Blow and Banner, p. 106, pl. XIV, Fig. D.
1966 *Globigerina (Globigerinita) dissimilis Cushman and Bermudez.* – McTavish, pl. 2. Fig. 15–17, 27–28.

Description:

Test medium, low trochospiral, consisting of 3 whorls. The first whorl consists of about 5 chambers, the last whorl of 4 inflated, partially embracing chambers. Periphery distinctly lobulate. Wall calcareous, perforate, finely hispid. Sutures depressed throughout. Umbilicus invisible owing to the presence of a bulla. The bulla extends from the apertural face of the last chamber across the umbilicus to the margin of the opposite chamber. Primary aperture interiomarginal, umbilical; accessory apertures are indistinct.

Diameter: 0.48 mm.

Occurrence: In the *G. ampliapertura* Zone, Eger bore-hole.

Cushman and Bermudez (1937) described *Globigerina dissimilis* from the Eocene of Cuba.

GLOBIGERINITA MARTINI MARTINI BLOW AND BANNER

(Plate 11, Fig. 2a–d, 3a, b)

1962 *Globigerinita martini martini Blow and Banner*, p. 110. pl. XIV, O.
1966 *Globigerina (Globigerinita) martini Blow and Banner.* – McTavish, pl. 2. Fig. 12–14.

Description:

Test small, low trochospiral, consists of about three whorls. The last whorl is composed of 3 rapidly increasing inflated chambers. Periphery strongly lobulate. Wall calcareous, coarsely perforate, hispid. Sutures distinct, depressed. Umbilicus deep, covered by a small bulla: the bulla is attached to the umbilical margin of the first and the final chamber of the last whorl.

Diameter: 0.2 mm.

Occurrence: In sample No. 13, Eger bore-hole, and sample No. 322, Törökbálint.

Stratigraphic range: Globigerinita martini martini was recorded by Blow and Banner (1962) from the upper part of the *Truncorotaloides rohri* Zone (middle Eocene) to the top of the *Globigerina turritilina turritilina* Zone (upper Eocene).

GLOBIGERINITA UNICAVA PRIMITIVA BLOW AND BANNER

(Plate 12, Fig. 1a–d)

1962 *Globigerinita unicava primitiva.* – Blow and Banner, p. 114, pl. XIV, J–L.

Description:

Test small, subquadrate, low trochospiral, consists of three whorls of rapidly enlarging, embracing chambers. The last whorl has 4 chambers, ovoid in axial profile. Axial periphery rounded, equatorial periphery weakly lobate. Wall calcareous, perforate, surface hispid. Sutures radial to weakly curved. Umbilicus deep and not covered by the bulla. The bulla is subquadrate in outline, its wall is much thinner and finely perforate. Aperture broad, extends along the margin of the bulla.

Diameter: 0.32 mm.

Occurrence: In sample No. 16, Eger bore-hole.

Blow and Banner (1962) described this subspecies from the *Truncorotaloides rohri* Zone, (middle Eocene), to the top of the *Globigerina oligocaenica* Zone, (Oligocene) East Africa.

Remarks: This species differs from *G. unicava unicava* in having a subquadrate test, in possessing more depressed later chambers and a more restricted bulla of subtriangular outline which incompletely covers the umbilicus.

GLOBIGERINITA UNICAVA UNICAVA (BOLLI, LOEBLICH AND TAPPAN)

(Plate 11, Fig. 4a–d, 5a, b)

1957 *Catapsydrax unicavus.* Bolli, Loeblich and Tappan, p. 37, pl. 7. Fig. 9a–c. p. 116, pl. 37, Fig. 7a–b.

1960 *Catapsydrax unicavus Bolli, Loeblich and Tappan.* – Jenkins, p. 356, pl. 3. Fig. 7a–c.

1962 *Globigerinita unicava unicava (Bolli, Loeblich and Tappan).* – Blow and Banner, p. 113, pl. XIV. Fig. M, N.

1966 *Globigerina (Globigerinita) unicava Bolli, Loeblich and Tappan.* – McTavish, pl. 2, Fig. 19, 22–23.

Description:

Test medium, trochospiral, subquadrate, of about three whorls. The first whorl consists of 5 chambers, the last of 4 chambers. The chambers are rapidly enlarging, inflated and partially embracing. Periphery lobulate. Wall calcareous, perforate, surface smooth, pitted, weakly hispid. Umbilicus deep, broad. Aperture interiomarginal, umbilical, covered by a small bulla which is attached at the side; the bulla is subquadrate in outline.

Diameter: 0.30 mm.

Occurrence: In the *Globigerina ouachitaensis ouachitaensis* and *Globigerina ampliapertura* Zones, Eger bore-hole; also Novaj.

This species was illustrated and described by Bolli, Loeblich and Tappan (1957) from the *Globigerina ciperoensis ciperoensis* Zone, Upper Oligocene, Trinidad.

GENUS GLOBIGERINOIDES CUSHMAN, 1927
GLOBIGERINOIDES PRIMORDIUS BLOW AND BANNER

(Plate 11, Fig. 6a – d)

1962 *Globigerinoides quadrilobata primordius.* – Blow and Banner (in Eames et al.), p. 115, pl. IX Dd – Ff, Fig. 14 (iii, viii).
1964 *Globigerinoides cf. G. primordius Blow and Banner.* – Jenkins, p. 29, tab. 1.
1966 *Globigerinoides cf. G. primordius Blow and Banner.* – Jenkins, p. 8, pl. 2, Fig. 7a – c.

Description:

Test small, low trochospiral consisting of 2 1/2 whorls. The last whorl is composed of 4 chambers. Chambers of the last whorl subspherical, slightly embracing, increasing slowly in size as added. Periphery lobulate, rounded. Wall calcareous, coarsely perforate, surface cancellate. Sutures depressed, radial on both the spiral and the umbilical sides. Umbilicus narrow. Only two apertures are present. A sutural aperture is a small hole without a lip in the wall of the last chamber; the primary aperture is intraumbilical, in the form of an arch with a rim.

Diameter: 0.28 mm.

Occurrence: Rare in sample No. 1287, Ipolytarnóc.

Globigerinoides primordius was described by Blow and Banner (in Eames et al., 1962) from the *Globorotalia kugleri* Zone of Trinidad.

GENUS GLOBOQUADRINA FINLAY, 1947
GLOBOQUADRINA DEHISCENS (CHAPMAN, PARR AND COLLINS)

(Plate 13, Fig. 2a – d)

1957 *Globoquadrina dehiscens (Chapman, Parr and Collins).* – Bolli, p. 111, pl. 24, Fig. 3a – 4a.
1959 *Globoquadrina dehiscens dehiscens (Chapman, Parr and Collins).* – Blow, p. 182, pl. 8, Fig. 49a – c.
1960 *Globoquadrina dehiscens (Chapman, Parr and Collins)* subsp. dehiscens (Chapman, Parr and Collins). – Jenkins, pp. 354 – 355, pl. 3. Fig. 3a – c.
1964 *Globoquadrina dehiscens (Chapman, Parr and Collins).* – Jenkins, p. 29, table 1.
1966 *Globoquadrina dehiscens (Chapman, Parr and Collins).* – Jenkins, p. 6, pl. 1, Fig. 19a – c, pl. 2, Fig. 1.

Description:

Test small, low trochospiral, composed of 3 whorls: each whorl composed of 4 chambers. Chambers subangular. Periphery truncate. Wall calcareous, perforate, surface pitted. Sutures slightly depressed, gently curved on the spiral side, radial on the umbilical side. Aperture interiomarginal, covered by an apertural flap.

Diameter: 0.25 mm.

Occurrence: In sample No. 1280, Ipolytarnóc.

Globoquadrina dehiscens was originally described from the Balcombian rocks of Victoria, Australia by Chapman et al. (1934).

GLOBOQUADRINA LARMEUI AKERS

(Plate 13, Fig. 1a – d)

1955 *Globoquadrina larmeui.* – Akers, p. 661, pl. 65. Fig. 4a – c.
1960 *Globoquadrina larmeui Akers.* – Jenkins, p. 355, pl. 3. Fig. 2a – c.
1964 *Globoquadrina cf. G. larmeui Akers.* – Jenkins, p. 29, tab. 1.
1966 *Globoquadrina larmeui Akers.* – Jenkins, p. 7. pl. 2. Fig. 2a – c.

Description:

Test small, low trochospiral, composed of 2 1/2 whorls. The last whorl composed of 4 chambers, chambers spherical. Equatorial periphery lobate, axial periphery rounded. Wall calcareous, perforate, surface cancellate. Sutures distinctly depressed, radial to slightly curved on both the spiral and the umbilical sides. Aperture slit-like, opening at the base of the last chamber, covered by a small labrum-like projection.

Diameter: 0.28 mm.

Occurrence: In sample No. 1287 at Ipolytarnóc.

Stratigraphic range:

Akers (1955) first described *G. larmeui* from the Middle Miocene of Louisiana, USA.

GLOBOQUADRINA VENEZUELANA (HEDBERG)

(Plate 12, Fig. 2a – d, 3a – d)

1937 *Globigerina venezuelana.* – Hedberg, p. 681, pl. 92. Fig. 7.
1955 *Globigerina venezuelana Hedberg.* – Weiss, p. 310, 1. 3, Fig. 16 – 17.
1956 *Globigerina venezuelana Hedberg.* – Drooger, p. 190, pl. 1. Fig. 13.
1957 *Globigerina venezuelana Hedberg.* – Bolli, p. 110, pl. 23, Fig. 6a – 8b, p. 161, pl. 35. Fig. 16 – 17.
1959 *Globigerina venezuelana Hedberg.* – Drooger and Magné, pl. 1, Fig. 3a – c.
1961 *Globigerina venezuelana Hedberg.* – Gordon p. 452, pl. 1, Fig. 4a – c.
1963 *Globigerina venezuelana Hedberg.* – Passagno, p. 56, pl. 3, Fig. 3 – 7.
1966 *Globoquadrina venezuelana (Hedberg).* – McTavish, p. 28. pl. 4. Fig. 18, 24 – 25.

Description:

Test large, trochospiral, consisting of about 2 whorls of rapidly enlarging, partially embracing chambers, the 4 chambers of the last whorl enlarging gradually as added, subglobular; the final chamber is reduced in size. Periphery rounded and lobulate. Wall calcareous, perforate, strongly reticulate. Sutures on spiral side slightly curved, depressed: on the umbilical side, radial, depressed. Aperture interiomarginal. Umbilicus deep, quadrangular.

Diameter: 0.52 mm.

Occurrence: In both the *Globigerina ampliapertura* and *Globorotalia opima opima* Zones, Eger bore-hole, Novaj.

Hedberg (1937) described this species from the Carapite formation, Oligocene, Venezuela.

Globigerina venezuelana was found by Weiss (1955) in the Oligocene of north western Peru.

Drooger and Magné (1959) recorded it from the Oligocene, of Algeria.

SUBFAMILY GLOBOROTALIINAE CUSHMAN, 1927

GENUS GLOBOROTALIA CUSHMAN, 1927

GLOBOROTALIA CONTINUOSA BLOW

(Plate 13, Fig. 3a–f)

1959 *Globorotalia opima continuosa.* – Blow, p. 218–219, pl. 19. Fig. 125a–c.
1960 *Globorotalia opima Bolli subsp. continuosa Blow.* – Jenkins, p. 366, pl. 5, Fig. 4a–c, 5a–c.
1964 *Globorotalia continuosa Blow.* – Jenkins, p. 29. tab. 1.
1966 *Globorotalia opima continuosa Blow.* – McTavish, p. 28, pl. 4. Fig. 2–3, 8.
1966 *Globorotalia continuosa Blow.* – Jenkins, p. 9. pl. 1. Fig. 9a–c.

Description:

Test medium, low trochospiral, composed of 3 whorls, the last whorl composed of 4 chambers rapidly increasing in size. Chambers inflated, subspherical, ovate. Periphery rounded, distinctly lobulate. Wall calcareous, perforate, finely hispid. Sutures depressed in both spiral and umbilical sides. Umbilical narrow. Aperture a high arch with a distinctive lip.

Diameter: 0.36 mm.

Occurrence: Abundant in sample No. 1283, Ipolytarnóc.

Blow (1959) was first to record this species from the Miocene of Venezuela, where it ranges from the *Catapsydrax stainforthi* Zone, to the *Sphaeroidinella seminula* Zone.

GLOBOROTALIA EXTENS JENKINS

(Plate 13, Fig. 5a – d)

1960 *Globorotalia extens.* – Jenkins, p. 360, pl. 4, Fig. 4a – c, 5a – c.

Description:

Test minute, low trochospiral, composed of 3 whorls. The last whorl is composed of, 5 chambers, increasing rapidly in size as added; chambers ovoid. Axial periphery rounded, equatorial periphery lobate. Wall calcareous, perforate, surface pitted. Sutures on both the spiral and the umbilical sides depressed. Umbilicus narrow. Aperture a low arch, slit-like, extraumbilical.

Diameter: 0.22 mm.

Occurrence: Freqent in sample No. 322, *Globorotalia opima opima* Zone, Törökbálint.

This species was described by Jenkins (1960) from the *Globoquadrina dehiscens dehiscens* Zone to the *Globigerina woodi* Zone, southeastern Australia.

GLOBOROTALIA OBESA BOLLI

(Plate 13, Fig. 4a – f)

1957 *Globorotalia obesa.* – Bolli, p. 119, pl. 29. Fig. 2a – 3.
1959 *Globorotalia obesa Bolli.* – Blow, p. 218, pl. 19. Fig. 124a – c.
1960 *Globorotalia obesa Bolli.* – Jenkins, p. 364, pl. 5. Fig. 2a – c.
1964 *Globorotalia cf. G. obesa Bolli.* – Jenkins, p. 29, tabl. 1.
1966 *Globorotalia cf. G. obesa Bolli.* – McTavish, p. 28, pl. 4. Fig. 20 – 21, 26.
1966 *Globorotalia obesa Bolli.* – Jenkins, p. 10, pl. 2, Fig. 10a – c.

Description:

Test small, low trochospiral, of 2 1/2 whorls. The last whorl is composed of 4 chambers, increasing rapidly in size. Chambers inflated, spherical. Periphery strongly lobulate, rounded. Wall calcareous perforate, hispid. Sutures depressed, radial on both the spiral and the umbilical sides, Umbilicus deep. Aperture a high arch, extraumbilical.

Diameter: 0.33 mm.

Occurrence: Abundant in samples Nos. 1281, 1283, Ipolytarnóc.

Bolli (1957) described this species from the *Catapsydrax dissimilis* Zone to the *Globorotalia menardii* Zone, (Miocene), Cipero for mation, Trinidad.

GLOBOROTALIA OPIMA NANA BOLLI

(Plate 14, Fig. 3a – e, 4a, b)

1957 *Globorotalia opima nana Bolli.* – Bolli, p. 118, pl. 28. Fig. 3a – c.
1958 *Globigerina sp.* – Batjes, p. 161, pl. XI. Fig. 8.
1962 *Globorotalia (Turborotalia) opima nana Bolli.* – Blow and Banner, p. 119, pl. XIII. Fig. Q – S.

1963 *Globigerina opima nana (Bolli).* – Hofker, p. 199, Abb. 1–3.
1963 *Globorotalia opima nana Bolli.* – Pessagno, p. 58, pl. 2. Fig. 1–2.
1966 *Globorotalia opima nana Bolli.* – McTavish, p. 28, pl. 4, Fig. 4, 9–10.

Description:

Test small, low trochospiral, of three whorls; each whorl composed of about four chambers, slowly enlarging, semicircular in outline. Wall coarsely perforate and cancellate. Periphery slightly lobulate. Sutures distinct, slightly depressed, radial on both spiral and umbilical side. Umbilicus narrow, almost closed and shallow. Aperture slit-like, bordered by a distinct lip.

Diameter: 0.3 mm.

Occurrence: Abundant in the *Globorotalia opima opima* Zone, Eger bore-hole, Eger profile, Novaj and Törökbálint; rare in Ipolytarnóc.

Globorotalia opima nana was first described by Bolli 1957 from the *Globorotalia opima opima* zone, Oligocene, Cipero formation, Trinidad.

Batjes (1958) described it as *Globigerina sp.* from the Boon clay, Oligocene of Belgium.

GLOBOROTALIA OPIMA OPIMA BOLLI

(Plate 14, Fig. 1a–d, 2a–d)

1957 *Globorotalia opima opima.* – Bolli, p. 117, pl. 28, Fig. 1a–2.
1959 *Globigerina opima (Bolli).* – Drooger and Magné, pl. 1. Fig. 4a–c.
1960 *Globorotalia opima Bolli subsp. opima Bolli.* – Jenkins, p. 366, pl. 5, Fig. 3a–c.
1963 *Globorotalia opima opima Bolli.* – Pessagno, p. 58, pl. 1, Fig. 4–6, pl. 2. Fig. 18.

Description:

Test small, trochospiral, of 2 1/2 whorls, each whorl composed of about 4–5 chambers. Chambers of the last whorl increase rapidly in size as added. Periphery lobulate. Sutures radial, depressed on both spiral and umbilical sides. Wall calcareous, perforate, surface pitted. Umbilicus narrow, deep. Aperture arch-like, with a small lip.

Diameter: 0.45 mm.

Occurrence: Abundant in the *Globorotalia opima opima* zone, the Eger bore-hole, Eger profile, at Novaj and Törökbálint.

This species was described by Bolli (1957) from the *Globorotalia opima opima* zone, Oligocene, Cipero formation, Trinidad.

Drooger and Magné (1959) illustrated it from the Oligocene of Kef Irhoud, Algeria.

GLOBOROTALIA PERMICRA BLOW AND BANNER

(Plate 15, Fig. 1a–d)

Globorotalia (Turborotalia) permicra. – Blow and Banner p. 120, pl. XII. N–P.

Description:

Test minute, low trochospiral, consisting of two whorls of chambers slowly enlarging in the first whorl and rapidly enlarging in the later whorl.

Chambers subovoid. Periphery lobulate. Wall calcareous, perforate, surface finely pitted. Sutures distinctly depressed. Umbilicus narrow and deep. Aperture arched, extending from the umbilicus to the periphery, bordered by a narrow lip.

Diameter: 0.25 mm.

Occurrence: Abundant in sample No. 308, Novaj.

Blow and Banner (1962) described this species from the *Globigerina turritilina turritilina* zone, uppermost Eocene, to the *G. oligocaenica* zone, Oligocene, of the Lindi area, East Africa.

GLOBOROTALIA POSTCRETACEA (MYATLIUK)

(Plate 14, Fig. 5a–e)

1950 *Globigerina postcretacea.* – Myatliuk, p. 280, pl. 4. Fig. 3a–b.
1953 *Globigerina postcretacea Myatliuk.* – Subbotina, p. 60, pl. 2. Fig. 16a–20c.
1962 *Globorotalia (Turborotalia) postcretacea (Myatliuk).* – Blow and Banner, p. 120, pl. XII, Fig. G–J.

Description:

Test minute, low trochospiral, consisting of about 2 1/2 whorls, each whorl composed of 5 chambers moderatly enlarging in size as added; chambers subovoid. Periphery rounded, distinctly lobulate. Wall calcareous, perforate, surface weakly hispid, especially near the umbilicus. Sutures depressed, slightly curved on the spiral side, radial on the umbilical side. Umbilicus narrow. Aperture arched; extends from the umbilicus to the periphery.

Diameter: 0.28 mm.

Occurrence: Frequent only in sample No. 322, Törökbálint.

Myatliuk (1950) described this species from beds thought to be of Oligocene age in the Ukraine.

It was described by Subbotina (1953) from the lower part of the Caucasian Oligocene.

GLOBOROTALIA SAGINATA JENKINS

(Plate 15, Fig. 2a – f)

1966 *Globorotalia saginata.* – Jenkins, p. 10, pl. 2, Fig. 11a – c.

Description:

Test small, low trochospiral, composed of 2 whorls. The 4 chambers of the last whorl increase fairly rapidly in size. Periphery rounded, lobulate. Wall calcareous, distinctly perforate. Sutures depressed, curved on both the spiral and the umbilical sides. Aperture in the form of a low arch, umbilical, extending toward the periphery. Umbilicus very narrow.

Diameter: 0.35 mm.

Occurrence: Abundant in the *Globigerina ciperoensis ciperoensis* Zone, sample No. 1281, Ipolytarnóc.

Jenkins (1966) recorded this species from the Aquitanian-Burdigalian of France.

GLOBOROTALIA TESTARUGOSA JENKINS

(Plate 15, Fig. 3a – f)

1960 *Globorotalia testarugosa.* – Jenkins, p. 368, pl. 5. Fig. 8a – c.

Description:

Test small, low trochospiral, composed of 2 1/2 whorls; last whorl composed of 4 chambers; chambers inflated, increasing rapidly in size as added. Periphery rounded, lobulate. Wall calcareous, coarsely perforate. Sutures depressed, radial on the spiral side, slightly curved on the umbilical side. Umbilicus narrow.

Diameter: 0.33 mm.

Occurrence: Rare in sample No. 1287, Ipolytarnóc.

Jenkins (1960) recorded this species from the pre-*Globoquadrina dehiscens dehiscens* Zone, Lower Miocene, southeast Australia.

GENUS GLOBOROTALOIDES BOLLI, 1957

GLOBOROTALOIDES SUTERI BOLLI

(Plate 15, Fig. 4a – c)

1957 *Globorotaloides suteri.* – Bolli, p. 117, pl. 27, Fig. 9a – 13b, p. 166, pl. 37, Fig. 10a – 12.

1958 *Globigerina globularis Roemer.* – Batjes, p. 161 – 162, pl. 11. Fig. 3a – c, 5a – c.

1962 *Globorotaloides suteri Bolli.* – Blow and Banner, p. 112, pl. XIII, Fig. N-p.

Description:

Test medium, low trochospiral, consisting of about 2 $^1/_2$ whorls, the last whorl with 4 chambers, increasing rapidly in size as added; chambers ovate.

Periphery lobulate. Wall calcareous, perforate, surface cancellate. Sutures on the spiral side slightly curved, on the umbilical side radial, depressed. Umbilicus open, partly covered by a small bulla-like chamber. Aperture interiomarginal.

Diameter: 0.37 mm.

Occurrence: Scarce enough in the *Globorotalia opima opima* Zone, Eger bore-hole.

Bolli (1957) described and illustrated this species from the *Globigerina ampliapertura* Zone, Oligocene, Cipero formation, Trinidad.

Batjes (1958) described if as *G. globularis* from the Oligocene of Belgium.

Blow and Banner (in Eames et al. 1962) recorded this species from the upper Lutetian to the middle part of the Aquitanian in East Africa.

It has been observed by Blow and Banner in the Aquitanian of southeastern Sicily.

GLOBOROTALOIDES VARIABILIS BOLLI
(Plate 15, Fig. 5a–d)

1957 *Globorotaloides variabilis.* – Bolli, p. 117, pl. 27 Fig. 15a–20c.
1966 *Globorotaloides variabilis Bolli.* – Mc Tavish, p. 30, pl. 5, Fig. 32–33.

Description:

Test medium, low trochospiral, composed of 2 $^1/_2$ whorls. The last whorl consists of 4–5 chambers, increasing rapidly in size as added. Chambers ovate. Periphery subacute. Wall calcareous, perforate, surface cancellate. Sutures depressed, radial to slightly curved on both the spiral and the umbilical sides. Umbilicus open, slightly or partly covered by a bulla-like chamber. Aperture slit-like, interiomarginal.

Diameter: 0.35 mm.

Occurrence: Rare in sample No. 1283, Ipolytarnóc.

This species was first described by Bolli (1957) from the *Globorotalia fohsi barisanensis* Zone to the *Globorotalia menardii* Zone, Miocene, Cipero formation, Trinidad.

REFERENCES

Akers, W. H. (1955): Some planktonic Foraminifera of the American Gulf Coast and suggested correlation with Caribbean Tertiary. Journ. Paleont., Vol. 29. no. 4 pp. 647–664.,

Báldi, T. – Kecskeméti, T. – Nyirő M. R. and Drooger, C. W. (1961 : Neue Angaben zur Grenzziehung zwischen Chatt und Aquitan in der Umgebung von Eger (Nordungarn). Ann. Hist.-Nat. Mus. Nat. Hung. 53, pp. 67–132.

Báldi, T. (1964): Über das Alter des "Pectunculussandes" von Törökbálint und das Problem der Oligocän-Miozän-Grenze. Ann. Hist.-Nat. Mus. Nat. Hung. 56. pp. 135–152.

Báldi, T. (1966 : Die oberoligozäne Molluskenfauna von Eger und die Neuuntersuchung der Schichtfolge. Ann. Hist.-nat. Mus. Nat. Hung. 58. pp. 69–101.

Bandy, O. L. (1964): The type of Globigerina quadrilobata d'Orbigny. Cushman Lab. Foram. Res., Contr., Vol. 15, pt. 1, pp. 36–37.

Banner, F. T. and Blow, W. H. (1959): The classification and stratigraphical distribution of the Globigerinaceae. Paleontology, Vol. 3, pt. 1. pp. 1–27. pls. 1–3.

Banner, F. T. and Blow, W. H. (1960 : Some primary types of species belonging to the Superfamily Globigerinaceae. Cushman Found. Foram. Res. Contr., Vol. 11. pp. 1 – 41 pls. 1 – 8.

Batjes, D. A. J. (1938): Foraminifera of the Oligocene of Belgium. Inst. Royal des Sciences Naturelles de Belgique, Mem. 143, pp. 1 – 188, pls. 1 – 13.

Berggren, W. A. (1963 : Review and discussion: Micropaleontology, Vol. 9. no. 4 pp. 467 – 473.

Blow, W. H. (1956): Origin and evolution of the foraminiferal genus Orbulina d'Orbigny. Micropaleontology, Vol. 2, pp. 57 – 70.

Blow, W. H. (1957): Transatlantic correlation of Miocene sediments. Micropaleontology, Vol. 3. pp. 77 – 79.

Bolli, H. M. (1957): Planktonic Foraminifera from the Oligocene-Miocene Cipero and Lengua Formations of Trinidad, B.W.I.U.S. Nat. Mus. Bull. 215, pp. 97 – 123, pls. 22 – 29.

Bolli, H. M. (1966): Zonation of Cretaceous to Pliocene marine sediments based on Planktonic Foraminifera. Asoc. Ven. Geol. Min. Petr., Bol. Inf., v. 9, n. 1, pp. 1 – 32.

Bolli, H. M., Loeblich, A. R. and Tappan, H. (1957): Planktonic foraminiferal families Hantkeninidae, Orbulinidae, Globorotaliidae and Globotruncanidae. U.S. Nat. Mus. Bull. 215, pp. 3 – 50, pls. 1 – 11.

Cita, M. B. and Silva, I. P. (1967): Evoluzione della fauna planctonica nell' intervallo stratigrafico compreso fra il Langhianotipo ed il Tortoniano – tipe e zonazione del Miocene Piemontese. IV Congresso del Comitato per la Stratigrafia del Neogene Mediterraneo. Bologna.

Csepreghy-Mezneries, I. (1962): Das problem des Chatt-Aquitans in wissenschaftsgeschichtlicher Beleuchtung. Ann. Hist. Nat. Mus. Nat. Hung., 54. pp. 57 – 71.

Csepreghy-Mezneries, I. (1967): As Ipolytarnóc burdigalai fauna. Földtani Közl. 97. 2. pp. 177 – 185.

Cushman, J. A. (1948): Foraminifera, their classification and economic use. Harvard Univ. Press. pp. 1 – 605. Cambridge.

Drooger, C. W. (1956): Transatlantic correlation of the Oligo-Miocene by means of Foraminifera. Micropaleontology, Vol. 2. no. 2 – pp. 183 – 192, pl. 1.

Drooger, C. W. and Batjes, D. A. J. (1959): Planktonic foraminifera in the Oligocene and Miocene of the North Sea basin. Koninkl. Nederl. Akad. van. Weten., ser. B., 62, no. 3, pp. 172 – 186.

Drooger C. W. and Magné, J. (1959): Miogypsinids and planktonic foraminifera of the Algerian Oligocene and Miocene. Micropaleontology, Vol. 5. no. 3. pp. 273 – 284. 2 pls.

Eames, F. E. – Banner, F. T. – Blow, W. H. – Clarke, W. J. (1962): Fundamentals of Mid-Tertiary stratigraphical correlation. Cambridge Univ. Press. pp. 163.

Ellis, B. F. – Messina, A. R. (1940): Catalogue of Foraminifera. New York. Amer. Mus. Nat. Hist. Spec. Publ.

Gordon, V. A. (1961): Planktonic foraminifera and the correlation of the Middle Tertiary rocks of Puerto Rico. Micropaleontology, Vol. 7. no. 4, pp. 451 – 460, pls. 1 – 2.

Hofker, J. (1963): Einige planktonische Foraminiferen aus dem borealen europäischen Oligozän. N. Jb. Geol. Paleont. Abh. Vol. 118. pp. 197 – 206.

Hornibrook, N. De B. (1958 : New Zealand Upper Cretaceous and Tertiary foraminifera, zones and some overseas correlation. Micropaleontology, Vol. 4, no. 1. pp. 25 – 38, pl. 1. 1

Jenkins, D. G. (1960): Planktonic foraminifera from the Lakes Entrance oil shaft, Victoria, Australia. Micropaleontology, Vol. 6, no. 4. pp. 345 – 371, pls. 1 – 5.

Jenkins, D. G. (1964): Preliminary Account of the type Aquitanian-Burdigalian Planktonic Foraminifera. Cushman Found. Foram. Res. Contr. Vol. 15, pp. 28 – 29.

Jenkins, D. G. (1964a): A new planktonic foraminiferal subspecies from the Australian Lower Miocene. Micropaleontology, Vol. 10. no. 1, p. 72, Textfig. 1.

Jenkins, D. G. (1965): Planktonic foraminifera zone and new taxa from the Danian to Lower Miocene of New Zealand. N. Z. Jour. Geol. Geophys. Vol. 8, p. 1088 – 1126.

Jenkins, D. G. (1965a): Planktonic foraminifera and Tertiary intercontinental correlation. Micropaleontology, Vol. 11. no. 3. p. 265 – 277.

Jenkins, D. G. (1966): Planktonic foraminifera from the type Aquitanian-Burdigalian of France. Cushman Found. Foram. Res. Contr. Vol. 17, pt. 1, pp. 1 – 15, pls. 1 – 3.

Majzon, L. (1942): Újabb adatok az egri oligocén rétegek faunájához és a paleogén-neogén határkérdés. Földtani Közl. 72, p. 29 – 39.

Majzon, L. (1950): Újabb őslénytani adatok Ipolytarnócról. Földtani Közl. 80, pp. 262–265.
Majzon, L. (1966): Foraminifera vizsgálatok. Akadémiai Kiadó, pp. 1–939, pls. 1–118, Budapest.
Mc Tavish, R. A. (1966): Planktonic foraminifera from the Malaita Group, British Solomon Islands. Micropaleontology, Vol. 12, no. 1, pp. 1–36. pls. 1–7.
Nyirő, M. R. (1963): Beiträge zur Foraminiferen-Fauna der Oligozän-Schichten von Törökbálint. Ann. Hist.-Nat. Mus. Nat. Hung. 55. pp. 61–70.
Nyirő, M. R. (1967): Az Ipolytarnóc tengeri rétegek Foraminifera-faunája. Földt. Közl. 97. 2. pp. 186–193. 3 pls.
Pessagno, E. A. (1963): Planctonic Foraminifera from the Juana Diaz Formation, Puerto Rico. Micropaleontology, vol. 9, no. 1. pp. 53–60. pls. 1–3.
Pokorny, V. (1958): Grundzüge der zoologischen Mikropaleontologie, Bd. 1, pp. 1–582, VEB Deutscher Verlag der Wissenschaften Berlin.
Reiss, Z. and Gvirtzman, G. (1964): Subsurface Neogene stratigraphy of Israel. Comm. Medit. Neogene Strat. Proc. III. Sess., Bern.
Said, R. and El-Heiny, I. (1967): Planktonic foraminifera from the Miocene rocks of the Gulf of Suez region, Egypt. Contr. Cushman Found. Foram. Res. Vol. 18. pt. 1, pp. 14–26, 2 tab. 3 fig.
Subbotina, N. N. (1953): Globigerinidae, Hantkeninidae and Globorotaliidae. Vses. Neft. Nauchno-Issled. Geol. Razved. Inst. (VNIGRI), Fossil foraminifera of the USSR Trudy, vypusk, 76, pp. 1–296, pls. 1–41.
Weiss, L. (1955): Planktonic index foraminifera of northwestern Peru. Micropaleontology, Vol. 1. no. 1, pp. 301–319. pls. 1–3.

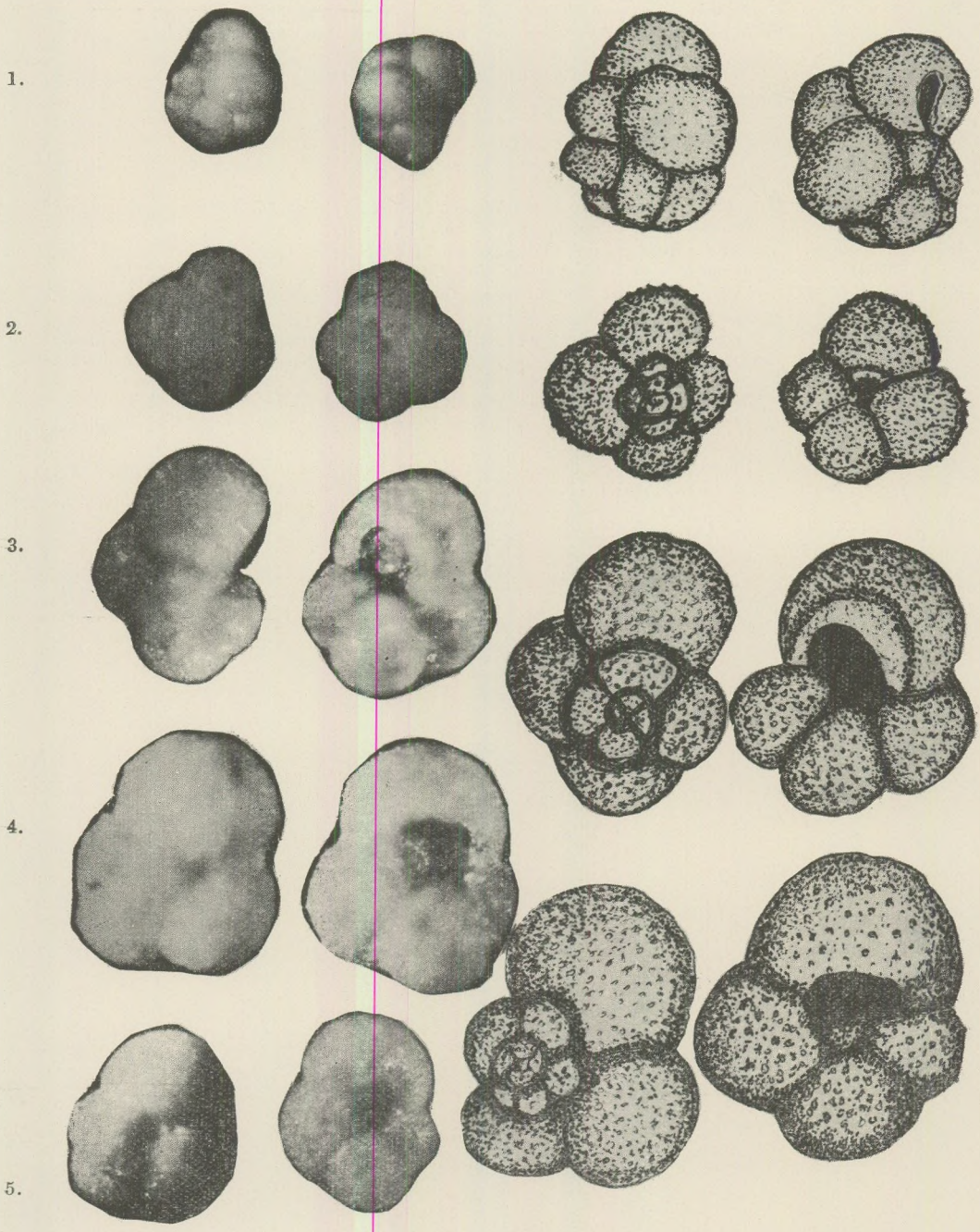
1.
2.
3.
4.
5.
a.
b.
c.
d.

Plate 1.

1a – d

Cassigerinella chipolensis (Cushman and Ponton)
1a,c; 1b,d: opposite sides

Photo X110; drawing X125
Ipolytarnóc, sample No. 1283

2a – d

Globigerina bollii Cita and Premoli
2a,c: Spiral view; 2b,d: Umbilical view

Photo X90; drawing X120
Ipolytarnóc, sample No. 1288

3a – d

Globigerina ampliapertura Bolli
3a,c: Spiral view; 3a,d: Umbilical view

Photo X90; drawing X120
Eger bore-hole, sample No. 60

4a – d

Globigerina ampliapertura Bolli
4a,c: Spiral view; 4b,d: Umbilical view

Photo X90; drawing X120
Eger bore-hole, sample No. 121a

5a,b

Globigerina ampliapertura Bolli
5a: Spiral view; 5b: Umbilical view

Photo X90; drawing X120
Eger bore-hole, sample No. 104

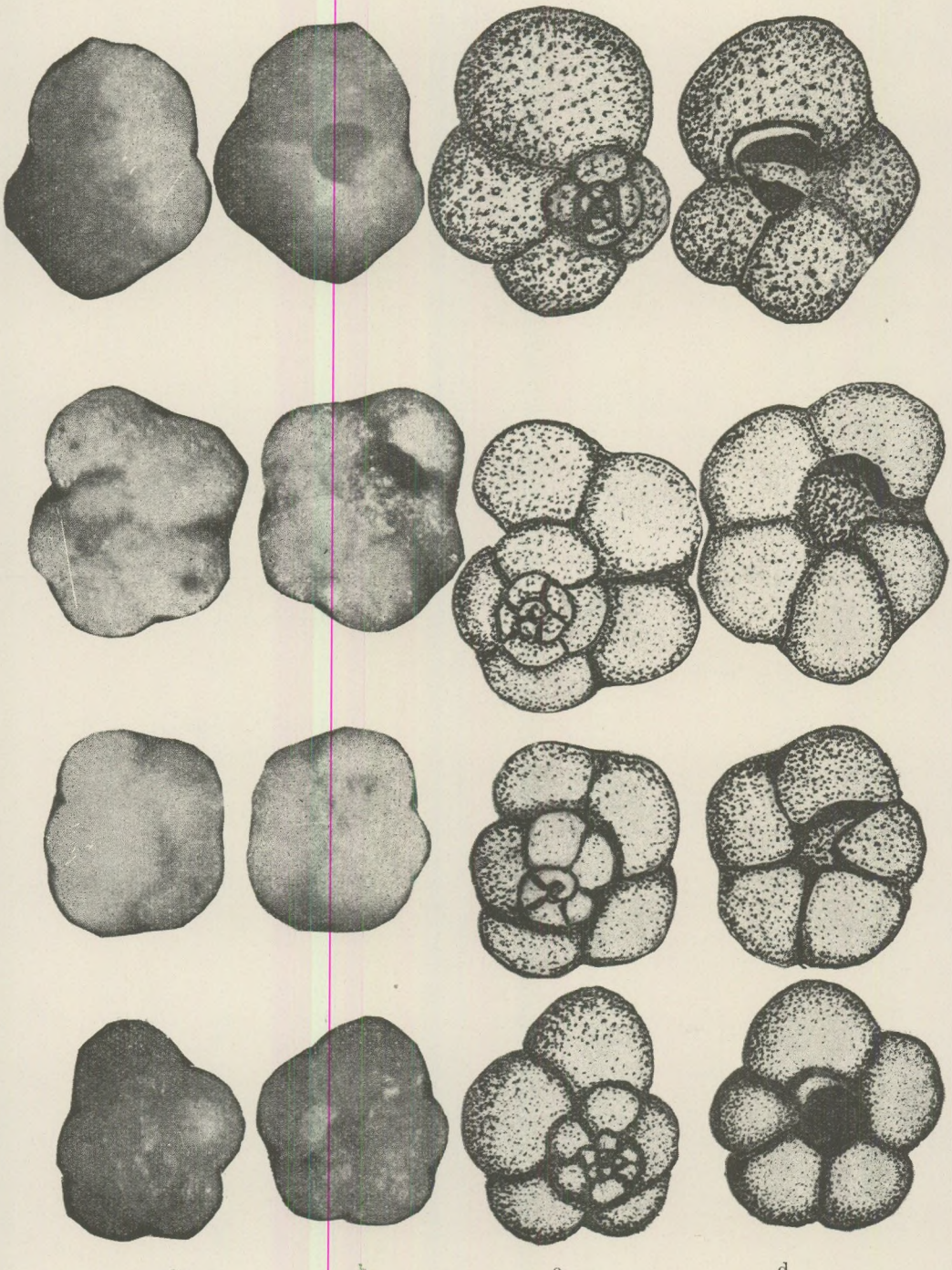
1.
2.
3.
4.
a.
b.
c.
d.

Plate 2.
(All photos X90; drawings X120)

1a – d

Globigerina brazieri Jenkins
1a,c: Spiral view; 1b,d: Umbilical view

Ipolytarnóc, sample No. 1283

2a – d

Globigerina ciperoensis ciperoensis Bolli
2a,c: Spiral view; 2b,d: Umbilical view

Eger bore-hole, sample No. 8

3a – d

Globigerina ciperoensis ciperoensis Bolli
3a,c: Spiral view; 3b,d: Umbilical view

Novaj, sample No. 309

4a – d

Globigerina ciperoensis ciperoensis Bolli
4a,c: Spiral view; 4b,d: Umbilical view

Ipolytarnóc, sample No. 1287

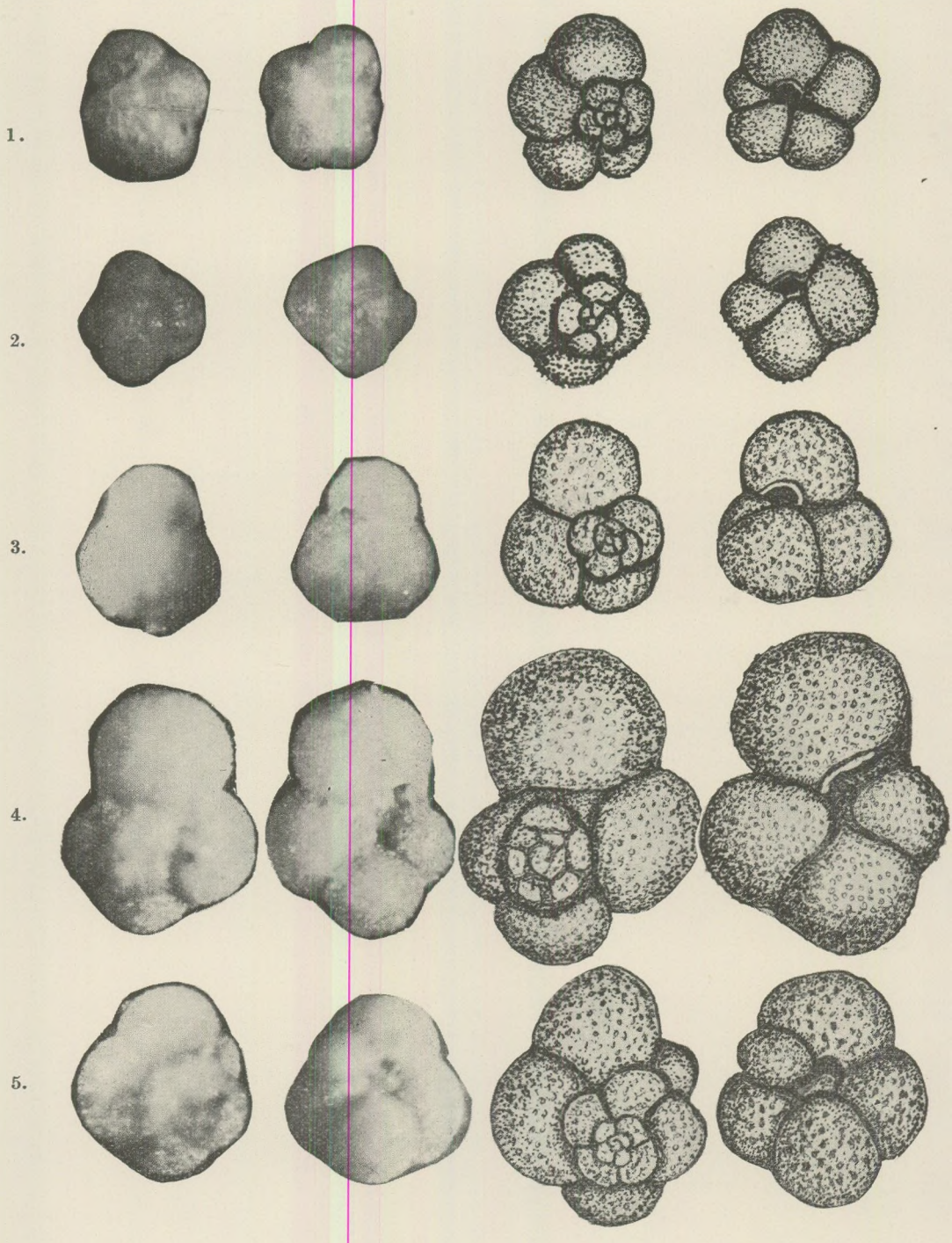
1.
2.
3.
4.
5.
a.
b.
c.
d.

Plate 3.
(All photos X90, drawings X120)

1a – d

Globigerina ciperoensis angulisuturalis Bolli
1a,c: Spiral view; 1b,d: Umbilical view

Ipolytarnóc, sample No. 1287

2a – d

Globigerina foliata Bolli
2a,c: Spiral view; 2b,d: Umbilical view

Ipolytarnóc, sample No. 1287

3a – d

Globigerina druryi Akers
3a,c; Spiral view; 3b,d: Umbilical view

Eger bore-hole, sample No. 29

4a – d

Globigerina ciperoensis angustiumbilicata Bolli
4a,c: Spiral view; 4b,d: Umbilical view

Eger bore-hole, sample 26

5a – d

Globigerina corpulenta Subbotina
4a,c: Spiral view; 4b,d: Umbilical view

Eger bore-hole, sample 29

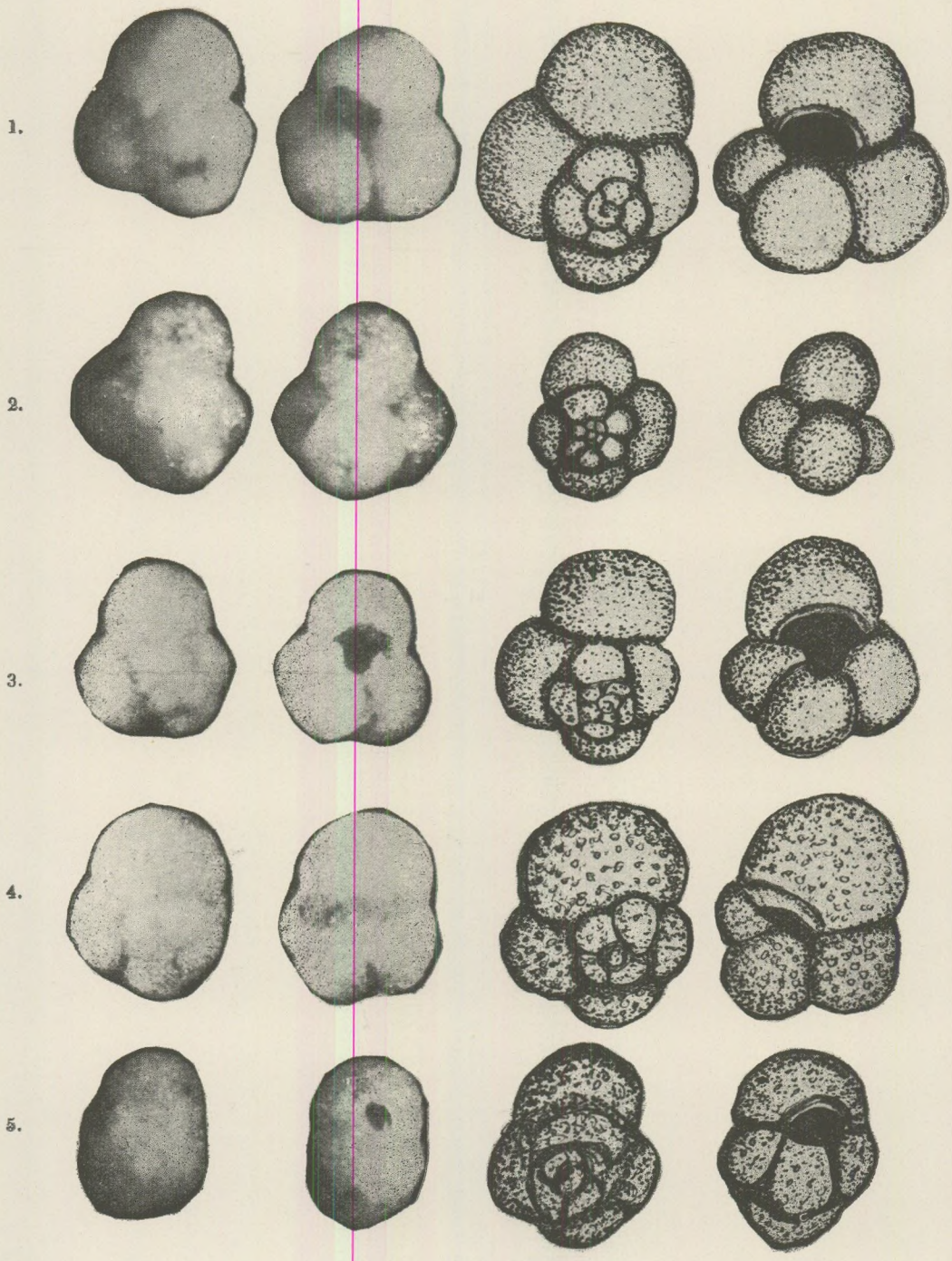
1.
2.
3.
4.
5.
a.
b.
c.
d.

Plate 4.

(All photos X90; drawings X120 except 2a – d)

1a – d

Globigerina euapertura Jenkins
1a,c: Spiral view; 1b,d: Umbilical view

Novaj, sample 309

2a – d

Globigerina juvenilis Bolli
2a,c: Spiral view; 2b,d: Umbilical view

Photo X160, drawing X120
Ipolytarnóc, sample No. 1287

3a – d

Globigerina labiacrassata Jenkins
3a,c: Spiral view; 3b,d: Umbilical view

Eger profile, sample No. 18

4a – d

Globigerina linaperta Finlay
4a,c: Spiral view; 4b,d: Umbilical view

Novaj sample No. 308

5a – d

Globigerina nepenthes Todd
5a,c: Spiral view; 5b,d: Umbilical view

Ipolytarnóc sample No. 1283

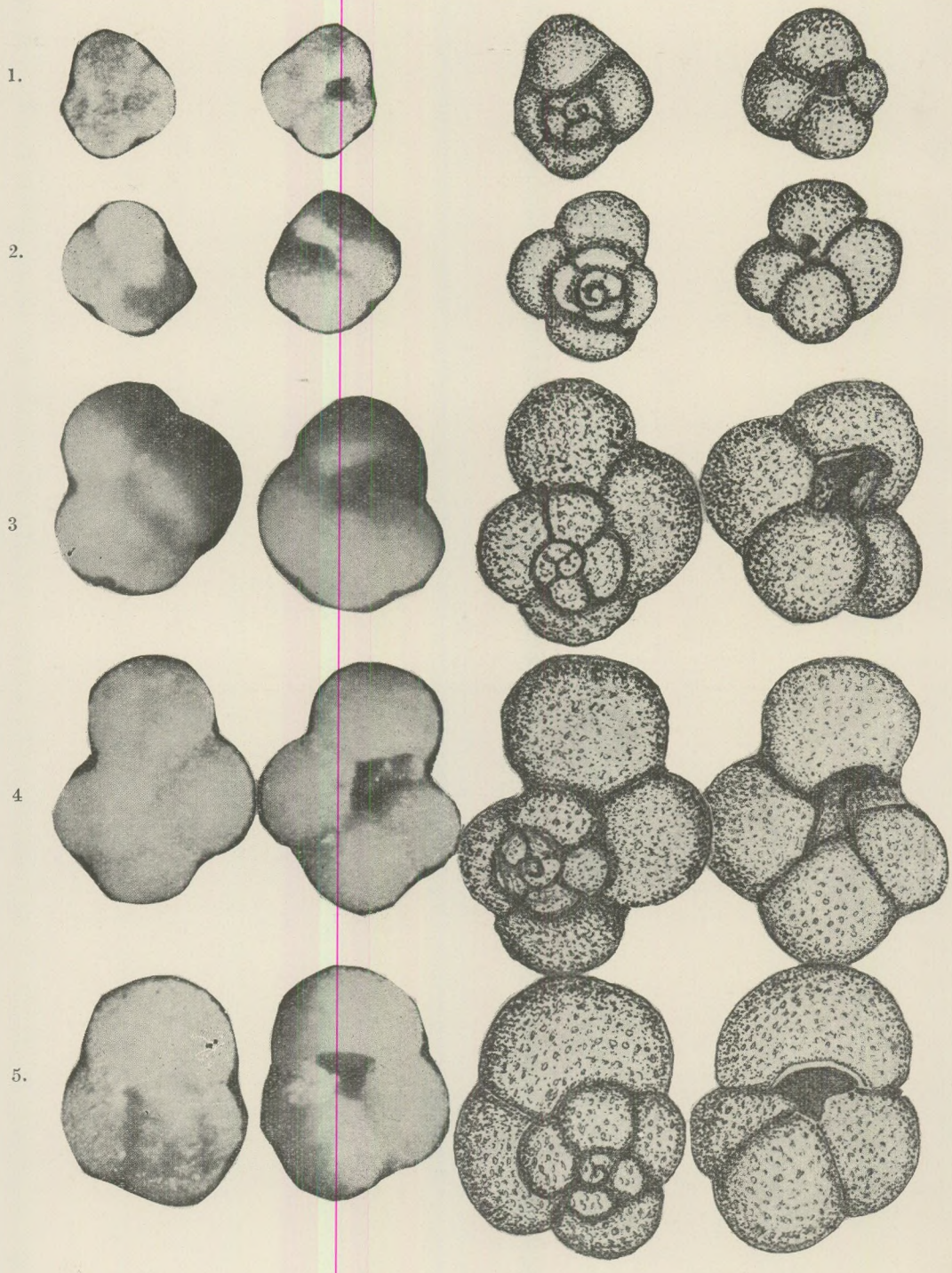
1.
2.
3
4
5.
a.
b.
c.
d.

Plate 5.
(All photos X90, drawings X120)

1a–d
Globigerina parva Bolli
1a,c: Spiral view; 1b,d: Umbilical view
Eger bore-hole, sample No. 5

2a–d
Globigerina parva Bolli
2a,c: Spiral side; 2b,d: Umbilical side
Novaj, sample No. 457

3a–d
Globigerina ouachitaensis gnaucki Blow and Banner
3a,c: Spiral side; 3b,d: Umbilical side
Eger bore-hole, sample No. 123a

4a–d
Globigerina ouachitaensis gnaucki Blow and Banner
4a,c: Spiral view; 4c,d: Umbilical view
Eger bore-hole, sample No. 26

5a–d
Globigerina ouachitaensis ouachitaensis Howe and Wallace
5a,c: Spiral view; 5b,d: Umbilical view
Eger bore-hole, sample No. 120

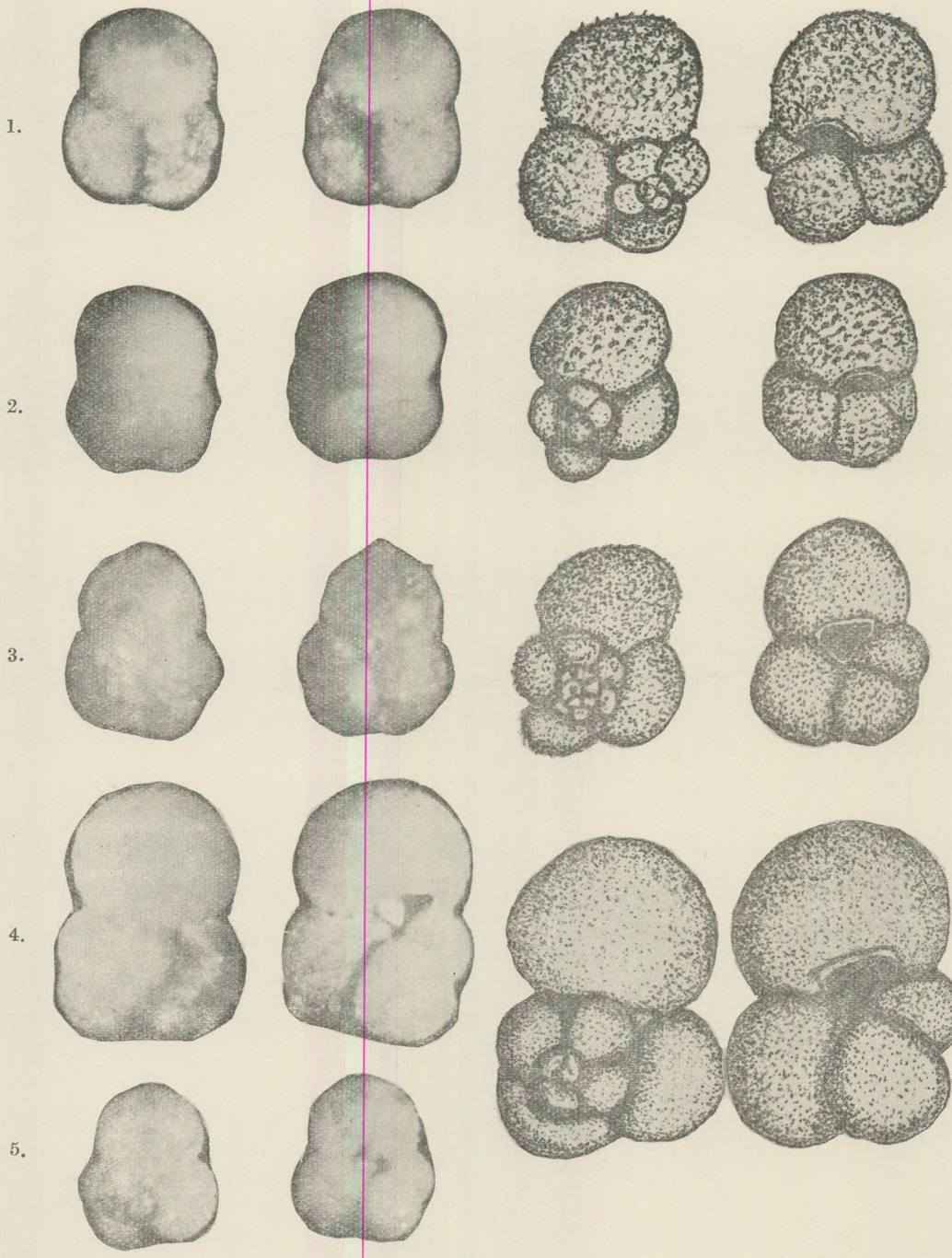
1.
2.
3.
4.
5.
a.
b.
c.
d.

Plate 6

(All photos X90, drawings X120)

1a – d

Globigerina praebulloides leroyi Blow and Banner
1a,c: Spiral view; 1b,d: Umbilical view

Eger profile, sample No. 8

2a – d

Globigerina praebulloides leroyi Blow and Banner
2a,c: Spiral side; 2b,d: Umbilical side

Ipolytarnóc, sample No. 1287

3a – d

Globigerina praebulloides praebulloides Blow
3a,c: Spiral view; 3b,d: Umbilical view

Ipolytarnóc, sample No. 1283

4a – d

Globigerina praebulloides praebulloides Blow
4a,c: Spiral view, 4b,d: Umbilical view

Eger bore-hole, sample No. 11

5a – d

Globigerina praebulloides leroyi Blow and Banner
5a: Spiral view; 5b: Umbilical view

Novaj, sample No. 308

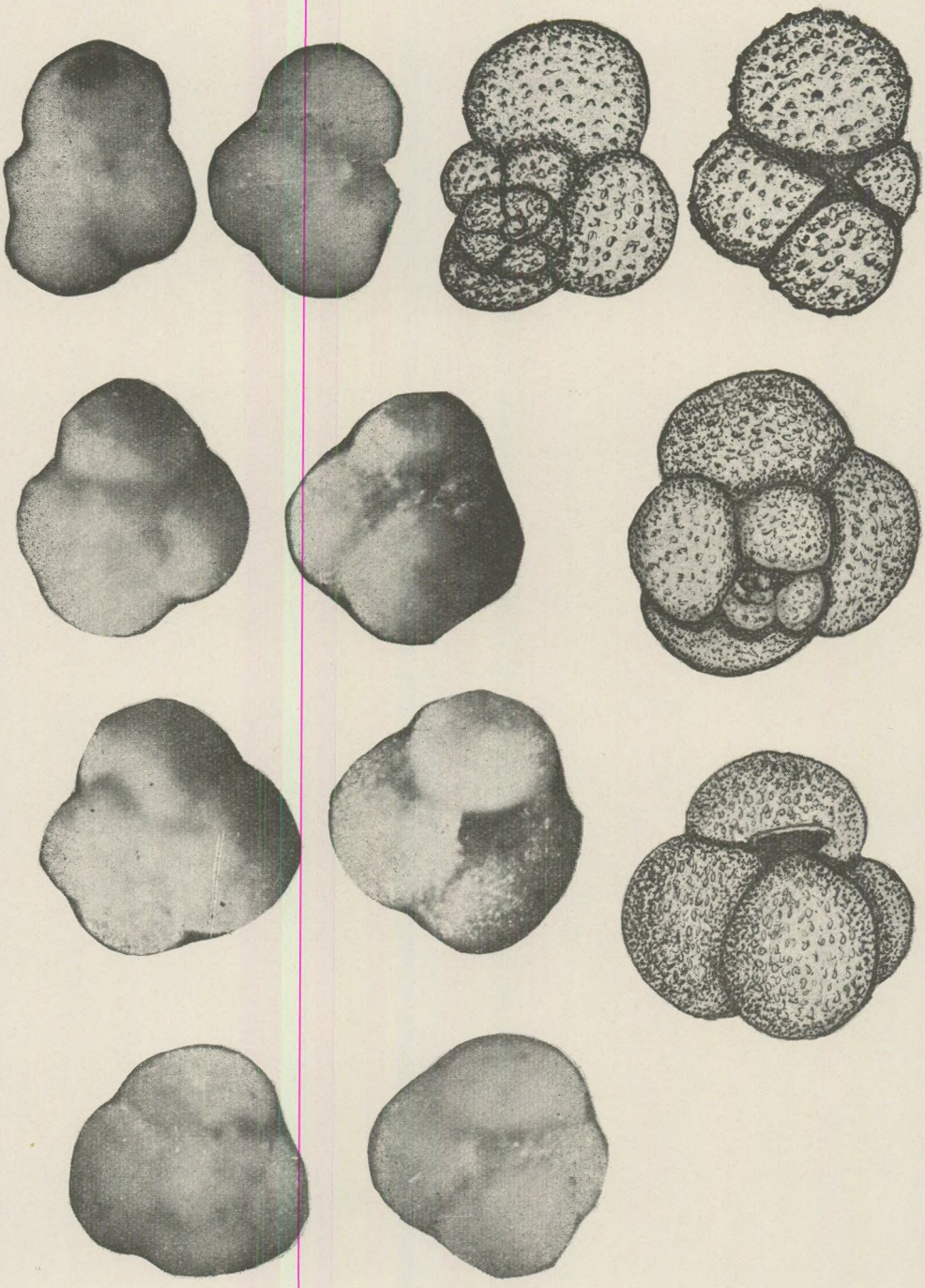

1a – d

2a – b

3a, b
2d

4a, b

Plate 7

(All photos X90, drawings X120)

1a – d

Globigerina praebulloides occlusa Blow and Banner
1a,c: Spiral side; 1b,d: Umbilical side

Novaj, sample No. 308

2a – d

Globigerina senilis Bandy
2a,c: Spiral view; 2b,d: Umbilical view

Eger bore-hole, sample No. 25

3a – b

Globigerina senilis Bandy
3a, Spiral view; 3b, Umbilical view

Eger bore-hole, sample No. 21

4a – b

Globigerina senilis Bandy
4a: Spiral view; 4b: Umbilical view

Eger bore-hole, sample No. 26

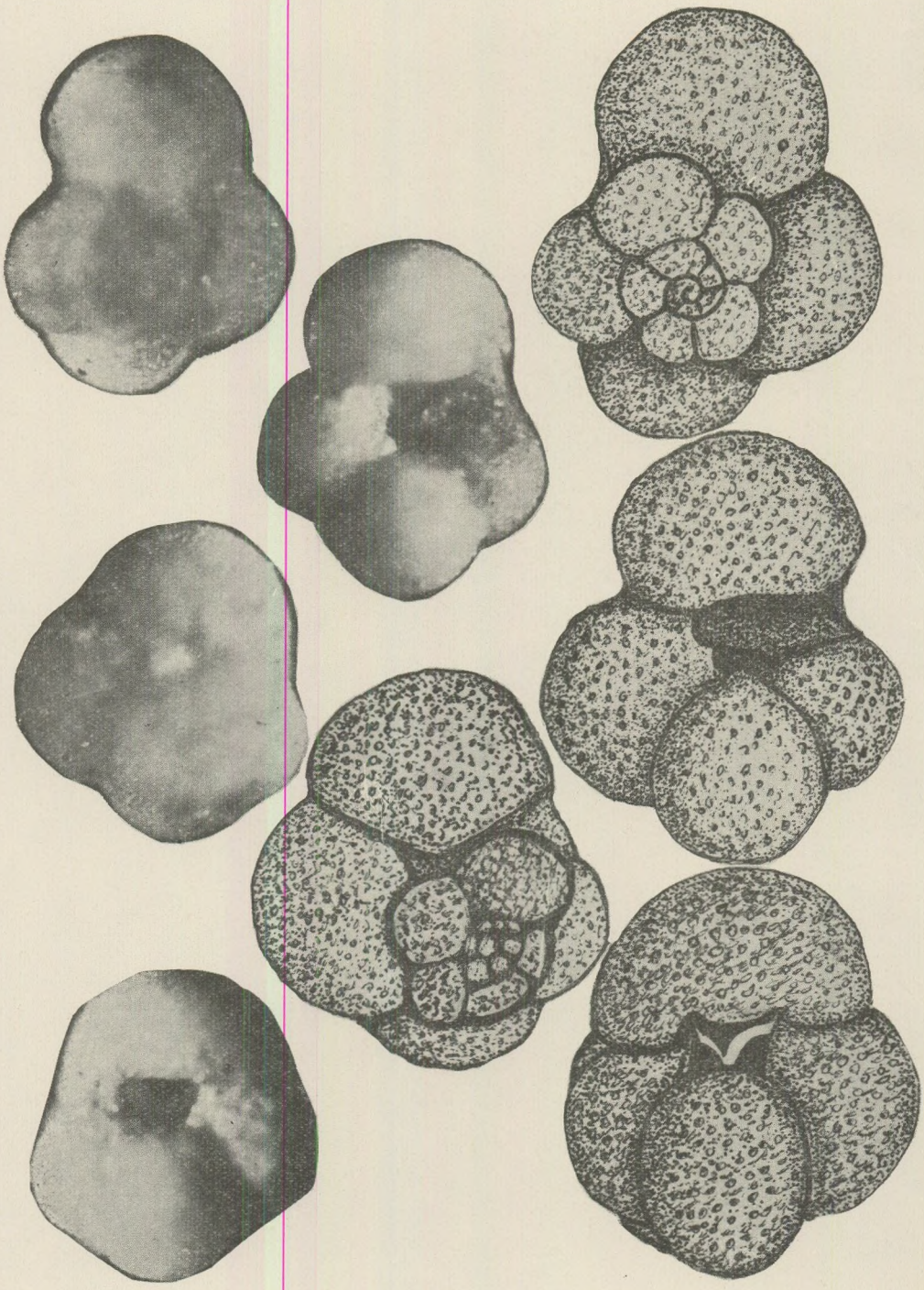

1a, c

1b

2a, 1d

2c

2b, d

Plate 8

(All photos X90; drawings X120)

1a – d

Globigerina sp.

1a,c: Spiral view; 1b,d: Umbilical view

Eger bore-hole, sample No. 13

2a – d

Globigerina rohri Bolli

2a,c: Spiral view; 2b,d: Umbilical view

Eger bore-hole, sample No. 10a

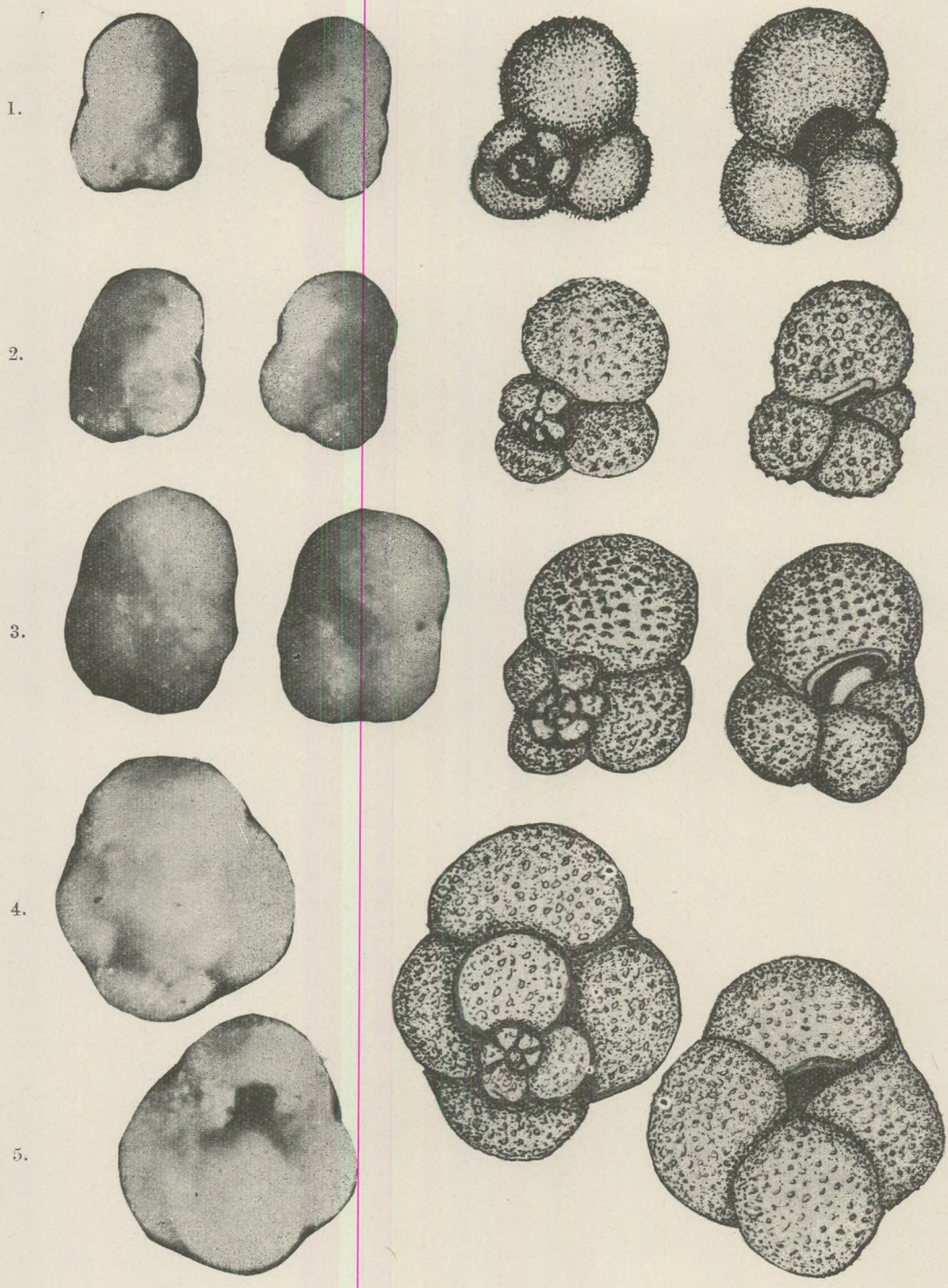
1.
2.
3.
4.
5.
a.
b.
c.
d.

Plate 9

(All photos X90; drawings X120)

1a – d

Globigerina trilocularis d'Orbigny
1a,c: Spiral view; 1b,d: Umbilical view

Eger bore-hole, sample No. 97

2a – d

Globigerina trilocularis d'Orbigny
2a,c: Spiral view; 2b,d: Umbilical view

Eger bore-hole, sample No. 13

3a – d

Globigerina woodi woodi Jenkins
3a,c: Spiral view; 3b,d: Umbilical view

Ipolytarnóc, sample No. 1283

4a – d

Globigerina yeguaensis Weinzierl and Applin
4a,c: Spiral view; 4b,d: Umbilical view

Eger bore-hole, sample No. 13

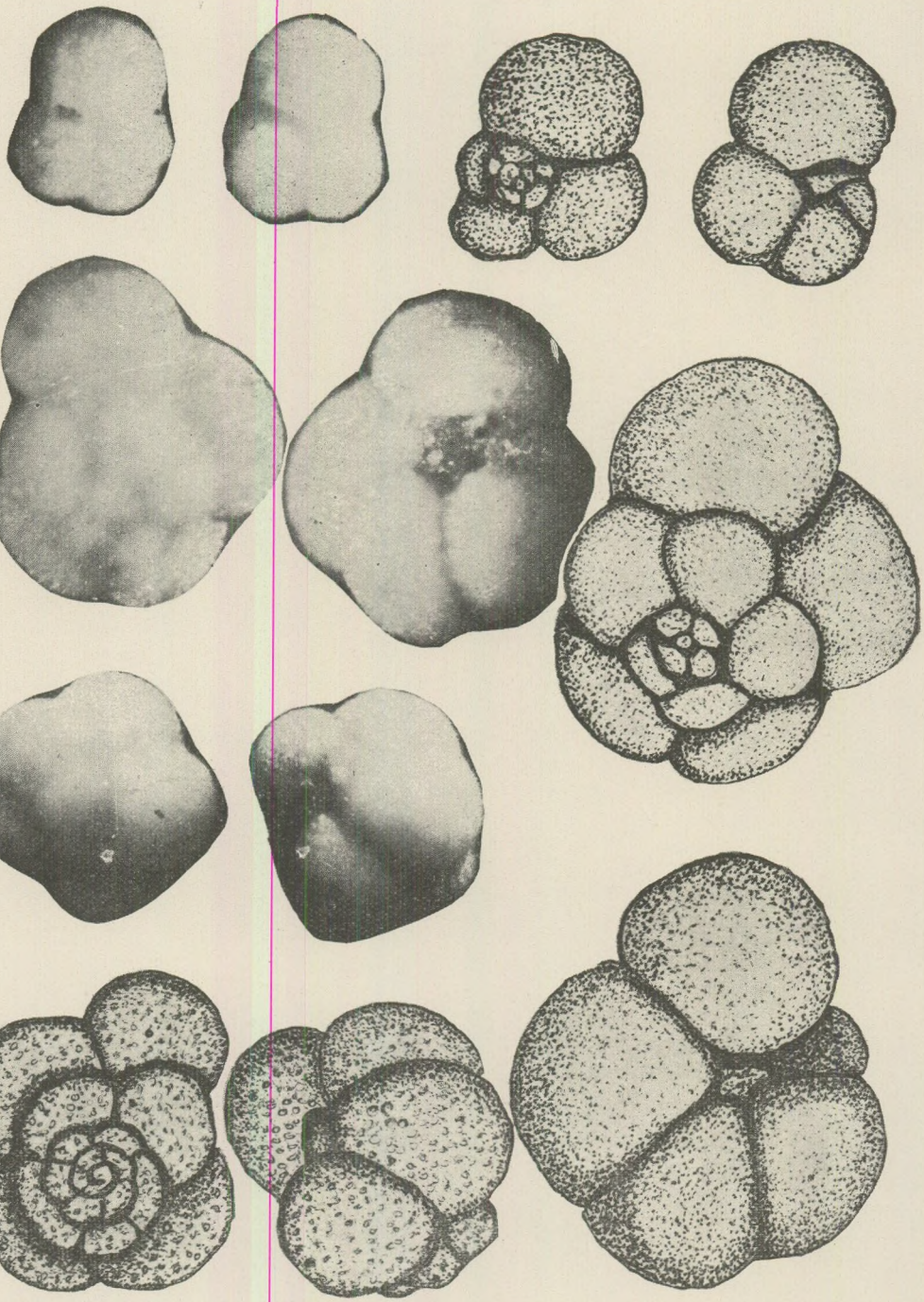

1a – d

2a – c

3a, b

3c, d
2d

Plate 10

(All photos X90, drawings X120)

1a – d

Globigerina woodi connecta Jenkins

1a,c: Spiral view; 1b,d: Umbilical view

Ipolytarnóc, sample No. 1280

2a – d

Globigerina turritilina praeturritilina Blow and Banner

2a,c: Spiral view; 2b,d: Umbilical view

Eger bore-hole, sample No. 8

3a – d

Globigerina turritilina turritilina Blow and Banner

3a,c: Spiral view; 3b,d: Umbilical view

Eger bore-hole, sample No. 25

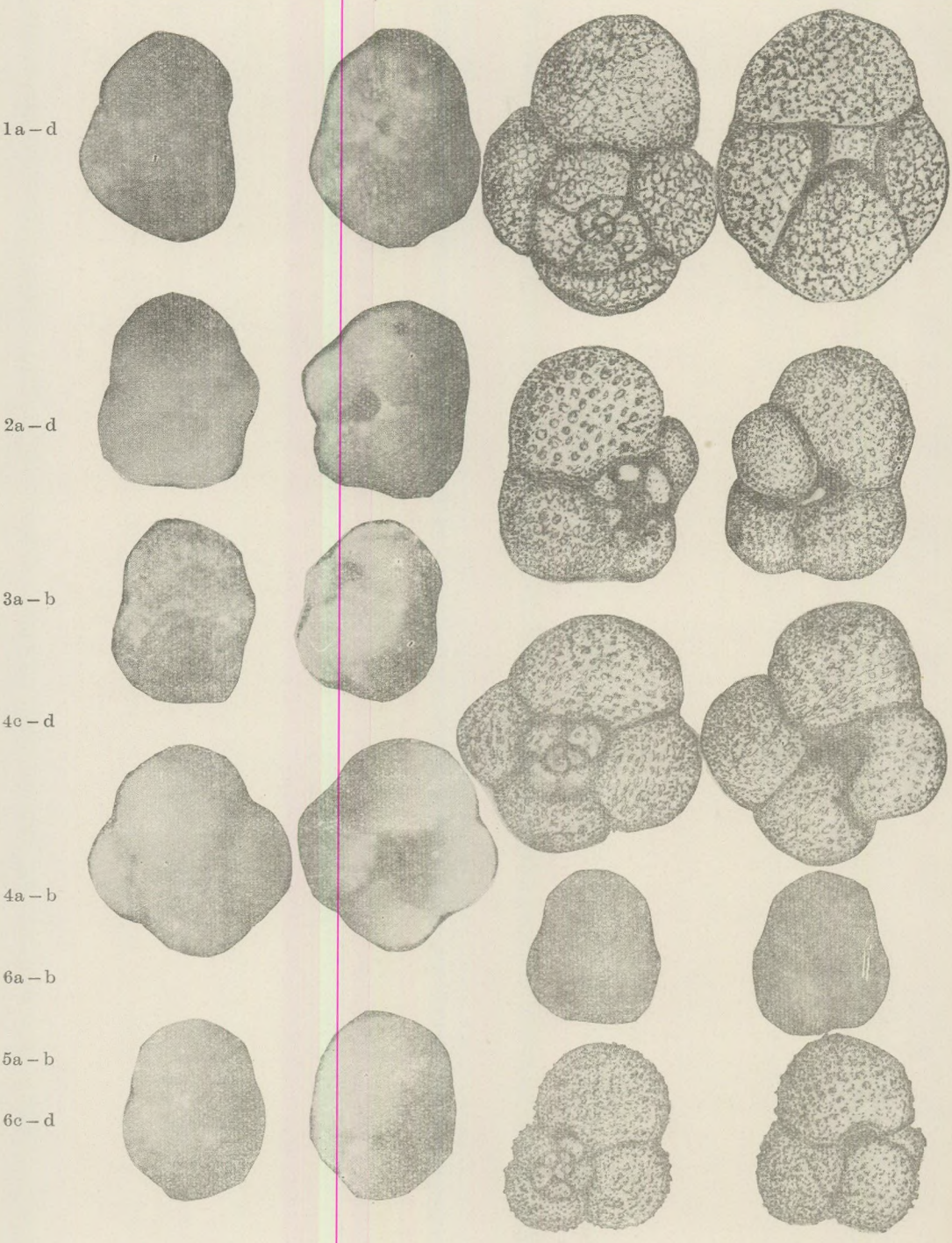
1a – d
2a – d
3a – b
4c – d
4a – b
6a – b
5a – b
6c – d

Plate 11
(All photos X90; drawings X120)

1a – d
Globigerinita dissimilis (Cushman and Bermudez)
1a,c: Spiral side; 1b,d: Umbilical side
Eger bore-hole, sample No. 10

2a – d
Globigerinita martini martini Blow and Banner
2a,c: Spiral view; 2b,d: Umbilical view
Eger bore-hole, sample No. 13

3a,b
Globigerinita martini martini Blow and Banner
3a: Spiral view; 3b: Umbilical view
Törökbálint, sample No. 322

4a – d
Globigerinita unicava unicava (Bolli, Loeblich and Tappan)
4a,c: Spiral view; 4b,d: Umbilical view
Eger bore-hole, sample No. 21

5a – b
Globigerinita unicava unicava (Bolli, Loeblich and Tappan)
5a: Spiral view; 5b: Umbilical view
Eger bore-hole, sample No. 26

6a – d
Globigerinoides primordius Blow and Banner
6a,c: Spiral side; view: Umbilical view
Ipolytarnóc, sample No. 1287

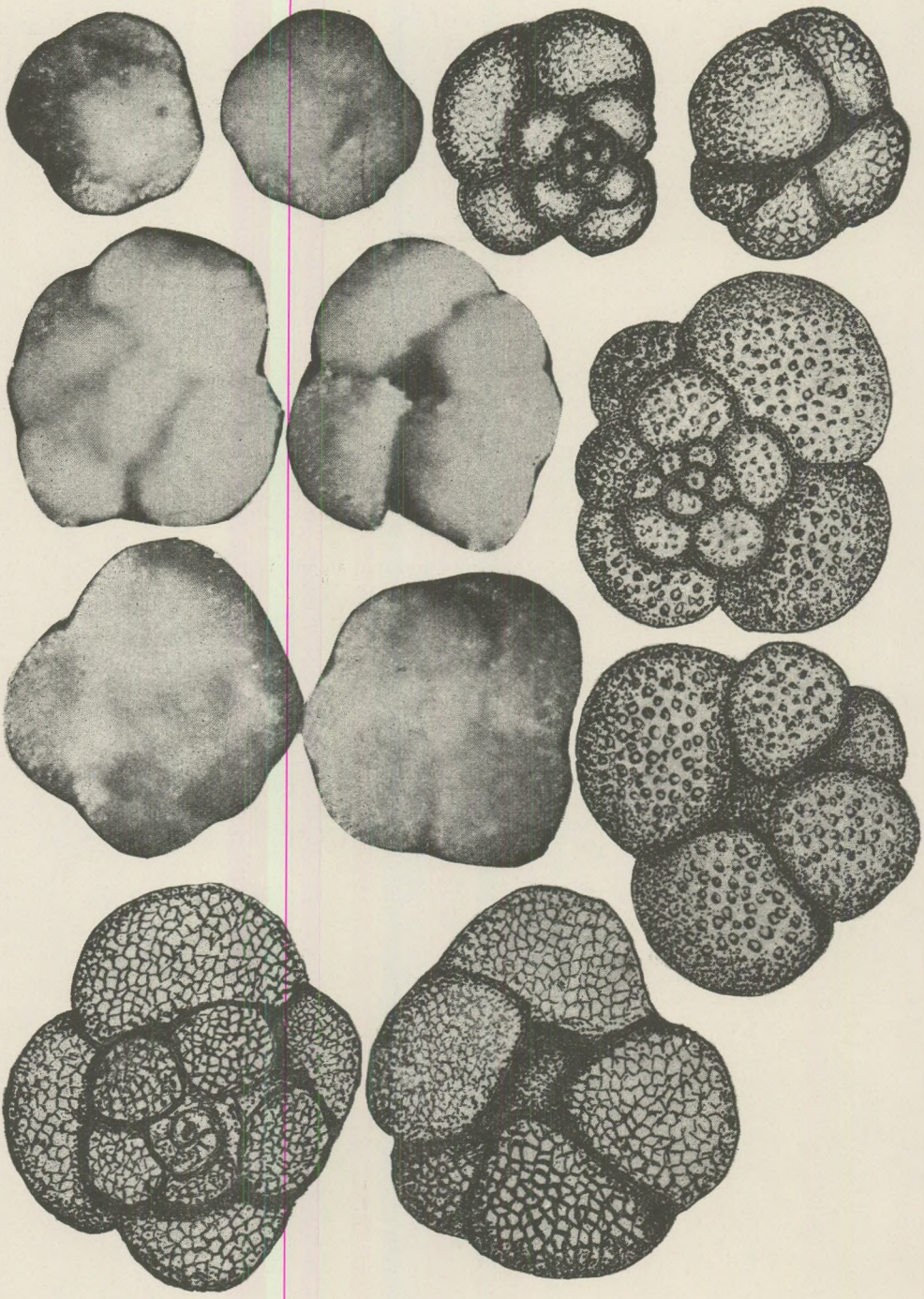

1a – d

2a – c

3a. b
2d

3c, d

Plate 12
(All photos X90, drawings X120)

1a – d

Globigerinita unicava primitiva Blow and Banner
1a,c: Spiral view; 1b,d: Umbilical view

Eger bore-hole, sample No. 16

2a – d

Globoquadrina venezuelana (Hedberg)
2a,c: Spiral view; 2b,d: Umbilical view

Eger bore-hole, sample No. 9

3a – d

Globoquadrina venezuelana (Hedberg)
3a,c: Spiral view; 3b,d: Umbilical view

Novaj, sample No. 457

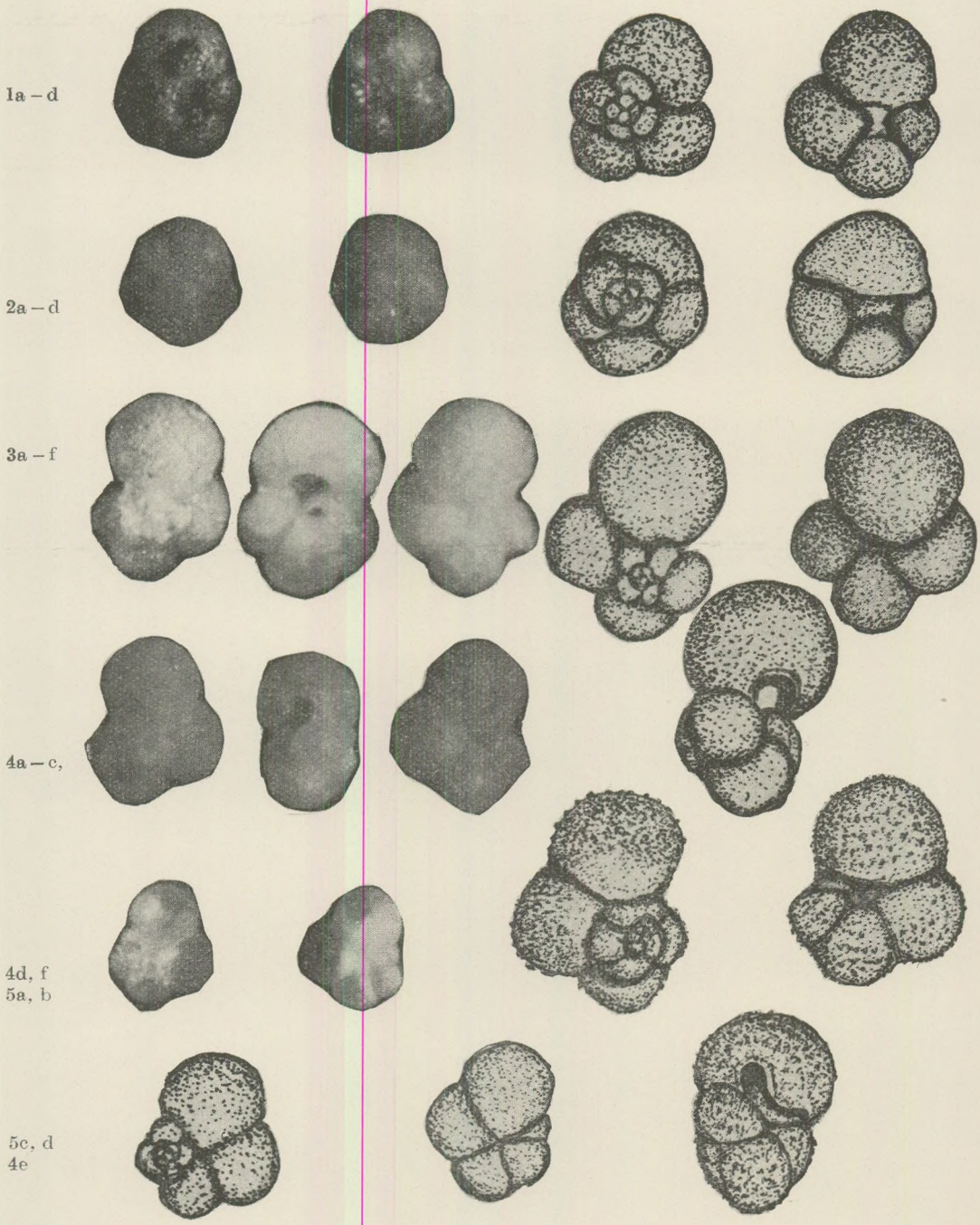
1a – d
2a – d
3a – f
4a – c,
4d, f
5a, b
5c, d
4e

Plate 13

(All photos X90, drawings X120)

1a – d

Globoquadrina larmeui Akers

1a,c: Spiral view; 1b,d: Umbilical view

Ipolytarnóc, sample No. 1287

2a – d

Globoquadrina dehiscens (Chapman, Parr and Collins)

2a,c: Spiral view; 2b,d: Umbilical view

Ipolytarnóc, sample No. 1280

3a – f

Globorotalia continuosa Blow

3a,c: Spiral view; 3b,e: lateral view; 3c,f: Umbilical view

Ipolytarnóc, sample No. 1283

4a – f

Globorotalia obesa Bolli

4a,d: Spiral view; 4b,e: lateral view; 4c,f: Umbilical view

Ipolytarnóc, sample No. 1283

5a – d

Globorotalia extens Jenkins

5a,c: Spiral view; 5b,d: Umbilical view

Törökbálint, sample No. 322

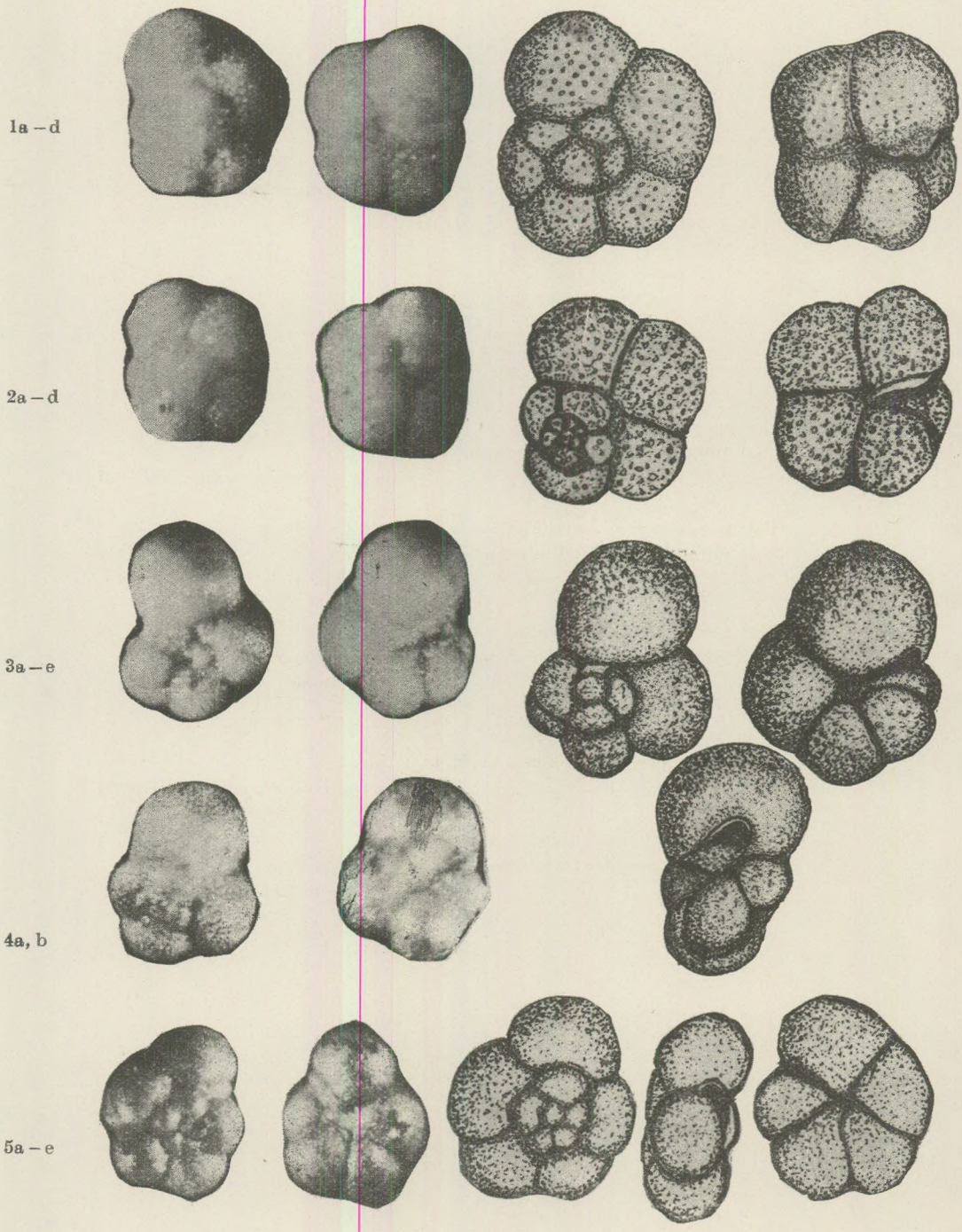
1a – d
2a – d
3a – e
4a, b
5a – e

Plate 14

(All photos X90, drawings X120)

1a – d

Globorotalia opima opima Bolli

1a,c: Spiral view; 1b,d: Umbilical view

Eger bore-hole, sample No. 8

2a – d

Globorotalia opima opima Bolli

2a,c: Spiral view; 2b,d: Umbilical view

Eger profile, sample No. 18

3a – e

Globorotalia opima nana Bolli

3a,c: Spiral view; 3d: Lateral view; 3b,e: Umbilical view

Eger bore-hole, sample No. 8

4a,b

Globorotalia opima nana Bolli

4a: Spiral view; 4b: Umbilical view

Eger bore-hole, sample No. 8

5a – e

Globorotalia postcreacea (Myatliuk)

5a,c: Spiral view; 5d: Lateral view; 5b,e: Umbilical view

Törökbálint, sample No. 322

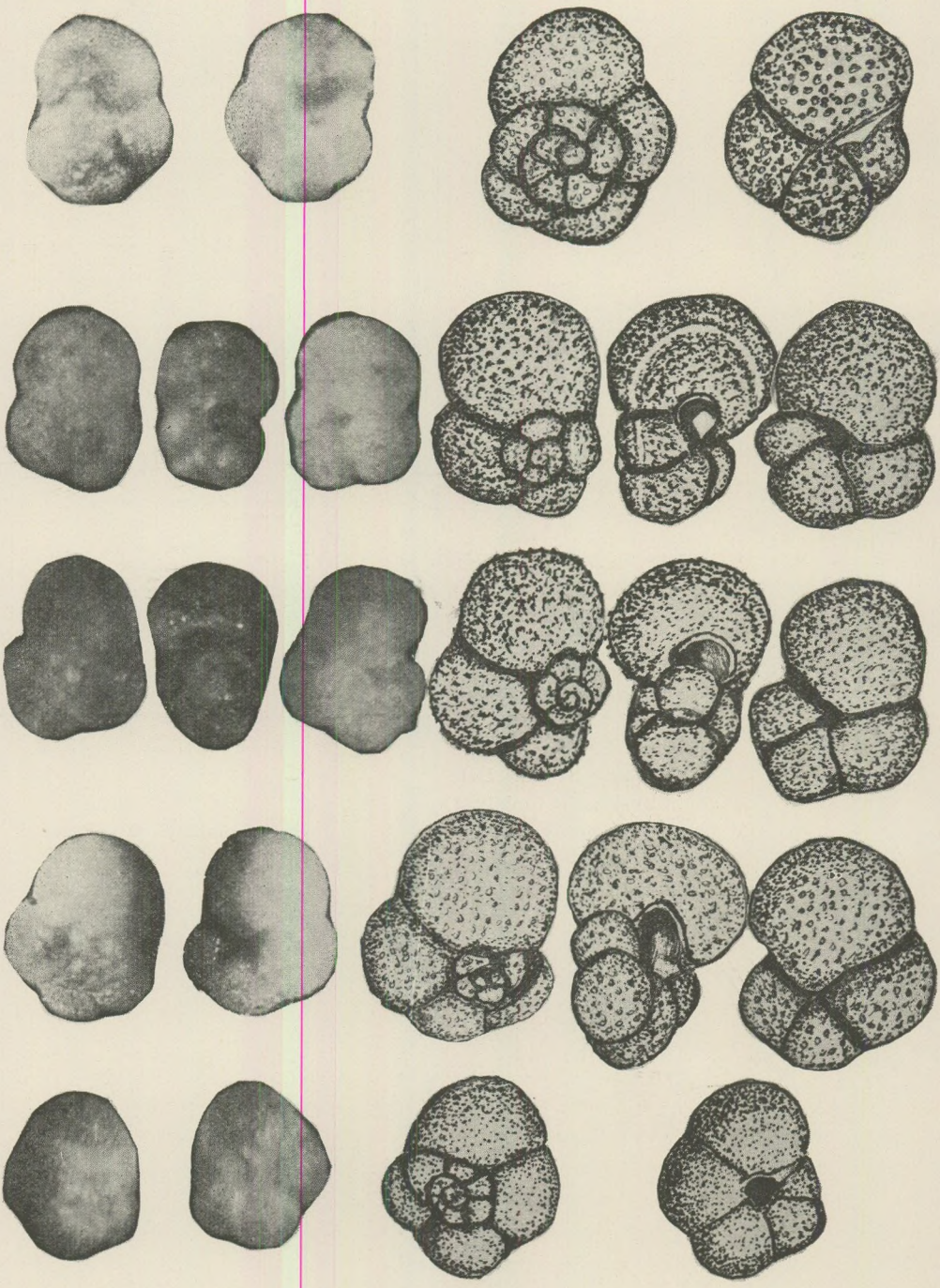

1a – d

2a – f

3a – f

4a – e

5a – d

Plate 15
(All photos X90, drawings X120)

1a–d
Globorotalia permicra Blow and Banner
1a,c: Spiral view; 1b,d: Umbilical view
Novaj, sample No. 308

2a–f
Globorotalia saginata Jenkins
2a,d: Spiral view; 2b,e: Lateral view; 2c,f: Umbilical view
Ipolytarnóc, sample No. 1287

3a–f
Globorotalia testarugosa Jenkins
3a,d: Spiral view; 3b,e: Lateral view; 3c,f: Umbilical view
Ipolytarnóc, sample No. 1287

4a–e
Globorotaloides suteri Bolli
4a,c: Spiral view: 4d: Lateral view; 4b,e: Umbilical view
Eger bore-hole, sample No. 8

5a–d
Globorotaloides variabilis Bolli
5a,c: Spiral view; 5b,d: Umbilical view
Ipolytarnóc, sample No. 1283

1.

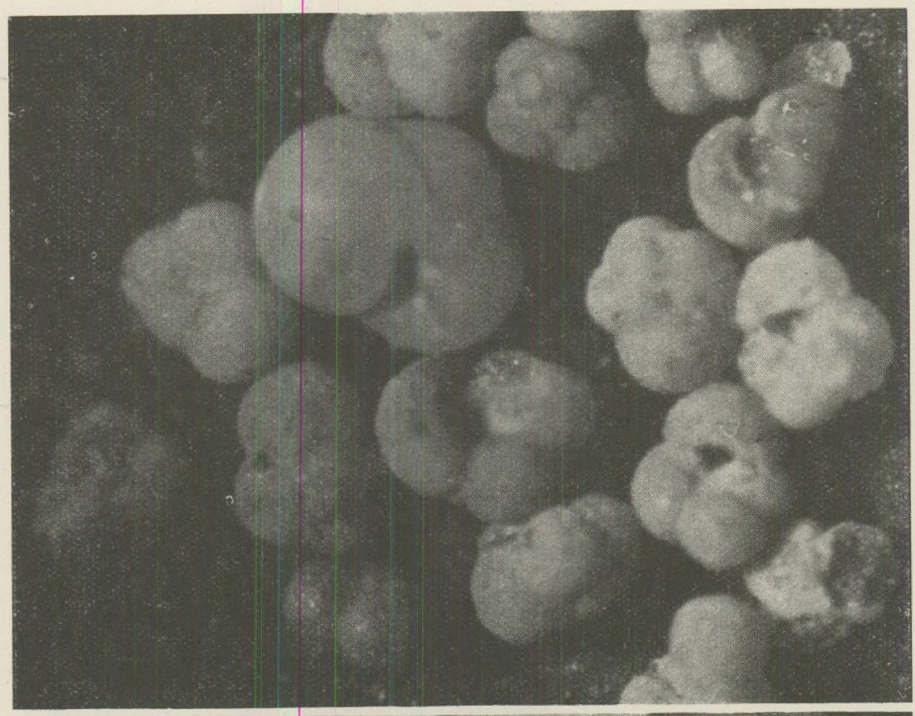

2.

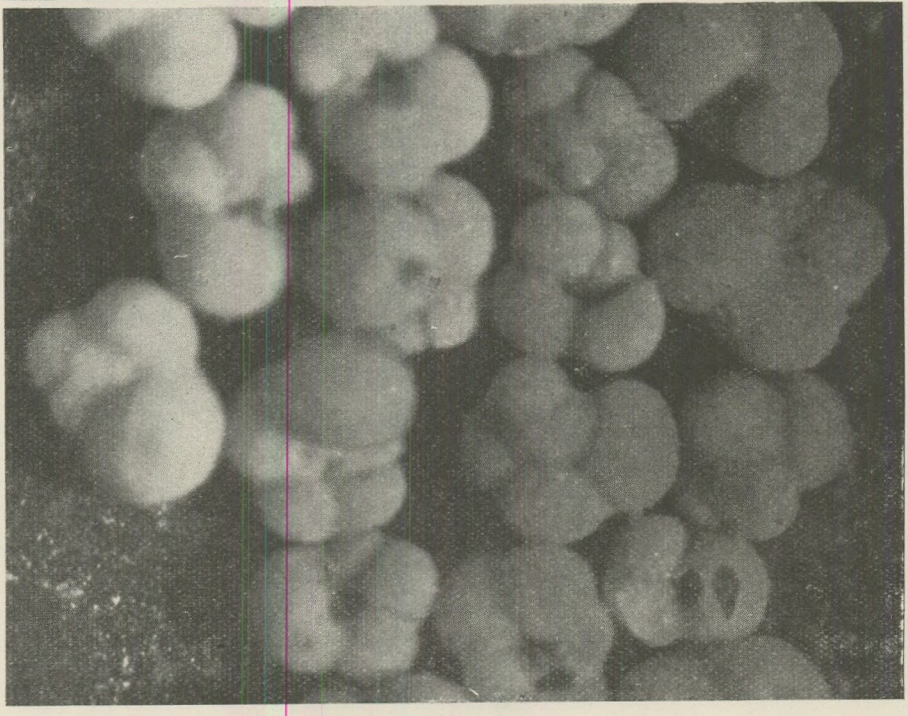

Plate 16

1. **Globigerina ouachitaensis ouachitaensis Zone X75**
Eger bore-hole

2. **Globigerina ampliapertura Zone X75**
Eger bore-hole

1.

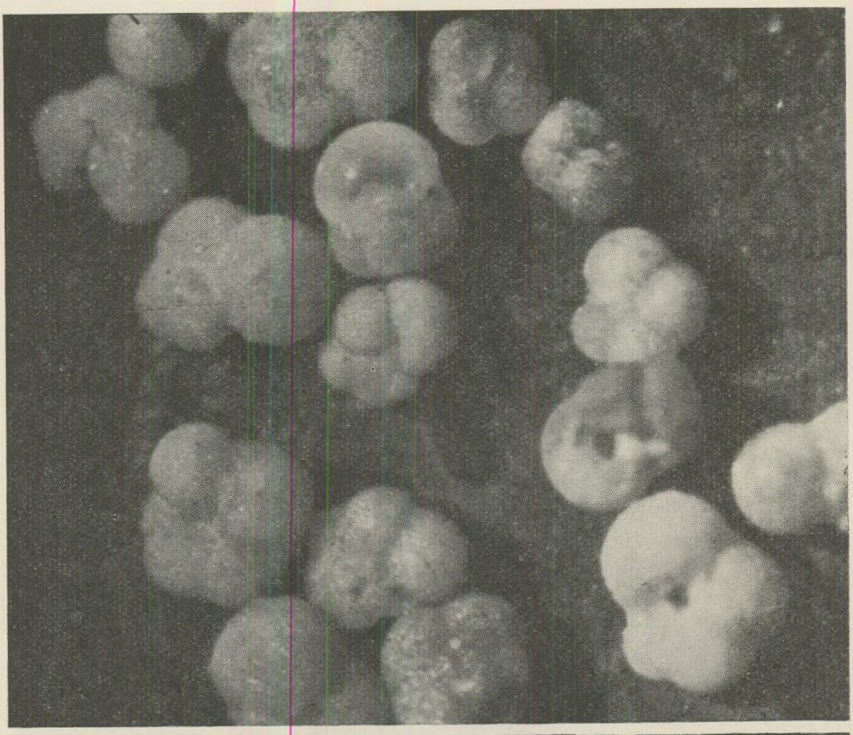

2.

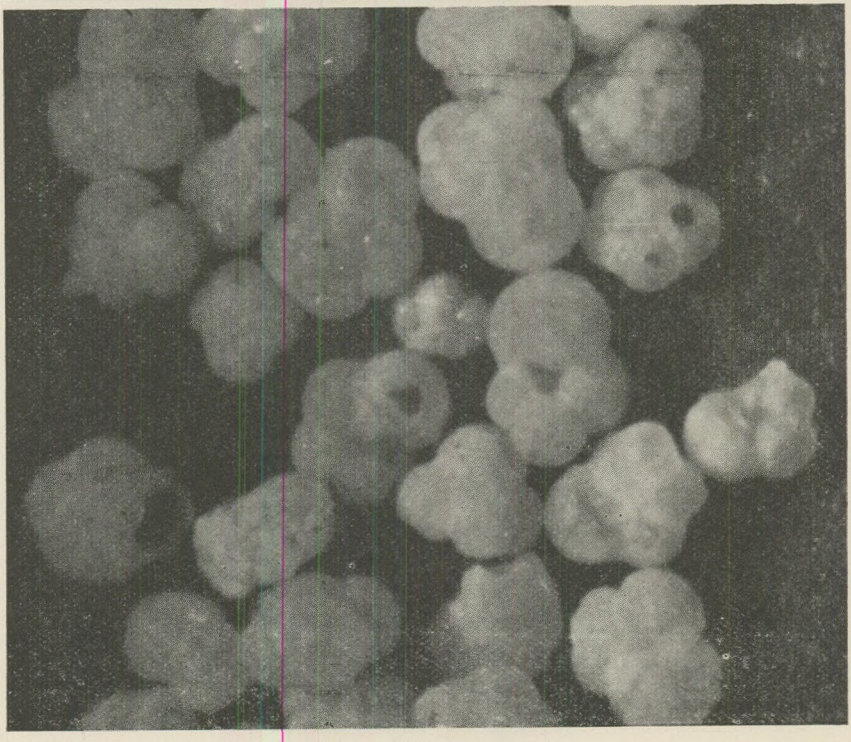

Plate 17

1. Globorotalia opima opima Zone X75

Eger bore-hole

2. Globigerina ciperoensis ciperoensis Zone X75

Ipolytarnóc

INDEX

A kiadásért felelős: az Eötvös Loránd Tudományegyetem rektora
A kézirat nyomdába érkezett: 1968. január — Megjelent: 1968. szeptember
Terjedelem: 17,5 (A/5) ív — Példányszám: 500
Készült mono szedéssel, íves magasnyomással, az MSZ 5061—59 és az 5602—55
szabvány szerint
68.309. Állami Nyomda, Budapest